Heterogeneous photochemistry of atmospheric dusts and organic films

by

Sarah Anne Styler

A thesis submitted in conformity with the requirements for the degree of Doctor of Philosophy

Department of Chemistry
University of Toronto

Heterogeneous photochemistry of atmospheric dusts and organic films

Sarah Anne Styler
Doctor of Philosophy
Department of Chemistry, University of Toronto
2014

Abstract

Little is currently known regarding the nature and consequences of interactions between photoactive surfaces, including mineral dust and 'urban film', and gas-phase pollutants in urban environments. In order to address this knowledge gap, this thesis explores the photochemical reactivity of these environmental surfaces in controlled laboratory settings.

The photoenhanced ozonation of pyrene, a toxic product of incomplete combustion, proceeds at different rates and via different mechanisms at three model 'urban film' surfaces. These results are important because they suggest that the reactivity of a molecule on simplified surfaces may not accurately reflect its reactivity in the real environment.

The photooxidation of isopropanol at the surface of TiO_2, here used as a proxy for the photoactive component of mineral dust, yields gas-phase acetone. This chemistry is amplified by nitrate, a major surficial component of atmospherically processed dust.

These results suggest that dust has the potential to convert non-absorbing species to photochemically active species, and thereby serve as a source of reactive organic radicals for further gas- or surface-phase chemistry.

Oxalic acid, the most atmospherically abundant dicarboxylic acid, is efficiently oxidized to gas-phase CO_2 at the surface of Mauritanian sand and Icelandic volcanic ash. These experiments indicate that the lifetime of oxalic acid may be limited in arid regions by Fe and Ti-catalyzed aerosol-phase photochemistry.

Fluorotelomer alcohols (FTOHs), a class of industrial chemicals used in the production of surface coatings, undergo photooxidation at the surface of sand and ash to yield toxic and persistent perfluorinated carboxylic acids (PFCAs). These results provide the first evidence that the metal-catalyzed heterogeneous oxidation of FTOHs may act as a local source of aerosol-phase PFCAs.

Illumination of Nigerien sand in the presence of gas-phase SO_2 leads to the formation of surface-sorbed sulfate. This chemistry proceeds more efficiently on fine sand than on coarse sand. In chamber experiments, the illumination of SO_2 in the presence of realistically produced dust aerosol results in new particle formation. Together, these results suggest that SO_2 photochemistry at the dust surface has the potential to change not only dust hygroscopicity but also the net scattering potential of dust-containing air masses.

Acknowledgments

I would first like to thank Carol Shields, in whose novels I found Larry, florist-turned-mazemaker, and Fay, mermaid researcher. Through these characters, she instilled in me a desire to make of my life something fantastic, something memorable. I would also like to thank the thermal baths in Budapest, Hungary, for reminding me that there is *actual molten rock* thousands of kilometres below me, and thereby providing me with an ongoing, literal source of perspective.

It's impossible for me to imagine a better mentor than my supervisor, Dr. Jamie Donaldson. It's difficult, when one begins graduate work, to see a place for oneself in the 'exalted halls' of academia, and I have Jamie to thank for knowing before I could even begin to imagine it that there is room for me, here.

My research within the Donaldson group was funded by a PGS-D scholarship from NSERC and by the Queen Elizabeth II/Edwin Walter and Margery Warren Scholarship in Science and Technology. I thank these organizations and donors for their support of basic science research, which not only serves as a necessary foundation for all applied work but also has as its inherently valuable goal — and this is important — the betterment of our understanding of the Earth's complexity.

Jamie encourages his students to take advantage of departmental and university-wide support for graduate students' professional development. I would like to thank the Centre for Global Change Science for the award of two separate fellowships. The first funded a six-week research trip to Université Paris-Est Créteil Val-de-Marne, where I participated in the first introduction of mineral dust into the CESAM environmental chamber. The second supported my travel to Taicang, China, where I attended the first Sino-European Summer School on Atmospheric Chemistry. I would also like to thank the Department of Chemistry for the award of two Special Opportunity Travel Grants, the first of which allowed me to present my work at a conference in Melbourne and to meet with atmospheric science researchers at three Australian universities, and the second of which supported two weeks of follow-up research on SO_2 photochemistry in the CESAM atmospheric chamber.

The Donaldson group is truly peerless! I'm so happy to have shared this journey with you, and I can only hope that I've given you a small percentage of the insight and perspective that you've given me. If I write it here, it has to happen: see you in Vienna, Sumi.

I would also like to thank the members of my doctoral committee, Dr. Jennifer Murphy and Dr. Jonathan Abbatt, for their mentorship and advice throughout my

time in the program. In some fields, it seems, the committee is just a formality, but here, I've always felt as though Jen and Jon have cared about my progress as a scientist and my future within the field. This support has been immensely valuable.

I am grateful to my research collaborators in Lyon and Paris, Dr. Christian George, Dr. Jean-François Doussin, and Dr. Paola Formenti. I've learned so much from each of you, and I look forward to future collaborations. Special thanks are also due to Edouard Pangui, who has been an excellent guide to the intricacies of CESAM, and Dr. Claudia Di Biagio, whom I will probably email daily to discuss particle data.

The Department of Chemistry has a truly stellar support staff. I'd like to especially thank Ahmed Bobat, John Ford, and Johnny Lo in the machine shop for all of their wonderful creations and expert troubleshooting; Dan Mathers for his assistance in ANALEST; and Anna Liza Villavelez for her friendly assistance. I'd also like to thank David Rogerson in the Department of Physics for his exceptionally patient assistance with a last-minute soldering request.

Bethea, Anne, Erin, Kim, Larissa, Laurie, Sabrina, and Teri, girlfriends extraordinaire, thank you for the brilliant conversations and wonderful travel experiences, from Toronto to Tegucigalpa and from Chicago to Condesa: you've taught me so much not only about what it means to be a feminist but also about what it means to live fearlessly and to dance with style. I'm so lucky to have met each of you.

Adam, I love you. This last year has been more wonderful than I could have ever imagined, and it would take more than a thesis to describe the beauty, wonder, and intrigue that you've brought to my life. I'd be happy if I could spend all of my summer evenings sitting beside you on the bench in the Roncesvalles parkette, watching the ever-changing LEDs at KK Thai and Chinese Express and discussing the marketing missteps of Gourmet Pizza by the Slice (GPBTS) while enjoying cones from Cinema Convenience.

Finally, above all else, I would like to thank my family: Mom, for teaching me to be curious about the world and for believing in me, always; Sean, for daytime phone support and much-needed perspective; Daniel and Annalisa, for general hilarity we'll always have Red Lobster; Nana and Grampy, for being the kindest, most loving grandparents one could ever ask for; Uncle Charlie, Uncle Jim, and Aunt Lil, for everything; and Great-Uncle Ron, for his enthusiastic support of my various endeavours. I love each of you so much.

These acknowledgements have been written on two separate trans-Atlantic flights, which somehow seems fitting, since this degree has brought me around the world and back. I'm so lucky to have had this opportunity, and I wouldn't change a thing.

Table of Contents

List of Tables, Figures, and Schemes

Preface

With the exception of Chapters 1, 6, and 7, the chapters of this thesis are based upon a series of published manuscripts. The results presented in Chapter 6 have been accepted for presentation at the 2013 meeting of the American Geophysical Union, and will be included in a future publication. The following paragraphs outline the contributions made to each chapter.

Chapter 1
Introduction

Contributions:

The manuscript was written by Sarah A. Styler, with critical comments from D. James Donaldson.

Chapter 2
Substrate effects in the photoenhanced ozonation of pyrene

Published as:

Styler, S.A.; Loiseaux, M.-E.; Donaldson, D.J. "Substrate effects in the photoenhanced ozonation of pyrene" in *Atmospheric Chemistry and Physics* 2011, 11, 1243 1253.

Contributions:

Experiments at the aqueous surface were carried out by Marie-Eve Loiseaux under the direction of Sarah A. Styler. All other experiments were designed and performed by Sarah A. Styler. The manuscript was written by Sarah A. Styler, with critical comments from D. James Donaldson.

Chapter 3
Photooxidation of Atmospheric Alcohols on Laboratory Proxies for Freshly Emitted and Atmospherically Processed Mineral Dust

Published as:

Styler, S.A.; Donaldson, D.J. "Photooxidation of Atmospheric Alcohols on Laboratory Proxies for Mineral Dust" in *Environmental Science & Technology* 2011, 45, 10004 10012.

Contributions:

All experiments were conducted by Sarah A. Styler. The manuscript was written by Sarah A. Styler, with critical comments from D. James Donaldson.

Chapter 4
Heterogeneous photochemistry of oxalic acid on Mauritanian sand and Icelandic volcanic ash

Published as:

Styler, S.A.; Donaldson, D.J. "Heterogeneous photochemistry of oxalic acid on Mauritanian sand and Icelandic volcanic ash" in *Environmental Science & Technology* 2012, 46, 8756 8763.

Contributions:

All experiments were designed and conducted by Sarah A. Styler. Milos Markovic provided assistance with ion chromatography. The manuscript was written by Sarah A. Styler, with critical comments from D. James Donaldson.

Chapter 5
Heterogeneous photooxidation of fluorotelomer alcohols: a new source of aerosol-phase perfluorinated carboxylic acids

Published as:

Styler, S.A.; Myers, A.L.; Donaldson, D.J. "Heterogeneous photooxidation of fluorotelomer alcohols: a new source of aerosol-phase perfluorinated carboxylic acids" in *Environmental Science & Technology* 2013, 47 (12), 6358 6367.

Contributions:

Anne L. Myers designed the extraction and analysis procedure for surface-sorbed perfluorinated species, and carried out this procedure with assistance from Sarah A. Styler. All other experiments were designed and conducted by Sarah A. Styler. The manuscript was written by Sarah A. Styler (with the exception of experimental and supporting material related to the extraction and analysis of surface-sorbed perfluorinated species, which was written by Anne L. Myers), with critical comments from Anne L. Myers and D. James Donaldson.

Chapter 6
Light-induced interactions of SO_2 with authentically generated mineral dust

Contributions:

Sarah A. Styler designed the overall experimental strategy with assistance from D. James Donaldson, Jean-Francois. Doussin, and Paola Formenti. All experiments performed at the University of Toronto were designed and conducted by Sarah A. Styler. Experiments in the CESAM atmospheric chamber were performed by Sarah A. Styler with assistance from Paola Formenti, Jean-François Doussin, Claudia di Biagio, and Edouard Pangui. The manuscript was written by Sarah A. Styler, with critical comments from D. James Donaldson.

Chapter 7
Conclusions and future directions

Contributions:

The manuscript was written by Sarah A. Styler, with critical comments from D. James Donaldson.

Chapter 1

Introduction

Contributions:

The manuscript was written by Sarah A. Styler, with critical comments from D. James Donaldson.

1.1 Mineral dust: sources, composition, and transport

Large quantities of mineral dust are released into the atmosphere on an annual basis: according to one recent estimate, the annual emission flux from the Saharan desert is ~ 2000 Tg.[1] However, North Africa is not the only dust source region: emissions from Australia, East Asia, and the Arabian Peninsula also contribute to global dust loadings.[2, 3] Once emitted, dust undergoes efficient long-range transport: Figure 1-1 shows the main routes of dust transport from major deserts and dust source regions.[3]

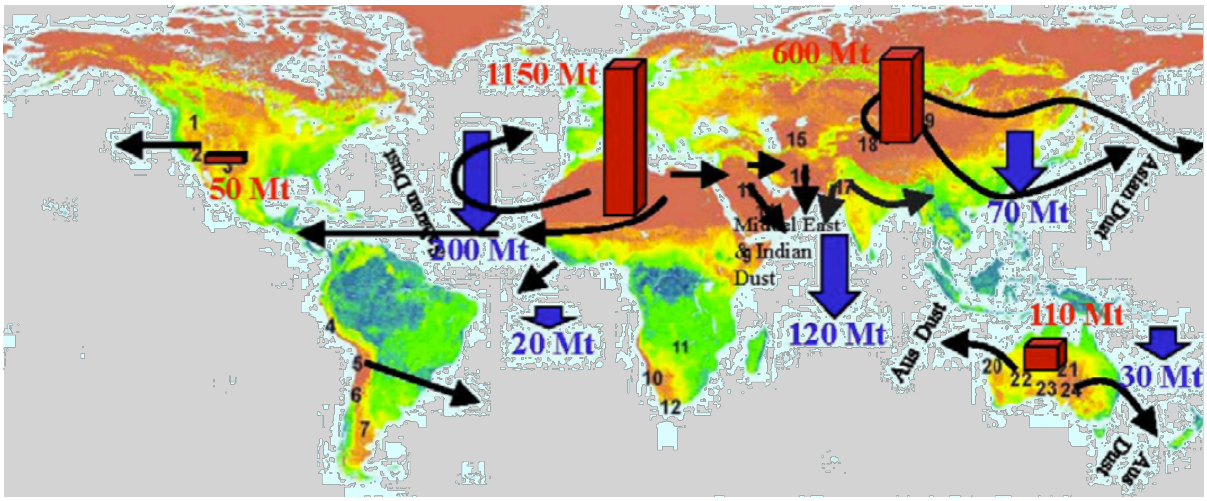

Figure 1-1 Global dust emission sources (red bars), transport routes (black arrows), and oceanic deposition sinks (blue arrows). Locations of the world's major deserts are numbered as follows: Great Basin (1), Sonoran (2), Chihuahua (3), Peruvian (4), Atacama (5), Monte (6), Patagonia (7), Sahara (8), Somali–Chabli (9), Namib (10), Kalahari (11), Karroo (12), Arabian (13), Rub al Khali (14), Turkestan (15), Iranian (16), Thar (17), Taklimakan (18), Gobi (19), Great Sandy (20), Simpson (21), Gibson (22), Great Victoria (23), and Sturt (24). Figure (with adapted caption) reprinted from Aeolian Research Volume 2, Shao *et al.*, Dust cycle: an emerging core theme in Earth system science, 181–204, copyright 2011 with permission from Elsevier[3]

As a result of this efficient transport, mineral dust contributes to aerosol populations even far from source regions: Saharan dust, for example, has been detected in the

southeastern United States,[4] Hong Kong,[5] and southern Italy,[6] and trans-Pacific transport of Asian dust has been shown to contribute to visibility reductions in the western United States.[7]

	Harmattan (Sahara / Sahel)	China	Arizona	Global Dust	Global Rocks
SiO_2	60.95	60.26	57.92	59.9	58.93
Al_2O_3	11.02	11.40	12.21	14.13	14.98
Fe_2O_3	4.50	2.91	4.72	6.85	6.1
MgO	0.76	--	3.01	2.60	3.81
CaO	2.31	--	2.01	3.94	4.84
TiO_2	0.82	0.65	0.74	--	--

Table 1-1 Average elemental composition of dust from global source regions (adapted from Goudie and Middleton; not all components are shown[8]).

As shown in Table 1-1, dust from all global source regions is dominated by SiO_2 and Al_2O_3, and the concentrations of these oxides are similar to those found in rocks.[8] Despite these similarities, dust composition displays continent- and regional-scale heterogeneities: for example, Saharan dusts are typically higher in iron oxides than Asian dusts,[9] and the relative abundance of illite and kaolinite in the clay fraction of Saharan dust varies with source latitude.[10, 11]

The size distribution of airborne dust does not stay constant during transport: by measuring dust size distributions in the Canary Islands and Puerto Rico, Maring and co-workers were able to show that preferential removal of dust particles with diameter > 7.3 μm occurred during trans-Atlantic transport from North Africa.[12] Similarly, in a

study designed to investigate long-range transport of dust from the Chinese interior to Japan, the authors found that the peak of the dust mass size distribution was larger in Beijing, China, a near-source receptor region, than in Yamaguchi, a distant Japanese receptor region.[13]

Long-range transport also has implications for aerosol mineralogy: for example, while the relative concentration of quartz in advected Saharan dust has been observed to decrease during trans-Atlantic transport from the Cape Verde Islands to Barbados, the relative concentration of mica/illite clays has been observed to increase.[14] This preferential retention of the clay fraction of mineral dust, which has been attributed to the relatively more rapid gravitational settling of the quartz fraction,[14] has also been observed for Asian dust during its transport to the North Pacific.[15]

Studies have shown that trace elements, including Fe and Ti, are often enriched in the finer size fraction of mineral dust.[16, 17] In an individual-particle study of airborne mineral dust samples collected over Morocco, for example, Fe and Ti were often found as grains associated with clay mineral aggregates.[18] Given the preferential atmospheric retention of the lighter, clay-sized fraction, these observations imply that the trace metal content and, for reasons that will be discussed later in this chapter, the photoactivity of advected dust will be enhanced during long-range transport.

1.2 Atmospheric consequences of reactions on dust surfaces

During transport, dust mixes with other atmospheric species, including those present in industrial[19] and urban[20] pollutant plumes. In the following sections, the role that these processes play not only in determining the physical, chemical, and toxicological characteristics of dust particles but also in influencing the tropospheric oxidant budget will be discussed.

1.2.1 Changes in dust native optical properties

The mixing of dust with pollutant plumes changes its propensity to absorb and scatter incoming solar radiation, and therefore its influence upon the global radiation budget. The mechanisms by which pollution–dust interactions lead to changes in dust optical properties are complex and still the topic of much research discussion (see *e.g.* a recent review by Formenti *et al.*[21]). As noted in a recent study by Liu and coworkers, pollutant-induced changes in optical properties are more pronounced for Asian dust, which passes over heavily populated industrial and urban centres before being transported over the Pacific.[22]

The absorptive character of freshly emitted mineral dust is composition-dependent, and largely determined by its hematite content.[9, 23, 24] The absorption of coarse-mode mineral dust, however, can be enhanced by coagulation/internal mixing with absorbing pollutants, including black/elemental carbon (EC).[25] Even when black carbon is only externally mixed with dust, as was the case in one study in Dakar, Senegal,[26] this mixing leads to a change in the "effective" absorption properties of the dust layer as measured using remote sensing techniques.[22]

The mixing of dust with pollutant plumes can also result in the transfer of other carbonaceous compounds – organic (OC) or "brown carbon" – to the dust surface.[27-29] An illustration of this effect is presented in Figure 1-2. More evidence for the existence of mixed dust–carbonaceous aerosol was provided by Deboudt and coworkers, who found that mixing of African dust with biomass burning and anthropogenic emissions led to the formation of a carbonaceous coating on the dust surface.[30] Since organic carbon also absorbs in the actinic region (although to a lesser extent than black carbon/soot),[31, 32] dust–organic interactions would also be expected to alter the absorption properties of dust aerosol.

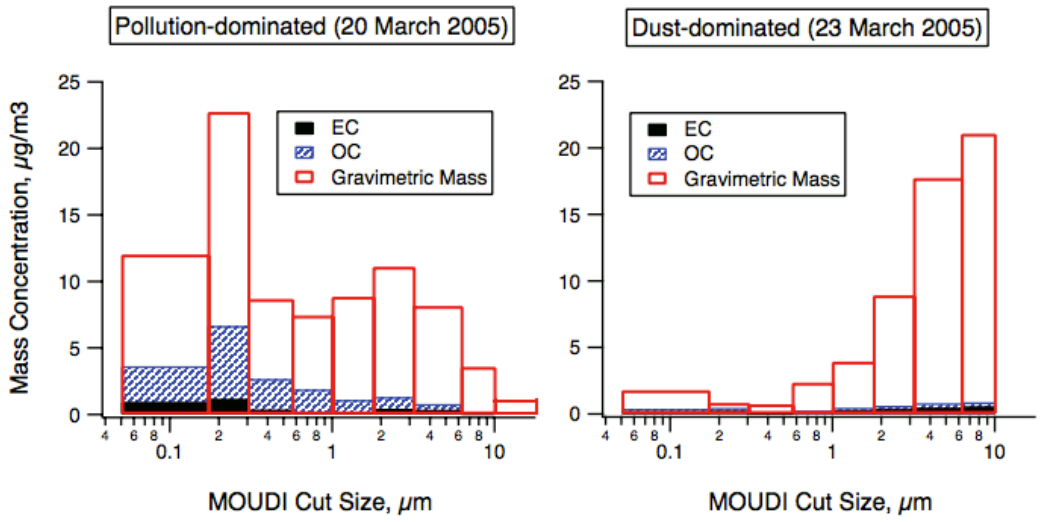

Figure 1-2 Size-segregated mass concentrations of elemental (EC) and organic (OC) carbon measured during the EAST-AIRE campaign near Beijing. Although most carbonaceous mass was in the fine mode during pollution-dominated periods, significantly more carbon (~ 50%) was present in the coarse mode during dust-dominated periods. Image and caption adapted from Yang *et al.*[27]

Although the formation of soluble coatings on dust surfaces via the uptake of acidic pollutant gases is not expected to have a significant influence on dust scattering properties,[33] pollutant dust interactions can have an indirect negative influence on the net scattering efficiency of air masses via the transfer of scattering mass (*e.g.* sulfate and nitrate) from the optically effective accumulation mode to the coarse dust surface.[25, 34, 35] This effect can be highly significant: in a study performed using data from the ACE-Asia and TRACE-P experiments, Tang *et al.* reported that 10 30% of sulfate and more than 80% of nitrate resided in the supermicron mode during dust events.[36]

1.2.2 Changes in dust-mediated cloud formation

1.2.2.1 Dust as cloud condensation nuclei (CCN)

According to Köhler theory, the cloud condensation nuclei (CCN) activity of a particle depends exclusively on its size, surface tension, and on the quantity of soluble material contained within it.[37] The bulk of studies investigating the CCN activity of mineral dust, which is largely insoluble, have therefore focused on its hygroscopic conversion through atmospheric processing (*vide infra*).

In recent years, however, a growing body of field[38] and laboratory[39] evidence supports the hypothesis that freshly emitted dust particles can also act as CCN. Although some studies have attributed the CCN activity of unprocessed dust to small quantities of hygroscopic material contained within it,[39] others have suggested that dust CCN activity does not require deliquescent material but is rather controlled by efficient adsorption of water multilayers to the dust clay fraction.[40, 41]

Dust hygroscopicity can be enhanced during atmospheric transport by the acid-induced formation of soluble nitrate and sulfate surface coatings.[42-45] In a recent Korean study designed to measure the composition and hygroscopicity of advected Asian dust, for example, Kim and Park found that dust which had previously passed over highly polluted industrial areas was internally mixed with hygroscopic sulfate from condensation of H_2SO_4 and/or $(NH_4)_2SO_4$.[29] The timescale associated with acid processing can be quite rapid: according to one laboratory study, insoluble calcite can be converted to soluble and hygroscopic calcium nitrate within several hours at atmospherically relevant HNO_3 concentrations.[46]

The reactivity of dust toward atmospheric acids displays a strong dependence upon particle mineralogy. In a laboratory study of calcium-containing minerals, for example, Krueger and coworkers found that while calcite ($CaCO_3$) and dolomite ($CaMg(CO_3)_2$) reacted with gas-phase HNO_3, gypsum (Ca_2SO_4) did not.[47] This mineral-dependent

processing has also been observed in the field: a study of coarse particulate matter in Beijing, China, found that sulfate and nitrate were more strongly associated with carbonates than silicates.[48]

A number of field studies have found that mineral dust is often internally mixed with oxalic acid and other carboxylic acids.[49, 50] Since oxalic acid is highly soluble and hygroscopic,[51] this mixing might be expected to result in the formation of a soluble coating, which would enhance the CCN activity of the dust acid mixture over that of the dust itself. However, laboratory studies have shown that this is not always the case: reaction of oxalic acid with calcite, for example, which results in the formation of insoluble calcium oxalate, does not result in an enhancement in CCN activity.[52, 53] In addition, a recent field study performed in Japan showed that a large portion of aerosol-phase oxalic acid was present as insoluble zinc and calcium oxalates, which would also not contribute to dust hygroscopicity.[54]

1.2.2.2 Dust as ice nuclei (IN)

Mineral dust aerosols are efficient ice nuclei (IN), even at substantial distances from source regions: African dust aerosols have been shown to contribute to ice nucleating aerosol populations in Florida[55] and in the Amazon basin,[56] for example, and both Saharan and Asian dust have been recently shown to contribute to ice-induced precipitation in the western United States.[57] Although the IN activity of unprocessed mineral dust was originally attributed largely to clay minerals, including illite, kaolinite, and montmorillonite,[58] two recent studies have shown that the comparatively minor feldspar mineral component also plays a significant role in determining this property.[59, 60]

Although acid processing generally enhances mineral dust's CCN activity, it often has the opposite effect on its IN activity: sulfuric acid, for example, has been shown to impede the IN activity of Arizona test dust and illite,[61, 62] perhaps via an acid-induced reduction in ordered water structures at the air dust interface[63] or via the conversion

of ice-active silicates to non-active metal sulfates.[64] The same is not true for all acids, however: while exposure to nitric acid impairs depositional ice nucleation by Arizona test dust, it promotes sub-saturation condensation ice nucleation.[65]

The exposure of Arizona test dust to secondary organic aerosol formed from the biogenic monoterpene α-pinene has also been shown to reduce its IN activity.[66] This reduction was correlated with the fractional organic surface coating of the dust,[66] which suggests that exposure of mineral dust to organic species contained within urban or industrial pollutant plumes would suppress its IN activity relative to that of freshly emitted dust. To date, however, no studies have investigated the effect(s) of urban or industrial organic pollutants upon dust IN activity.

1.2.3 Changes in dust toxicity

Although the majority of studies on the health effects of airborne particulate matter have focused on particles < 2.5 μm in diameter (PM2.5; see *e.g.* work by Laden *et al.*[67]), recent research has begun to focus on the contribution of the coarse fraction of PM10 (particles with diameters 2.5 10 μm) to adverse health effects.[68, 69]

Epidemiological studies in areas affected by advected dust have shown that dust episodes are correlated with hospital admissions for a variety of respiratory,[70, 71] cerebrovascular,[71, 72] and cardiovascular[73] illnesses. Although the mechanisms by which dust mediates these adverse effects are not fully understood, it has been hypothesized that microorganisms, toxic organic pollutants, and metals at the dust surface may all contribute to dust toxicity.[74]

Field research has suggested that organic contamination of advected dust can arise via a number of pathways, including mobilization of contaminated source material,[75, 76] adsorption of organic pollutants during transport over polluted regions,[77, 78] and uptake of pollutants in urban receptor regions.[78, 79] These pathways are often location-dependent: for example, PCDD/F contamination of coarse particulate matter in

Taiwan during an Asian dust storm episode was attributed in a background location to long-range transport of contaminated PM from mainland China and in the Taipei urban region to local contamination by municipal waste incinerators.[79]

A number of studies have shown that dust can also serve as a vector for transport of toxic trace metals, including Pb, Cd, Sn, and Cr.[80-83] As was the case for organic contaminants, this can arise via the entrainment of polluted source soils[81] and/or via the scavenging of atmospheric pollutants during the transport of advected dust over polluted urban[81] and industrial[82, 83] regions.

Our understanding of these issues is complicated by the fact that these pathways often operate in concert: results obtained in an Israeli sampling campaign designed to study the mineral-dust mediated transport of anthropogenic pollutants showed that suspended dust was contaminated with pesticides, presumably as a result of its transport over rural agricultural areas; lead, which most likely adsorbed to the dust surface during its transport over the polluted Cairo basin; and PAH, which adsorbed to the dust in the urban receptor regions under study.[81, 84]

1.2.4 Changes in dust solubility

Approximately 25% of dust emitted to the atmosphere is deposited to the oceans,[3] where its soluble iron component serves to enhance primary productivity in iron-limited marine ecosystems.[85] Although this "fertilization" effect which has the potential to influence climate via the photosynthesis-mediated oceanic uptake of atmospheric CO_2 [86] has received much research attention, major questions still exist regarding the factors that determine aerosol iron solubility.

The solubility of iron depends strongly on its oxidation state and bound nature, both of which are mineralogy-dependent, and ranges from 0.01% for hematite to ~4% for clay-associated iron.[87] By contrast, iron solubility in aerosols can reach 80%.[88] Although recent evidence suggests that iron-containing anthropogenic combustion

aerosols may contribute significantly to these elevated solubility values, and therefore to the total flux of soluble iron to the oceans,[88, 89] it is also known that atmospheric processing of mineral dusts enhances the solubility of iron contained within them.[90, 91]

Since iron solubility is enhanced under acidic conditions,[92, 93] one potential anthropogenically mediated dissolution mechanism involves the acidification of dust via the uptake and subsequent heterogeneous oxidation of anthropogenic SO_2.[20, 94, 95] Exposure to anthropogenic SO_2 has also been suggested to facilitate the liberation of structural iron contained within the clay mineral chlorite and its subsequent conversion to the significantly more soluble ferrihydrite.[96]

Laboratory experiments have shown that dust iron solubility is also enhanced under dark conditions by complexation with anthropogenically derived organic ligands, including oxalate.[97, 98] Oxalate and other electron-donating carboxylates, including formate, acetate, and butyrate, also promote the photoreduction of iron (III) oxyhydroxides and the formation of soluble iron (II).[99, 100] As will be discussed in Chapter 4, mineral dust oxalate photochemical interactions may also play a significant role in determining the atmospheric lifetime of oxalic acid in arid environments.[101]

1.2.5 New particle formation

As outlined in the previous sections, the interaction of mineral dust with SO_2 may lead to the formation of surface-bound sulfate, which reduces the dust's IN activity, enhances its CCN ability, and promotes the acid-mediated solubilization of iron contained within it.

In one very recent study, the interaction of illuminated mineral dust with SO_2 was shown to result in the formation of large quantities of nanometer-sized particles.[102] This process, which is believed to occur via the nucleation of H_2SO_4 produced by oxidation of SO_2 by gas-phase hydroxyl radicals produced by the illuminated mineral dust, represents a new pathway for H_2SO_4-induced particle formation under low dust loadings.

1.2.6 Changes in tropospheric trace gas concentrations

In their pioneering model study, which was performed when direct measurements of trace gas uptake by mineral aerosol were virtually non-existent, Dentener and coworkers suggested that heterogeneous chemistry at the mineral dust surface has the potential to change the trace gas composition of the surrounding atmosphere.[103] This suggestion has been borne out by measurements made in a large number of field campaigns: Figure 1-3, for example, shows a distinct anti-correlation between North African coarse aerosol and gas-phase ozone concentrations at Mount Cimone, Italy.[104]

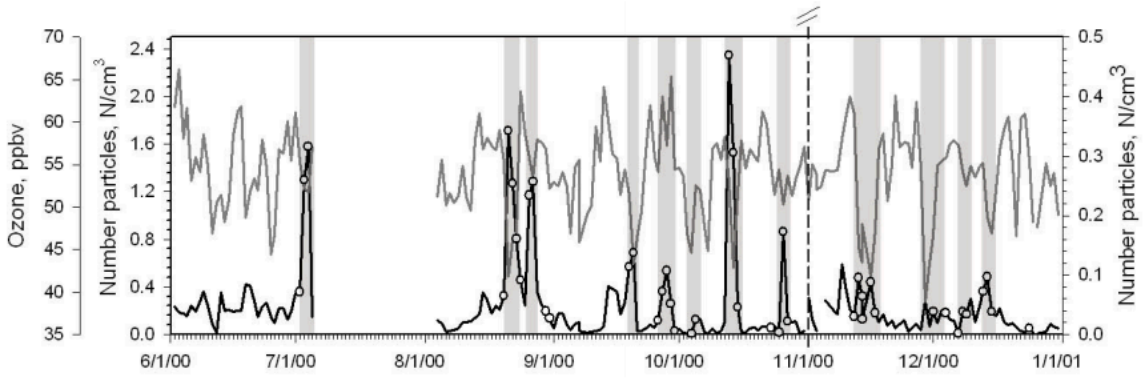

Figure 1-3 Daily coarse aerosol concentration (black line) and daily de-trended ozone (grey line; see Bonasoni *et al.* for details[104]) recorded at Mt. Cimone during the period June–December 2000 (for coarse aerosol: November–December right scale). White circles represent days during which back-trajectories originated from North Africa. Coloured bars indicate the periods of the dust transport events. Image taken from Bonasoni *et al.*[104]

It is universally agreed that dust has a strong influence on gas-phase HNO_3 concentrations.[20, 35, 105] In a study performed as part of the ACE-Asia campaign, for example, Tang and coworkers found reductions in HNO_3 of up to 95% during a high-dust period.[106] By contrast, field studies have shown that the O_3-depleting influence of dust plumes is highly variable: while significant dust-induced O_3 reductions have been observed in some studies,[20, 105-108] other studies have reported minimal O_3 depletion in

dust plumes.[109, 110] Although dust can theoretically influence O_3 directly (*i.e.* by direct uptake of O_3 on dust[111]) or indirectly (*i.e.* by uptake of O_3 precursors, including HNO_3), most studies have attributed global O_3 reductions to the latter pathway,[107, 112] in part because direct O_3 uptake on dust is limited by surface passivation.[113]

Dust can also influence the tropospheric oxidant budget by reducing the local actinic flux.[108, 114, 115] For example, the results of a modeling study suggest dust-induced reductions in actinic flux during the Megacity Initative: Local and Global Research Observations (MILAGRO) experiment in Mexico City were responsible for a 5 20% reduction in photochemical production of OH and a ~ 10 ppbv reduction in O_3 concentrations.[115] A similar dampening of photolysis rates was suggested to be partially responsible for enhanced carbonyl concentrations measured during a severe dust episode in Beijing, China.[116]

During the Mineral Dust and Tropospheric Chemistry (MINATROC) study, Salisbury and coworkers measured the influence of a Saharan dust event on the gas-phase concentrations of methanol, formaldehyde, acetone, and acetaldehyde.[117] Although these authors found no discernable effect on these concentrations, they emphasized that these results were specific to the region and specific set of atmospheric conditions under study, and thus do not preclude the existence of dust organic interactions under different circumstances. To date, however, no other field studies have attempted to assess the effect of dust on the concentration of gas-phase organic species.

1.3 How are heterogeneous reactions studied in the laboratory?

Given the complexity and spatiotemporal variability of real atmospheric surfaces, the vast majority of our knowledge regarding heterogeneous chemistry under both dark and light conditions comes from laboratory experiments, which typically measure

surface-phase reaction rates and/or gas-phase uptake coefficients. This section focuses on the methods by which reaction mechanisms and parameters can be extracted from laboratory results, the experimental techniques by which heterogeneous reactions are currently studied, and the challenges associated with the extrapolation of results obtained under idealized laboratory conditions to the real atmosphere, with all its attendant complexity.

1.3.1 Mechanistic frameworks

1.3.1.1 The Langmuir–Hinshelwood mechanism for surface reactions

In the gas phase, the rate of bimolecular reactions depends linearly on the concentrations of both reactants.[118] The same is not true for heterogeneous bimolecular reactions. The pseudo-first-order reactive loss rate k_{obs} of surface-bound species upon exposure to gas-phase ozone, for example, generally approaches a maximum value – often termed k^{I}_{max} or A – at high gas-phase ozone concentrations. This behaviour has recently been observed for the ozonation of anthracene at the mineral dust surface;[119] the oxidation of soot by ozone;[120] and, as will be discussed in Chapter 2, the ozonation of pyrene solid films and pyrene at the air–aqueous and air–octanol interfaces.[121]

In general terms, this non-linear dependence implies that the heterogeneous reactions of surface-sorbed organic molecules with gas-phase oxidants proceeds by a Langmuir–Hinshelwood mechanism, in which the oxidant adsorbs to the surface prior to reaction and the rate of reaction is thus equal to the product of the surface oxidant concentration $[Ox_{surf}]$ and the second-order rate coefficient for reaction at the surface k^{II}:[122]

$$k_{obs} = k^{II}[Ox_{surf}]$$

If $[Ox_{surf}]$ behaves according to a Langmuir adsorption isotherm, then it can be modeled using the following equation:

$$[Ox_{surf}] = \frac{N_{surf}\,[Ox_{gas}]}{[Ox_{gas}]+B}$$

In this equation, N_{surf} is the maximum number of sites available for oxidant adsorption, B represents the ratio of surface desorption to adsorption, and [Ox_{gas}] represents the gas-phase oxidant concentration.[123] In cases where little to no oxidant dissolution in the bulk phase occurs, B can be approximated as the inverse of its gas surface partition coefficient, K_{Ox}.[124] At high [Ox_{gas}], the surface becomes "saturated"; that is, no further adsorption of oxidant is possible. At this point, the reaction rate becomes independent of [Ox_{gas}]. Under these conditions, the dependence of k_{obs} upon [Ox_{gas}] can be written as:

$$k_{obs} = \frac{k^{II} N_{surf}\,[Ox_{gas}]}{[Ox_{gas}]+B}$$

This dependence can then be fit to an equation of the following form, where A is equal to $k^{II}N_{surf}$:[124]

$$k_{obs} = \frac{A\,[Ox_{gas}]}{[Ox_{gas}]+B}$$

Since the A parameter in the Langmuir-Hinshelwood model is in part a function of the bimolecular rate constant k^{II}, for surficial oxidation, its magnitude depends on the identities of both the oxidant and the surface-sorbed organic species. For example, in their investigation of the reaction of polycyclic aromatic hydrocarbons (PAH) with ozone at the surface of model urban films, Kahan and coworkers found that the A parameter was an order of magnitude greater for benzo[a]pyrene than for phenanthrene.[124]

The A parameter can also be influenced by co-sorbed species at the reaction surface. For example, studies have shown that the A parameter for the reaction of ozone with

anthracene[125] and pyrene[126] adsorbed at the air aqueous interface is lower in the presence of monolayer films of small carboxylic acids. Quantum chemical calculations suggest that this effect arises via the sequestration of ozone by the carboxylic acid moiety at the aqueous surface.[126]

While *A* values are in large part a function of the identity of the surface-sorbed species, *B* values are primarily determined by the extent to which the gas-phase oxidant partitions to the reaction substrate. *B* values for the reaction of ozone with PAHs have been measured for a wide variety of substrates, including water,[127] water with monolayers of octanol and octanoic acid,[126] and soot aerosols.[128] Generally, ozone displays a propensity for non-polar surfaces: *B* values for soot aerosols (3.57×10^{12} molecules cm^{-3})[128] and phenylsiloxane oil aerosols (1×10^{13} molecules cm^{-3})[129] are significantly lower than those for polar surfaces such as water (2.15×10^{15} molecules cm^{-3}),[127] which implies a correspondingly higher equilibrium partitioning to non-polar surfaces. Preliminary calculations suggest that the propensity of ozone for non-polar surfaces may arise from stronger substrate ozone binding interactions at these surfaces.[129]

1.3.1.2 The resistor model for trace gas uptake

The uptake of trace gases by environmental surfaces is often reported in terms of an uptake coefficient (typically denoted as γ), which describes the ratio of the net flux from the gas phase to the surface to the total gas surface collision flux.[130] As the uptake coefficient is a purely empirical quantity, it does not itself provide mechanistic insight into the set of simultaneous processes gas-phase diffusion, adsorption, desorption, and reaction at the particle surface and/or in its bulk that together determine its magnitude. One method by which mechanistic information can be extracted from empirical uptake coefficients is the use of the resistor model, which treats the measured uptake coefficient γ as a set of decoupled processes combined either in series or in parallel. Although this model was first applied in the atmospheric community to the study of gas liquid interactions,[131] it has more recently been adapted to the study of

gas-phase uptake by solid particles (see Amman *et al.*[132] for a full derivation).

In cases where uptake coefficients are large and gas-phase diffusion is insufficient to replenish reagent concentrations near the substrate surface, there is an effective reduction in the collision rate of gas-phase species (here denoted by *X*) with the substrate surface.[132] As shown in the following equation, this is accounted for by the gas-phase diffusional resistance term Γ_{diff}:[132]

$$\gamma_{obs} = \frac{1}{\gamma_X} + \frac{1}{\Gamma_{diff}}$$

Generally, laboratory experiments are conducted at reduced pressures, which minimizes the influence of gas-phase diffusion. Under these conditions, $\gamma_{obs} = \gamma_X$ and the following equation applies, where $1/S_0$ is a resistance to mass accommodation at the particle surface (where the surface accommodation coefficient S_0 is defined here as the probability that *X* neither immediately leaves the surface nor reacts immediately upon collision) and $1/\Gamma_{surf}$ is a resistance to surface reaction:[132]

$$\frac{1}{\gamma_{obs}} = \frac{1}{S_0} + \frac{1}{\Gamma_{surf}}$$

In cases where uptake of *X* is limited by a Langmuir Hinshelwood-type reaction with a surface-sorbed species *Y* (*i.e.* where $S_0 >> /\Gamma_{surf}$), the following equation applies:[132]

$$\gamma_{obs} = \frac{4k_{surf}\,[Y_{surf}]\,K}{c_X\sigma_X(K[X_{gas}]+1)}$$

Here, k_{surf} is the bimolecular rate coefficient for reaction at the particle surface, *K* is the Langmuir partitioning constant for the gas-phase species, $[X_{gas}]$ is the gas-phase concentration of reagent *X*, $[Y_{surf}]$ is the surface concentration of the adsorbed species *Y*, c_X is the mean thermal velocity of *X*, and σ_X is the surface area occupied by a single molecule of *X*.[132]

This formalism is useful because it makes clear that the reaction-dominated uptake coefficient of gas-phase species by particles scales linearly with the concentration of surface-sorbed reagents and that, at elevated gas-phase concentrations, the uptake coefficient will decrease with increasing gas-phase concentration. An illustration of the latter point is provided by Figure 1-4, which shows the uptake coefficient of gas-phase ozone by solid pyrene films as a function of ozone concentration.[133]

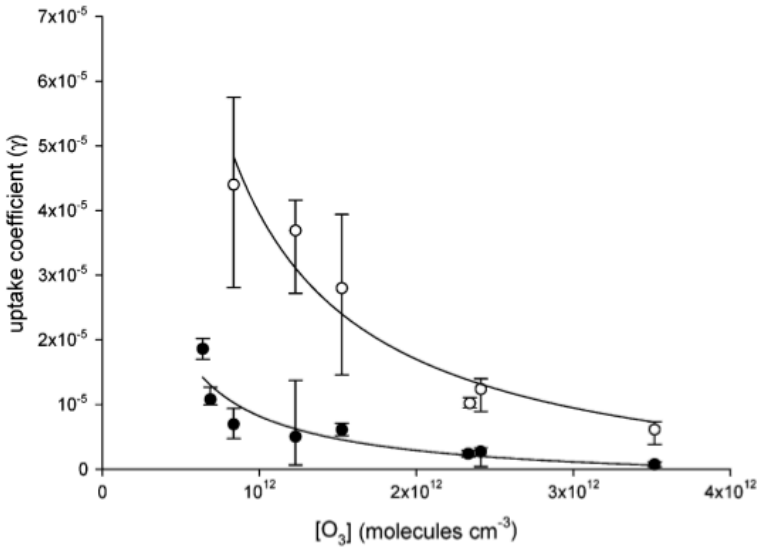

Figure 1-4 Steady-state uptake coefficients for the reaction of ozone with solid pyrene films under both dark (solid circles) and light (hollow circles) as a function of gas-phase ozone concentration. Reproduced from Styler *et al.*[133] with permission from the PCCP Owner Societies.

1.3.2 Experimental techniques

The laboratory community makes use of a number of techniques to interrogate reactions at atmospheric surfaces. Since an excellent overview of the theory underlying these techniques is available in a recent review paper by Kolb and coworkers,[134] this section will focus primarily upon their application, advantages, and disadvantages in the context of mineral dust chemistry and photochemistry.

1.3.2.1 Knudsen cells

Although the Knudsen cell was developed in the early twentieth century,[135] its first application to the study of reaction rates and measurements occurred in the 1960s at the Stanford Research Institute.[136] Since its development, it has found much use in the study of heterogeneous atmospheric processes, including the interaction of a wide variety of inorganic[113, 137, 138] and, to a lesser extent, organic [139-141] trace gases with mineral surfaces. The design and construction of a three-compartment version of this cell, which allows for the investigation of light-induced chemistry in the presence and absence of gas-phase oxygen, was a major component of the present thesis work. A schematic of the final iteration of this photochemical Knudsen cell is shown in Figure 5A-1.[142]

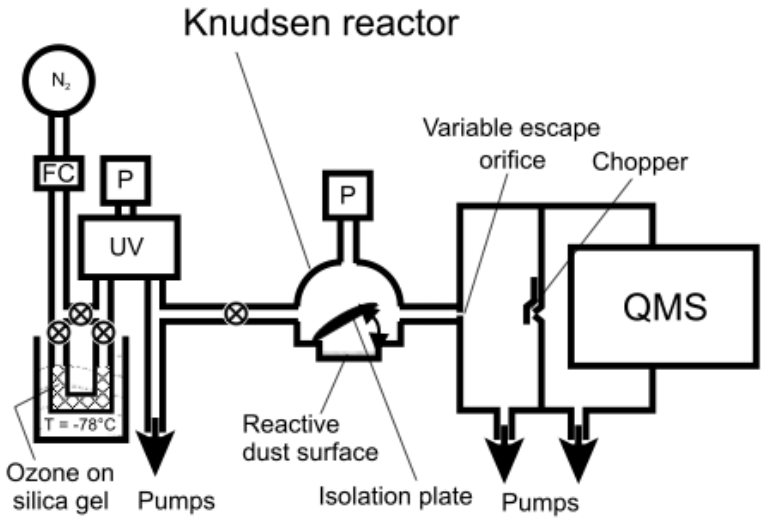

Figure 1-5 A schematic of a simple Knudsen cell, from Hanisch and Crowley.[113]

A schematic of a simple Knudsen cell is shown in Figure 1-5.[113] In this apparatus, gas-phase probe reagents are introduced into the cell and their effusion through a small exit orifice is measured using mass spectrometry. Generally, Knudsen cells are

operated in the molecular-flow pressure regime, where the mean free path of gas-phase reagents exceeds the cell dimensions such that gas surface collisions outnumber gas-phase collisions. Under these conditions, the change in effusion of a gas through the exit orifice of the Knudsen cell upon exposure to a solid substrate is directly related to the probability of loss from the gas phase upon a single collision with the substrate, and an uptake coefficient for reaction can be calculated using the following equation:[118]

$$\gamma = \frac{A_0}{A_S}\left(\frac{I-I_0}{I_0}\right)$$

Here, A_0 and A_S are the geometric areas of the exit orifice and the sample holder, respectively, I_0 is the mass spectral signal obtained with the sample holder closed, and I is the signal obtained with the sample open.

One of the main advantages of this apparatus is that the low pressure reached in the reaction chamber obviates the need to consider gas-phase diffusion limitations to reaction (see Section 1.3.2.2). Conversely, these low pressures also prevent the ambient-temperature study of relatively volatile substrates, such as aqueous H_2SO_4, and do not permit the investigation of the influence of relative humidity upon reactions. In addition, the use of bulk mineral samples also requires researchers to scale observed uptake coefficients by the substrate surface area available for reaction, which is not always simple to determine and which has been the subject of much debate in the literature (see Section 1.3.3.2).

1.3.2.2 Coated-wall and aerosol flow tubes

In coated-wall flow tubes, the substrate of interest is coated on the inner surface of a glass (typically quartz or Pyrex) tube, which is subsequently placed within a temperature- and pressure-controlled assembly.[143] Gas-phase reagents are introduced into the flow tube through a movable injector. In aerosol flow tubes, by contrast, the particles themselves are typically entrained in an inert gas flow and introduced into a

flow of reagent gas using a movable injector.[102] A simple aerosol flow tube schematic is shown in Figure 1-6.[144] In this particular apparatus, a constant aerosol flux is maintained within the flow reactor and, as is the case for coated-wall reactors, the reagent gas is introduced using a movable injector.

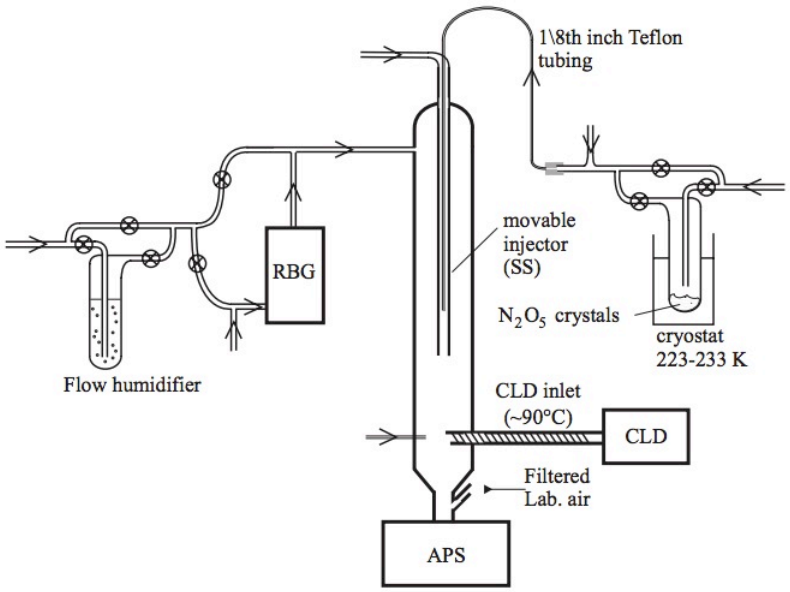

Figure 1-6 A schematic of the aerosol flow tube apparatus used by Wagner *et al.*[144] for the study of N_2O_5 uptake at the surface of authentic and synthetic mineral samples. Here, a rotating brush generator (RBG) is used to entrain particles in a N_2 flow, a chemiluminescence detector (CLD) is used to detect NO at the exit of the flow tube, and an aerodynamic particle sizer (APS) is used to characterize the dust particle size distribution.

In both of these types of experiment, the gas-phase reagent concentration is measured at a number of injector positions, and thus as a function of gas substrate interaction time. The pseudo-first-order loss rate k_{obs} determined from these measurements can then be used to calculate a surface area-scaled uptake coefficient for reaction using the following equation, where c is the mean thermal velocity of the gas-phase reagent, r is the radius of the flow tube, and S is the surface area of the mineral sample:[133]

$$\gamma = \frac{k_{obs}\, 2r}{c\, S}$$

In cases where uptake coefficients are large and radial diffusion in the flow tube is thus insufficient to replenish reagent concentrations near the substrate surface, this equation is not valid. In order to account for such diffusional limitations, uptake coefficients obtained in coated-wall flow tubes are often corrected using the Cooney Kim Davis (CKD) method, which estimates Γ_{diff} (see Section 1.3.1.2).[133, 145, 146]

Coated-wall and aerosol flow tubes have been widely used to investigate the chemistry and photochemistry of inorganic[144, 147-150] and, to a much lesser extent, organic[151] species at the surface of authentic and synthetic mineral samples. One of the main advantages of these techniques is that they can be operated at or near atmospheric pressure and thus permit the study of reactions as a function of relative humidity (see Section 1.3.3.3 for a discussion of the role that adsorbed water plays in chemistry at the mineral dust surface).

Aerosol flow tubes present three distinct advantages over coated-wall flow reactors. First, although the surface area of a coated-wall flow tube itself is exactly calculable, the surface area of a heterogeneous, multilayer solid coating is less so. In aerosol flow tubes, available (external) surface areas for reaction can be calculated directly using particle size distributions obtained from aerodynamic particle sizer (APS) or scanning mobility particle sizer (SMPS) data,[134] after correction for particle non-sphericity.[152] Second, uptake coefficients determined using aerosol flow tubes do not require correction for gas diffusion into underlying sample layers, which is the case for uptake coefficients determined using porous bulk powder or film samples.[153, 154]

Third, and perhaps most importantly, they permit *in situ* analysis of reaction-induced changes in particle properties: in one study, Sullivan and co-workers exposed $CaCO_3$ particles to HNO_3 in an aerosol flow reactor at a range of relative humidities and then used an aerosol time-of-flight mass spectrometer (ATOFMS) and cloud condensation

nuclei counter (CCNc) coupled to the flow tube to measure changes in particle composition specifically, the formation of calcium nitrate and hygroscopicity, respectively.[46]

1.3.2.3 Atmospheric reaction chambers

Atmospheric reaction chambers are large volumes, typically constructed from PTFE[155] or stainless steel,[156] which allow for the introduction of gas-phase reagents and/or particle-phase species. Changes in gas- and particle-phase compositions as a result of photochemical or dark reactions within the chamber are monitored using a range of *in situ* and offline techniques. While atmospheric reaction chambers have been widely used for the determination of gas-phase reaction rates[157] and secondary organic aerosol (SOA) chemistry,[158] the majority of chamber studies involving mineral dust have focused on its cloud nucleating properties rather than its chemical transformations.[159]

To date, the only published chamber experiments exploring mineral dust chemistry have emerged from the environmental aerosol chamber developed by Grassian and coworkers.[160] This 150 L stainless steel chamber can be equipped with a UV-Vis spectrometer and/or single-pass FTIR system for the measurement of gas-phase reagents and, in its most recent iteration, allows for the illumination of reaction mixtures using a solar simulator located on its upper face.[161-163]

Thus far, experiments conducted in this chamber have investigated the fate of gas-phase species on individual mineral dust components, including oxides, clays, and carbonates,[164-166] but have yet to employ authentic dust samples. In these experiments, particle introduction is accomplished with a flow of high-pressure gas, which is used to inject particles (generally in the submicron size range) through a nozzle/impactor assembly and into the chamber. This technique promotes particle mixing within the chamber, which is typically accomplished within one minute.[160]

Figure 1-7 shows the results of a typical experiment using this assembly, in this case investigating O_3 uptake by suspended Fe_2O_3 aerosol as a function of relative humidity.[164] In these types of experiments, heterogeneous uptake coefficients can be determined using the following equation:[163]

$$\gamma = \frac{4k}{c\,S[C_{mass}]}$$

Here, c is the mean thermal velocity of the gas-phase reagent, k is the pseudo-first-order rate coefficient for loss of gas-phase reagent, $[C_{mass}]$ is the mass concentration of mineral particles within the chamber, and S is the surface area of the mineral sample.

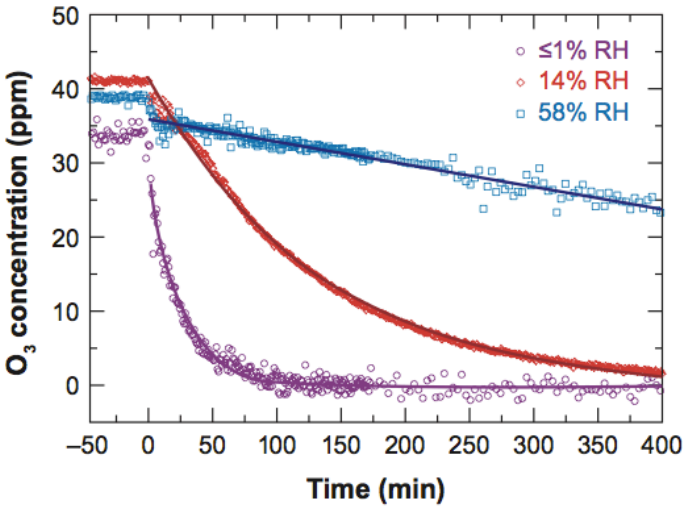

Figure 1-7 Ozone decay on α-Fe_2O_3 as a function of relative humidity. Image reprinted with permission from Cwiertny *et al.*;[163] original data from Prince *et al.*[164]

As can be seen in Figure 1-7, one of the main advantages of chamber experiments is that they allow reactions to be followed for hours, rather than seconds or minutes. Under these conditions (although not in this particular case), experiments can be performed at gas-phase reagent concentrations that more closely resemble those

found in the environment than those typically used in flow-tube studies. This is especially important for heterogeneous environmental samples, where the influence of high-reactivity, low-abundance surface sites may be underestimated under conditions of rapid surface saturation.

Recent, as-yet unpublished experiments from the CESAM chamber at the Laboratoire Inter-universitaire des Systèmes Atmosphériques (LISA), have aimed to expand the scope of the mineral dust chamber studies performed to date. CESAM is a 4200 L stainless steel chamber equipped with a wide variety of instrumentation for the analysis of gas-phase and particulate species contained within it.[156] In these experiments, which will be presented in full at the Fall 2013 meeting of the American Geophysical Union and in preliminary form in Chapter 6, the interaction of SO_2 with mineral dust was investigated as a function of relative humidity and illumination conditions.[167]

One of the main advances associated with these experiments was the use of realistically produced mineral dust particles (i.e. rather than individual dust components or sieved source sands). These particles, which had a median diameter of 1.1 μm, were generated from Nigerien and Chinese desert sands using a procedure designed to mimic the sandblasting process that leads to dust emission in the real environment.[23]

The large size of the CESAM chamber is beneficial because it allows for simultaneous sampling by multiple instruments; in its current configuration, it can support a total outflow of 20 L min^{-1}. In the experiments referenced here, for example, the chamber was interfaced not only to an SO_2 monitor but also to two GRIMM optical particle counters, a WELAS light-scattering spectrometer, a condensation particle counter (CPC), a scanning mobility particle sizer (SMPS), an aethalometer, a nephelometer, and an aerodynamic particle sizer (APS). These complementary techniques provide a

rich dataset that would not be available under lower-flow conditions, such as those present in coated-wall or aerosol flow tubes.

1.3.2.4 Surface spectroscopic techniques

A number of studies have employed diffuse reflectance infrared Fourier transform spectroscopy (DRIFTS) to investigate the interaction of mineral surfaces with gas-phase oxidants, including NO_2,[168] ozone,[169] N_2O_5,[170] and mixtures of SO_2 with O_3[171] and NO_2.[137]

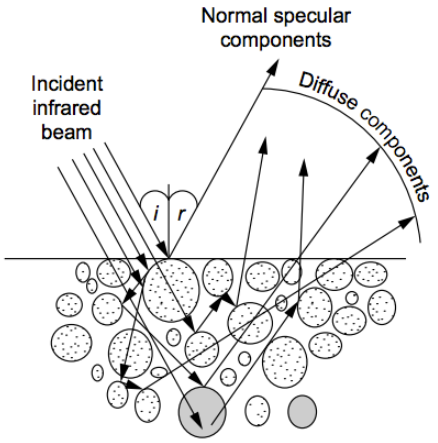

Figure 1-8 Mechanisms generating the infrared spectrum of a powdered sample. Figure from Armaroli *et al*.[172]

The DRIFTS technique exploits the fact that the diffuse component of a reflected infrared beam has penetrated particles in the sample and thus contains information regarding the sample's absorption properties in the IR region (see Figure 1-8).[172] Unlike transmission spectra, however, which display a linear correlation between the measured signal and the concentration of the absorbing species, the appearance of DRIFTS spectra is also influenced by particle packing density, refractive index, and particle dimensions.[172] Since all of these properties vary from sample to sample especially in the case of real environmental samples, which are particularly

heterogeneous the DRIFTS technique is not ideally suited for quantitative analysis.[172] However, keeping in mind these limitations, quantitative data can be extracted from DRIFTS spectra by applying the Kubelka-Munk equation (see Armaroli *et al.* for a full explanation of this process), which provides spectra similar to those obtained in transmission-mode infrared spectroscopy.[172]

In a typical DRIFTS experiment, a mineral dust sample is exposed to the gas-phase species of interest while changes in its surface composition are monitored as a function of time. Uptake coefficients for product formation can then be determined using the following equation:[173]

$$\gamma = \frac{d[P]}{dt\, Z}$$

Here, $[P]$ represents the concentration of product at the mineral surface and Z represents the product of the concentration of gas-phase species and the collision frequency.[173] Since DRIFTS spectra are not inherently quantitative, the surface concentration of products must be determined by calibration against absolute techniques: in their study of N_2O_5 uptake by Saharan dust, for example, Seisel and coworkers calibrated nitrate absorbance bands by extracting and analyzing samples using ion chromatography.[170]

One of the main advantages of the DRIFTS technique is that it provides direct, *in situ* information regarding the speciation and binding environment of surface-sorbed products information that is generally inaccessible from gas-phase uptake measurements. It has been used, for example, to probe the ozone-initiated oxidation of sulfite to sulfate on the surface of $CaCO_3$.[174]

Another technique for monitoring changes in concentration of surface-sorbed species is glancing-angle laser-induced fluorescence. This technique, which was developed in our laboratory, has been used to study a wide variety of atmospherically relevant

reactions, including the ozonation of anthracene[127] and chlorophyll[175] at the air aqueous interface and a number of PAH at the surface of organic films.[124] In addition, the experiments described in Chapter 2, which investigated the interaction of ozone with pyrene at a number of proxies for atmospheric surfaces, were performed using this technique.[121]

A schematic of a laser-induced fluorescence apparatus, here used to investigate the reaction of ozone with pyrene solid films,[133] is shown in Figure 1-9.

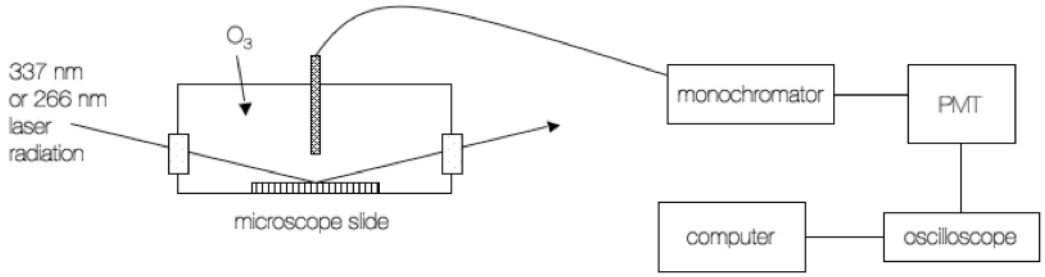

Figure 1-9 Laser-induced fluorescence apparatus for the investigation of the interaction of ozone with pyrene solid films.

In this experimental technique, the excitation laser is aligned such that it impinges the reaction surface at a glancing angle. Fluorescence thus excited is collected by a liquid light guide, passed through a monochromator, and detected by a photomultiplier tube (PMT). The PMT output is sent to a digital oscilloscope, and the resultant fluorescence curve is read and stored for later analysis. During reactions, the loss in fluorescence intensity of the surface-sorbed species is measured as a function of time; then, an exponential fit to the loss curve yields a pseudo-first-order reaction rate k_{obs}.

One major advantage of this technique is that it allows for reactions to be followed *in situ*, thereby eliminating the need for time-consuming extraction and quantification

steps.[176] In addition, because it is a surface-sensitive technique, it provides information about the reactivity of the uppermost surface-sorbed molecules without interference from molecules present in underlying sample layers and subject to burial-induced reductions in apparent reactivity (see work by Zhou and coworkers[177]).

At first glance, an obvious disadvantage of this technique is that it requires the molecules under study to be fluorescent. However, with some creativity, additional systems can be studied: Clifford *et al.*, for example, studied the kinetics of the reaction of ozone with bromide at the air aqueous interface by monitoring pH changes associated with the reaction using a surface-sensitive fluorescent pH probe.[178]

1.3.3 Challenges and considerations in translating laboratory measurements to the "real world"

1.3.3.1 Choosing representative laboratory models

The bulk of laboratory experiments investigating mineral dust reactivity have been performed using individual dust components (*e.g.* metal oxides, clays, and carbonates) and/or standard reference dust (*e.g.* Arizona test dust). Fewer experiments have been conducted using "real" environmental samples depositional dust and source soils, for example. In this section, the benefits and disadvantages associated with the use of model and environmentally sourced samples will be discussed.

Experiments performed using model substrates are useful in part because they allow for the comparison of values and (associated uncertainties) obtained using different experimental techniques and, by extension, a metric by which to assess the strengths and limitations of each technique. Together, experiments performed using identical substrates provide large datasets, which are useful in assessing uncertainties in reported values (see *e.g.* the recent compilation of evaluated heterogeneous kinetic data by Crowley and coworkers[130]) and against which new techniques can be validated.

In addition, study of simple, well-characterized systems permits a mechanistic, molecular-level understanding of individual reactions and processes an understanding that may be obscured in more complex, variable systems, where observed results may represent the vector sum of a number of unknown elementary processes. For example, while it is obviously useful to measure the ozone uptake coefficient of real depositional dust samples, it is impossible to infer the behaviour of one desert dust sample from that of another without understanding which components of dust drive its reactivity (see Chen *et al.*[161] for an illustration of mineral-dependent ozone reactivity) and where in the real sample these 'active' components are located.

Of course, model systems are not without limitations even the simple act of choosing a model system requires one to make value judgments regarding the model systems worth studying. An excellent example of the pitfalls associated with this sort of assumption-making is provided by the ice nucleation community, which studied extensively the IN properties of clay minerals, including montmorillonite a valid choice, given their prevalence in advected dust samples only to find that the much less abundant (and much less abundantly studied) feldspar minerals contribute disproportionately to dust's IN activity.[58, 59]

A successful model study not only requires a researcher to fully understand the model system but also requires her to develop a "transfer function" between results observed on model surfaces and results observed in the real environment. While this is certainly not an easy task, it often receives much less attention than is warranted. As an example, consider that the bulk of studies exploring the iron mediation of ozone chemistry at the mineral dust surface have been conducted using α-Fe_2O_3, or hematite[164, 179] this, despite the fact that iron in dust is present not only as pure iron oxide but also as oxyhydroxides (*e.g.* goethite) and in association with aluminosilicate clays.[21, 180] The implicit, and largely unexamined, assumption in these laboratory studies is that an understanding of the behaviour of ozone in the presence of iron-

containing dust can be directly gleaned from an understanding of its behaviour in the presence of hematite.

As outlined in the preceding sections, the physicochemical properties of mineral dust change during transport. When performing experiments using depositional dust samples, therefore, it is difficult to know whether observed reactivity (or lack of reactivity) arises from inherent dust characteristics or from characteristics imparted during atmospheric processing. Indeed, a number of studies have found that the reactivity of mineral dust changes significantly during simulated processing: for example, a study by Usher and coworkers found that the reactivity of Al_2O_3 particles toward ozone decreased when the particles were pre-treated with HNO_3, which blocked adsorptive sites, but increased when they were pre-treated with SO_2, which produced sulfite and/or bisulfate species capable of reaction with ozone[181] In addition, a very recent study by Zhao and coworkers showed that the uptake of H_2O_2 by $CaCO_3$ particles displayed a complex dependence upon relative humidity and prior exposure to SO_2 and HNO_3 (although exposure to SO_2 universally enhanced H_2O_2 uptake, again via formation of reactive surface sulfite).[182]

One simple way of avoiding the uncertainties associated with this "unknown" processing is to use the smallest – and thus most subject to long-range transport – size fraction of sand/soil material obtained from dust source regions. To date, however, this technique has seen little experimental application: while several studies have investigated chemistry and photochemistry on finely ground source sands,[101, 142, 150, 183] the as-yet unpublished work presented in Chapter 6 of this thesis represents the first experimental investigation of photochemistry at the surface of (roughly) size-selected source material. A further improvement on this strategy, which is also presented in Chapter 6, involves the use of dust generated in the laboratory from source samples in a manner that reflects dust generation processes in the real atmosphere.

The issues discussed in this section are by no means restricted to the study of mineral dust: another illustration of challenges associated with the use of laboratory models for complex systems is provided by Chapter 2 of this thesis, which focuses on the heterogeneous photochemical oxidation of pyrene, a model polycyclic aromatic hydrocarbon (PAH), at the surface of a variety of proxies for soot and "urban grime".

1.3.3.2 Defining available surface areas

Knudsen cells have been used to quantify uptake of atmospheric trace gases by a variety of liquid and powdered surfaces, including soot,[184] mineral dust,[185] organic films,[186] and cold sulfuric acid.[187] As outlined in Section 1.3.2.1, uptake coefficients can be determined using the following equation, where A_0 is the geometric areas of the exit orifice, I_0 is the mass spectral signal obtained with the sample holder closed, and I is the signal obtained with the sample open:[118]

$$\gamma = \frac{A_0}{A_s}\left(\frac{I-I_0}{I_0}\right)$$

A major challenge associated with use of this equation is the fact that determination of environmentally relevant uptake coefficients requires researchers to decide how to represent the surface area of sample, A_S, accessed by each gas-phase molecule over the time-scale of uptake experiments.

In the case of liquids, which present a clearly defined surface area for uptake, A_S can be defined as the geometric area of the sample holder.[186, 187] In the case of powdered samples, however, the situation is less trivial. Use of the geometric surface area implies the assumption that each gas-phase molecule collides only once with the solid-phase surface.[185] However, as shown in Figure 1-10, gas-phase molecules may also diffuse into underlying layers, which can also contribute to observed uptake – if so, uptake coefficients determined using only the geometric surface area of the sample will be significant overestimates.[185]

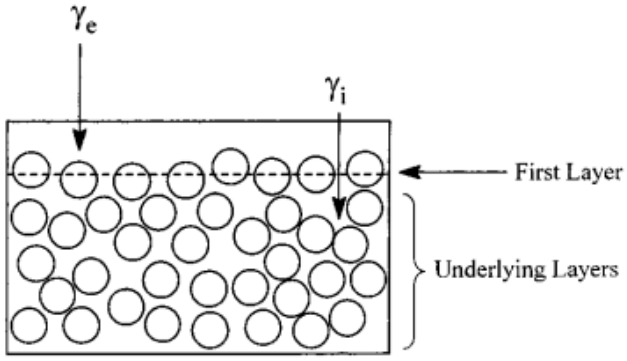

Figure 1-10 In powdered samples, both external (γ_e) and internal (γ_i) sample layers can contribute to observed uptake coefficients. Reprinted (adapted) with permission from Underwood *et al.* Determining accurate kinetic parameters of potentially important heterogeneous atmospheric reactions on solid particle surfaces with a Knudsen cell reactor. *J. Phys. Chem. A* **2000**, *104*, (4), 819–829.[185] Copyright 2000 American Chemical Society.

Although a comprehensive solution to this issue has been developed (the 'KML' model[188]), it requires knowledge of the diffusion constant of the gas of interest through the powdered sample, which is difficult to measure and which varies as a function of both substrate identity and sample packing.[185]

In 2000, Underwood and coworkers suggested a simpler approach, which involves the measurement of uptake coefficients at sample masses small enough to allow the gas-phase probe molecules to access the entire sample via diffusion over the time-scale of the uptake experiment.[185] In this linear mass-dependent (LMD) regime, the sample surface area available for reaction is simply its total Brunauer Emmett Teller (BET) surface area.[185] At elevated sample masses, gas-phase molecules may not be able to access the entire sample over the time-scale of the uptake experiment. In this 'plateau' regime, additional sample mass will not lead to a change in the apparent measured uptake coefficient. An illustration of the LMD and plateau regimes is provided in Figure 1-11 for the uptake of gas-phase NO_2 by Fe_2O_3 powder.[185]

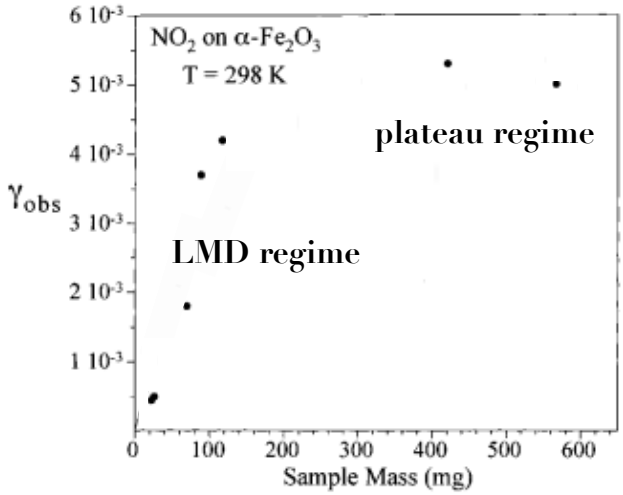

Figure 1-11 Illustration of the linear mass-dependent (LMD) and plateau regimes for the uptake of NO_2 by Fe_2O_3. Reprinted (adapted) with permission from Underwood *et al.* Determining accurate kinetic parameters of potentially important heterogeneous atmospheric reactions on solid particle surfaces with a Knudsen cell reactor. *J. Phys. Chem. A* **2000**, *104*, (4), 819–829.[185] Copyright 2000 American Chemical Society.

It should be noted that the scaling of uptake coefficients by the total external and internal sample area (*i.e.* the BET surface area, which is typically determined using N_2) may not always be appropriate. For example, BET-scaled uptake coefficients may be underestimates for larger adsorbate molecules, which may not be able to access all adsorptive sites accessible to N_2.[185] In addition, studies investigating the uptake of HNO_3 and N_2O_5 by mineral dust, for example, have provided evidence that the use of the geometric sample surface area may be more appropriate.[138, 144] As noted by Kolb and coworkers,[134] this is an area deserving of future study; at present, it seems prudent to regard BET-scaled and geometric uptake coefficients determined in laboratory experiments as lower and upper limits, respectively, to uptake coefficients in the real environment.

1.3.3.3 Effects of surface-sorbed water

Adsorption of water by mineral surfaces is efficient: for a variety of metal oxides, including Fe_2O_3, TiO_2, Al_2O_3, and MgO, monolayer water coverage is achieved at

relative humidities ranging from 24 30%.[189] The same is true at the surface of model dusts: using thermogravimetric analysis (TGA) for the study of water adsorption on Arizona test dust, Gustafsson and coworkers were able to show that monolayer coverage occurred at a relative humidity of approximately 10%.[190] The water uptake behaviour of China loess and Saharan sand is similar to that of single-component clays, which suggests that the water uptake capacity of dust is dominated by its clay fraction.[191, 192] This adsorbed water plays a significant and complex role in chemistry and photochemistry at atmospheric surfaces.[193]

In some cases, gas-phase water competes with inorganic and organic adsorbates for available surface sites: this effect, which manifests as a reduction in uptake of gas-phase species at elevated relative humidities, has been observed for ozone uptake by soot,[128] Fe_2O_3 and Al_2O_3 aerosols,[164] and solid pyrene films;[133] hydrogen peroxide uptake on calcium carbonate particles;[182] and HO_2 uptake by Arizona test dust.[194] By contrast, surface-sorbed water promotes the uptake of some soluble species: the uptake of gas-phase nitric acid on oxide particles[195] and Arizona test dust,[152] for example, is enhanced at high relative humidities. This effect has been attributed to solvation of nitrate anion by the water layer present at the dust surface.[195]

At the surface of illuminated semiconductor-containing dusts (see Section 1.4.2.3), adsorbed water can also promote uptake of gas-phase species by acting as a source of reactive hydroxyl radical (•OH).[196] This effect has been observed for the uptake of formaldehyde[151] and ammonia[197] by illuminated TiO_2 surfaces, which both increase with increasing relative humidity.

Although mineral dust is primarily emitted in arid regions, advected dust is subjected to a variety of humidity regimes during its long-range transport. In order to capture the full range of potential chemistry and photochemistry at the dust surface, therefore, it is important that laboratory experiments be conducted in the presence of surface-sorbed water. While it is possible to perform flow tube and chamber experiments at

elevated relative humidities, the same is not true for Knudsen cells, which by necessity (see Section 1.3.2.4) are operated at low pressures and therefore in the absence of gas-phase water.

The inability to perform experiments in the presence of gas-phase water is not as much an experimental liability as it might first seem, however, since the absence of gas-phase water does not preclude the presence of surface-sorbed water: in an ATR-FTIR study of water uptake by Chinese and Saharan dust, Navea and coworkers[191] observed absorbance from hydroxyl groups even after overnight evacuation at <5% RH; in the case of Chinese dust, absorbance from molecular water was even present. These authors attributed this hysteresis in water removal to the strong adsorptive capacity of swelling clay minerals present within the dust.[191]

The participation of strongly sorbed water has been invoked to explain unexpectedly weak RH dependences in the uptake of ozone by Al_2O_3[198] and the uptake of N_2O_5 by Saharan dust deposited in the Cape Verde islands.[144] The latter observation is especially striking, since it implies that the clay fraction of Saharan dust contains sufficient water to catalyze the heterogeneous hydrolysis of N_2O_5, independent of local RH conditions.

1.4 Influence of light upon reactions at atmospheric surfaces

Until very recently, the vast majority of laboratory experiments investigating the interaction of trace gases with solid surfaces were performed under dark conditions. The 2010 IUPAC evaluation of heterogeneous reactions on solid surfaces, for example, presents only one instance the interaction of NO_2 with mineral dust in which uptake coefficients were determined under both light and dark conditions.[130]

In their 2010 review of the state of knowledge regarding heterogeneous uptake of trace gases by atmospheric surfaces, Kolb and coworkers explicitly outlined the need for an improved understanding of heterogeneous photochemistry, including that promoted by light-absorbing species contained within mineral dust, soot, and organic aerosol.[134] The following sections aim to provide an overview of current knowledge regarding both direct and substrate-promoted (*i.e.* indirect, or 'photosensitized') photochemistry occurring at atmospheric surfaces.

1.4.1 Direct photochemistry on atmospheric surfaces

Atmospherically processed mineral dust contains a number of surface-sorbed chromophores, including nitrate and polycyclic aromatic hydrocarbons (PAH),[43, 84] which can undergo direct photochemistry at the particle surface. The heterogeneous photochemistry of these light-absorbing species has been the subject of much research study (see *e.g.* representative work from the laboratories of Dabestani[199] and Grassian[200]). Several broad-picture insights from these investigations will be outlined briefly here.

First, the light-induced chemistry of adsorbed species may occur more efficiently than the corresponding chemistry in the gas phase. For example, the photolysis of HNO_3 at the surface of Pyrex glass proceeds ~ 2 orders of magnitude more quickly than in the gas phase or in aqueous solution.[201] This observation has been attributed to an enhancement in the absorption cross section of surface-sorbed HNO_3 over that observed in the gas phase.[202]

Second, the photochemistry of adsorbed species is substrate-dependent: the photolysis of PAH at the surface of fly ash and carbon black, for example, proceeds much more slowly than at the surface of silica and alumina.[203, 204] This suppression has been attributed to the competitive absorption of incoming radiation by the colored fly ash substrate and/or to the efficient non-reactive quenching of PAH excited states by

transition metal ions present at the fly ash surface.[204] The products of photolytic processes may also display a substrate dependence: at the Al_2O_3 surface, adsorbed nitrite produced from nitrate photolysis undergoes rapid secondary photolysis to yield gas-phase NO;[200] in porous aluminosilicates, by contrast, photochemically produced nitrite is stabilized against further reaction.[205]

Finally, and perhaps most importantly, the direct photochemistry of adsorbed species has the potential to alter the composition of the surrounding atmosphere. For example, the photolysis of adsorbed nitrate at the surface of Al_2O_3, which has been used as a surrogate for mineral dust, leads to the production of gas-phase NO, NO_2, and N_2O.[162, 200, 206] These results suggest that mineral dust is best considered a temporary reservoir rather than a permanent sink of NO_x.

1.4.2 Photosensitized chemistry: mechanisms and substrates

Many atmospheric surfaces absorb incoming solar radiation, and may thereafter promote, or 'photosensitize', reactions of photochemically inactive adsorbates. In the following sections, the primary mechanisms via which atmospheric surfaces can promote photochemical reactions of adsorbed species will be discussed in the context of results from recent laboratory experiments. A summary of outstanding questions in the field will not be presented in this section but rather will be used in Section 1.5 to provide context for the thesis work.

According to one conceptual model, which is illustrated in Scheme 1-1, there are two primary photosensitization mechanisms available to excited-state sensitizers. In Type I photosensitization, the excited sensitizer undergoes a charge-transfer reaction – either with an adsorbed gas-phase reagent or with another aerosol-phase species – to yield radicals or radical ions, which ultimately results in the formation of oxidized products.[207] In Type II photosensitization, the excited sensitizer transfers its energy to oxygen, which results in the formation of singlet oxygen and returns the sensitizer to

its ground state. The singlet oxygen thus formed is then available for reaction with the substrate itself or with other aerosol-phase species.[207]

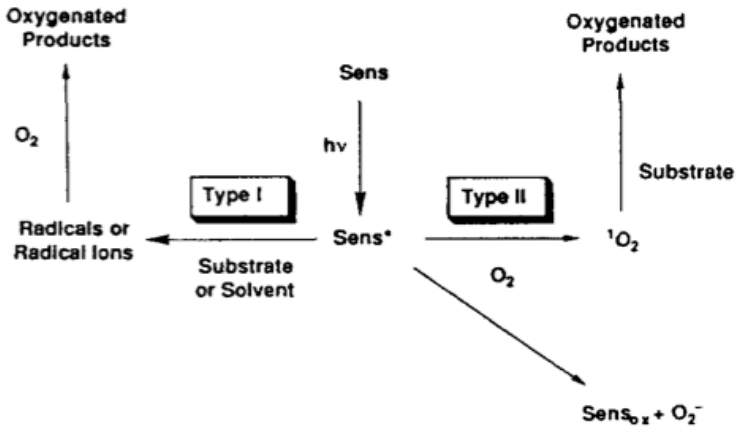

Scheme 1-1 Type I and Type II photosensitization. Reprinted with permission from Foote (1991).[207]

The following sections will outline recent developments in the study of substrate-mediated photochemistry. The first two sections will focus on Type II and Type I photosensitization, respectively. The last will focus on semiconductor-mediated photochemistry, which does not fit into the conceptual model described above but nonetheless represents a potentially important atmospheric reactive pathway.

1.4.2.1 Type II photosensitization: energy transfer

Elevated ozone uptake coefficients in the presence of light have been observed for a number of photoactive solid surfaces, including pyrene,[133] benzophenone,[208] laboratory-generated soot,[120] and components of biomass burning aerosol.[209]

As illustrated in Scheme 1-2, this photoenhancement is believed to proceed in some cases via a Type II mechanism,[207] in which the quenching of the excited-state substrate

leads to the formation of the second electronically excited state of oxygen, $O_2(^1\sum_g^+)$, which in turn reacts with adsorbed ozone.[133, 208]

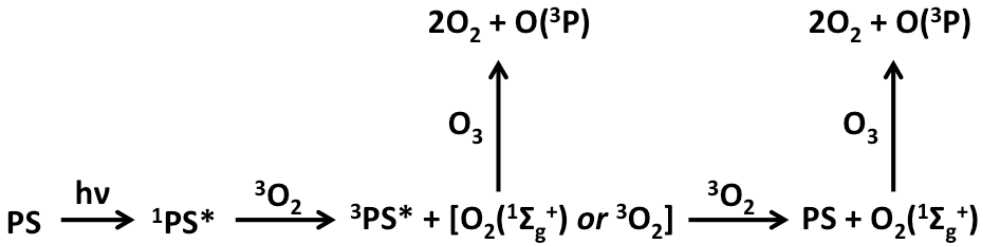

Scheme 1-2 Energy-transfer reaction pathways available to a generic photoactive substrate (PS) in the presence of O_3.

Singlet oxygen formation has also been implicated in the uptake of the biogenic volatile organic compounds limonene and isoprene by illuminated seed aerosols containing humic acid,[210] a well-known singlet oxygen source in aqueous solution.[211]

Singlet oxygen-mediated processes in atmospheric particulate matter need not involve the participation of additional gas-phase adsorbates: for example, studies have shown that singlet oxygen produced from the illumination of a wide variety of surface-sorbed PAH can in some cases react with the PAH itself to produce oxidized products.[212]

1.4.2.2 Type I photosensitization: charge transfer

In a pioneering set of papers, the research group of Christian George reported the photoenhanced uptake of NO_2 and concurrent production of HONO at the surface of humic acid and other model compounds used as laboratory proxies for the organic component of tropospheric aerosol.[213-215] Since this time, light-enhanced uptake of NO_2 has also been observed for a number of additional substrates, including pyrene,[216] soot,[217] and proxies for atmospheric polyphenolic compounds.[218]

As shown in Scheme 1-3, this photoenhancement is believed to proceed via a Type I mechanism,[207] in which a charge-transfer complex is formed between adsorbed NO_2 and the excited substrate. In this photosensitization mechanism, excited-state substrate molecules ultimately act as electron donors, thereby reducing NO_2 to nitrite anion, which can subsequently be protonated and released into the gas phase.[207, 216, 217]

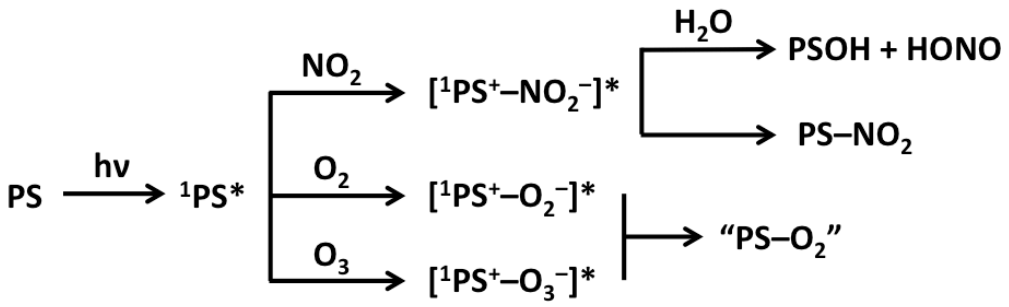

Scheme 1-3 Charge-transfer reaction pathways available to a generic photoactive substrate (PS) in the presence of NO_2, O_2, or O_3. PS–NO_2 and "PS–O_2" denote nitro- and oxygenated products, respectively.

The interaction of excited substrates with NO_2 has also been shown to result in the formation of nitrated products, some of which can subsequently photolyze to yield additional HONO.[219] Indirect evidence for the yield of these nitrated products is provided by experiments performed at the pyrene surface, which found that only ~ 50% of NO_2 loss in the presence of light could be accounted for by the production of gas-phase nitrogen oxides (NO and HONO).[216]

As outlined in the previous section, the photoenhanced uptake of ozone by a variety of substrates is believed to occur via a singlet oxygen-mediated mechanism, which from the perspective of the substrate itself can be viewed as a purely photophysical (*i.e.* non-destructive) process. In some cases, however, the ozone-induced reaction of the substrate *itself* is also accelerated in the presence of light: the ozone-induced losses of solid

pyrene films,[133] silica-sorbed veratraldehyde,[220] and 3,4,5-trimethoxybenzaldehyde,[221] for example, all proceed more quickly with illumination. This accelerated reactivity, which has been attributed to the formation and subsequent degradation of charge-transfer complexes between the substrate and adsorbed ozone,[133] is discussed in more detail in Chapter 2.

In some cases, the photoenhanced loss of ozone at the surface of organic films can also occur via a charge-transfer pathway.[175, 222, 223] The light-enhanced uptake of ozone by humic acid films, for example, which occurs more rapidly at higher pH, is believed to occur via an electron transfer from photoexcited phenolate moieties to adsorbed ozone.[222]

As was the case for energy-transfer processes, charge-transfer reactions can also occur between condensed-phase species without the participation of gas-phase adsorbates. For example, the photosensitized oxidation of sea-salt halides by benzophenone is believed to occur via reactive quenching of the benzophenone triplet state,[224] and the first step in the formation of oligomeric products from illuminated solutions of phenol in the presence of the photosensitizer anthraquinone-2-sulfonate (AQ2S) is believed to be the oxidation of phenol by the AQ2S triplet state.[225]

The formation of charge-transfer complexes is not specific to organic substrates: for example, the photoinduced dissolution of Fe_2O_3 in the presence of oxalic acid is believed to occur via a ligand-to-metal charge-transfer complex, which decomposes to yield dissolved Fe(II).[100] This mechanism will be described in more detail in Chapter 5, which focuses on the photochemistry of oxalic acid in the presence of Fe_2O_3 and iron-containing sand and ash.

1.4.2.3 Semiconductor-mediated photochemistry

As noted in Section 1.1, mineral dust contains substantial quantities of Fe_2O_3 and TiO_2, both of which are semiconductors and thus would be expected to promote the

photochemical processing of adsorbed species.[8] Although the bulk of research in TiO_2 photocatalysis has been conducted in the context of air and water purification,[226-228] a number of recent studies have investigated its participation in photochemical processes of atmospheric significance. Specifically, TiO_2 has been shown to promote the photooxidation of adsorbed nitrate,[229] sulfite,[230] and ammonia[197] and the photoenhanced uptake of NO_2,[143] formaldehyde,[151] and O_3.[161]

Figure 1-12 provides a mechanistic summary of the photoinduced processes that can occur at the TiO_2 surface. As illustrated in this diagram, illumination of TiO_2 results in the formation of electron hole pairs. The holes thus formed can oxidize adsorbed species directly or can react with adsorbed water to form hydroxyl radical, which can in turn serve as a surficial oxidant.[161, 231] The photoproduced electrons can react with adsorbed oxygen, which results in the formation of reactive superoxide radical ($O_2^{\bullet}$), or directly reduce adsorbed species.[231]

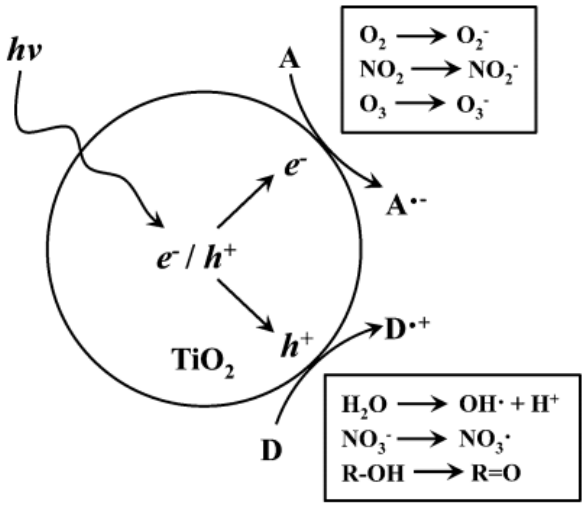

Figure 1-12 Photoredox processes at the surface of illuminated TiO_2. The formation of electron–hole pairs can result in the reduction of electron acceptors (A) by photogenerated electrons and the oxidation of electron donors (D) by photogenerated holes. Image reprinted (adapted) with permission from Chen *et al.* Titanium dioxide photocatalysis in atmospheric chemistry. *Chem. Rev*. **2012**, 112, (11), 5919–5948.[232] Copyright 2012 American Chemical Society.

Although fewer studies have investigated the role that Fe_2O_3 may play in atmospheric photochemistry, laboratory work has shown that it can catalyze the aqueous photooxidation of pyrene, [233]sulfur dioxide,[234] oxalic acid,[235] phenol,[236] and chlorinated phenols.[237] The photochemistry of organic compounds at the surface of Fe_2O_3 is explored further in Chapters 4 and 5.

A small number of field and laboratory studies have explored inorganic photochemistry at the surface of authentic mineral dust samples, including that of surface-sorbed nitrate[238] and gas-phase NO_2.[150, 239] Fewer studies still have focused on the photochemistry of organic species at the surface of mineral dust and other photoactive substrates. The current state of knowledge in this area will be summarized in the next section.

1.5 Introduction to the thesis work

1.5.1 Current knowledge and outstanding questions

Despite the best efforts of a small group of (primarily laboratory) researchers, a fully comprehensive understanding of heterogeneous atmospheric photochemistry at the surface of dust and other photoactive substrates remains elusive. As demonstrated by the illustrative work presented in the previous section, the vast majority of publications in this nascent field have focused on the heterogeneous photochemistry of inorganic pollutants much less is currently known regarding the heterogeneous photochemistry of gas-phase organic species typical of urban environments.

Investigations of substrate-catalyzed organic photochemistry are scattered throughout the catalytic, agricultural, and environmental literature, however, and this section represents an attempt to concisely summarize the current state of knowledge in this field. Since an excellent atmospherically focused review of current knowledge in the field of TiO_2-catalyzed organic photochemistry was published recently by Chen and

coworkers,[232] this section will focus on organic photochemistry at the surface of authentic environmental samples.

In a 1978 paper, Pierotti and coworkers reported modest but significant reductions in gas-phase concentrations of CCl_4 and CH_3CCl_3 over the Sahara in the presence of dust.[240] Laboratory studies have since found that the photochemistry of CH_3CCl_3 on aluminosilicate clays,[241] fluorochloromethanes with desert sand,[242] and CCl_3F on soil and fly ash[243] can be a sink for these species, which are otherwise considered largely recalcitrant under tropospheric conditions. A full understanding of CH_3CCl_3 loss pathways is especially important because the slow atmospheric decay of this species since its restriction under the Montreal Protocol, which has been assumed to proceed primarily via reaction with OH, has been used extensively to infer global OH concentrations.[244]

A small number of studies have investigated the photocatalytic activity of coal fly ash. While some studies have found that it promotes the photodegradation of adsorbed PAH,[245, 246] others have found that it stabilizes adsorbed PAH against photooxidation.[247, 248] Fly ash has also been shown to promote the photooxidation of adsorbed ethanol and methyl-tert-butyl-ether (MTBE).[249]

In an effort to understand the post-application behaviour of pesticides, a large number of studies have investigated their photolysis at the surface of clay minerals and whole soils.[250-254] These studies have shown that pesticide degradation can mediated by hydroxyl radical[253] and/or singlet oxygen[251] produced at the illuminated surface of clays and soils. There is no question that this large body of work (see *e.g.* a substantial 2004 review article by Katagi[250]) has the potential to provide useful mechanistic insights to researchers studying photochemical processes catalyzed by terrigenous aerosol.

As alluded to above, illumination of environmental surfaces may lead to the production of reactive radicals. More focused mechanistic studies have shown that the illumination of soil surfaces[255] and perhaps surprisingly non-transition-metal oxides[256] leads to the production of singlet oxygen; that hydroxyl radical is produced by Fe_2O_3,[257] montmorillonite,[258] and other clays[259] in illuminated aqueous solutions; and that H_2O_2 is produced in suspensions of desert sand.[260]

Together, these results suggest that a multitude of mechanisms exist by which mineral dust and other photoactive surfaces could influence the fate of semi-volatile organic species in polluted environments. A comprehensive understanding of these mechanisms is lacking, however: prior to the work presented in this thesis, the only direct experimental evidence of dust-mediated chemistry of organic pollutants came from a single study, which measured the photooxidation of toluene at the surface of volcanic ash and desert sand.[261] As will be outlined in the following section, the primary goal of this thesis is to improve our understanding of the photochemical interactions of urban pollutants with photoactive surfaces.

1.5.2 Thesis outline and goals

Significant uncertainties remain regarding the role that photochemical reactions occurring on dust and other photoactive surfaces may play in influencing the concentration and lifetime of gas-phase pollutants in urban environments. In order to address these uncertainties, this thesis explores the photochemical reactivity of these environmental surfaces in controlled laboratory settings. The body of this thesis is organized into five chapters, each of which explores a different aspect of atmospheric heterogeneous photochemistry.

Chapter 2 reports the results of an investigation of the effect of light upon the reaction of ozone with pyrene, a carcinogenic product of incomplete combustion present on the surface of soot and "urban grime". These experiments, which were performed on

three model surfaces designed to mimic the range of reactive environments available to pyrene under real atmospheric conditions, aimed to answer the following main questions:

- Does the reaction of ozone with pyrene display a light enhancement?
- Does the photochemical behaviour of pyrene depend on the chemical characteristics of the environment in which it is located?

Chapter 3 focuses on the photochemistry of atmospherically relevant alcohols at the surface of TiO_2, which was employed as a simple laboratory proxy for the photoactive component of mineral dust. The first main goal of this project was to develop a new technique, the photochemical Knudsen cell reactor, for the study of heterogeneous atmospheric photochemistry. The work presented in this chapter, which was conducted using this custom-built apparatus, aimed to answer the following specific questions:

- Does the photooxidation of alcohols occur efficiently at the TiO_2 surface?
- What are the gas-phase products of alcohol photooxidation?
- How does the presence of nitrate influence alcohol photochemistry at the TiO_2 surface?

Chapter 4 focuses on the photochemistry of oxalic acid, the most atmospherically abundant dicarboxylic acid, at the surface of Mauritanian sand and Icelandic volcanic ash. The overall goal of this work, which is one of the first studies of organic photochemistry at the surface of real environmental samples, was to discover whether mineral dust-catalyzed photochemistry could serve as an additional sink for this species under arid conditions. Specifically, this project used simultaneous gas- and surface-phase measurements to answer the following questions:

- Does mineral dust catalyze the photooxidation of surface-sorbed oxalic acid?
- Is this photooxidation mediated by Fe and Ti present in the dust?

Chapter 5 presents an exploration of the dust- and ash-mediated photochemistry of fluorotelomer alcohols (FTOHs), a class of chemicals used in the production of water- and oil-repelling surface coatings. This project, which was performed using a variety of gas- and surface-phase analytical techniques, aimed to answer the following questions:

- Do FTOHs partition to atmospheric surfaces?
- What are the gas- and particulate-phase products of FTOH photooxidation?
- Does FTOH photooxidation produce surface-sorbed perfluorinated carboxylic acids (PFCAs; a toxic, recalcitrant, and bioaccumulative class of chemicals)?

Chapter 6 moves away from dust-catalyzed organic chemistry; instead, it focuses on the light-mediated interactions of SO_2 with sand samples from Niger and China. This project, which was performed in part in the CESAM atmospheric chamber at the Université Paris Est Créteil, attempted to answer the following questions:

- Does illuminated desert sand catalyze the production of surface-sorbed sulfate in the presence of gas-phase SO_2?
- How does the efficiency of this process depend on sand particle size (and, thus, composition)?
- Does the interaction of SO_2 with illuminated dust result in new particle formation?

The results obtained in these studies provide insight into the behaviour of a wide variety of urban pollutants sorbed to photoactive surfaces. Overall, this thesis represents a first step toward an assessment of the absolute importance of the surface-catalyzed photochemistry in determining the atmospheric lifetime and ultimate fate of these pollutants. The concluding chapter, Chapter 7, provides a summary not only of the experiments conducted as part of this thesis but also of the broader health and climate implications of photochemical processes catalyzed by atmospheric surfaces, and, finally, outlines a set of recommendations for future work in this field.

1.6 References

1. Tegen, I.; Schepanski, K.; Heinold, B., Comparing two years of Saharan dust source activation obtained by regional modelling and satellite observations. *Atmos. Chem. Phys.* **2013,** *13*, (5), 2381 2390.

2. Tanaka, T. Y.; Chiba, M., A numerical study of the contributions of dust source regions to the global dust budget. *Global Planet. Change* **2006,** *52*, (1 4), 88 104.

3. Shao, Y.; Wyrwoll, K.-H.; Chappell, A.; Huang, J.; Lin, Z.; McTainsh, G. H.; Mikami, M.; Tanaka, T. Y.; Wang, X.; Yoon, S., Dust cycle: an emerging core theme in Earth system science. *Aeolian Res.* **2011,** *2*, (4), 181 204.

4. Prospero, J. M., Long-term measurements of the transport of African mineral dust to the southeastern United States: implications for regional air quality. *J. Geophys. Res.–Atmos.* **1999,** *104*, (D13), 15917 15927, doi:10.1029/1999JD900072.

5. Lee, Y. C.; Yang, X.; Wenig, M., Transport of dusts from East Asian and non-East Asian sources to Hong Kong during dust storm related events 1996 2007. *Atmos. Environ.* **2010,** *44*, (30), 3728 3738.

6. Caggiano, R.; Fiore, S.; Lettino, A.; Macchiato, M.; Sabia, S.; Trippetta, S., $PM_{2.5}$ measurements in a Mediterranean site: Two typical cases. *Atmos. Res.* **2011,** *102*, (1 2), 157 166.

7. Fairlie, T. D.; Jacob, D. J.; Park, R. J., The impact of transpacific transport of mineral dust in the United States. *Atmos. Environ.* **2007,** *41*, (6), 1251 1266.

8. Goudie, A. S.; Middleton, N. J., Saharan dust storms: nature and consequences. *Earth Sci. Rev.* **2001,** *56*, (1 4), 179 204.

9. Sokolik, I. N.; Toon, O. B., Incorporation of mineralogical composition into models of the radiative properties of mineral aerosol from UV to IR wavelengths. *J. Geophys. Res.–Atmos.* **1999,** *104*, (D8), 9423 9444.

10. Caquineau, S.; Gaudichet, A.; Gomes, L.; Magonthier, M. C.; Chatenet, B., Saharan dust: clay ratio as a relevant tracer to assess the origin of soil-derived aerosols. *Geophys. Res. Lett.* **1998,** *25*, (7), 983 986.

11. Scheuvens, D.; Schutz, L.; Kandler, K.; Ebert, M.; Weinbruch, S., Bulk composition of northern African dust and its source sediments: a compilation. *Earth Sci. Rev.* **2013,** *116*, 170 194.

12. Maring, H.; Savoie, D. L.; Izaguirre, M. A.; Custals, L.; Reid, J. S., Mineral dust aerosol size distribution change during atmospheric transport. *J. Geophys. Res.–Atmos.* **2003,** *108*, (D19).

13. Mori, I.; Nishikawa, M.; Tanimura, T.; Quan, H., Change in size distribution and chemical composition of kosa (Asian dust) aerosol during long-range transport. *Atmos. Environ.* **2003,** *37*, (30), 4253 4263.

14. Glaccum, R. A.; Prospero, J. M., Saharan aerosols over the tropical North Atlantic: mineralogy. *Mar. Geol.* **1980,** *37*, (3 4), 295 321.

15. Arnold, E.; Merrill, J.; Leinen, M.; King, J., The effect of source area and atmospheric transport on mineral aerosol collected over the North Pacific Ocean. *Global Planet. Change* **1998,** *18*, (3 4), 137 159.

16. Castillo, S.; Moreno, T.; Querol, X.; Alastuey, A.; Cuevas, E.; Herrmann, L.; Mounkaila, M.; Gibbons, W., Trace element variation in size-fractionated African desert dusts. *J. Arid Environ.* **2008,** *72*, (6), 1034 1045.

17. Jeong, G. Y., Bulk and single-particle mineralogy of Asian dust and a comparison with its source soils. *J. Geophys. Res.–Atmos.* **2008,** *113*, (D2).

18. Scheuvens, D.; Kandler, K.; Kupper, M.; Lieke, K.; Zorn, S. R.; Ebert, M.; Schutz, L.; Weinbruch, S., Individual-particle analysis of airborne dust samples collected over Morocco in 2006 during SAMUM 1. *Tellus Ser. B* **2011,** *63*, (4), 512 530.

19. Rodriguez, S.; Alastuey, A.; Alonso-Perez, S.; Querol, X.; Cuevas, E.; Abreu-Afonso, J.; Viana, M.; Perez, N.; Pandolfi, M.; de la Rosa, J., Transport of desert dust mixed with North African industrial pollutants in the subtropical Saharan Air Layer. *Atmos. Chem. Phys.* **2011,** *11*, (13), 6663 6685.

20. Li, J.; Wang, Z.; Zhuang, G.; Luo, G.; Sun, Y.; Wang, Q., Mixing of Asian mineral dust with anthropogenic pollutants over East Asia: a model case study of a super-duststorm in March 2010. *Atmos. Chem. Phys.* **2012,** *12*, (16), 7591 7607.

21. Formenti, P.; Schuetz, L.; Balkanski, Y.; Desboeufs, K.; Ebert, M.; Kandler, K.; Petzold, A.; Scheuvens, D.; Weinbruch, S.; Zhang, D., Recent progress in understanding physical and chemical properties of African and Asian mineral dust. *Atmos. Chem. Phys.* **2011,** *11*, (16), 8231 8256.

22. Liu, Z.; Fairlie, T. D.; Uno, I.; Huang, J.; Wu, D.; Omar, A.; Kar, J.; Vaughan, M.; Rogers, R.; Winker, D.; Trepte, C.; Hu, Y.; Sun, W.; Lin, B.; Cheng, A., Transpacific transport and evolution of the optical properties of Asian dust. *J. Quant. Spectrosc. Radiat. Transfer* **2013,** *116*, 24 33.

23. Alfaro, S. C.; Lafon, S.; Rajot, J. L.; Formenti, P.; Gaudichet, A.; Maille, M., Iron oxides and light absorption by pure desert dust: an experimental study. *J. Geophys. Res.–Atmos.* **2004,** *109*, (D8).

24. Derimian, Y.; Karnieli, A.; Kaufman, Y. J.; Andreae, M. O.; Andreae, T. W.; Dubovik, O.; Maenhaut, W.; Koren, I., The role of iron and black carbon in aerosol light absorption. *Atmos. Chem. Phys.* **2008,** *8*, (13), 3623 3637.

25. Clarke, A. D.; Shinozuka, Y.; Kapustin, V. N.; Howell, S.; Huebert, B.; Doherty, S.; Anderson, T.; Covert, D.; Anderson, J.; Hua, X.; Moore, K. G.; McNaughton, C.; Carmichael, G.; Weber, R., Size distributions and mixtures of dust and black carbon aerosol in Asian outflow: physiochemistry and optical properties. *J. Geophys. Res.–Atmos.* **2004,** *109*, (D15).

26. Petzold, A.; Veira, A.; Mund, S.; Esselborn, M.; Kiemle, C.; Weinzierl, B.; Hamburger, T.; Ehret, G.; Lieke, K.; Kandler, K., Mixing of mineral dust with urban pollution aerosol over Dakar (Senegal): impact on dust physico-chemical and radiative properties. *Tellus B* **2011,** *63*, (4), 619 634.

27. Yang, M.; Howell, S. G.; Zhuang, J.; Huebert, B. J., Attribution of aerosol light absorption to black carbon, brown carbon, and dust in China interpretations of atmospheric measurements during EAST-AIRE. *Atmos. Chem. Phys.* **2009,** *9*, (6), 2035 2050.

28. Leaitch, W. R.; Macdonald, A. M.; Anlauf, K. G.; Liu, P. S. K.; Toom-Sauntry, D.; Li, S. M.; Liggio, J.; Hayden, K.; Wasey, M. A.; Russell, L. M.; Takahama, S.; Liu, S.; van Donkelaar, A.; Duck, T.; Martin, R. V.; Zhang, Q.; Sun, Y.; McKendry, I.; Shantz, N. C.; Cubison, M., Evidence for Asian dust effects from aerosol plume measurements during INTEX-B 2006 near Whistler, BC. *Atmos. Chem. Phys.* **2009,** *9*, (11), 3523 3546.

29. Kim, J. S.; Park, K., Atmospheric aging of Asian dust particles during long-range transport. *Aerosol Sci. Technol.* **2012,** *46*, (8), 913 924.

30. Deboudt, K.; Flament, P.; Choel, M.; Gloter, A.; Sobanska, S.; Colliex, C., Mixing state of aerosols and direct observation of carbonaceous and marine coatings on African dust by individual particle analysis. *J. Geophys. Res.–Atmos.* **2010,** *115*, D24207, doi:10.1029/2010JD013921.

31. Kirchstetter, T. W.; Novakov, T.; Hobbs, P. V., Evidence that the spectral dependence of light absorption by aerosols is affected by organic carbon. *J. Geophys. Res.–Atmos.* **2004,** *109*, (D21).

32. Andreae, M. O.; Gelencser, A., Black carbon or brown carbon? The nature of light-absorbing carbonaceous aerosols. *Atmos. Chem. Phys.* **2006,** *6*, 3131 3148.

33. Bauer, S. E.; Mishchenko, M. I.; Lacis, A. A.; Zhang, S.; Perlwitz, J.; Metzger, S. M., Do sulfate and nitrate coatings on mineral dust have important effects on radiative properties and climate modeling? *J. Geophys. Res.–Atmos.* **2007,** *112*, (D6).

34. Howell, S. G.; Clarke, A. D.; Shinozuka, Y.; Kapustin, V.; McNaughton, C. S.; Huebert, B. J.; Doherty, S. J.; Anderson, T. L., Influence of relative humidity upon pollution and dust during ACE-Asia: size distributions and implications for optical properties. *J. Geophys. Res.–Atmos.* **2006,** *111*, (D6).

35. McNaughton, C. S.; Clarke, A. D.; Kapustin, V.; Shinozuka, Y.; Howell, S. G.; Anderson, B. E.; Winstead, E.; Dibb, J.; Scheuer, E.; Cohen, R. C.; Wooldridge, P.; Perring, A.; Huey, L. G.; Kim, S.; Jimenez, J. L.; Dunlea, E. J.; DeCarlo, P. F.; Wennberg, P. O.; Crounse, J. D.; Weinheimer, A. J.; Flocke, F., Observations of heterogeneous reactions between Asian pollution and mineral dust over the eastern North Pacific during INTEX-B. *Atmos. Chem. Phys.* **2009,** *9*, (21), 8283 8308.

36. Tang, Y. H.; Carmichael, G. R.; Seinfeld, J. H.; Dabdub, D.; Weber, R. J.; Huebert, B.; Clarke, A. D.; Guazzotti, S. A.; Sodeman, D. A.; Prather, K. A.; Uno, I.; Woo, J. H.; Yienger, J. J.; Streets, D. G.; Quinn, P. K.; Johnson, J. E.; Song, C. H.; Grassian, V. H.; Sandu, A.; Talbot, R. W.; Dibb, J. E., Three-dimensional simulations of inorganic aerosol distributions in east Asia during spring 2001. *J. Geophys. Res.–Atmos.* **2004,** *109*, (D19).

37. Seinfeld, J. H.; Pandis, S. N., *Atmospheric Chemistry and Physics—From Air Pollution to Climate Change, 2nd edition*. 2nd edition ed.; J. Wiley: New York, United States, 2006.

38. Twohy, C. H.; Kreidenweis, S. M.; Eidhammer, T.; Browell, E. V.; Heymsfield, A. J.; Bansemer, A. R.; Anderson, B. E.; Chen, G.; Ismail, S.; DeMott, P. J.; Van den Heever, S. C., Saharan dust particles nucleate droplets in eastern Atlantic clouds. *Geophys. Res. Lett.* **2009,** *36*.

39. Koehler, K. A.; Kreidenweis, S. M.; DeMott, P. J.; Petters, M. D.; Prenni, A. J.; Carrico, C. M., Hygroscopicity and cloud droplet activation of mineral dust aerosol. *Geophys. Res. Lett.* **2009,** *36*.

40. Kumar, P.; Sokolik, I. N.; Nenes, A., Measurements of cloud condensation nuclei activity and droplet activation kinetics of fresh unprocessed regional dust samples and minerals. *Atmos. Chem. Phys.* **2011,** *11*, (7), 3527 3541.

41. Karydis, V. A.; Kumar, P.; Barahona, D.; Sokolik, I. N.; Nenes, A., On the effect of dust particles on global cloud condensation nuclei and cloud droplet number. *J. Geophys. Res.–Atmos.* **2011,** *116*.

42. Sullivan, R. C.; Guazzotti, S. A.; Sodeman, D. A.; Prather, K. A., Direct observations of the atmospheric processing of Asian mineral dust. *Atmos. Chem. Phys.* **2007,** *7*, 1213 1236.

43. Li, W. J.; Shao, L. Y., Observation of nitrate coatings on atmospheric mineral dust particles. *Atmos. Chem. Phys.* **2009,** *9*, (6), 1863 1871.

44. Kojima, T.; Buseck, P. R.; Iwasaka, Y.; Matsuki, A.; Trochkine, D., Sulfate-coated dust particles in the free troposphere over Japan. *Atmos. Res.* **2006,** *82*, (3 4), 698 708.

45. Fan, S. M.; Horowitz, L. W.; Levy, H.; Moxim, W. J., Impact of air pollution on wet deposition of mineral dust aerosols. *Geophys. Res. Lett.* **2004,** *31*, (2).

46. Sullivan, R. C.; Moore, M. J. K.; Petters, M. D.; Kreidenweis, S. M.; Roberts, G. C.; Prather, K. A., Timescale for hygroscopic conversion of calcite mineral particles through heterogeneous reaction with nitric acid. *Phys. Chem. Chem. Phys.* **2009,** *11*, (36), 7826 7837.

47. Krueger, B. J.; Grassian, V. H.; Cowin, J. P.; Laskin, A., Heterogeneous chemistry of individual mineral dust particles from different dust source regions: the importance of particle mineralogy. *Atmos. Environ.* **2004,** *38*, (36), 6253 6261.

48. Matsuki, A.; Iwasaka, Y.; Shi, G. Y.; Zhang, D. Z.; Trochkine, D.; Yamada, M.; Kim, Y. S.; Chen, B.; Nagatani, T.; Miyazawa, T.; Nagatani, M.; Nakata, H., Morphological and chemical modification of mineral dust: observational insight into the heterogeneous uptake of acidic gases. *Geophys. Res. Lett.* **2005,** *32*, (22).

49. Takahama, S.; Liu, S.; Russell, L. M., Coatings and clusters of carboxylic acids in carbon-containing atmospheric particles from spectromicroscopy and their implications for cloud-nucleating and optical properties. *J. Geophys. Res.–Atmos.* **2010,** *115*.

50. Sullivan, R. C.; Prather, K. A., Investigations of the diurnal cycle and mixing state of oxalic acid in individual particles in Asian aerosol outflow. *Environ. Sci. Technol.* **2007,** *41*, (23), 8062 8069.

51. Kumar, P. P.; Broekhuizen, K.; Abbatt, J. P. D., Organic acids as cloud condensation nuclei: laboratory studies of highly soluble and insoluble species. *Atmos. Chem. Phys.* **2003,** *3*, 509 520.

52. Gierlus, K. M.; Laskina, O.; Abernathy, T. L.; Grassian, V. H., Laboratory study of the effect of oxalic acid on the cloud condensation nuclei activity of mineral dust aerosol. *Atmos. Environ.* **2012,** *46*, 125 130.

53. Sullivan, R. C.; Moore, M. J. K.; Petters, M. D.; Kreidenweis, S. M.; Roberts, G. C.; Prather, K. A., Effect of chemical mixing state on the hygroscopicity and cloud nucleation properties of calcium mineral dust particles. *Atmos. Chem. Phys.* **2009,** *9*, (10), 3303 3316.

54. Furukawa, T.; Takahashi, Y., Oxalate metal complexes in aerosol particles: implications for the hygroscopicity of oxalate-containing particles. *Atmos. Chem. Phys.* **2011,** *11*, (9), 4289 4301.

55. DeMott, P. J.; Sassen, K.; Poellot, M. R.; Baumgardner, D.; Rogers, D. C.; Brooks, S. D.; Prenni, A. J.; Kreidenweis, S. M., African dust aerosols as atmospheric ice nuclei. *Geophys. Res. Lett.* **2003,** *30*, (14).

56. Prenni, A. J.; Petters, M. D.; Kreidenweis, S. M.; Heald, C. L.; Martin, S. T.; Artaxo, P.; Garland, R. M.; Wollny, A. G.; Poeschl, U., Relative roles of biogenic emissions and Saharan dust as ice nuclei in the Amazon basin. *Nat. Geosci.* **2009,** *2*, (6), 401 404.

57. Creamean, J. M.; Suski, K. J.; Rosenfeld, D.; Cazorla, A.; DeMott, P. J.; Sullivan, R. C.; White, A. B.; Ralph, F. M.; Minnis, P.; Comstock, J. M.; Tomlinson, J. M.; Prather, K. A., Dust and biological aerosols from the Sahara and Asia influence precipitation in the Western U.S. *Science* **2013,** *339*, (6127), 1572 1578.

58. Hoose, C.; Moehler, O., Heterogeneous ice nucleation on atmospheric aerosols: a review of results from laboratory experiments. *Atmos. Chem. Phys.* **2012,** *12*, (20), 9817 9854.

59. Yakobi-Hancock, J. D.; Ladino, L. A.; Abbatt, J. P. D., Feldspar minerals as efficient deposition ice nuclei. *Atmos. Chem. Phys. Discuss.* **2013,** *13*, 17299 17326.

60. Atkinson, J. D.; Murray, B. J.; Woodhouse, M. T.; Whale, T. F.; Baustian, K. J.; Carslaw, K. S.; Dobbie, S.; O'Sullivan, D.; Malkin, T. L., The importance of feldspar for ice nucleation by mineral dust in mixed-phase clouds. *Nature* **2013,** *498*, (7454), 355 358.

61. Cziczo, D. J.; Froyd, K. D.; Gallavardin, S. J.; Moehler, O.; Benz, S.; Saathoff, H.; Murphy, D. M., Deactivation of ice nuclei due to atmospherically relevant surface coatings. *Environ. Res. Lett.* **2009,** *4*, (4), 044013.

62. Sullivan, R. C.; Petters, M. D.; DeMott, P. J.; Kreidenweis, S. M.; Wex, H.; Niedermeier, D.; Hartmann, S.; Clauss, T.; Stratmann, F.; Reitz, P.; Schneider, J.; Sierau, B., Irreversible loss of ice nucleation active sites in mineral dust particles caused by sulphuric acid condensation. *Atmos. Chem. Phys.* **2010,** *10*, (23), 11471 11487.

63. Yang, Z.; Bertram, A. K.; Chou, K. C., Why do sulfuric acid coatings influence the ice nucleation properties of mineral dust particles in the atmosphere? *J. Phys. Chem. Lett.* **2011,** *2*, (11), 1232 1236.

64. Niedermeier, D.; Hartmann, S.; Clauss, T.; Wex, H.; Kiselev, A.; Sullivan, R. C.; DeMott, P. J.; Petters, M. D.; Reitz, P.; Schneider, J.; Mikhailov, E.; Sierau, B.; Stetzer, O.; Reimann, B.; Bundke, U.; Shaw, R. A.; Buchholz, A.; Mentel, T. F.; Stratmann, F., Experimental study of the role of physicochemical surface processing on the IN ability of mineral dust particles. *Atmos. Chem. Phys.* **2011,** *11*, (21), 11131 11144.

65. Sullivan, R. C.; Minambres, L.; DeMott, P. J.; Prenni, A. J.; Carrico, C. M.; Levin, E. J. T.; Kreidenweis, S. M., Chemical processing does not always impair heterogeneous ice nucleation of mineral dust particles. *Geophys. Res. Lett.* **2010,** *37*.

66. Mohler, O.; Benz, S.; Saathoff, H.; Schnaiter, M.; Wagner, R.; Schneider, J.; Walter, S.; Ebert, V.; Wagner, S., The effect of organic coatings on the heterogeneous ice nucleation efficiency of mineral dust aerosols. *Environ. Res. Lett.* **2008,** *3*, (2).

67. Laden, F.; Neas, L. M.; Dockery, D. W.; Schwartz, J., Association of fine particulate matter from different sources with daily mortality in six US cities. *Environ. Health Perspect.* **2000,** *108*, (10), 941 947.

68. Brunekreef, B.; Forsberg, B., Epidemiological evidence of effects of coarse airborne particles on health. *Eur. Resp. J.* **2005,** *26*, (2), 309 318.

69. Karanasiou, A.; Moreno, N.; Moreno, T.; Viana, M.; de Leeuw, F.; Querol, X., Health effects from Sahara dust episodes in Europe: literature review and research gaps. *Environ. Int.* **2012,** *47*, 107 114.

70. Kanatani, K. T.; Ito, I.; Al-Delaimy, W. K.; Adachi, Y.; Mathews, W. C.; Ramsdell, J. W.; Toyama Asian Desert Dust and Asthma Study Team, Desert dust

exposure is associated with increased risk of asthma hospitalization in children. *Am. J. Respir. Crit. Care Med.* **2010,** *182*, (12), 1475 1481.

71. Alessandrini, E. R.; Stafoggia, M.; Faustini, A.; Gobbi, G. P.; Forastiere, F., Saharan dust and the association between particulate matter and daily hospitalisations in Rome, Italy. *Occup. Environ. Med.* **2013,** *70*, (6), 432 434.

72. Kang, J.-H.; Liu, T.-C.; Keller, J.; Lin, H.-C., Asian dust storm events are associated with an acute increase in stroke hospitalisation. *J. Epidemiol. Community Health* **2013,** *67*, (2), 125 131.

73. Neophytou, A. M.; Yiallouros, P.; Coull, B. A.; Kleanthous, S.; Pavlou, P.; Pashiardis, S.; Dockery, D. W.; Koutrakis, P.; Laden, F., Particulate matter concentrations during desert dust outbreaks and daily mortality in Nicosia, Cyprus. *J. Exposure Sci. Environ. Epidemiol.* **2013,** *23*, (3), 275 280.

74. Garrison, V. H.; Foreman, W. T.; Genualdi, S.; Griffin, D. W.; Kellogg, C. A.; Majewski, M. S.; Mohammed, A.; Ramsubhag, A.; Shinn, E. A.; Simonich, S. L., Saharan dust a carrier of persistent organic pollutants, metals and microbes to the Caribbean? *Rev. Biol. Trop.* **2006,** *54*, (Suppl. 3), 9 21.

75. Tamamura, S.; Sato, T.; Ota, Y.; Wang, X. L.; Tang, N.; Hayakawa, K., Long-range transport of polycyclic aromatic hydrocarbons (PAHs) from the eastern Asian continent to Kanazawa, Japan with Asian dust. *Atmos. Environ.* **2007,** *41*, (12), 2580 2593.

76. Ladji, R.; Yassaa, N.; Balducci, C.; Cecinato, A., Organic components of Algerian desert dusts. *Chemosphere* **2010,** *81*, (7), 925 931.

77. Thuan, N. T.; Chi, K. H.; Wang, S.-H.; Chang, M. B.; Lin, N.-H.; Sheu, G.-R.; Peng, C.-M., Atmospheric PCDD/F measurement in Taiwan and Southeast Asia during Dongsha Experiment. *Atmos. Environ.* **2013,** *78*, 195 202.

78. Hou, X. M.; Zhuang, G. S.; Sun, Y.; An, Z. S., Characteristics and sources of polycyclic aromatic hydrocarbons and fatty acids in PM2.5 aerosols in dust season in China. *Atmos. Environ.* **2006,** *40*, (18), 3251 3262.

79. Chi, K. H.; Hsu, S. C.; Wang, S. H.; Chang, M. B., Increases in ambient PCDD/F and PCB concentrations in Northern Taiwan during an Asian dust storm episode. *Sci. Total Environ.* **2008,** *401*, (1 3), 100 108.

80. Marx, S. K.; Kamber, B. S.; McGowan, H. A., Scavenging of atmospheric trace metal pollutants by mineral dusts: inter-regional transport of Australian trace metal pollution to New Zealand. *Atmos. Environ.* **2008,** *42*, (10), 2460 2478.

81. Erel, Y.; Dayan, U.; Rabi, R.; Rudich, Y.; Stein, M., Trans-boundary transport of pollutants by atmospheric mineral dust. *Environ. Sci. Technol.* **2006,** *40*, (9), 2996 3005.

82. Han, J. S.; Moon, K. J.; Ahn, J. Y.; Hong, Y. D.; Kim, Y. J.; Ryu, S. Y.; Cliff, S. S.; Cahill, T. A., Characteristics of ion components and trace elements of fine

particles at Gosan, Korea in springtime from 2001 to 2002. *Environ. Monit. Assess.* **2004,** *92*, (1–3), 73–93.

83. Lee, P. K.; Youm, S. J.; Jo, H. Y., Heavy metal concentrations and contamination levels from Asian dust and identification of sources: a case study. *Chemosphere* **2013,** *91*, (7), 1018–1025.

84. Falkovich, A. H.; Schkolnik, G.; Ganor, E.; Rudich, Y., Adsorption of organic compounds pertinent to urban environments onto mineral dust particles. *J. Geophys. Res.–Atmos.* **2004,** *109*, D02208, doi:10.1029/2003JD003919.

85. Schulz, M.; Prospero, J. M.; Baker, A. R.; Dentener, F.; Ickes, L.; Liss, P. S.; Mahowald, N. M.; Nickovic, S.; Garcia-Pando, C. P.; Rodriguez, S.; Sarin, M.; Tegen, I.; Duce, R. A., Atmospheric transport and deposition of mineral dust to the ocean: implications for research needs. *Environ. Sci. Technol.* **2012,** *46*, (19), 10390–10404.

86. Mahowald, N. M.; Engelstaedter, S.; Luo, C.; Sealy, A.; Artaxo, P.; Benitez-Nelson, C.; Bonnet, S.; Chen, Y.; Chuang, P. Y.; Cohen, D. D.; Dulac, F.; Herut, B.; Johansen, A. M.; Kubilay, N.; Losno, R.; Maenhaut, W.; Paytan, A.; Prospero, J. A.; Shank, L. M.; Siefert, R. L., Atmospheric iron deposition: global distribution, variability, and human perturbations. *Ann. Rev. Mar. Sci.* **2009,** *1*, 245–278.

87. Journet, E.; Desboeufs, K. V.; Caquineau, S.; Colin, J.-L., Mineralogy as a critical factor of dust iron solubility. *Geophys. Res. Lett.* **2008,** *35*, (7).

88. Sholkovitz, E. R.; Sedwick, P. N.; Church, T. M.; Baker, A. R.; Powell, C. F., Fractional solubility of aerosol iron: synthesis of a global-scale data set. *Geochim. Cosmochim. Acta* **2012,** *89*, 173–189.

89. Chen, H. H.; Laskin, A.; Baltrusaitis, J.; Gorski, C. A.; Scherer, M. M.; Grassian, V. H., Coal fly ash as a source of iron in atmospheric dust. *Environ. Sci. Technol.* **2012,** *46*, (4), 2112–2120.

90. Shi, Z.; Krom, M. D.; Jickells, T. D.; Bonneville, S.; Carslaw, K. S.; Mihalopoulos, N.; Baker, A. R.; Benning, L. G., Impacts on iron solubility in the mineral dust by processes in the source region and the atmosphere: a review. *Aeolian Res.* **2012,** *5*, 21–42.

91. Baker, A. R.; Croot, P. L., Atmospheric and marine controls on aerosol iron solubility in seawater. *Mar. Chem.* **2010,** *120*, (1–4), 4–13.

92. Cwiertny, D. M.; Baltrusaitis, J.; Hunter, G. J.; Laskin, A.; Scherer, M. M.; Grassian, V. H., Characterization and acid-mobilization study of iron-containing mineral dust source materials. *J. Geophys. Res.–Atmos.* **2008,** *113*, (D5).

93. Shi, Z.; Bonneville, S.; Krom, M. D.; Carslaw, K. S.; Jickells, T. D.; Baker, A. R.; Benning, L. G., Iron dissolution kinetics of mineral dust at low pH during simulated atmospheric processing. *Atmos. Chem. Phys.* **2011,** *11*, (3), 995–1007.

94. Meskhidze, N.; Chameides, W. L.; Nenes, A.; Chen, G., Iron mobilization in mineral dust: can anthropogenic SO_2 emissions affect ocean productivity? *Geophys. Res. Lett.* **2003,** *30*, (21).

95. Solmon, F.; Chuang, P. Y.; Meskhidze, N.; Chen, Y., Acidic processing of mineral dust iron by anthropogenic compounds over the north Pacific Ocean. *J. Geophys. Res.–Atmos.* **2009,** *114*.

96. Takahashi, Y.; Higashi, M.; Furukawa, T.; Mitsunobu, S., Change of iron species and iron solubility in Asian dust during the long-range transport from western China to Japan. *Atmos. Chem. Phys.* **2011,** *11*, (21), 11237 11252.

97. Paris, R.; Desboeufs, K. V.; Journet, E., Variability of dust iron solubility in atmospheric waters: investigation of the role of oxalate organic complexation. *Atmos. Environ.* **2011,** *45*, (36), 6510 6517.

98. Paris, R.; Desboeufs, K. V., Effect of atmospheric organic complexation on iron-bearing dust solubility. *Atmos. Chem. Phys.* **2013,** *13*, (9), 4895 4905.

99. Pehkonen, S. O.; Siefert, R.; Erel, Y.; Webb, S.; Hoffmann, M. R., Photoreduction of iron oxyhydroxides in the presence of important atmospheric organic compounds. *Environ. Sci. Technol.* **1993,** *27*, (10), 2056 2062.

100. Siffert, C.; Sulzberger, B., Light-induced dissolution of hematite in the presence of oxalate: a case study. *Langmuir* **1991,** *7*, (8), 1627 1634.

101. Styler, S. A.; Donaldson, D. J., Heterogeneous photochemistry of oxalic acid on Mauritanian sand and Icelandic volcanic ash. *Environ. Sci. Technol.* **2012,** *46*, (16), 8756 8763.

102. Dupart, Y.; King, S. M.; Nekat, B.; Nowak, A.; Wiedensohler, A.; Herrmann, H.; David, G.; Thomas, B.; Miffre, A.; Rairoux, P.; D'Anna, B.; George, C., Mineral dust photochemistry induces nucleation events in the presence of SO_2. *PNAS* **2012,** *109*, (51), 20842 20847.

103. Dentener, F. J.; Carmichael, G. R.; Zhang, Y.; Lelieveld, J.; Crutzen, P. J., Role of mineral aerosol as a reactive surface in the global troposphere. *J. Geophys. Res.–Atmos.* **1996,** *101*, (D17), 22869 22889.

104. Bonasoni, P.; Cristofanelli, P.; Calzolari, F.; Bonafe, U.; Evangelisti, F.; Stohl, A.; Sajani, S. Z.; van Dingenen, R.; Colombo, T.; Balkanski, Y., Aerosol ozone correlations during dust transport episodes. *Atmos. Chem. Phys.* **2004,** *4*, 1201 1215.

105. Hanke, M.; Umann, B.; Uecker, J.; Arnold, F.; Bunz, H., Atmospheric measurements of gas-phase HNO_3 and SO_2 using chemical ionization mass spectrometry during the MINATROC field campaign 2000 on Monte Cimone. *Atmos. Chem. Phys.* **2003,** *3*, 417 436.

106. Tang, Y. H.; Carmichael, G. R.; Kurata, G.; Uno, I.; Weber, R. J.; Song, C. H.; Guttikunda, S. K.; Woo, J. H.; Streets, D. G.; Wei, C.; Clarke, A. D.; Huebert, B.; Anderson, T. L., Impacts of dust on regional tropospheric chemistry during the ACE-

Asia experiment: a model study with observations. *J. Geophys. Res.–Atmos.* **2004,** *109*, (D19).

107. de Reus, M.; Fischer, H.; Sander, R.; Gros, V.; Kormann, R.; Salisbury, G.; Van Dingenen, R.; Williams, J.; Zollner, M.; Lelieveld, J., Observations and model calculations of trace gas scavenging in a dense Saharan dust plume during MINATROC. *Atmos. Chem. Phys.* **2005,** *5*, 1787 1803.

108. Zhu, S.; Butler, T.; Sander, R.; Ma, J.; Lawrence, M. G., Impact of dust on tropospheric chemistry over polluted regions: a case study of the Beijing megacity. *Atmos. Chem. Phys.* **2010,** *10*, (8), 3855 3873.

109. Fairlie, T. D.; Jacob, D. J.; Dibb, J. E.; Alexander, B.; Avery, M. A.; van Donkelaar, A.; Zhang, L., Impact of mineral dust on nitrate, sulfate, and ozone in transpacific Asian pollution plumes. *Atmos. Chem. Phys.* **2010,** *10*, (8), 3999 4012.

110. Li, J. W.; Han, Z. W., A modeling study of the impact of heterogeneous reactions on mineral aerosol surfaces on tropospheric chemistry over East Asia. *Particuology* **2010,** *8*, (5), 433 441.

111. de Reus, M.; Dentener, F.; Thomas, A.; Borrmann, S.; Strom, J.; Lelieveld, J., Airborne observations of dust aerosol over the North Atlantic Ocean during ACE 2: indications for heterogeneous ozone destruction. *J. Geophys. Res.–Atmos.* **2000,** *105*, (D12), 15263 15275.

112. Bauer, S. E.; Balkanski, Y.; Schulz, M.; Hauglustaine, D. A.; Dentener, F., Global modeling of heterogeneous chemistry on mineral aerosol surfaces: influence on tropospheric ozone chemistry and comparison to observations. *J. Geophys. Res.–Atmos.* **2004,** *109*, (D2).

113. Hanisch, F.; Crowley, J. N., Ozone decomposition on Saharan dust: an experimental investigation. *Atmos. Chem. Phys.* **2003,** *3*, 119 130.

114. Bian, H. S.; Zender, C. S., Mineral dust and global tropospheric chemistry: relative roles of photolysis and heterogeneous uptake. *J. Geophys. Res.–Atmos.* **2003,** *108*, (D21).

115. Ying, Z.; Tie, X.; Madronich, S.; Li, G.; Massie, S., Simulation of regional dust and its effect on photochemistry in the Mexico City area during MILAGRO experiment. *Atmos. Environ.* **2011,** *45*, (15), 2549 2558.

116. Pang, X. B.; Mu, Y. J.; Lee, X. Q.; Zhang, Y. J.; Xu, Z., Influences of characteristic meteorological conditions on atmospheric carbonyls in Beijing, China. *Atmos. Res.* **2009,** *93*, (4), 913 919.

117. Salisbury, G.; Williams, J.; Gros, V.; Bartenbach, S.; Xu, X.; Fischer, H.; Kormann, R.; de Reus, M.; Zoellner, M., Assessing the effect of a Saharan dust storm on oxygenated organic compounds at Izana, Tenerife (July August 2002). *J. Geophys. Res.–Atmos.* **2006,** *111*, (D22).

118. Finlayson-Pitts, B. J.; Pitts, J. N., *Chemistry of the upper and lower atmosphere*. Academic Press: San Diego, CA, 2000.

119. Ma, J.; Liu, Y.; Ma, Q.; Liu, C.; He, H., Heterogeneous photochemical reaction of ozone with anthracene adsorbed on mineral dust. *Atmos. Environ.* **2013,** *72*, 165 170.

120. Zelenay, V.; Monge, M. E.; D'Anna, B.; George, C.; Styler, S. A.; Huthwelker, T.; Ammann, M., Increased steady state uptake of ozone on soot due to UV/Vis radiation. *J. Geophys. Res.-Atmos.* **2011,** *116*, (D11), DOI: 10.1029/2010JD015500.

121. Styler, S. A.; Loiseaux, M. E.; Donaldson, D. J., Substrate effects in the photoenhanced ozonation of pyrene. *Atmos. Chem. Phys.* **2011,** *11*, (3), 1243 1253.

122. Adamson, A. W., *Physical Chemistry of Surfaces, 5th ed.* John Wiley and Sons: Toronto, Ontario, Canada, 1990.

123. Donaldson, D. J., Adsorption of atmospheric gases at the air-water interface. I. NH_3. *J. Phys. Chem. A* **1999,** *103*, (1), 62 70.

124. Kahan, T. F.; Kwamena, N. O. A.; Donaldson, D. J., Heterogeneous ozonation kinetics of polycyclic aromatic hydrocarbons on organic films. *Atmos. Environ.* **2006,** *40*, (19), 3448 3459.

125. Mmereki, B. T.; Donaldson, D. J.; Gilman, J. B.; Eliason, T. L.; Vaida, V., Kinetics and products of the reaction of gas-phase ozone with anthracene adsorbed at the air aqueous interface. *Atmos. Environ.* **2004,** *38*, (36), 6091 6103.

126. Henderson, E. A.; Donaldson, D. J., Influence of organic coatings on pyrene ozonolysis at the air aqueous interface. *J. Phys. Chem. A* **2012,** *116*, (1), 423 429.

127. Mmereki, B. T.; Donaldson, D. J., Direct observation of the kinetics of an atmospherically important reaction at the air aqueous interface. *J. Phys. Chem. A* **2003,** *107*, (50), 11038 11042.

128. Poschl, U.; Letzel, T.; Schauer, C.; Niessner, R., Interaction of ozone and water vapor with spark discharge soot aerosol particles coated with benzo[a]pyrene: O_3 and H_2O adsorption, benzo[a]pyrene degradation, and atmospheric implications. *J. Phys. Chem. A* **2001,** *105*, (16), 4029 4041.

129. Kwamena, N. O. A.; Staikova, M. G.; Donaldson, D. J.; George, I. J.; Abbatt, J. P. D., Role of the aerosol substrate in the heterogeneous ozonation reactions of surface-bound PAHs. *J. Phys. Chem. A* **2007,** *111*, (43), 11050 11058.

130. Crowley, J. N.; Ammann, M.; Cox, R. A.; Hynes, R. G.; Jenkin, M. E.; Mellouki, A.; Rossi, M. J.; Troe, J.; Wallington, T. J., Evaluated kinetic and photochemical data for atmospheric chemistry: Volume V heterogeneous reactions on solid substrates. *Atmos. Chem. Phys.* **2010,** *10*, (18), 9059 9223.

131. Davidovits, P.; Kolb, C. E.; Williams, L. R.; Jayne, J. T.; Worsnop, D. R., Mass accommodation and chemical reactions at gas liquid interfaces. *Chem. Rev.* **2006,** *106*, (4), 1323 1354.

132. Ammann, M.; Poschl, U.; Rudich, Y., Effects of reversible adsorption and Langmuir Hinshelwood surface reactions on gas uptake by atmospheric particles. *Phys. Chem. Chem. Phys.* **2003,** *5*, (2), 351 356.

133. Styler, S. A.; Brigante, M.; D'Anna, B.; George, C.; Donaldson, D. J., Photoenhanced ozone loss on solid pyrene films. *Phys. Chem. Chem. Phys.* **2009,** *11*, (36), 7876 7884.

134. Kolb, C. E.; Cox, R. A.; Abbatt, J. P. D.; Ammann, M.; Davis, E. J.; Donaldson, D. J.; Garrett, B. C.; George, C.; Griffiths, P. T.; Hanson, D. R.; Kulmala, M.; McFiggans, G.; Poeschl, U.; Riipinen, I.; Rossi, M. J.; Rudich, Y.; Wagner, P. E.; Winkler, P. M.; Worsnop, D. R.; O' Dowd, C. D., An overview of current issues in the uptake of atmospheric trace gases by aerosols and clouds. *Atmos. Chem. Phys.* **2010,** *10*, (21), 10561 10605.

135. Knudsen, M., Experimental determination of the pressure of saturated mercury steam at 0 degrees and at higher temperatures. *Ann. Phys.* **1909,** *29*, (6), 179 193.

136. Golden, D. M.; Spokes, G. N.; Benson, S. W., Very low-pressure pyrolysis (VLPP): versatile kinetic tool. *Angew. Chem. Int. Ed.* **1973,** *12*, (7), 534 546.

137. Ullerstam, M.; Johnson, M. S.; Vogt, R.; Ljungstrom, E., DRIFTS and Knudsen cell study of the heterogeneous reactivity of SO_2 and NO_2 on mineral dust. *Atmos. Chem. Phys.* **2003,** *3*, 2043 2051.

138. Hanisch, F.; Crowley, J. N., Heterogeneous reactivity of gaseous nitric acid on Al_2O_3, $CaCO_3$, and atmospheric dust samples: A Knudsen cell study. *J. Phys. Chem. A* **2001,** *105*, (13), 3096 3106.

139. Li, P.; Perreau, K. A.; Covington, E.; Song, C. H.; Carmichael, G. R.; Grassian, V. H., Heterogeneous reactions of volatile organic compounds on oxide particles of the most abundant crustal elements: Surface reactions of acetaldehyde, acetone, and propionaldehyde on SiO_2, Al_2O_3, Fe_2O_3, TiO_2, and CaO. *J. Geophys. Res.–Atmos.* **2001,** *106*, (D6), 5517 5529.

140. Hatch, C. D.; Gough, R. V.; Tolbert, M. A., Heterogeneous uptake of the C-1 to C-4 organic acids on a swelling clay mineral. *Atmos. Chem. Phys.* **2007,** *7*, (16), 4445 4458.

141. Grassian, V. H., Heterogeneous uptake and reaction of nitrogen oxides and volatile organic compounds on the surface of atmospheric particles including oxides, carbonates, soot and mineral dust: implications for the chemical balance of the troposphere. *Int. Rev. Phys. Chem.* **2001,** *20*, (3), 467 548.

142. Styler, S. A.; Myers, A. L.; Donaldson, D. J., Heterogeneous photooxidation of fluorotelomer alcohols: a new source of aerosol-phase perfluorinated carboxylic acids. *Environ. Sci. Technol.* **2013,** *47*, (12), 6358 6367.

143. Ndour, M.; D'Anna, B.; George, C.; Ka, O.; Balkanski, Y.; Kleffmann, J.; Stemmler, K.; Ammann, M., Photoenhanced uptake of NO_2 on mineral dust: laboratory experiments and model simulations. *Geophys. Res. Lett.* **2008,** *35*, (5).

144. Wagner, C.; Hanisch, F.; Holmes, N.; de Coninck, H.; Schuster, G.; Crowley, J. N., The interaction of N_2O_5 with mineral dust: aerosol flow tube and Knudsen reactor studies. *Atmos. Chem. Phys.* **2008,** *8*, (1), 91 109.

145. Cooney, D. O.; Kim, S. S.; Davis, E. J., Analyses of mass transfer in hemodialyzers for laminar blood flow and homogeneous dialysate. *Chem. Eng. Sci.* **1974,** *29*, (8), 1731-1738.

146. Murphy, D. M.; Fahey, D. W., Mathematical treatment of the wall loss of a trace species in denuder and catalytic converter tubes. *Anal. Chem.* **1987,** *59*, (23), 2753 2759.

147. Pradhan, M.; Kyriakou, G.; Archibald, A. T.; Papageorgiou, A. C.; Kalberer, M.; Lambert, R. M., Heterogeneous uptake of gaseous hydrogen peroxide by Gobi and Saharan dust aerosols: a potential missing sink for H_2O_2 in the troposphere. *Atmos. Chem. Phys.* **2010,** *10*, (15), 7127 7136.

148. Vlasenko, A.; Huthwelker, T.; Gaggeler, H. W.; Ammann, M., Kinetics of the heterogeneous reaction of nitric acid with mineral dust particles: an aerosol flowtube study. *Phys. Chem. Chem. Phys.* **2009,** *11*, (36), 7921 7930.

149. Adams, J. W.; Rodriguez, D.; Cox, R. A., The uptake of SO_2 on Saharan dust: a flow tube study. *Atmos. Chem. Phys.* **2005,** *5*, 2679 2689.

150. Ndour, M.; Nicolas, M.; D'Anna, B.; Ka, O.; George, C., Photoreactivity of NO_2 on mineral dusts originating from different locations of the Sahara desert. *Phys. Chem. Chem. Phys.* **2009,** *11*, (9), 1312 1319.

151. Sassine, M.; Burel, L.; D'Anna, B.; George, C., Kinetics of the tropospheric formaldehyde loss onto mineral dust and urban surfaces. *Atmos. Environ.* **2010,** *44*, (40), 5468 5475.

152. Vlasenko, A.; Sjogren, S.; Weingartner, E.; Stemmler, K.; Gaggeler, H. W.; Ammann, M., Effect of humidity on nitric acid uptake to mineral dust aerosol particles. *Atmos. Chem. Phys.* **2006,** *6*, 2147 2160.

153. Li, P.; Al-Abadleh, H. A.; Grassian, V. H., Measuring heterogeneous uptake coefficients of gases on solid particle surfaces with a Knudsen cell reactor: complications due to surface saturation and gas diffusion into underlying layers. *J. Phys. Chem. A* **2002,** *106*, (7), 1210 1219.

154. Abbatt, J. P. D.; Lee, A. K. Y.; Thornton, J. A., Quantifying trace gas uptake to tropospheric aerosol: recent advances and remaining challenges. *Chem. Soc. Rev.* **2012,** *41*, (19), 6555 6581.

155. Iinuma, Y.; Kahnt, A.; Mutzel, A.; Boege, O.; Herrmann, H., Ozone-driven secondary organic aerosol production chain. *Environ. Sci. Technol.* **2013,** *47*, (8), 3639 3647.

156. Wang, J.; Doussin, J. F.; Perrier, S.; Perraudin, E.; Katrib, Y.; Pangui, E.; Picquet-Varrault, B., Design of a new multi-phase experimental simulation chamber

for atmospheric photosmog, aerosol and cloud chemistry research. *Atmos. Meas. Tech.* **2011,** *4*, (11), 2465 2494.

157. Paulson, S. E.; Seinfeld, J. H., Development and evaluation of a photooxidation mechanism for isoprene. *J. Geophys. Res.–Atmos.* **1992,** *97*, (D18), 20703 20715.

158. Hallquist, M.; Wenger, J. C.; Baltensperger, U.; Rudich, Y.; Simpson, D.; Claeys, M.; Dommen, J.; Donahue, N. M.; George, C.; Goldstein, A. H.; Hamilton, J. F.; Herrmann, H.; Hoffmann, T.; Iinuma, Y.; Jang, M.; Jenkin, M. E.; Jimenez, J. L.; Kiendler-Scharr, A.; Maenhaut, W.; McFiggans, G.; Mentel, T. F.; Monod, A.; Prevot, A. S. H.; Seinfeld, J. H.; Surratt, J. D.; Szmigielski, R.; Wildt, J., The formation, properties and impact of secondary organic aerosol: current and emerging issues. *Atmos. Chem. Phys.* **2009,** *9*, (14), 5155 5236.

159. Mohler, O.; Field, P. R.; Connolly, P.; Benz, S.; Saathoff, H.; Schnaiter, M.; Wagner, R.; Cotton, R.; Kramer, M.; Mangold, A.; Heymsfield, A. J., Efficiency of the deposition mode ice nucleation on mineral dust particles. *Atmos. Chem. Phys.* **2006,** *6*, 3007 3021.

160. Prince, A. P.; Wade, J. L.; Grassian, V. H.; Kleiber, P. D.; Young, M. A., Heterogeneous reactions of soot aerosols with nitrogen dioxide and nitric acid: atmospheric chamber and Knudsen cell studies. *Atmos. Environ.* **2002,** *36*, (36 37), 5729 5740.

161. Chen, H. H.; Stanier, C. O.; Young, M. A.; Grassian, V. H., A kinetic study of ozone decomposition on illuminated oxide surfaces. *J. Phys. Chem. A* **2011,** *115*, (43), 11979 11987.

162. Chen, H. H.; Navea, J. G.; Young, M. A.; Grassian, V. H., Heterogeneous photochemistry of trace atmospheric gases with components of mineral dust aerosol. *J. Phys. Chem. A* **2011,** *115*, (4), 490 499.

163. Cwiertny, D. M.; Young, M. A.; Grassian, V. H., Chemistry and photochemistry of mineral dust aerosol. In *Annu. Rev. Phys. Chem.*, 2008; Vol. 59, pp 27 51.

164. Mogili, P. K.; Kleiber, P. D.; Young, M. A.; Grassian, V. H., Heterogeneous uptake of ozone on reactive components of mineral dust aerosol: An environmental aerosol reaction chamber study. *J. Phys. Chem. A* **2006,** *110*, (51), 13799 13807.

165. Navea, J. G.; Xu, S.; Stanier, C. O.; Young, M. A.; Grassian, V. H., Effect of ozone and relative humidity on the heterogeneous uptake of octamethylcyclotetrasiloxane and decamethylcyclopentasiloxane on model mineral dust aerosol components. *J. Phys. Chem. A* **2009,** *113*, (25), 7030 7038.

166. Prince, A. P.; Kleiber, P. D.; Grassian, V. H.; Young, M. A., Reactive uptake of acetic acid on calcite and nitric acid reacted calcite aerosol in an environmental reaction chamber. *Phys. Chem. Chem. Phys.* **2008,** *10*, (1), 142 152.

167. Styler, S. A.; Doussin, J.-F.; Formenti, P.; Donaldson, D. J., Light-induced SO_2 chemistry at the mineral dust surface. Submitted abstract, 2013 AGU Fall Meeting.

168. Zhang, Z.; Shang, J.; Zhu, T.; Li, H.; Zhao, D.; Liu, Y.; Ye, C., Heterogeneous reaction of NO_2 on the surface of montmorillonite particles. *J. Env. Sci. China* **2012,** *24*, (10), 1753 1758.

169. Roscoe, J. M.; Abbatt, J. P. D., Diffuse reflectance FTIR study of the interaction of alumina surfaces with ozone and water vapor. *J. Phys. Chem. A* **2005,** *109*, (40), 9028 9034.

170. Seisel, S.; Borensen, C.; Vogt, R.; Zellner, R., Kinetics and mechanism of the uptake of N_2O_5 on mineral dust at 298 K. *Atmos. Chem. Phys.* **2005,** *5*, 3423 3432.

171. Ullerstam, M.; Vogt, R.; Langer, S.; Ljungstrom, E., The kinetics and mechanism of SO_2 oxidation by O_3 on mineral dust. *Phys. Chem. Chem. Phys.* **2002,** *4*, (19), 4694 4699.

172. Armaroli, T.; Becue, T.; Gautier, S., Diffuse reflection infrared spectroscopy (DRIFTS): application to the in situ analysis of catalysts. *Oil Gas Sci. Technol.* **2004,** *59*, (2), 215 237.

173. Borensen, C.; Kirchner, U.; Scheer, V.; Vogt, R.; Zellner, R., Mechanism and kinetics of the reactions of NO_2 or HNO_3 with alumina as a mineral dust model compound. *J. Phys. Chem. A* **2000,** *104*, (21), 5036 5045.

174. Wu, L. Y.; Tong, S. R.; Wang, W. G.; Ge, M. F., Effects of temperature on the heterogeneous oxidation of sulfur dioxide by ozone on calcium carbonate. *Atmos. Chem. Phys.* **2011,** *11*, (13), 6593 6605.

175. Reeser, D. I.; Jammoul, A.; Clifford, D.; Brigante, M.; D'Anna, B.; George, C.; Donaldson, D. J., Photoenhanced reaction of ozone with chlorophyll at the seawater surface. *J. Phys. Chem. C* **2009,** *113*, (6), 2071 2077.

176. Kwamena, N. O. A.; Earp, M. E.; Young, C. J.; Abbatt, J. P. D., Kinetic and product yield study of the heterogeneous gas-surface reaction of anthracene and ozone. *J. Phys. Chem. A* **2006,** *110*, (10), 3638 3646.

177. Zhou, S.; Lee, A. K. Y.; McWhinney, R. D.; Abbatt, J. P. D., Burial effects of organic coatings on the heterogeneous reactivity of particle-borne benzo[a]pyrene (BaP) toward ozone. *J. Phys. Chem. A* **2012,** *116*, (26), 7050 7056.

178. Clifford, D.; Donaldson, D. J., Direct experimental evidence for a heterogeneous reaction of ozone with bromide at the air aqueous interface. *J. Phys. Chem. A* **2007,** *111*, (39), 9809 9814.

179. Michel, A. E.; Usher, C. R.; Grassian, V. H., Reactive uptake of ozone on mineral oxides and mineral dusts. *Atmos. Environ.* **2003,** *37*, (23), 3201 3211.

180. Deboudt, K.; Gloter, A.; Mussi, A.; Flament, P., Redox speciation and mixing state of iron in individual African dust particles. *J. Geophys. Res.–Atmos.* **2012,** *117*.

181. Usher, C. R.; Michel, A. E.; Stec, D.; Grassian, V. H., Laboratory studies of ozone uptake on processed mineral dust. *Atmos. Environ.* **2003,** *37*, (38), 5337 5347.

182. Zhao, Y.; Chen, Z.; Shen, X.; Huang, D., Heterogeneous reactions of gaseous hydrogen peroxide on pristine and acidic gas-processed calcium carbonate particles: effects of relative humidity and surface coverage of coating. *Atmos. Environ.* **2013,** *67*, 63 72.

183. Underwood, G. M.; Li, P.; Al-Abadleh, H.; Grassian, V. H., A Knudsen cell study of the heterogeneous reactivity of nitric acid on oxide and mineral dust particles. *J. Phys. Chem. A* **2001,** *105*, (27), 6609 6620.

184. Al-Abadleh, H. A.; Grassian, V. H., Heterogeneous reaction of NO_2 on hexane soot: a Knudsen cell and FT-IR study. *J. Phys. Chem. A* **2000,** *104*, (51), 11926 11933.

185. Underwood, G. M.; Li, P.; Usher, C. R.; Grassian, V. H., Determining accurate kinetic parameters of potentially important heterogeneous atmospheric reactions on solid particle surfaces with a Knudsen cell reactor. *J. Phys. Chem. A* **2000,** *104*, (4), 819 829.

186. Donaldson, D. J.; Mmereki, B. T.; Chaudhuri, S. R.; Handley, S.; Oh, M., Uptake and reaction of atmospheric organic vapours on organic films. *Faraday Discuss.* **2005,** *130*, 227 239.

187. Williams, L. R.; Manion, J. A.; Golden, D. M.; Tolbert, M. A., Laboratory measurements of heterogeneous reactions on sulfuric acid surfaces. *J. Appl. Meteorol.* **1994,** *33*, (7), 785 790.

188. Keyser, L. F.; Moore, S. B.; Leu, M. T., Surface reaction and pore diffusion in flow-tube reactors. *J. Phys. Chem.* **1991,** *95*, (14), 5496 5502.

189. Ma, Q. X.; He, H.; Liu, Y. C., In-situ DRIFTS study of hygroscopic behavior of mineral aerosol. *J. Environ. Sci. China* **2010,** *22*, (4), 555 560.

190. Gustafsson, R. J.; Orlov, A.; Badger, C. L.; Griffiths, P. T.; Cox, R. A.; Lambert, R. M., A comprehensive evaluation of water uptake on atmospherically relevant mineral surfaces: DRIFT spectroscopy, thermogravimetric analysis and aerosol growth measurements. *Atmos. Chem. Phys.* **2005,** *5*, 3415 3421.

191. Navea, J. G.; Chen, H. H.; Huang, M.; Carmichel, G. R.; Grassian, V. H., A comparative evaluation of water uptake on several mineral dust sources. *Environ. Chem.* **2010,** *7*, (2), 162 170.

192. Schuttlefield, J. D.; Cox, D.; Grassian, V. H., An investigation of water uptake on clays minerals using ATR-FTIR spectroscopy coupled with quartz crystal microbalance measurements. *J. Geophys. Res.–Atmos.* **2007,** *112*, (D21).

193. Rubasinghege, G.; Grassian, V. H., Role(s) of adsorbed water in the surface chemistry of environmental interfaces. *Chem. Comm.* **2013,** *49*, (30), 3071 3094.

194. Bedjanian, Y.; Romanias, M. N.; El Zein, A., Uptake of HO_2 radicals on Arizona Test Dust. *Atmos. Chem. Phys.* **2013,** *13*, (13), 6461 6471.

195. Goodman, A. L.; Bernard, E. T.; Grassian, V. H., Spectroscopic study of nitric acid and water adsorption on oxide particles: enhanced nitric acid uptake kinetics in the presence of adsorbed water. *J. Phys. Chem. A* **2001,** *105*, (26), 6443 6457.

196. Henderson, M. A., A surface science perspective on TiO_2 photocatalysis. *Surf. Sci. Rep.* **2011,** *66*, (6 7), 185 297.

197. Kebede, M. A.; Varner, M. E.; Scharko, N. K.; Gerber, R. B.; Raff, J. D., Photooxidation of ammonia on TiO_2 as a source of NO and NO_2 under atmospheric conditions. *J. Am. Chem. Soc.* **2013,** *135*, (23), 8606 8615.

198. Sullivan, R. C.; Thornberry, T.; Abbatt, J. P. D., Ozone decomposition kinetics on alumina: effects of ozone partial pressure, relative humidity and repeated oxidation cycles. *Atmos. Chem. Phys.* **2004,** *4*, 1301 1310.

199. Reyes, C. A.; Medina, M.; Crespo-Hernandez, C.; Cedeno, M. Z.; Arce, R.; Rosario, O.; Steffenson, D. M.; Ivanov, I. N.; Sigman, M. E.; Dabestani, R., Photochemistry of pyrene on unactivated and activated silica surfaces. *Environ. Sci. Technol.* **2000,** *34*, (3), 415 421.

200. Schuttlefield, J.; Rubasinghege, G.; El-Maazawi, M.; Bone, J.; Grassian, V. H., Photochemistry of adsorbed nitrate. *J. Am. Chem. Soc.* **2008,** *130*, (37), 12210 12211.

201. Zhou, X. L.; Gao, H. L.; He, Y.; Huang, G.; Bertman, S. B.; Civerolo, K.; Schwab, J., Nitric acid photolysis on surfaces in low-NO_x environments: significant atmospheric implications. *Geophys. Res. Lett.* **2003,** *30*, (23).

202. Zhu, C.; Xiang, B.; Zhu, L.; Cole, R., Determination of absorption cross sections of surface-adsorbed HNO_3 in the 290 330 nm region by Brewster angle cavity ring-down spectroscopy. *Chem. Phys. Lett.* **2008,** *458*, (4 6), 373 377.

203. Behymer, T. D.; Hites, R. A., Photolysis of polycyclic aromatic hydrocarbons adsorbed on fly ash. *Environ. Sci. Technol.* **1988,** *22*, (11), 1311 1319.

204. Korfmacher, W. A.; Wehry, E. L.; Mamantov, G.; Natusch, D. F. S., Resistance to photochemical decomposition of polycyclic aromatic hydrocarbon vapor adsorbed on coal fly ash. *Environ. Sci. Technol.* **1980,** *14*, (9), 1094 1099.

205. Gankanda, A.; Grassian, V. H., Nitrate photochemistry in NaY zeolite: product formation and product stability under different environmental conditions. *J. Phys. Chem. A* **2013,** *117*, (10), 2205 2212.

206. Rubasinghege, G.; Grassian, V. H., Photochemistry of adsorbed nitrate on aluminum oxide particle surfaces. *J. Phys. Chem. A* **2009,** *113*, (27), 7818 7825.

207. Foote, C. S., Definition of Type I and Type II photosensitized oxidation. *Photochem. Photobiol.* **1991,** *54*, (5), 659.

208. Jammoul, A.; Gligorovski, S.; George, C.; D'Anna, B., Photosensitized heterogeneous chemistry of ozone on organic films. *J. Phys. Chem. A* **2008,** *112*, (6), 1268 1276.

209. Forrester, S. M.; Knopf, D. A., Photosensitised heterogeneous oxidation kinetics of biomass burning aerosol surrogates by ozone using an irradiated rectangular channel flow reactor. *Atmos. Chem. Phys.* **2013,** *13*, (13), 6507 6522.

210. Monge, M. E.; Rosenorn, T.; Favez, O.; Mueller, M.; Adler, G.; Riziq, A. A.; Rudich, Y.; Herrmann, H.; George, C.; D'Anna, B., Alternative pathway for atmospheric particles growth. *PNAS* **2012,** *109*, (18), 6840 6844.

211. Frimmel, F. H., Photochemical aspects related to humic substances. *Environ. Int.* **1994,** *20*, (3), 373 385.

212. Dabestani, R.; Ivanov, I. N., A compilation of physical, spectroscopic and photophysical properties of polycyclic aromatic hydrocarbons. *Photochem. Photobiol.* **1999,** *70*, (1), 10 34.

213. Stemmler, K.; Ammann, M.; Donders, C.; Kleffmann, J.; George, C., Photosensitized reduction of nitrogen dioxide on humic acid as a source of nitrous acid. *Nature* **2006,** *440*, (7081), 195-198.

214. George, C.; Strekowski, R. S.; Kleffmann, J.; Stemmler, K.; Ammann, M., Photoenhanced uptake of gaseous NO_2 on solid organic compounds: a photochemical source of HONO? *Faraday Discuss.* **2005,** *130*, 195 210.

215. Stemmler, K.; Ndour, M.; Elshorbany, Y.; Kleffmann, J.; D'Anna, B.; George, C.; Bohn, B.; Ammann, M., Light induced conversion of nitrogen dioxide into nitrous acid on submicron humic acid aerosol. *Atmos. Chem. Phys.* **2007,** *7*, (16), 4237 4248.

216. Brigante, M.; Cazoir, D.; D'Anna, B.; George, C.; Donaldson, D. J., Photoenhanced uptake of NO_2 by pyrene solid films. *J. Phys. Chem. A* **2008,** *112*, (39), 9503 9508.

217. Monge, M. E.; D'Anna, B.; Mazri, L.; Giroir-Fendler, A.; Ammann, M.; Donaldson, D. J.; George, C., Light changes the atmospheric reactivity of soot. *PNAS* **2010,** *107*, (15), 6605 6609.

218. Sosedova, Y.; Rouviere, A.; Bartels-Rausch, T.; Ammann, M., UVA/Vis-induced nitrous acid formation on polyphenolic films exposed to gaseous NO_2. *Photochem. Photobiol. Sci.* **2011,** *10*, (10), 1680 1690.

219. Han, C.; Liu, Y.; He, H., Heterogeneous photochemical aging of soot by NO_2 under simulated sunlight. *Atmos. Environ.* **2013,** *64*, 270 276.

220. Net, S.; Gligorovski, S.; Pietri, S.; Wortham, H., Photoenhanced degradation of veratraldehyde upon the heterogeneous ozone reactions. *Phys. Chem. Chem. Phys.* **2010,** *12*, (27), 7603 7611.

221. Net, S.; Gligorovski, S.; Wortham, H., Light-induced heterogeneous ozone processing on organic coated particles: kinetics and condensed-phase products. *Atmos. Environ.* **2010,** *44*, (27), 3286 3294.

222. D'Anna, B.; Jammoul, A.; George, C.; Stemmler, K.; Fahrni, S.; Ammann, M.; Wisthaler, A., Light-induced ozone depletion by humic acid films and submicron aerosol particles. *J. Geophys. Res.–Atmos.* **2009,** *114*, (12), D12301, doi:10.1029/2008JD001237.

223. Baduel, C.; Monge, M. E.; Voisin, D.; Jaffrezo, J.-L.; George, C.; El Haddad, I.; Marchand, N.; D'Anna, B., Oxidation of atmospheric humic-like substances by ozone: a kinetic and structural analysis approach. *Environ. Sci. Technol.* **2011,** *45*, (12), 5238 5244.

224. Jammoul, A.; Dumas, S.; D'Anna, B.; George, C., Photoinduced oxidation of sea salt halides by aromatic ketones: a source of halogenated radicals. *Atmos. Chem. Phys.* **2009,** *9*, (13), 4229 4237.

225. De Laurentiis, E.; Maurino, V.; Minero, C.; Vione, D.; Mailhot, G.; Brigante, M., Could triplet-sensitised transformation of phenolic compounds represent a source of fulvic-like substances in natural waters? *Chemosphere* **2013,** *90*, (2), 881 884.

226. Carp, O.; Huisman, C. L.; Reller, A., Photoinduced reactivity of titanium dioxide. *Prog. Solid State Chem.* **2004,** *32*, (1 2), 33 177.

227. Gaya, U. I.; Abdullah, A. H., Heterogeneous photocatalytic degradation of organic contaminants over titanium dioxide: A review of fundamentals, progress and problems. *J. Photochem. Photobiol., C* **2008,** *9*, (1), 1 12.

228. Mo, J.; Zhang, Y.; Xu, Q.; Lamson, J. J.; Zhao, R., Photocatalytic purification of volatile organic compounds in indoor air: a literature review. *Atmos. Environ.* **2009,** *43*, (14), 2229 2246.

229. Monge, M. E.; George, C.; D'Anna, B.; Doussin, J. F.; Jammoul, A.; Wang, J.; Eyglunent, G.; Solignac, G.; Daele, V.; Mellouki, A., Ozone formation from illuminated titanium dioxide surfaces. *J. Am. Chem. Soc.* **2010,** *132*, (24), 8234 8235.

230. Baltrusaitis, J.; Jayaweera, P. M.; Grassian, V. H., Sulfur dioxide adsorption on TiO_2 nanoparticles: influence of particle size, coadsorbates, sample pretreatment, and light on surface speciation and surface coverage. *J. Phys. Chem. C* **2011,** *115*, (2), 492 500.

231. Hoffmann, M. R.; Martin, S. T.; Choi, W. Y.; Bahnemann, D. W., Environmental applications of semiconductor photocatalysis. *Chem. Rev.* **1995,** *95*, (1), 69 96.

232. Chen, H. H.; Nanayakkara, C. E.; Grassian, V. H., Titanium dioxide photocatalysis in atmospheric chemistry. *Chem. Rev.* **2012,** *112*, (11), 5919 5948.

233. Wang, Y.; Liu, C. S.; Li, F. B.; Liu, C. P.; Liang, J. B., Photodegradation of polycyclic aromatic hydrocarbon pyrene by iron oxide in solid phase. *J. Hazard. Mater.* **2009,** *162*, (2 3), 716 723.

234. Faust, B. C.; Hoffmann, M. R.; Bahnemann, D. W., Photocatalytic oxidation of sulfur dioxide in aqueous suspensions of alpha-Fe_2O_3. *J. Phys. Chem.* **1989,** *93*, (17), 6371 6381.

235. Zuo, Y. G.; Hoigne, J., Photochemical decomposition of oxalic, glyoxalic and pyruvic acid catalyzed by iron in atmospheric waters. *Atmos. Environ.* **1994,** *28*, (7), 1231 1239.

236. Dindar, B.; Icli, S., Unusual photoreactivity of zinc oxide irradiated by concentrated sunlight. *J. Photochem. Photobiol., A* **2001,** *140*, (3), 263 268.

237. Bandara, J.; Mielczarski, J. A.; Lopez, A.; Kiwi, J., 2. Sensitized degradation of chlorophenols on iron oxides induced by visible light: comparison with titanium oxide. *Appl. Catal., B* **2001,** *34*, (4), 321 333.

238. Ndour, M.; Conchon, P.; D'Anna, B.; Ka, O.; George, C., Photochemistry of mineral dust surface as a potential atmospheric renoxification process. *Geophys. Res. Lett.* **2009,** *36*.

239. Nie, W.; Wang, T.; Xue, L. K.; Ding, A. J.; Wang, X. F.; Gao, X. M.; Xu, Z.; Yu, Y. C.; Yuan, C.; Zhou, Z. S.; Gao, R.; Liu, X. H.; Wang, Y.; Fan, S. J.; Poon, S.; Zhang, Q. Z.; Wang, W. X., Asian dust storm observed at a rural mountain site in southern China: chemical evolution and heterogeneous photochemistry. *Atmos. Chem. Phys.* **2012,** *12*, (24), 11985 11995.

240. Pierotti, D.; Rasmussen, L. E.; Rasmussen, R. A., Sahara as a possible sink for trace gases. *Geophys. Res. Lett.* **1978,** *5*, (12), 1001 1004.

241. Kutsuna, S.; Chen, L.; Ohno, K.; Negishi, N.; Takeuchi, K.; Ibusuki, T.; Tokuhashi, K.; Sekiya, A., Laboratory study on heterogeneous decomposition of methyl chloroform on various standard aluminosilica clay minerals as a potential tropospheric sink. *Atmos. Chem. Phys.* **2003,** *3*, 1063 1082.

242. Benzoni, L.; Garbassi, F., Reactivity of fluorochloromethanes with desert sands. *Ber. Bunsen Ges. Phys. Chem.* **1984,** *88*, (4), 379 382.

243. Kutsuna, S.; Takeuchi, K.; Ibusuki, T., Adsorption and reaction of trichlorofluoromethane on various particles. *J. Atmos. Chem.* **1992,** *14*, (1 4), 1 10.

244. Prinn, R. G.; Weiss, R. F.; Miller, B. R.; Huang, J.; Alyea, F. N.; Cunnold, D. M.; Fraser, P. J.; Hartley, D. E.; Simmonds, P. G., Atmospheric trends and lifetime of CH_3CCl_3 and global OH concentrations. *Science* **1995,** *269*, (5221), 187 192.

245. Dlugi, R.; Güsten, H., The catalytic and photocatalytic activity of coal fly ashes. *Atmos. Environ.* **1983,** *17*, (9), 1765 1771.

246. Guillard, C.; Hoangvan, C.; Pichat, P.; Marme, F., Laboratory study of the respective roles of ferric oxide and released or added ferric ions in the photodegradation of oxalic acid in aerated liquid water. *J. Photochem. Photobiol., A* **1995,** *89*, (3), 221 227.

247. Miller, V.; Wehry, E. L.; Mamantov, G., Photochemical transformation of pyrene vapor deposited on eleven subfractions of a high-carbon coal stack ash. *Environ. Toxicol. Chem.* **1990,** *9*, (8), 975 980.

248. Dunstan, T. D. J.; Mauldin, R.; Zhong, J.; Hipps, A.; Wehry, E. L.; Mamantov, G., Adsorption and photodegradation of pyrene on magnetic, carbonaceous, and mineral subfractions of coal stack ash. *Environ. Sci. Technol.* **1989,** *23*, (3), 303 308.

249. Idriss, H.; Seebauer, E. G., Fast photoreactions of oxygenates on tropospheric fly ash particles. *J. Vac. Sci. Technol., A* **1996,** *14*, (3), 1627 1632.

250. Katagi, T., Photodegradation of pesticides on plant and soil surfaces. *Rev. Environ. Contam. Toxicol.* **2004,** *182*, 1 189.

251. Suzuki, Y.; Lopez, A.; Ponte, M.; Fujisawa, T.; Ruzo, L.; Toshiyuki, K., Photoinduced oxidation of the insecticide phenothrin on soil surfaces. *J. Agric. Food. Chem.* **2011,** *59*, (18), 10182 10190.

252. Lackhoff, M.; Niessner, R., Photocatalytic atrazine degradation by synthetic minerals, atmospheric aerosols, and soil particles. *Environ. Sci. Technol.* **2002,** *36*, (24), 5342 5347.

253. Menager, M.; Sarakha, M., Simulated solar light phototransformation of organophosphorus azinphos methyl at the surface of clays and goethite. *Environ. Sci. Technol.* **2013,** *47*, (2), 765 772.

254. Katagi, T., Photodegradation of the pyrethroid insecticide esfenvalerate on soil, clay minerals, and humic acid surfaces. *J. Agric. Food. Chem.* **1991,** *39*, (7), 1351 1356.

255. Gohre, K.; Miller, G., Singlet oxygen generation on soil surfaces. *J. Agric. Food. Chem.* **1983,** *31*, (5), 1104 1108.

256. Gohre, K.; Miller, G., Photochemical generation of singlet oxygen on non-transition-metal oxide surfaces. *J. Chem. Soc., Faraday Trans. 1* **1985,** *81*, (3), 793 800.

257. Baumanis, C.; Bloh, J.; Dillert, R.; Bahnemann, D., Hematite photocatalysis: dechlorination of 2,6-dichloroindophenol and oxidation of water. *J. Phys. Chem. C* **2011,** *115*, (51), 25442 25450.

258. Wu, F.; Li, J.; Peng, Z.; Deng, N., Photochemical formation of hydroxyl radicals catalyzed by montmorillonite. *Chemosphere* **2008,** *72*, (3), 407 413.

259. Gournis, D.; Karakassides, M. A.; Petridis, D., Formation of hydroxyl radicals catalyzed by clay surfaces. *Phys. Chem. Miner.* **2002,** *29*, (2), 155 158.

260. Kormann, C.; Bahnemann, D.; Hoffmann, M., Photocatalytic production of hydrogen peroxides and organic peroxides in aqueous suspensions of titanium dioxide, zinc oxide, and desert sand. *Environ. Sci. Technol.* **1988,** *22*, (7), 798 806.

261. Isidorov, V.; Klokova, E.; Povarov, V.; Kolkova, S., Photocatalysis on atmospheric aerosols: experimental studies and modeling. *Catal. Today* **1997,** *39*, 233 242.

Chapter 2

Substrate effects in the photoenhanced ozonation of pyrene

Reprinted (adapted) from Styler, S.A.; Loiseaux, M.-E.; Donaldson, D.J. "Substrate effects in the photoenhanced ozonation of pyrene" in *Atmospheric Chemistry and Physics* 2011, 11, 1243 1253.

Contributions:

Experiments at the aqueous surface were carried out by Marie-Eve Loiseaux under the direction of Sarah A. Styler. All other experiments were designed and performed by Sarah A. Styler. The manuscript was written by Sarah A. Styler, with critical comments from D. James Donaldson.

2.1 Introduction

In high-density urban environments, the percentage of land area covered by impervious surfaces roads, rooftops, side- walks, windows, and other surfaces that hinder the infiltration of water into soil[1] can reach 98%.[2] In 1998, Law and Diamond postulated that an organic film develops on these surfaces via the direct condensation of semi-volatile chemicals and/or via the deposition of secondary organic aerosols, which are in turn formed by the nucleation or condensation onto particles of the lower-vapour-pressure products of gas-phase reactions.[3] This organic coating, commonly referred to as "urban film", has been shown to enhance both the particle capture efficiency of the surface and the sorption of gas-phase chemicals to the surface, and thereby serve as a reservoir for hydrophobic organic compounds.[4, 5]

Chemical characterization of the organic fraction of urban film has revealed the presence of a variety of alkanes; a number of polar functional groups, including alcohols, esters, carboxylic acids, and carbohydrates; a large fraction of polymeric material; and a wide variety of compounds of toxicological significance.[6-11] Of particular interest to this study is the polycyclic aromatic hydrocarbon (PAH) profile observed in urban films: total PAH concentration has been shown to rise along a rural urban gradient[11] and can reach values as high as 62 000 ng m^{-2} in highly polluted urban environments.[6]

Generally, urban film contains an "aged" PAH profile as compared to that present in "fresh" vehicle exhaust: less reactive PAHs such as pyrene, phenanthrene, and fluoranthene dominate in the film while more reactive PAHs such as anthracene and benzo[a]pyrene are depleted.[5, 6, 11] This abundance pattern has been attributed to the rapid photo- oxidation of reactive PAH species, both in the gas phase and in the film itself.[6] Indeed, the results of one modelling study suggest that the large surface-area-to-volume ratio of urban film ($\sim 1.4 \times 10^7$) serves to promote chemical loss by re-

volatilization, wash-off, and photo- induced reactions.[12]

Motivated by these observations, our group has explored the role that organic films play in heterogeneous atmospheric reactive processes.[13-16] The heterogeneous ozonation of PAHs in solid films[16] and incorporated into artificial "window grime"[14] has been shown to proceed considerably faster than in the gas phase; in fact, the results of a modelling study suggest that ozonation on surface films is a major loss process for lower-volatility PAH species.[15] Given that the products of PAH ozonation are themselves photoactive,[17] these results imply that oxidative processes occurring within urban films may not only significantly influence the lifetime and relative abundance of PAH species but also promote other heterogeneous photoprocesses.

The products of PAH ozonation, which typically display enhanced toxicity,[18, 19] would not be expected to partition into the gas phase. Rather, their residence time in the film would be expected to be limited by rain-induced washoff, which has been shown to transfer the vast majority of PAH species to urban surface waters regardless of polarity.[20] This phenomenon has the potential to act as a pathway for contamination of urban soils and vegetation.

In recent years, a wide variety of studies have investigated heterogeneous photochemical processes occurring on solid organic surfaces[21-26] and organic compounds sorbed to silica particles,[27-29] where these surfaces have been envisaged as laboratory proxies for organic aerosol and urban film surfaces. These studies have shown that the heterogeneous reactive uptake of O_3 and NO_2 by a variety of photoactive organics is enhanced in the presence of light,[21-29] and have provided indications that such light-enhanced processes may alter aerosol wettability[21] and optical properties.[29] To date, however, the basic assumption underlying laboratory work in this area – that the reaction environment provided by simple proxy systems is sufficiently representative of that provided by real environmental surfaces – has yet to be comprehensively examined.

Guided by early experiments by Diamond et al.,[6] which showed that the urban film air and octanol air partition coefficients were comparable for a variety of PAH species, our group has previously used octanol as a proxy for the organic component of urban surface films.[14, 30] This, with the recent discovery that PAHs associate strongly with black carbon aerosol particles in the organic component of urban films,[10] leads one to expect that both solid PAH films and PAH-containing octanol films may be appropriate laboratory proxies for urban film surfaces. In this study, we test the assumption that photoenhanced processes are similar in these substrates by examining the influence of light upon the ozonation kinetics of pyrene, a representative PAH, at air octanol, air solid film, and air aqueous interfaces.

2.2 Materials and methods

2.2.1 Apparatus

The glancing-angle laser-induced fluorescence technique used in this study has been previously used by our group to investigate a range of heterogeneous oxidative processes.[14, 16, 31] All experiments described herein were conducted in the ~500 mL Teflon reaction chamber recently employed by Styler *et al.*[16] to study the ozonation kinetics of solid pyrene films. A quartz window present on the top of the reaction chamber allows for the illumination of samples. The chamber is also equipped with inlet and outlet ports for the introduction and venting of gaseous reagents. Gas-phase ozone was generated by passing a flow of high-purity oxygen (1 L min^{-1}, as measured by a mass flow meter) through a variable ozone generator. Prior to its introduction to the sample chamber, the ozone flow was directed through a 10-cm quartz-windowed absorption cell, where its concentration was determined by measuring the attenuation of the output of a 254-nm Hg pen-ray lamp passed through the cell.

Sample excitation was accomplished using either a pulsed nitrogen laser (337 nm) or a Nd:YAG-pumped tunable optical parametric oscillator (operated at 266 nm), which

were aligned such that the incoming beam passed through a quartz window, impinged on the sample surface at a glancing angle, and exited the chamber through a second quartz window opposite the first. The lasers were operated at a repetition rate of ~10 Hz and had pulse energies of ~260 μJ pulse^{-1} and ~3 mJ pulse^{-1}, respectively.

Pyrene fluorescence was collected perpendicular to the sample by a 7-mm diameter liquid light guide positioned ~1 cm above it. The fluorescence was imaged into a monochromator and the wavelength-resolved intensity was then detected by a photomultiplier tube, the output of which was sent to a digital oscilloscope. The resulting fluorescence decay curves were averaged over 16 laser shots; a 25 70 ns segment of each such averaged curve was sampled by a Lab-VIEW data-acquisition program and stored for later analysis.

2.2.2 Sample preparation

Octanol-based films[14, 30] were prepared by dispensing 20 μL of a 10^{-5} M or 10^{-2} M solution of pyrene in 1-octanol onto a microscope slide that had been previously greased with ~1 mg silicone stopcock grease (Dow Corning). A spatula was then used to smear the pyrene solution across the surface of the slide such that it became well mixed with the stopcock grease. Solid pyrene films were prepared by dispensing 20 μL of a 2.5 mM solution of pyrene in methanol onto a clean microscope slide and allowing the methanol to evaporate. The surface coverage of films prepared using this technique (~2.5 μg cm^{-2}) is of the same order of magnitude as the surface coverage used for our previous investigation of the ozonation of solid pyrene films.[16] In order to study the ozonation kinetics of pyrene at the air-aqueous interface, 2.4 mL of a 2.6×10^{-7} M solution of pyrene in 18 MΩ deionized water was used to fill a shallow Petri dish positioned below the liquid light guide. One set of experiments was also conducted with a five times more dilute pyrene solution.

2.2.3 Fluorescence spectra and ozonation kinetics studies

Wavelength-resolved fluorescence spectra of pyrene at the surface of the three substrates investigated in this study were obtained under an oxygen atmosphere. For each sample, the monochromator was manually scanned to monitor fluorescence intensity at 1-nm intervals over the wavelength range of interest.

Since pyrene fluorescence is efficiently quenched by oxygen,[14] all kinetics experiments began by allowing pure oxygen to flow through the reaction chamber. Once the pyrene fluorescence intensity reached a constant value, the ozone generator was turned on. The heterogeneous ozonation of pyrene at the surface of dilute octanol films and at the air aqueous interface was followed by monitoring the time-dependent decay of fluorescence from monomeric pyrene (*vide infra*) upon exposure to gas-phase ozone. Experiments at the air aqueous interface were performed at ozone concentrations ranging from 1.8×10^{15} molec cm^{-3} to 5.8×10^{15} molec cm^{-3}; fluorescence was measured at either 392 nm or 372 nm. Experiments at the air octanol interface were performed using ~8×10^{15} molec cm^{-3} ozone and monitored at 384 nm. The heterogeneous ozonation of solid pyrene films and pyrene at the surface of concentrated octanol films was followed by monitoring the time-dependent decrease in excimer fluorescence at 466 nm (*vide infra*) upon exposure to ~6×10^{15} and ~8×10^{15} molec cm^{-3} ozone, respectively. All reactions were performed at room temperature and atmospheric pressure.

Samples were illuminated using the optically filtered ($\lambda > 295$ nm) output of a 150 W xenon arc lamp (Oriel Corporation). The output of the light source was blocked for ~5 s prior to the acquisition of fluorescence intensity data in order to ensure that pyrene fluorescence excited by the laser was the only signal collected by the liquid light guide.

2.2.4 Chemicals

1-octanol (99%, Aldrich), pyrene (98%, Aldrich), and methanol (ACS grade, Aldrich) were used without purification. Oxygen gas (99.995%, BOC Gases) was used as delivered.

2.3 Results

2.3.1 Fluorescence spectra

The vibronic fine structure of pyrene monomer fluorescence shows a strong dependence upon the local solvent environment: in particular, the ratio of intensities of the third (III) to the first (I) peaks in the fluorescence emission spectrum is lower in more polar environments than in less polar ones.[32] Figure 2-1a compares the fluorescence emission spectrum observed for pyrene at the surface of dilute octanol solution with that observed for pyrene at the air aqueous interface.[14] The III/I ratio observed for pyrene at the air aqueous interface (~0.6) is considerably lower than that observed at the surface of dilute octanol films (~1.2). This observation suggests that pyrene experiences a more polar environment at the air aqueous interface than at the air octanol interface.

Figure 2-1b displays the fluorescence emission spectra of pyrene measured at the surface of dilute and concentrated solutions of pyrene in octanol and of pyrene at the surface of solid film samples. At high bulk solution concentrations, the fluorescence spectrum of pyrene at the surface of octanol films contains a broad, red-shifted, featureless band characteristic of emission from excimeric pyrene.[33] Solid pyrene films, by contrast, exhibit unstructured, excimer-type fluorescence exclusively.[34]

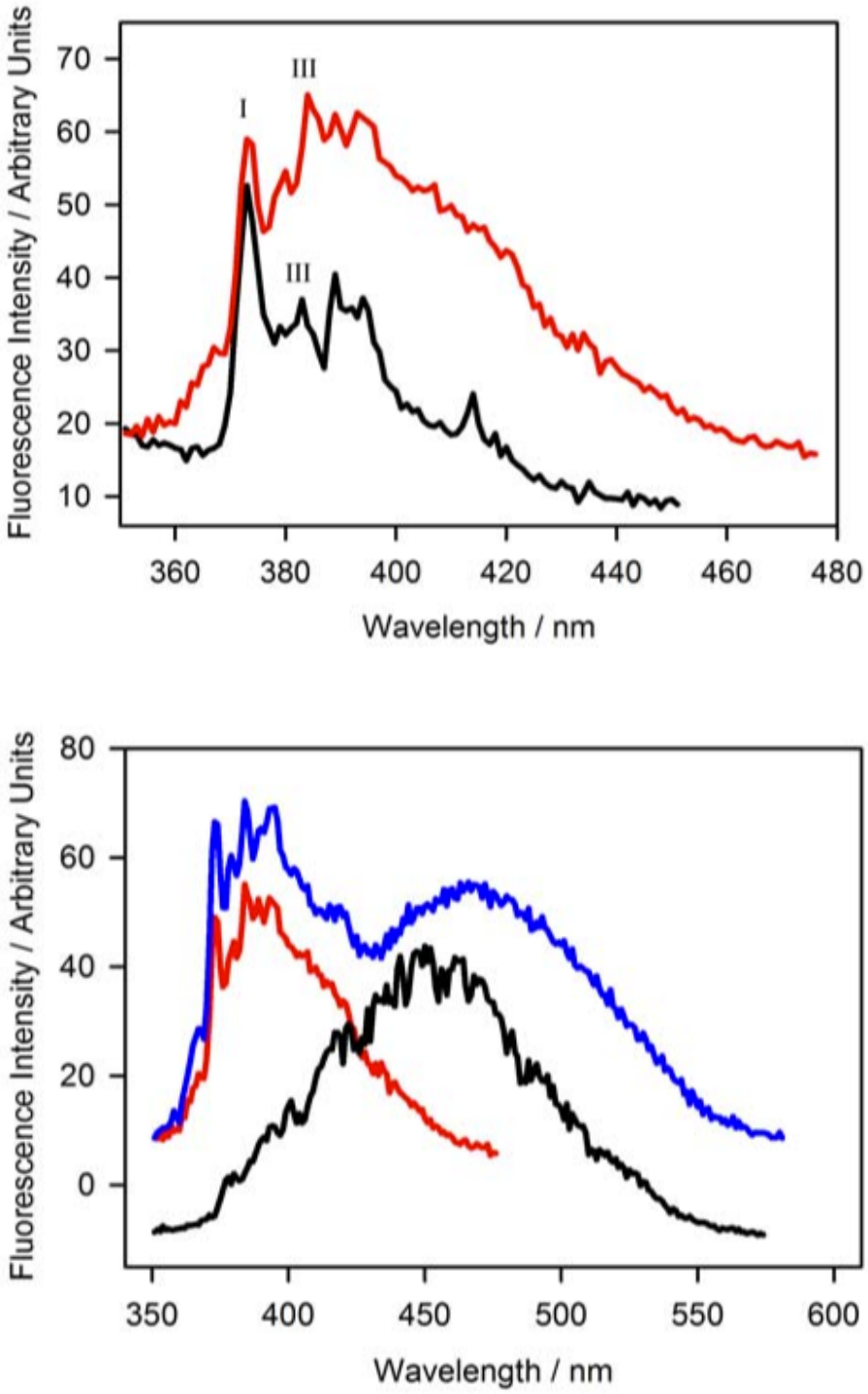

Figure 2-1 Fluorescence emission spectra of pyrene measured at the surface of a) 2.6×10^{-7} M solution of pyrene in deionized water (black) excited at 337 nm and 10^{-5} M pyrene in octanol (red) spread on silicone grease and excited at 337 nm; and b) 10^{-5} M (red) and 10^{-2} M (blue) pyrene in octanol spread on silicone grease and excited at 337 nm, and 2.5 μg cm^{-2} surface coverage solid pyrene film (black) prepared via evaporation from methanol solution and excited at 266 nm.

2.3.2 Dark ozonation kinetics

The heterogeneous ozonation kinetics of pyrene were determined by fitting the time-dependent loss in fluorescence intensity upon exposure to ozone to the exponential function:

$$I = I_0 e^{-k_{obs}t} + c \qquad (1)$$

Here, I_0 is the initial fluorescence intensity, I is the fluorescence intensity after time *t*, k_{obs} is the observed fluorescence decay rate due to reaction, and c is a constant that accounts for variations in background signal intensities. The values of k_{obs} obtained in this manner are displayed in Table 2-1.

Because ozone concentrations remained constant during each experiment, k_{obs} is a pseudo-first-order rate coefficient. As exemplified in Figure 2-2 by the quality of the fits for the heterogeneous ozonation of pyrene at the air aqueous interface, the reaction is first-order with respect to pyrene in all of the environments under study ($R^2 > 0.85$ for solid films and > 0.98 at the air aqueous and air octanol interfaces). The value of k_{obs} at the air octanol interface compares well with that previously observed by Kahan *et al.*[14] for pyrene at the surface of decanol-based urban film proxies. The k_{obs} obtained for solid pyrene films is similar to that obtained by our group under comparable experimental conditions.[16]

The solid symbols in Figures 2-3a and b show the dependence of k_{obs} on gas-phase ozone concentration for solid pyrene films[16] and pyrene at the air aqueous interface, respectively, under dark conditions. As shown by the hollow square in Figure 2-3b, a comparable k_{obs} is observed at the surface of a five times more dilute pyrene solution. This result implies that the kinetics observed at the air aqueous interface are not influenced by pyrene pyrene interactions. The solid lines in Fig. 3a and b illustrate fits to the data assuming a Langmuir Hinshelwood kinetic model, in which ozone adsorbs to the surface prior to reaction and the rate of reaction depends upon the

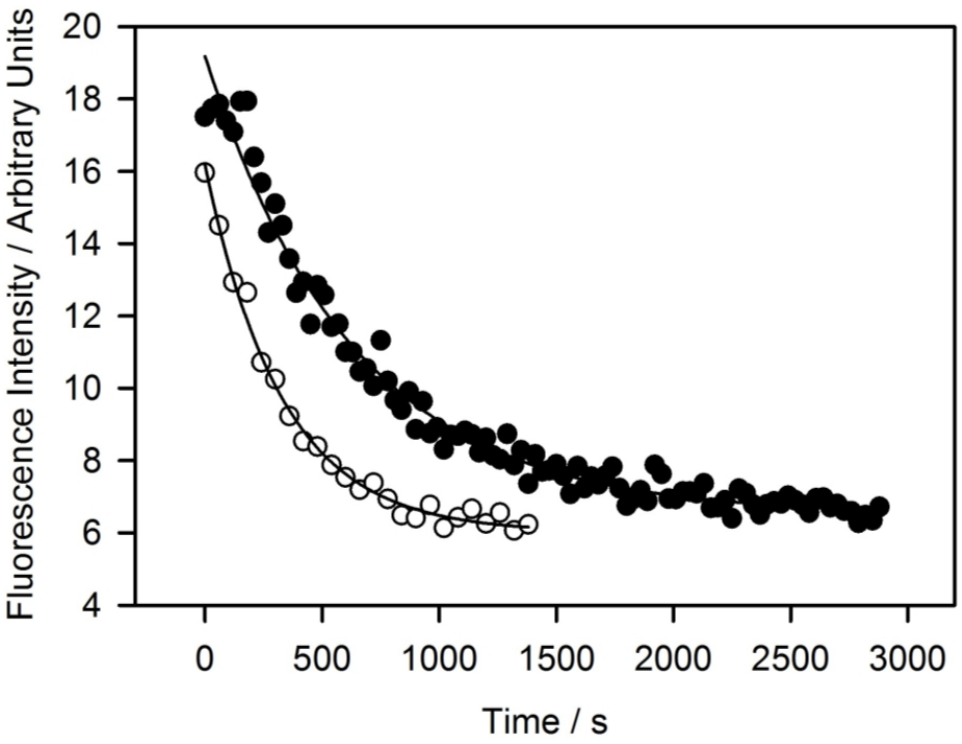

Figure 2-2 Decay in fluorescence emission intensity at the surface of 2.6×10^{-7} M pyrene in deionized water (337 nm excitation; 392 nm emission) upon exposure to ~6×10^{15} molecules cm^{-3} ozone. The solid circles show the dark reaction while the hollow circles show the light reaction. All experiments were performed at room temperature and atmospheric pressure.

---

surface concentration of both species.[35] Under these conditions, the dependence of k_{obs} upon gas-phase ozone concentration can be fit to an equation of the following form:

$$k_{obs} = \frac{A\,[O_3\,(g)]}{B + [O_3\,(g)]} \qquad (2)$$

Here, A is equal to the product of the bimolecular rate constant k^{II} and the maximum number of surface sites available for ozone adsorption N_{surf}, and B represents a ratio of surface desorption to adsorption from both bulk phases.[31] As shown in Table 2-1, the Langmuir Hinshelwood parameters obtained in the present study for pyrene at the

air-aqueous interface agree well with those previously obtained by Donaldson *et al.*[13]

2.3.3 Ozonation kinetics under illumination

At the highest ozone concentration employed in these experiments (~8 × 10^{15} molecules cm^{-3}), the average pseudo-first-order rate coefficient for ozonation of pyrene under illumination at the surface of both dilute and concentrated octanol films is the same as that observed in the dark. At an ozone concentration of ~6 × 10^{15} molecules cm^{-3}, the ozone-driven loss of pyrene at the air aqueous interface and at the surface of solid pyrene films displays a modest enhancement in the presence of light. These results are summarized in Table 2-1.

The average k_{obs} for the heterogeneous ozonation of solid-film pyrene increases from (2.44 ± 0.92) × 10^{-3} s^{-1} in the dark to (4.71 ± 0.81) × 10^{-3} s^{-1} upon illumination at an ozone concentration of ~6 × 10^{15} molec cm^{-3}. This enhancement, illustrated by the triangle symbols in Figure 2-3a, is comparable to that previously observed by our group for solid-film pyrene under similar conditions: at an ozone concentration of ~8 × 10^{15} molec cm^{-3}, the average k_{obs} increased from (3.2 ± 1.1) × 10^{-3} s^{-1} in darkness to (5.3 ± 1.5) × 10^{-3} s^{-1} in the presence of light.[16] The photolysis of solid-sorbed pyrene is known to be slow.[36, 37] With no ozone present, we observe only a slow evaporative loss of pyrene upon illumination.

The hollow symbols in Figures 2-3a and b show the dependence of k_{obs} on gas-phase ozone concentration for solid pyrene films[16] and pyrene at the air aqueous interface, respectively, under illuminated conditions. As shown by the intercept in Figure 2-3b, photochemical loss of pyrene at the water surface in the absence of ozone cannot fully account for the enhancement observed at the air aqueous interface. Unlike the pseudo-first-order ozonation rate of illuminated pyrene solid films, which displays a Langmuir Hinshelwood-type dependence on gas-phase ozone concentration,[16] the pseudo-first-order ozonation rate of pyrene at the air-aqueous interface varies linearly

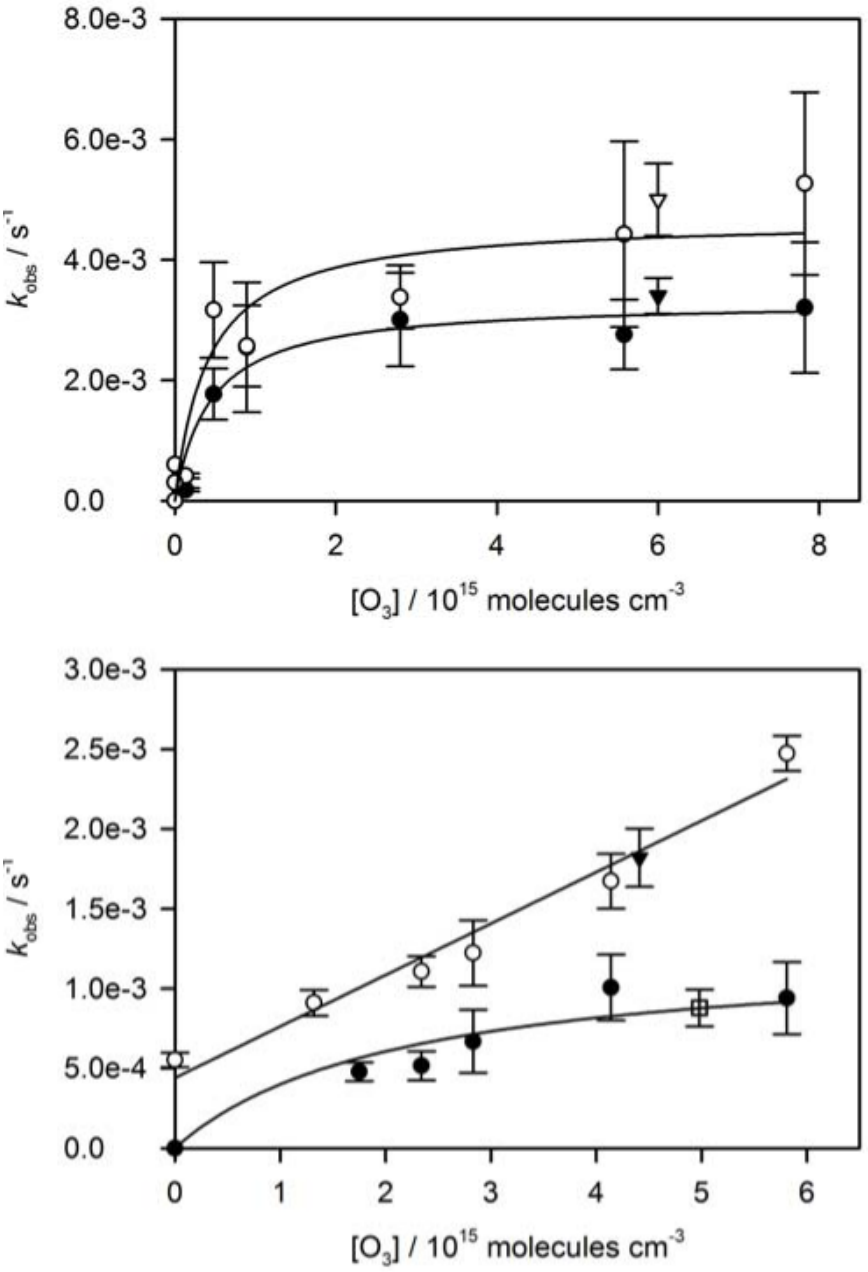

Figure 2-3 Heterogeneous loss rate of pyrene at the a) air–solid film and b) air–aqueous interface as a function of gas-phase ozone concentration. The solid circles represent the dark reaction while the hollow circles represent the light reaction. In a) the inverted triangles represent the current experiments; all other data is adapted from Styler et al. (2009). The inverted solid triangle in b) represents experiments performed using a 320 nm long-pass optical filter; all other experiments were performed using a 295 nm filter. The hollow square in b) represents experiments performed at the surface of five times more dilute aqueous pyrene solutions under dark conditions. All experiments were performed at room temperature and atmospheric pressure.

with gas-phase ozone concentration. At the surface of a substantially more dilute pyrene solution, we again observed a linear dependence of pyrene loss rate on ozone concentration (not shown in Figure 2-3).

In order to verify that the enhanced pyrene loss observed under illumination does not arise from reaction of pyrene with OH produced by the photolysis of ozone and subsequent reaction of $O(^1D)$ with water vapour, some experiments were performed using a 320 nm long-pass optical filter. $O(^1D)$ production under these conditions estimated using measured filter transmission spectra and literature values for ozone absorption cross section and $O(^1D)$ quantum yield[38] is expected to be two orders of magnitude lower than $O(^1D)$ production using the 295 nm long-pass filter. However, as illustrated by the solid inverted triangle in Figure 2-3b, we observed a near-identical k_{obs} in these experiments, which implies that OH production does not contribute to the observed kinetics.

2.4 Discussion

2.4.1 Heterogeneous ozonation of pyrene under dark conditions

Previous mechanistic studies of the reaction of gas-phase ozone with solid films of pyrene,[16] pyrene at the surface of dilute decanol-based urban film proxies,[14] and pyrene at the air aqueous interface[13] have shown that all three reactions proceed via a Langmuir-Hinshelwood mechanism, in which ozone adsorbs to the surface prior to reaction and the rate of reaction depends upon the surface concentration of both species.[35]

The Langmuir-Hinshelwood A parameter contains the two-dimensional rate coefficient for reaction: as shown in Table 2-1, its value for solid-film pyrene is approximately three times larger than for pyrene at the air-aqueous interface and approximately five times larger than for pyrene at the surface of octanol films. This

	k_{obs} (O_3) / 10^{-3} s^{-1}	k_{obs} ($h\nu$ + O_3) / 10^{-3} s^{-1}	k_{obs} ($h\nu$) / 10^{-3} s^{-1}	A / 10^{-3} s^{-1}	B / 10^{15} molec cm^{-3}
solid film	2.44 ± 0.92[a] 3.2 ± 1.1[b,c]	4.71 ± 0.81[a] 5.3 ± 1.5[b,c]	small evaporative loss	3.4 ± 0.3 (dark)[b,c] 5.0 ± 0.6 ($h\nu$)[b,c]	0.5 ± 0.2 (dark)[b,c] 0.6 ± 0.3 ($h\nu$)[b,c]
air octanol interface (10^{-5} M)	0.65±0.18b 0.7±0.1d	0.67[b]	--	--	--
air octanol interface (10^{-2} M)	0.63	0.55	--	--	--
air aqueous interface	1.7±0.7[a]	2.8±0.7[a]	0.55± 0.04[a]	1.5 (dark)[e] 1.3 ± 0.4 (dark)[a]	2.1 (dark)[e] 2.1 ± 1.6 (dark)[a]

Table 2-1 Kinetic parameters for pyrene loss as a function of proxy identity

result echoes previous observations of enhanced PAH reactivity in the solid state: the A parameters for the heterogeneous ozonation of both benzo[a]pyrene and anthracene are larger when they are sorbed to solid surfaces[39, 40] than when they are incorporated into octanol- or decanol-based films.[14]

It is tempting to propose that the heterogeneous ozonation kinetics of PAHs dissolved in organic films might be limited by the diffusion of PAHs from bulk solution to the air film boundary. After a thorough examination of this issue, however, Kwamena *et al.*[41] concluded that such liquid-phase diffusion constraints are likely not important. This suggests that the mechanism by which the reaction environment influences the heterogeneous reaction of PAHs with adsorbed ozone is chemical in nature.

In organic solvents, the rate-determining step for PAH ozonation is believed to be the formation of a charged π- or σ-complex with ozone via electrophilic attack.[42] This

implies that both the polarity of the reaction environment and the electrophilicity of ozone within the reaction environment may influence the rate of PAH ozonation. If such effects were important at interfaces, one would expect the heterogeneous ozonation rate of PAHs to vary as a function of surface polarity. Our work provides some support for this hypothesis: the pseudo-first-order rate coefficient for ozonation of pyrene at the air aqueous interface is somewhat larger than that observed for pyrene at the air octanol interface. However, this observation is far from universal: the Langmuir-Hinshelwood A parameter for the reaction of ozone with anthracene has been observed to be virtually identical ($\sim 2.5 \times 10^{-3}$ s^{-1}) when anthracene is present at the surface of "pure" water, water coated with a monolayer of 1-octanol, or decanol-based urban film proxies.[14, 31] Taken together, these results suggest that the role that the chemical nature of the surface plays in influencing the heterogeneous reaction of PAHs with adsorbed ozone under dark conditions is at best uncertain.

As illustrated in Fig. 2-1b, we observe broad, featureless, excimer-type fluorescence at the surface of both solid pyrene films and concentrated octanol films. On solid surfaces, excimeric emission by pyrene has been largely attributed to absorption and subsequent emission by weakly bound ground-state associated pairs.[36, 43] Evidence for the existence of higher aggregates in the solid state is provided by the absorption spectrum of thin pyrene films, which exhibits a long-wavelength tail.[44] The enhanced ozonation loss rate observed for PAHs in the solid-film environment as compared to the organic-film environment has been previously postulated to arise from an enhanced reactivity of such self-associated PAHs with ozone.[14] Indeed, it seems plausible that the extended electronic structure of the solid film and the resultant resonance stabilization of charged reaction intermediates might confer enhanced heterogeneous reactivity toward ozone.

Until recently, ground-state PAH aggregation was not believed to occur in solution: the broad, structureless emission observed for solution-phase pyrene and other PAHs

at high concentrations had been attributed exclusively to "dynamic" excimers transient dimers existing only in the excited state and formed by the interaction of an excited molecule with one in the ground state.[45] A number of recent studies, however, have suggested that ground-state associated pairs and/or aggregates, whose formation has been shown to be promoted by hydrophobic, π-stacking interactions,[46] may also contribute to the emission profile of concentrated pyrene solutions.[47-50] The role that these species play in the reactivity of pyrene at the air organic interface is currently unclear, however, and warrants further study.

2.4.2 Heterogeneous ozonation of pyrene under illumination

Some mechanistic insight into our observations can be provided by considering the various photochemical and photophysical deactivation pathways available to the singlet-state monomeric and excimeric pyrene species formed upon absorption of light in the presence of ozone and oxygen. These deactivation pathways are displayed schematically in Scheme 2-1.

First, singlet-state pyrene may form a charge-transfer complex with adsorbed ozone, which may subsequently undergo reactive decay to yield an oxygenated pyrene radical and molecular oxygen. This pathway, referred to in Scheme 2-1 and in the following discussion as an *A*-type pathway, is expected to lead to photoenhanced pyrene loss: indeed, we have previously invoked the existence of a charge-transfer complex between solid pyrene films and adsorbed ozone to explain the observed light-induced enhancement of the heterogeneous reaction rate for these two species.[16] Of course, singlet-state pyrene may also form a charge-transfer complex with adsorbed oxygen, giving rise to pyrene ions in the absence of ozone. However, in the present experiments, the photochemical loss rate of solid-film pyrene under a pure oxygen atmosphere was insignificant over the time scale of the ozonation reaction.

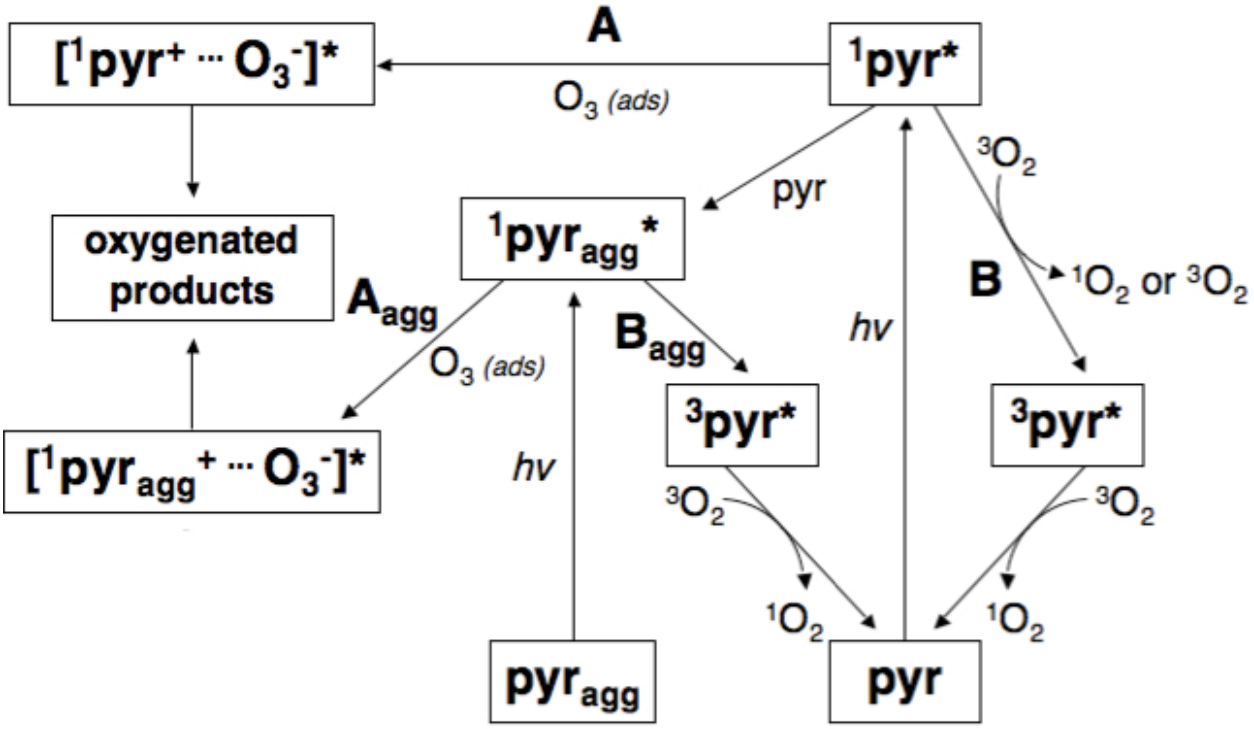

Scheme 2-1 Photophysical and photochemical deactivation pathways available to excited-state pyrene molecules.

Singlet-state pyrene may also be deactivated via oxygen- assisted intersystem crossing (with or without the production of excited singlet molecular oxygen, $O_2(^1\Delta_g)$;[51, 52] the resultant lower-energy triplet state may then be quenched by oxygen to yield ground-state pyrene with the concomitant production of $O_2(^1\Delta_g)$.[52, 53] Given that pyrene does not react efficiently with $O_2(^1\Delta_g)$,[36, 54] this pathway, referred to in Scheme 2-1 and in the following discussion as a *B*-type pathway, can be viewed purely as a photophysical deactivation process.

The relative importance of *A*-type and *B*-type pathways and thus the propensity of pyrene to undergo photoenhanced ozonation depends strongly on the nature of the reaction medium. In non-polar solvents such as octanol, *A*-type pathways are insignificant: although there is some evidence for the formation of contact charge-

transfer (CCT) complexes between pyrene and dissolved oxygen molecules in cyclohexane solution, the value of the CCT quenching constant is two orders of magnitude smaller than the dynamic, collision-based quenching constant.[55]

Our previous observations of order-of-magnitude enhancements in pyrene photolysis rates in bulk aqueous solution over those observed in organic solution[56] and our present failure to observe a light-induced enhancement in the heterogeneous ozonation of pyrene at the air octanol interface both provide additional evidence for the solvent dependence of these charge-transfer-type reactions. Persuasive evidence for the predominance of *B*-type pathways in non-polar solvents has been provided by a number of authors: the fraction of excited pyrene singlet states which yields triplet states upon quenching by oxygen, for example, has been shown to be unity in toluene[57] and cyclohexane.[52, 58]

As shown in Table 2-1, the heterogeneous ozonation of solid-film pyrene displays a modest enhancement upon illumination. These results are consistent with observations of *A*-type behaviour for solid-sorbed pyrene: pyrene is known to form charge-transfer complexes upon adsorption to reactive sites on silica gel;[59] at higher surface loadings on silica alumina and γ-alumina, pyrene radical cations react with parent molecules to form monopositive dimeric radical cations.[60]

Solid-phase pyrene is also known to undergo charge-transfer processes with adsorbed gaseous species: the formation of HONO upon reaction of an illuminated pyrene film with NO_2, for example, has been attributed to the photoreduction of NO_2 by excited-state pyrene.[22] Finally, pyrene photooxidation on surfaces is generally believed to proceed via an electron-transfer mechanism.[36, 61, 62] On silica gel, the pyrene radical cation has been shown to be an intermediate of the photooxidation process.[61]

A-type pathways are also common in polar solvents: a number of authors[51, 53, 57, 63] have attributed non-quantitative triplet yields for excited-state pyrene upon quenching by

oxygen in polar solvents to the existence of charge-transfer interactions between pyrene and oxygen that compete with oxygen-enhanced intersystem crossing; in some cases, absorbance attributable to the pyrene cation has been observed.[57] In addition, pyrene photooxidation in aqueous solution is be- lieved to occur via a charge-transfer process.[64, 65] Specifically, it is thought to occur either via the excitation of CCT pairs or via electron transfer to oxygen from the excited singlet state of pyrene; in both cases, the subsequent reaction of the resultant charge-transfer complex between the pyrene cation radical and superoxide yields oxidized products.[65]

As shown in Table 2-1 and illustrated in Figure 2-3b, the pseudo-first-order rate coefficient k_{obs} for the heterogeneous ozonation of pyrene at the air aqueous interface displays a modest enhancement upon illumination. Interestingly, this enhancement is accompanied by a change in kinetic mechanism: as illustrated in Figure 2-3b, while k_{obs} displays a Langmuir Hinshelwood-type dependence upon gas-phase ozone concentration under dark conditions, it increases linearly with gas-phase ozone concentration upon illumination. We attribute this change in mechanism to an increased favourability of *A*-type pathways at the highly polar air aqueous interface.

The linear dependence of k_{obs} upon gas-phase ozone concentration observed in the present experiments suggests that the charge-transfer reaction between pyrene and ozone at the air aqueous interface is sufficiently favourable to occur via a non-adsorptive Eley Rideal-type mechanism, in which reaction occurs upon the collision of a gas-phase ozone molecule with an adsorbed excited-state pyrene molecule.[35] At the aqueous surface, the ozonide anion thus formed can react to form hydroxyl radical, which can in turn react with adsorbed pyrene. The pyrene radical cation formed as a result of the initial charge-transfer reaction would be expected to react with water to form 1-hydroxypyrene and further oxidized products.[65] Our proposed mechanism can be summarized as follows:

Pyr + $h\nu$	→	Pyr*	*(3)*
Pyr* + O_3 *(ads)*	→	oxidized products	*(4)*
Pyr + O_3 *(g)*	→	$Pyr^+ + O_3$	*(5)*
O_3 + H_2O	→	OH + O_2 + OH	*(6)*
OH + Pyr	→	oxidized products	*(7)*
Pyr + H_2O	→	oxidized products	*(8)*

If the electron-transfer/hydrolysis steps (reactions 5 and 6) are sufficiently fast, the adsorbed concentration of ozone at the illuminated aqueous surface will be small. Under these conditions, loss of pyrene at the interface may be dominated by reaction with hydroxyl radical (reaction 7) rather than with adsorbed ozone (reaction 4). In this manner, the Langmuir Hinshelwood mechanism observed in the dark, which would involve reaction between co-adsorbed pyrene and ozone, would evolve into one in which the ozone dependence reflects the delivery of gas-phase ozone to the surface, where its reduction is very rapid. A similar mechanism has been proposed to explain the photoenhanced reaction of chlorophyll with ozone at the salt-water surface, which also shows a linear dependence on gas-phase ozone concentration.[66]

In summary, compelling evidence exists for the prevalence of charge-transfer pathways and thus the possibility for the photoenhanced loss of pyrene via the formation of charge- transfer complexes with adsorbed ozone for excited-state pyrene at the air solid film interface. By contrast, the deactivation of excited-state pyrene in non-polar environments is expected to proceed primarily via oxygen-assisted intersystem crossing. Indeed, the results obtained in this study fit well within this conceptual framework: we see a photoinduced enhancement of the heterogeneous ozonation rate of solid-film pyrene but not of pyrene at the non-polar air octanol film interface. At the highly polar air aqueous interface, our results suggest that a charge-

transfer mechanism between gas-phase ozone and adsorbed pyrene is activated upon illumination. We propose that the photoenhanced loss of pyrene at the air aqueous interface arises via the reaction of pyrene with photoproduced hydroxyl radical or via the reaction of pyrene cation radical with water.

2.5 Conclusions

Under dark conditions, our results suggest that the heterogeneous reactivity of pyrene toward ozone is influenced by a complex set of substrate substrate and substrate surface interactions. In the presence of light, the behaviour of pyrene at the surface of the three reaction environments under study differs more dramatically: while the heterogeneous ozonation of solid-film pyrene displays a light enhancement, the ozonation of pyrene at the air octanol film interface does not; moreover, the ozone-induced loss of pyrene at the illuminated air aqueous interface not only occurs more quickly than in the dark but also displays a different dependence upon gas-phase ozone concentration.

Our proposed mechanism of photoenhancement, which involves the transfer of charge from pyrene to either gas-phase or adsorbed ozone and which thus would be expected to be more favourable at the air solid film and air aqueous interfaces than at the non-polar air octanol film interface, fits well with these observations. In real environments, however, reactive molecules of interest are not present at bulk concentrations in a single solvent but rather are present as trace solutes in a complex matrix, the other components of which may alter their photophysical and photochemical properties. The work presented here on aqueous surfaces implies that photoenhanced processes may well be important for PAHs dispersed at low concentrations in aqueous environments. However, since real urban films have been shown to contain large quantities of sulfates, nitrates, and metals, which serve to increase the polarity of the medium and thus promote charge-transfer processes, and

which may serve as photocatalysts themselves,[8] our failure to observe light-enhanced ozonation at the air octanol interface may not be environmentally significant.

In summary, the results obtained in this study suggest that a variety of heterogeneous photoprocesses occurring in urban film proxies may depend strongly upon the type of surface that is used to mimic the urban film environment, and further caution that the use of proxies that only superficially resemble urban films may not necessarily give an accurate picture of reactions occurring in the environment.

2.6 References

1. Arnold, C. L.; Gibbons, C. J., Impervious surface coverage the emergence of a key environmental indicator. *J. Amer. Plann. Assoc.* **1996,** *62*, (2), 243 258.

2. Boyd, M. J.; Bufill, M. C.; Knee, R. M., Pervious and impervious runoff in urban catchments. *Hydrol. Sci. J.* **1993,** *38*, (6), 463 478.

3. Law, N. L.; Diamond, M. L., The role of organic films and the effect on hydrophobic organic compounds in urban areas: an hypothesis. *Chemosphere* **1998,** *36*, (12), 2607 2620.

4. Butt, C. M.; Diamond, M. L.; Truong, J.; Ikonomou, M. G.; Helm, P. A.; Stern, G. A., Semivolatile organic compounds in window films from lower Manhattan after the September 11th World Trade Center attacks. *Environ. Sci. Technol.* **2004,** *38*, (13), 3514 3524.

5. Liu, Q. T.; Diamond, M. L.; Gingrich, S. E.; Ondov, J. M.; Maciejczyk, P.; Stern, G. A., Accumulation of metals, trace elements and semi-volatile organic compounds on exterior window surfaces in Baltimore. *Environ. Pollut.* **2003,** *122*, (1), 51 61.

6. Diamond, M. L.; Gingrich, S. E.; Fertuck, K.; McCarry, B. E.; Stern, G. A.; Billeck, B.; Grift, B.; Brooker, D.; Yager, T. D., Evidence for organic film on an impervious urban surface: characterization and potential teratogenic effects. *Environ. Sci. Technol.* **2000,** *34*, (14), 2900 2908.

7. Liu, Q. T.; Chen, R.; McCarry, B. E.; Diamond, M. L.; Bahavar, B., Characterization of polar organic compounds in the organic film on indoor and outdoor glass windows. *Environ. Sci. Technol.* **2003,** *37*, (11), 2340 2349.

8. Lam, B.; Diamond, M. L.; Simpson, A. J.; Makar, P. A.; Truong, J.; Hernandez-Martinez, N. A., Chemical composition of surface films on glass windows and implications for atmospheric chemistry. *Atmos. Environ.* **2005,** *39*, (35), 6578 6586.

9. Simpson, A. J.; Lam, B.; Diamond, M. L.; Donaldson, D. J.; Lefebvre, B. A.; Moser, A. Q.; Williams, A. J.; Larin, N. I.; Kvasha, M. P., Assessing the organic composition of urban surface films using nuclear magnetic resonance spectroscopy. *Chemosphere* **2006,** *63*, (1), 142 152.

10. Unger, M.; Gustafsson, O., PAHs in Stockholm window films: evaluation of the utility of window film content as indicator of PAHs in urban air. *Atmos. Environ.* **2008,** *42*, (22), 5550 5557.

11. Gingrich, S. E.; Diamond, M. L., Atmospherically derived organic surface films along an urban rural gradient. *Environ. Sci. Technol.* **2001,** *35*, (20), 4031 4037.

12. Diamond, M. L.; Priemer, D. A.; Law, N. L., Developing a multimedia model of chemical dynamics in an urban area. *Chemosphere* **2001,** *44*, (7), 1655 1667.

13. Donaldson, D. J.; Mmereki, B. T.; Chaudhuri, S. R.; Handley, S.; Oh, M., Uptake and reaction of atmospheric organic vapours on organic films. *Faraday Discuss.* **2005,** *130*, 227 239.

14. Kahan, T. F.; Kwamena, N. O. A.; Donaldson, D. J., Heterogeneous ozonation kinetics of polycyclic aromatic hydrocarbons on organic films. *Atmos. Environ.* **2006,** *40*, (19), 3448 3459.

15. Kwamena, N. O. A.; Clarke, J. P.; Kahan, T. F.; Diamond, M. L.; Donaldson, D. J., Assessing the importance of heterogeneous reactions of polycyclic aromatic hydrocarbons in the urban atmosphere using the Multimedia Urban Model. *Atmos. Environ.* **2007,** *41*, (1), 37 50.

16. Styler, S. A.; Brigante, M.; D'Anna, B.; George, C.; Donaldson, D. J., Photoenhanced ozone loss on solid pyrene films. *Phys. Chem. Chem. Phys.* **2009,** *11*, (36), 7876 7884.

17. Mmereki, B. T.; Donaldson, D. J.; Gilman, J. B.; Eliason, T. L.; Vaida, V., Kinetics and products of the reaction of gas-phase ozone with anthracene adsorbed at the air aqueous interface. *Atmos. Environ.* **2004,** *38*, (36), 6091 6103.

18. Luster-Teasley, S. L.; Yao, J. J.; Herner, H. H.; Trosko, J. E.; Masten, S. J., Ozonation of chrysene: Evaluation of byproduct mixtures and identification of toxic constituent. *Environ. Sci. Technol.* **2002,** *36*, (5), 869 876.

19. Luster-Teasley, S. L.; Ganey, P. E.; DiOrio, M.; Ward, J. S.; Maleczka, R. E.; Trosko, J. E.; Masten, S. J., Effect of byproducts from the ozonation of pyrene: biphenyl-2,2',6,6'-tetracarbaldehyde and biphenyl-2,2',6,6'-tetracarboxylic acid on gap junction intercellular communication and neutrophil function. *Environ. Toxicol. Chem.* **2005,** *24*, (3), 733 740.

20. Labencki, T.; Diamond, M. L.; Motelay-Massai, A.; Truong, J.; Branfireun, B.; Dann, T., Variability in and mechanisms of PAH washoff from urban impervious surfaces. Unpublished work.

21. Nieto-Gligorovski, L.; Net, S.; Gligorovski, S.; Zetzsch, C.; Jammoul, A.; D'Anna, B.; George, C., Interactions of ozone with organic surface films in the presence of simulated sunlight: impact on wettability of aerosols. *Phys. Chem. Chem. Phys.* **2008,** *10*, (20), 2964 2971.

22. Brigante, M.; Cazoir, D.; D'Anna, B.; George, C.; Donaldson, D. J., Photoenhanced uptake of NO_2 by pyrene solid films. *J. Phys. Chem. A* **2008,** *112*, (39), 9503 9508.

23. Stemmler, K.; Ammann, M.; Donders, C.; Kleffmann, J.; George, C., Photosensitized reduction of nitrogen dioxide on humic acid as a source of nitrous acid. *Nature* **2006,** *440*, (7081), 195 198.

24. Jammoul, A.; Gligorovski, S.; George, C.; D'Anna, B., Photosensitized heterogeneous chemistry of ozone on organic films. *J. Phys. Chem. A* **2008,** *112*, (6), 1268 1276.

25. George, C.; Strekowski, R. S.; Kleffmann, J.; Stemmler, K.; Ammann, M., Photoenhanced uptake of gaseous NO_2 on solid organic compounds: a photochemical source of HONO? *Faraday Discuss.* **2005,** *130*, 195 210.

26. D'Anna, B.; Jammoul, A.; George, C.; Stemmler, K.; Fahrni, S.; Ammann, M.; Wisthaler, A., Light-induced ozone depletion by humic acid films and submicron aerosol particles. *J. Geophys. Res.–Atmos.* **2009,** *114*, (12), D12301, doi:10.1029/2008JD001237.

27. Net, S.; Nieto-Gligorovski, L.; Gligorovski, S.; Temime-Rousell, B.; Barbati, S.; Lazarou, Y. G.; Wortharn, H., Heterogeneous light-induced ozone processing on the organic coatings in the atmosphere. *Atmos. Environ.* **2009,** *43*, (9), 1683 1692.

28. Net, S.; Gligorovski, S.; Wortham, H., Light-induced heterogeneous ozone processing on organic coated particles: kinetics and condensed-phase products. *Atmos. Environ.* **2010,** *44*, (27), 3286 3294.

29. Nieto-Gligorovski, L. I.; Net, S.; Gligorovski, S.; Wortham, H.; Grothe, H.; Zetzsch, C., Spectroscopic study of organic coatings on fine particles exposed to ozone and simulated sunlight. *Atmos. Environ.* **2010,** *44*, (40), 5451 5459.

30. Handley, S. R.; Clifford, D.; Donaldson, D. J., Photochemical loss of nitric acid on organic films: a possible recycling mechanism for NO_x. *Environ. Sci. Technol.* **2007,** *41*, (11), 3898 3903.

31. Mmereki, B. T.; Donaldson, D. J., Direct observation of the kinetics of an atmospherically important reaction at the air aqueous interface. *J. Phys. Chem. A* **2003,** *107*, (50), 11038 11042.

32. Mmereki, B. T.; Donaldson, D. J., Laser-induced fluorescence of pyrene at an organic-coated air water interface. *Phys. Chem. Chem. Phys.* **2002,** *4*, (17), 4186 4191.

33. Forster, T.; Kasper, K., Ein konzentrationsumschlag der fluoreszenz des pyrens. *Z. Elektrochem.* **1955,** *59*, (10), 976 980.

34. Takahashi, Y.; Kitamura, T.; Uchida, K., Excimer emission from evaporated pyrene films. *J. Lumin.* **1980,** *21*, (4), 425 433.

35. Adamson, A. W., *Physical Chemistry of Surfaces, 5th edition*. John Wiley and Sons: Toronto, Ontario, Canada, 1990.

36. Reyes, C. A.; Medina, M.; Crespo-Hernandez, C.; Cedeno, M. Z.; Arce, R.; Rosario, O.; Steffenson, D. M.; Ivanov, I. N.; Sigman, M. E.; Dabestani, R., Photochemistry of pyrene on unactivated and activated silica surfaces. *Environ. Sci. Technol.* **2000,** *34*, (3), 415 421.

37. Behymer, T. D.; Hites, R. A., Photolysis of polycyclic aromatic hydrocarbons adsorbed on fly ash. *Environ. Sci. Technol.* **1988,** *22*, (11), 1311 1319.

38. Finlayson-Pitts, B. J.; Pitts, J. N., *Chemistry of the upper and lower atmosphere*. Academic Press: San Diego, CA, 2000.

39. Poschl, U.; Letzel, T.; Schauer, C.; Niessner, R., Interaction of ozone and water vapor with spark discharge soot aerosol particles coated with benzo[a]pyrene: O_3 and H_2O adsorption, benzo[a]pyrene degradation, and atmospheric implications. *J. Phys. Chem. A* **2001,** *105*, (16), 4029 4041.

40. Kwamena, N. O. A.; Earp, M. E.; Young, C. J.; Abbatt, J. P. D., Kinetic and product yield study of the heterogeneous gas-surface reaction of anthracene and ozone. *J. Phys. Chem. A* **2006,** *110*, (10), 3638 3646.

41. Kwamena, N. O. A.; Staikova, M. G.; Donaldson, D. J.; George, I. J.; Abbatt, J. P. D., Role of the aerosol substrate in the heterogeneous ozonation reactions of surface-bound PAHs. *J. Phys. Chem. A* **2007,** *111*, (43), 11050 11058.

42. Pryor, W. A.; Gleicher, G. J.; Church, D. F., Reaction of polycyclic aromatic hydrocarbons with ozone: linear free-energy relationships and tests of likely rate-determining steps using simple molecular-orbital correlations. *J. Org. Chem.* **1983,** *48*, (23), 4198 4202.

43. Barbas, J. T.; Dabestani, R.; Sigman, M. E., A mechanistic study of photodecomposition of acenaphthylene on a dry silica surface. *J. Photochem. Photobiol., A* **1994,** *80*, (1 3), 103 111.

44. Nautiyal, A.; Bisht, P. B., Steady-state and time-resolved studies of pyrene in solution and in single microcrystals. *J. Lumin.* **2010,** *130*, (10), 1829 1833.

45. Winnik, F. M., Photophysics of preassociated pyrenes in aqueous polymer solutions and in other organized media *Chem. Rev.* **1993,** *93*, (2), 587 614.

46. Jones, G.; Vullev, V. I., Ground- and excited-state aggregation properties of a pyrene derivative in aqueous media. *J. Phys. Chem. A* **2001,** *105*, (26), 6402 6406.

47. Khakhel', O. A., Absorption spectra of pyrene aggregates in saturated solutions. *J. Appl. Spectrosc.* **2001,** *68*, 280 286.

48. Boateng, S. Photophysical properties of pyrene, 2,7-diazapyrene, and 1,3-bis(β -naphthyl)propane. USA, 2007.

49. Andriessen, R.; Ameloot, M.; Boens, N.; Deschryver, F. C., Non a priori analysis of fluorescence decay surfaces of excited-state processes. 3. Intermolecular excimer formation of pyrene quenched by iodomethane. *J. Phys. Chem.* **1992,** *96*, (1), 314 326.

50. Krykunova, V.; Khakhel', O. A., Pyrene aggregation in liquid solutions. *Funct. Mater.* **1998,** *5*, 356 358.

51. Abdel-Shafi, A. A.; Wilkinson, F., Charge transfer effects on the efficiency of singlet oxygen production following oxygen quenching of excited singlet and triplet states of aromatic hydrocarbons in acetonitrile. *J. Phys. Chem. A* **2000,** *104*, (24), 5747 5757.

52. Abdel-Shafi, A. A.; Worrall, D. R.; Wilkinson, F., Singlet oxygen formation efficiencies following quenching of excited singlet and triplet states of aromatic hydrocarbons by molecular oxygen. *J. Photochem. Photobiol., A* **2001,** *142*, (2 3), 133 143.

53. Shold, D. M., Formation of singlet oxygen from aromatic excimers and monomers *J. Photochem.* **1978,** *8*, (1), 39 48.

54. Kubat, P.; Civis, S.; Muck, A.; Barek, J.; Zima, J., Degradation of pyrene by UV radiation. *J. Photochem. Photobiol., A* **2000,** *132*, (1 2), 33 36.

55. Brownrigg, J. T.; Kenny, J. E., Fluorescence intensities and lifetimes of aromatic hydrocarbons in cyclohexane solution: evidence of contact charge-transfer interactions with oxygen. *J. Phys. Chem. A* **2009,** *113*, (6), 1049 1059.

56. Donaldson, D. J.; Kahan, T. F.; Kwamena, N. O. A.; Handley, S. R.; Barbier, C., Atmospheric chemistry of urban surface films. In *Atmospheric Aerosols.* Valsaraj, K. T.; Kommalapati, R. R., Eds. ACS Symposium Series: Washington, DC, 2009.

57. Potashnik, R.; Goldschmidt, C. R.; Ottolenghi, M., Triplet state formation in the quenching of fluorescence by molecular oxygen. *Chem. Phys. Lett.* **1971,** *9*, (5), 424 425.

58. Kikuchi, K., A new method for determining the efficiency of enhanced intersystem crossing in fluorescence quenching by molecular oxygen. *Chem. Phys. Lett.* **1991,** *183*, (1 2), 103 106.

59. Ruetten, S. A.; Thomas, J. K., Fluorescence and triplet quantum yields of arenes on surfaces. *J. Phys. Chem. B* **1998,** *102*, (3), 598 606.

60. Mao, Y.; Thomas, J. K., Photochemical reactions of pyrene on surfaces of gamma-alumina and silica-alumina. *Langmuir* **1992,** *8*, (10), 2501 2508.

61. Mao, Y.; Thomas, J. K., Chemical reactions of molecular oxygen in surface-mediated photolysis of aromatic compounds on silica-based surfaces. *J. Phys. Chem.* **1995,** *99*, (7), 2048 2056.

62. Boscher, A.; David, B.; Guittoneau, S., Photodegradation of pyrene on solid phase. In *Environmental Chemistry*. Lichtfouse, E.; Schwarzbauer, J.; Robert, D., Eds. Springer Berlin: Heidelberg, Germany, 2005.

63. Sato, C.; Kikuchi, K.; Okamura, K.; Takahashi, Y.; Miyashi, T., New aspects on fluorescence quenching by molecular oxygen. 2. Inhibition of long-distance electron-transfer in acetonitrile *J. Phys. Chem.* **1995,** *99*, (46), 16925 16931.

64. Clark, C. D.; De Bruyn, W. J.; Ting, J.; Scholle, W., Solution medium effects on the photochemical degradation of pyrene in water. *J. Photochem. Photobiol., A* **2007,** *186*, (2 3), 342 348.

65. Sigman, M. E.; Schuler, P. F.; Ghosh, M. M.; Dabestani, R. T., Mechanism of pyrene photochemical oxidation in aqueous and surfactant solutions. *Environ. Sci. Technol.* **1998,** *32*, (24), 3980 3985.

66. Reeser, D. I.; Jammoul, A.; Clifford, D.; Brigante, M.; D'Anna, B.; George, C.; Donaldson, D. J., Photoenhanced reaction of ozone with chlorophyll at the seawater surface. *J. Phys. Chem. C* **2009,** *113*, (6), 2071 2077.

Chapter 3

Photooxidation of atmospheric alcohols on laboratory proxies for freshly emitted and atmospherically processed mineral dust

Contributions:

All experiments were conducted by Sarah A. Styler. The manuscript was written by Sarah A. Styler, with critical comments from D. James Donaldson.

3.1 Introduction

According to one recent estimate, 1600 Tg of mineral dust is released into the atmosphere on an annual basis.[1] Once aloft, dust particles can influence climate directly by absorbing and scattering incoming solar radiation and indirectly by influencing the formation, optical properties, and atmospheric lifetime of clouds.[2] Although dust events primarily originate in remote arid regions in North Africa, the Middle East, and central Asia, dust particles may undergo efficient long-range transport and thus have the potential to exert a strong influence upon air quality and human health in populated areas.[3-5]

Dust particles present a large surface area for reactive processes, and much recent evidence exists to suggest that they may influence the local and regional abundance of trace gases in the troposphere.[6-9] To date, laboratory studies of the heterogeneous reactivity of mineral dust have primarily focused on the uptake and transformation of inorganic trace gas species, including O_3, NO_2, HNO_3, NO_3, N_2O_5, and SO_2, on SiO_2, Al_2O_3, Fe_2O_3, and other metal oxide surfaces.[10-14] Evidence for the particular importance of nitrate processing on mineral dust surfaces has been provided by laboratory studies, which have shown substantial uptake of HNO_3 by a variety of mineral dust proxies,[12, 15, 16] and by direct observations of nitrate coatings on ambient mineral dust particles[17] and significant reductions in gas-phase nitric acid concentrations in dust plumes.[6]

Given that mineral dust contains a variety of semiconducting metal oxides, including TiO_2 and Fe_2O_3,[18, 19] it may play a significant role in influencing the uptake and photochemical transformation of trace gas species.[20] In recent years, a number of studies have investigated the photochemistry of inorganic gas-phase species on TiO_2 particles, which have been used as proxies for the photoactive component of mineral dust. These studies have shown that actinic illumination of TiO_2 surfaces containing

adsorbed nitrate leads to the production of NO and NO_2,[21] that uptake of gas-phase NO_2 on illuminated TiO_2 surfaces leads to the near-quantitative loss of NO_2 and the production of HONO,[22] and that reactive uptake of ozone to TiO_2 films is enhanced in the presence of light.[23]

Although a substantial body of literature exists regarding the TiO_2-catalyzed phototransformation of organic pollutants, work in this area has primarily focused on the development of techniques to optimize the mineralization of organic pollutants in wastewater and indoor air.[24-26] In an attempt to address the current gap in knowledge regarding the atmospheric significance of photooxidative reactions of organic species adsorbed to mineral dust, the phototransformations of isopropanol, n-propanol, and cyclohexene on the surface of TiO_2 and mixed TiO_2 SiO_2 films were investigated using a novel photochemical Knudsen cell effusion reactor. Although isopropanol and *n*-propanol are transparent in the actinic region,[27] their photooxidation products, acetone and propionaldehyde, are not;[28] this study sought to establish whether photochemistry on mineral dust surfaces may play a role in changing the optical properties of volatile organic compounds. Such changes could alter their atmospheric oxidative pathways and therefore influence both their HO_x formation efficiencies and their propensity to participate in radical-initiated secondary organic aerosol (SOA) formation reactions. Further experiments were performed to investigate the influence of cosorbed nitrate on the organic photooxidation processes observed at the TiO_2 surface.

3.2 Materials and methods

3.2.1 The photochemical Knudsen cell

Knudsen cells are low-pressure effusion reactors that have been used in the atmospheric chemistry community to measure the uptake of gas-phase molecules by surfaces of environmental interest, including that of organic species by mineral dust.[29,

[30] The present experiments were performed using a novel photochemical Knudsen cell, which is a modification of one previously used by our group to investigate the nonreactive uptake of a variety of gas-phase organic species by squalene and oleic acid films.[31] A schematic of this apparatus is shown in Figure 3-1.

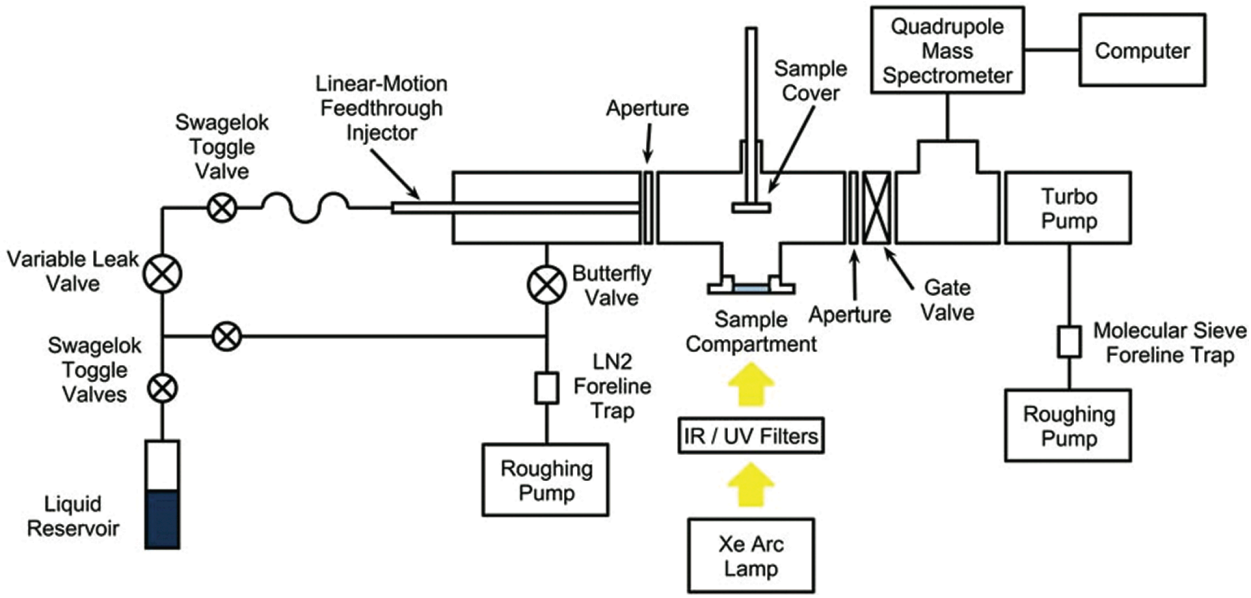

Figure 3-1 Schematic drawing of the photochemical Knudsen cell

The reactor consists of a 730 cm^3 stainless-steel T-shaped chamber, the bottom flange of which has a 3.2 cm diameter orifice. A quartz window in the center of this flange creates a 4.8 cm^3 sample compartment and allows for the illumination of samples from below. Pressures within the reactor are maintained using a turbopump, with baseline pressures typically ranging from 3 – 5 × 10^{-2} Pa. Gas-phase species effuse out of the cell through a 3 mm diameter exit orifice and are detected using a quadrupole mass spectrometer (QMS) with 70 eV electron-impact ionization. Gas-phase reagents are drawn from the vapor above an ice-cooled liquid reservoir and introduced to the reactor through a length of flexible tubing connected to a 1/4" stainless-steel injector

tube, which terminates at the entrance to the cell. Gas flow through the sample introduction system is controlled using a variable leak valve.

An isolation flange (with a Viton O-ring) attached to a stainless-steel rod passing through a compression fitting on the top of the reactor is used to cover the sample compartment. When the flange is lowered, samples are shielded from gas-phase reagents present in the cell. Because the volume of the sample compartment amounts to $< 1\%$ of the chamber volume, raising or lowering the isolation cover does not change the pressure within the reactor measurably.

3.2.2 Sample preparation

Unmodified dust samples were prepared by pipetting a slurry, made up of 10 50 mg of TiO_2 or TiO_2 SiO_2 in $\sim$ 2 mL of deionized water, into a shallow Pyrex sample holder (3.045 cm diameter) and heating the sample holder overnight in a 433 K oven. No further efforts were made to remove adsorbed water from the samples. Some dust samples were prepared from slurries made using aqueous solutions of $AgNO_3$ or KNO_3 (10 mM, 2 mL). In order to minimize thermal decomposition of $AgNO_3$,[32] samples prepared using this solution were heated under milder conditions (1.5 h at $\sim$ 373 K). Samples prepared using KNO_3 solutions were treated in an identical manner.

3.2.3 Uptake experiments

Before each uptake experiment, the Pyrex sample holder containing the substrate of interest was placed into the reactor on top of the quartz window (see Figure 3-1), and the apparatus was evacuated until the background pressure within the Knudsen reactor reached 3 5 $\times$ 10^{-2} Pa. At this point, back- ground levels of the *m/z* of interest were measured using the QMS. Next, the isolation cover was lowered and gas-phase isopropanol, *n*-propanol, or cyclohexene was introduced to the cell at total partial pressures ranging from 0.09 0.2 Pa. When a stable pressure was achieved, the

isolation cover was retracted to expose the mineral dust sample to the gas-phase reagent. Uptake of the gas-phase species by the sample gave rise to a prompt decrease in the QMS signal at the corresponding *m/z*, followed by a slower increase toward its initial value. When the isolation cover was closed, the signal returned to its initial value. This sequence is displayed in Figure 3-2.

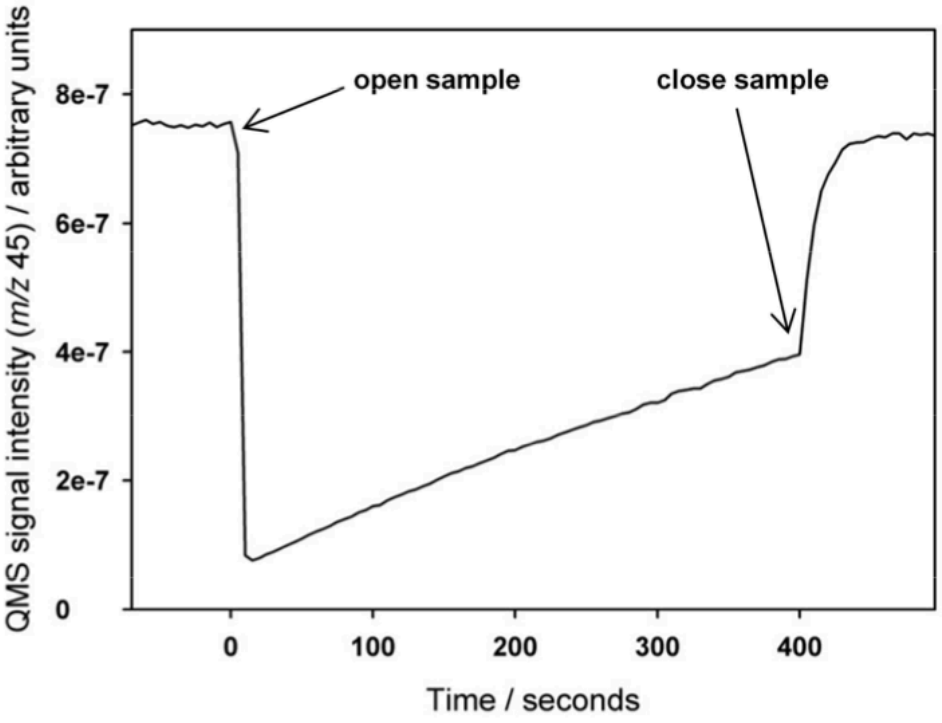

Figure 3-2 Results of a typical uptake experiment performed under dark conditions. Each experiment began by establishing a constant QMS signal at the *m/z* of interest (for isopropanol, *m/z* 45). Then, the sample cover was retracted to expose the gas-phase species to the solid film. Finally, the sample cover was closed and the QMS signal returned to its original level.

Experiments were performed under both dark and illuminated conditions. Illumination of samples was accomplished using a 150 W xenon arc lamp (Oriel Corporation), the output of which resembles the actinic radiation spectrum. The illumination beam was directed through the quartz base of the sample holder flange

and the Pyrex sample holder, with the latter also serving as a long-pass optical filter, eliminating $\lambda < 310$ nm. A water filter in the path of the beam was used to remove infrared radiation. Although we did not measure the lamp intensity, chemical actinometry experiments previously performed using this lamp suggest that the UV visible illumination under our experimental conditions was at least an order of magnitude smaller than the midday summer solar irradiance in Toronto.[33]

3.2.4 Chemicals

Titanium dioxide (anatase, ≥ 99%, Sigma Aldrich), silicon dioxide (99.9%, Alfa Aesar), potassium nitrate (ACS grade, ACP Chemicals), and silver nitrate were used as received. Isopropanol (≥ 99.5%, ACS grade, Sigma Aldrich), *n*-propanol (ACP Chemicals), and cyclohexene (99%, Sigma Aldrich) were subjected to multiple freeze pump thaw cycles prior to use.

3.3 Results

3.3.1 System characterization: uptake of isopropanol by TiO_2 under dark conditions

We characterized the Knudsen reactor by measuring the dark uptake of gas-phase isopropanol by TiO_2 under a variety of experimental conditions. Exposure of the TiO_2 sample to gas-phase isopropanol was accompanied by an immediate and substantial reduction in the isopropanol signal (*m/z* 45) measured by the QMS. This reduction in signal intensity was greatest when the sample cover was first raised and decreased gradually with exposure time as available adsorptive sites at the TiO_2 surface became saturated. The results of a typical experiment are shown in Figure 3-2. In these and all subsequent experiments, initial loss of the signal intensity of the *m/z* of interest was used to calculate an initial uptake coefficient for reaction at the TiO_2 surface.

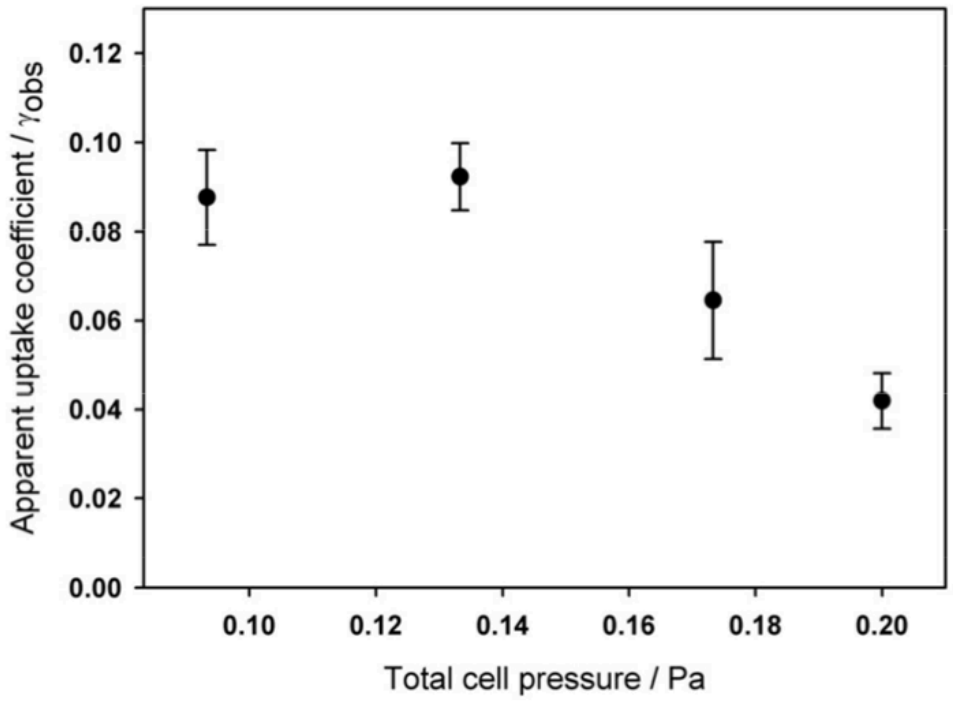

Figure 3-3 Apparent dark uptake coefficients for isopropanol onto TiO_2 films (film mass 20 mg) as a function of total cell pressure. Each data point represents the mean of 3 trials, with 1-σ error bars.

Generally, Knudsen cells are operated in the molecular-flow pressure regime, where the mean free path of the molecule of interest exceeds the cell dimensions such that gas-phase collisions are significantly outnumbered by gas surface collisions. In this pressure regime, the change in effusion of a gas through the exit orifice of the Knudsen cell upon exposure to a solid substrate is directly related to the probability of loss from the gas phase upon a single collision with the substrate. The apparent initial uptake coefficient for reaction γ_{obs}[34]

$$\gamma_{obs} = \frac{A_h}{A_s} \frac{I_0 - I}{I} \qquad (1)$$

depends on A_h and A_s, the geometric areas of the escape aperture and sample holder, respectively; I_0, the signal recorded by the QMS for the gas-phase species of interest with the sample cover closed; and I, the signal recorded by the QMS immediately after the sample cover is opened.

In order to determine the pressure range for our cell for which use of this equation was appropriate, we performed uptake experiments for isopropanol on TiO_2 as a function of total cell pressure. As shown in Figure 3-3, the apparent uptake coefficient did not depend upon cell pressure for cell pressures below 0.13 Pa. At higher cell pressures, however, a decrease in γ_{obs} with increasing cell pressure was observed. These observations are consistent with those obtained in earlier work using this apparatus.[35] All experiments reported here were performed at a total cell pressure of ~ 9×10^{-2} Pa (background pressure ~ 3.5×10^{-2} Pa).

Relating the observed uptake to environmentally relevant uptake coefficients requires knowledge of the total surface area of sample accessed by gas-phase molecules over the time scale of the uptake experiment (see Li *et al.*[36] for a comprehensive discussion of the complexities associated with the interpretation of apparent uptake coefficients obtained using powdered samples). Use of the geometric surface area of the sample, A_s, assumes that the sample surface area equals that of the sample holder. However, dust particles have high specific surface areas;[29] moreover, gas-phase molecules may diffuse into underlying sample layers. In both instances, uptake coefficients determined using only the geometric surface area of the sample holder will be significant overestimates.

In order to investigate the extent to which apparent uptake coefficients measured in the present experiments were governed by diffusion into underlying sample layers, we

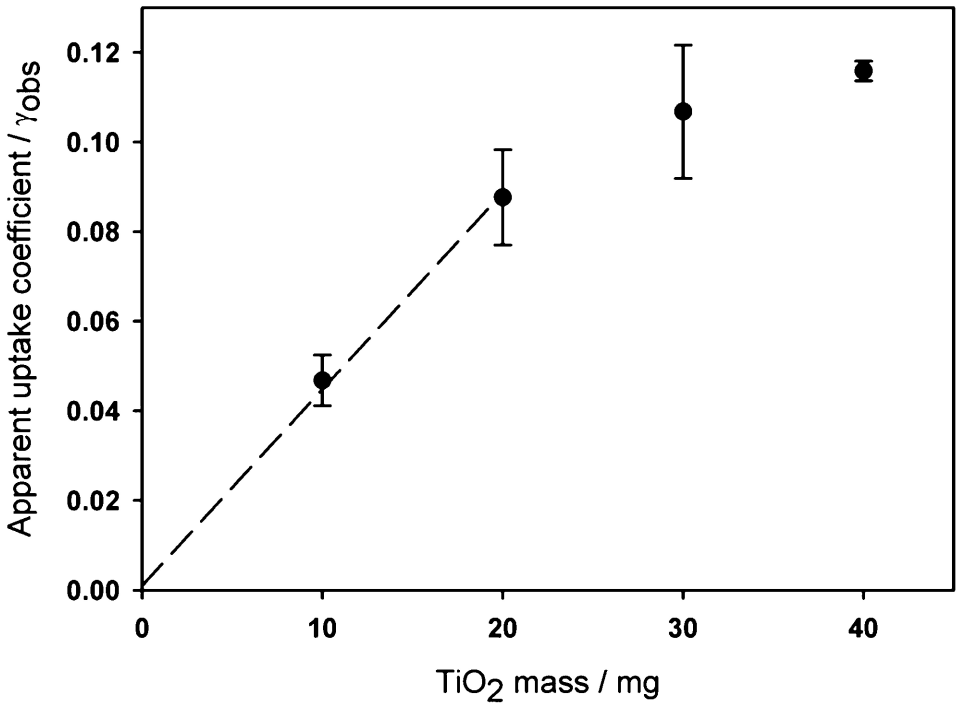

Figure 3-4 Apparent dark uptake coefficients for isopropanol onto TiO_2 films as a function of film mass. The dashed line is a linear fit to the data for film masses ≤ 20 mg. Each data point represents the mean of 3 or more trials, with 1-σ error bars.

---

measured uptake coefficients for isopropanol as a function of TiO_2 mass. As illustrated in Figure 3-4, the behavior of the apparent uptake coefficient as a function of sample mass can be divided into two regimes. At higher sample masses, γ_{obs} increased only slightly as a function of sample mass. This weak dependence upon sample mass, which has been previously observed for the uptake of volatile organic compounds by a variety of metal oxide surfaces,[29, 30] implies that these sample masses were in the so-called "plateau" region,[37] where the total sample amount was high enough that gas-phase molecules could not access the entire sample over the time scale of the uptake experiment, and so only its upper layers were important for uptake. At sample masses below 20 mg, however, γ_{obs} increased linearly with sample mass. This observation

implies that, over the time scale of the uptake experiment, gas-phase isopropanol was able to access the entire sample via diffusion and, therefore, that it may be appropriate to scale our observed uptake coefficients by the Brunauer Emmett Teller (BET) surface area of our sample (~ 50 m^2/g).[29] However, given that the uptake of gas-phase organic species by mineral dust has been shown to vary with relative humidity, in part as a result of competition between sorbing species and water vapor for available surface sites,[38, 39] this approach may not be applicable for our samples, which are expected to contain significant amounts of surface-sorbed water molecules. For this reason, and because we are most interested in photoinduced changes in uptake, we report apparent uptake coefficients alone. All experiments reported below were performed using total film masses of 20 mg, which is in the linear regime of Figure 3-4.

3.3.2 Photochemistry of isopropanol and *n*-propanol on TiO_2

In order to investigate the heterogeneous photooxidation of isopropanol, TiO_2 films were exposed to gas-phase isopropanol under dark conditions until surface saturation, here defined as the point when the isopropanol signal (*m/z* 45) returned to its original (pre-exposure to the substrate) level. With gas-phase isopropanol still flowing through the cell, the films were then subjected to the following course of illumination: 15 min on; 5 min off; 10 min on; 5 min off. Representative results obtained in these experiments are presented in Figure 3-5.

As shown in Figure 3-5a, illumination resulted in an immediate increase in the QMS signal associated with *m/z* 43 and a concomitant decrease in the signal associated with *m/z* 45. Given that *m/z* 45 is characteristic only of isopropanol while *m/z* 43 is present in the EI ionization spectrum of both isopropanol and acetone,[40] these results suggest that illumination led to the conversion of isopropanol to acetone on the TiO_2 surface.[41] The changes in the signal intensities at the two masses were quite similar, which suggests that the conversion of isopropanol to acetone occurred with near-unit efficiency.

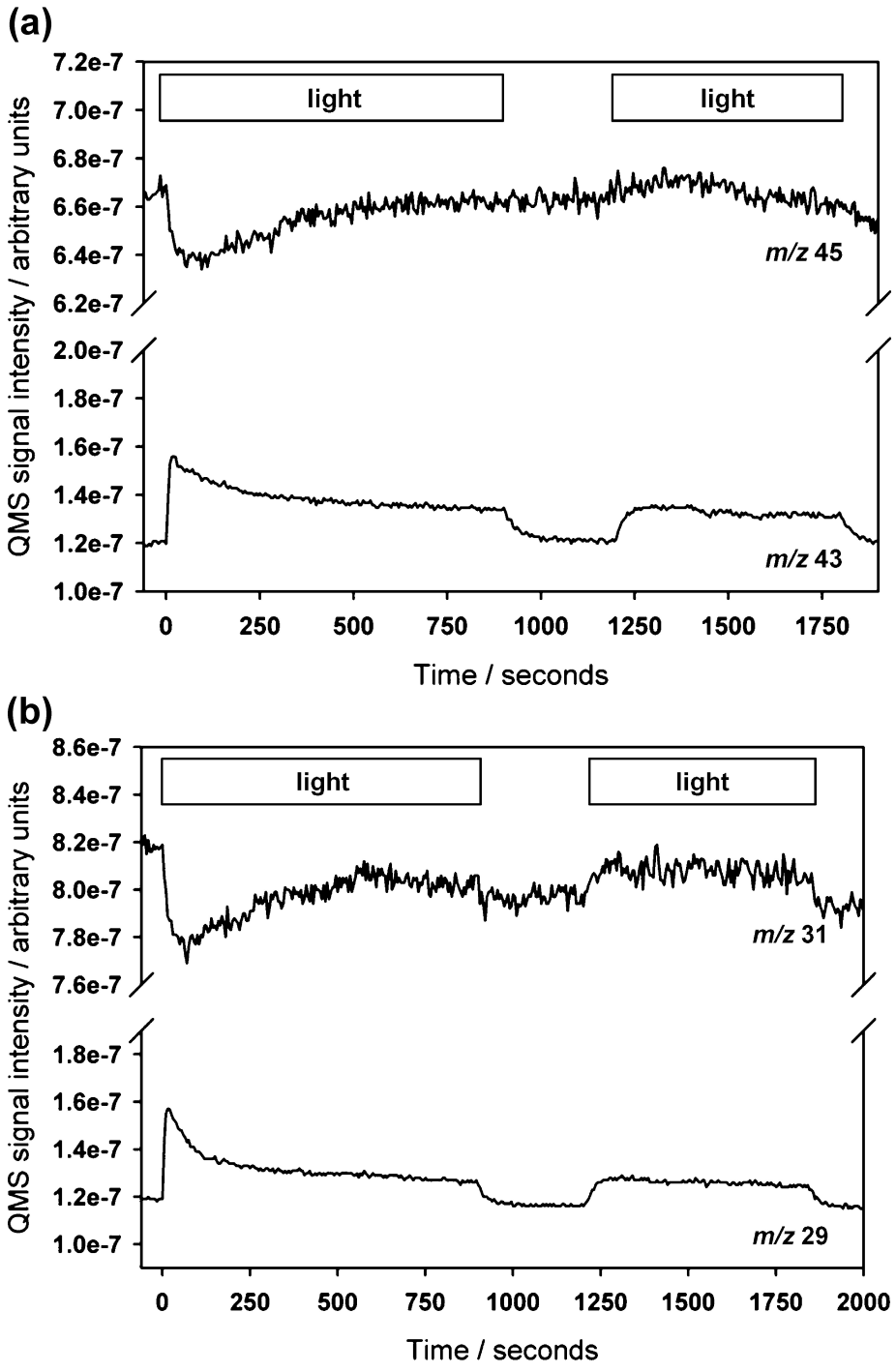

Figure 3-5 Representative QMS trace for conversion of (a) isopropanol (*m/z* 45) to acetone (*m/z* 43) and (b) *n*-propanol (*m/z* 31) to propionaldehyde (*m/z* 29) at the illuminated TiO_2 surface (film mass 20 mg). In both plots, time = 0 indicates when the sample was first illuminated.

Figure 3-5a further shows that acetone production ceased immediately at the end of the first illumination cycle; at the same time, the gas-phase isopropanol signal gradually increased to its pre-illumination value. Interestingly, while the production of acetone resumed immediately when the second illumination cycle commenced, the loss of gas-phase isopropanol was less apparent. We tentatively attribute this observation to the "poisoning" of TiO_2 adsorptive sites, presumably as a result of accumulation of acetone and/or its less volatile aldol condensation product, mesityl oxide, on the TiO_2 surface.[42-44]

In order to verify that the observed photooxidation reaction was not specific to secondary alcohols, we performed an identical set of experiments using TiO_2 films saturated with *n*-propanol. As shown in Figure 3-5b, illumination led to an increase in a QMS signal associated with propionaldehyde (*m/z* 29) and a concurrent decrease in the QMS signal associated with n-propanol (*m/z* 31). Again, these observations suggest that illumination of the *n*-propanol-saturated TiO_2 surface promoted the heterogeneous photooxidation of *n*-propanol to propionaldehyde[45] with near-unit efficiency. Figure 3-5b also shows that the initial photoenhanced uptake of *n*-propanol was not maintained over long time-scales. This observation provides further evidence that the TiO_2 surface was gradually deactivated as a result of accumulation of oxidation products.

3.3.3 Isopropanol photooxidation on TiO_2 is enhanced by co-sorbed nitrate

In order to investigate the influence of co-sorbed nitrate on the photooxidation of isopropanol, the same experiments were performed using TiO_2 films prepared from KNO_3- or $AgNO_3$-containing slurries. As shown in Figure 3-6, both isopropanol uptake and acetone production were significantly enhanced in the presence of $AgNO_3$ or KNO_3 relative to their respective values using unmodified TiO_2 films. The enhancement in acetone production effected by $AgNO_3$ was greater than that effected by KNO_3. The loss of isopropanol mass intensity was closely matched by the increase

in acetone signal, which is again consistent with very efficient conversion of the alcohol to the ketone. Finally, as illustrated in Figure 3-6, illumination of the KNO_3-doped films in the presence of isopropanol also led to the production of gas-phase NO (*m/z* 30). However, no such NO production was observed for illuminated $AgNO_3$-doped films in the presence of isopropanol.

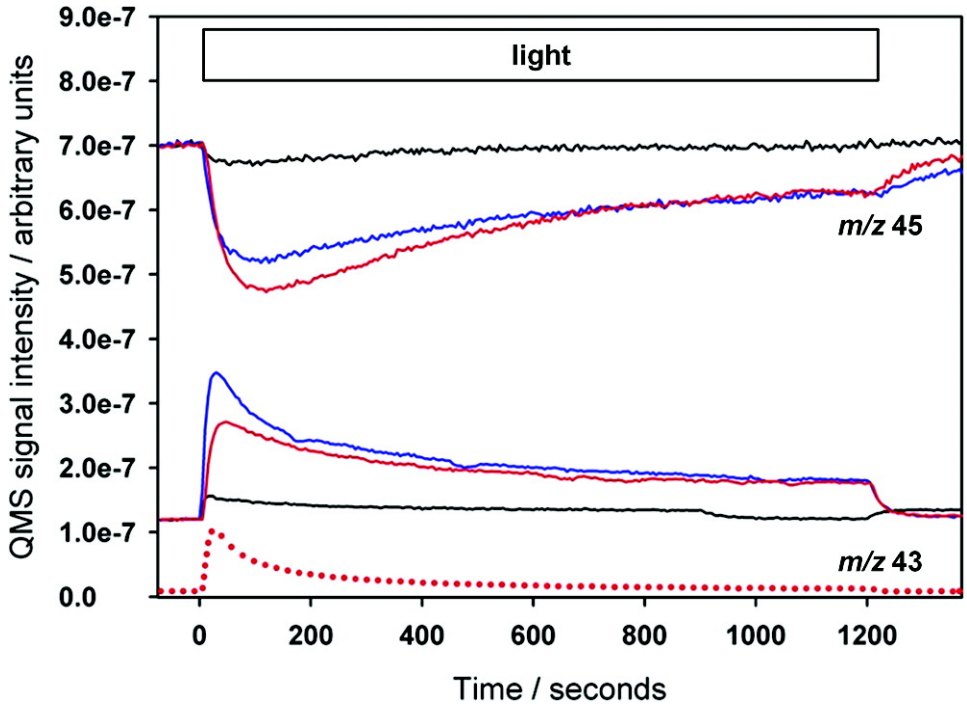

Figure 3-6 Representative QMS trace for conversion of isopropanol (*m/z* 45) to acetone (*m/z 43*) at the illuminated TiO_2 surface (film mass 20 mg) in the presence of cosorbed nitrate ion. The red trace represents reaction in the presence of cosorbed KNO_3, while the blue trace represents reaction in the presence of cosorbed $AgNO_3$. For comparison, the black trace reproduces results shown in Figure 3-5 for an unmodified TiO_2 film. The dotted red trace represents production of NO (*m/z* 30) by the KNO_3-doped film in the presence of gas-phase isopropanol. In both plots, time = 0 indicates when the sample was first illuminated.

Evidence for the source(s) of this enhancement was provided by a set of experiments using a variety of optical filters. When a 320 nm long-pass filter was used, which

should suppress direct photolysis of nitrate at the TiO_2 surface,[46] the enhancement persisted. However, when the sample was illuminated only with radiation with wavelengths longer than the TiO_2 absorption threshold (384 nm[24]), all photochemistry ceased. Together, these observations imply that the observed photochemistry was mediated by TiO_2 and that its enhancement in the presence of nitrate did not arise from the production of OH at the TiO_2 surface via direct nitrate photolysis.

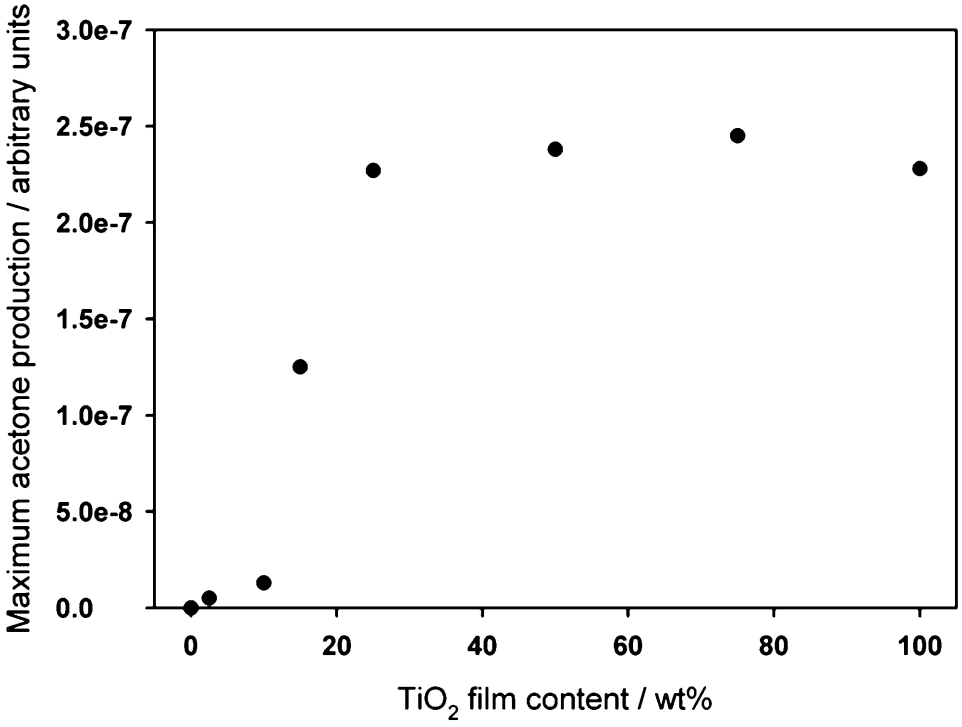

Figure 3-7 Maximum acetone production at the surface of $AgNO_3$-doped mixed SiO_2–TiO_2 samples as a function of TiO_2 film content. The total mass of all samples was 20 mg.

The elemental abundance of Ti in Saharan mineral dust samples varies with the geochemistry of the source region: typical values range from less than one to several percent by mass.[18, 19, 47, 48] In order to mimic the environment presented by real mineral

dust, which is primarily composed of SiO_2 (~60%),[3] we performed a set of experiments using $AgNO_3$-doped mixed SiO_2 TiO_2 samples. The results of these experiments, which are shown in Figure 3-7, show that the production of acetone from these films increased monotonically with increasing TiO_2 film content for films prepared with $\leq$ 25 wt % TiO_2. These observations provide additional evidence that the reaction was mediated by TiO_2. For films prepared with > 25 wt % TiO_2, however, the production of acetone no longer increased with increasing TiO_2 content. We attribute this high-TiO_2 plateau to the use of films with thicknesses greater than the optical penetration depth of our illumination source: assuming a TiO_2 density of 3.85 g cm^{-3} and a 380-nm absorption coefficient of ~104 cm^{-1},[49] a 20 mg film prepared with 25 wt % TiO_2, which corresponds to a film thickness of ~1.8 μm, would be expected to absorb ~98% of incoming radiation at this wavelength and virtually all of that at shorter wavelengths.

3.3.4 Cyclohexene reactivity at the illuminated TiO_2 surface

Motivated by our observations of nitrate-enhanced photooxidation of isopropanol, we also performed a set of experiments to probe the possible oxidation of cyclohexene, a representative alkene, at the illuminated TiO_2 surface. In these experiments, TiO_2 films prepared from KNO_3-containing slurries were exposed to gas-phase cyclohexene under dark conditions. Then, with gas-phase cyclohexene still present, the films were illuminated. Representative results from these experiments are presented in Figure 3-8.

No change in the cyclohexene signal (*m/z* 67) was observed upon exposure to the KNO_3-doped TiO_2 surface in the dark. In addition, no change in cyclohexene signal was observed upon exposure to unmodified TiO_2 films under light or dark conditions. However, as illustrated in Figure 3-8, we did observe a small uptake of cyclohexene by illuminated KNO_3-doped TiO_2 films. These observations suggest that a loss process for gas-phase cyclohexene was activated upon illumination of the KNO_3- doped TiO_2 surface. By contrast, in control experiments using KNO_3-doped SiO_2 films under both

dark and illuminated conditions, we saw no cyclohexene uptake. We conclude that the photoinduced cyclohexene loss observed at the KNO_3-doped TiO_2 surface did not arise from the reaction of cyclohexene with hydroxyl radical produced either via TiO_2 surface photochemistry or via direct nitrate anion photolysis. Interestingly, no production of NO was observed in these experiments.

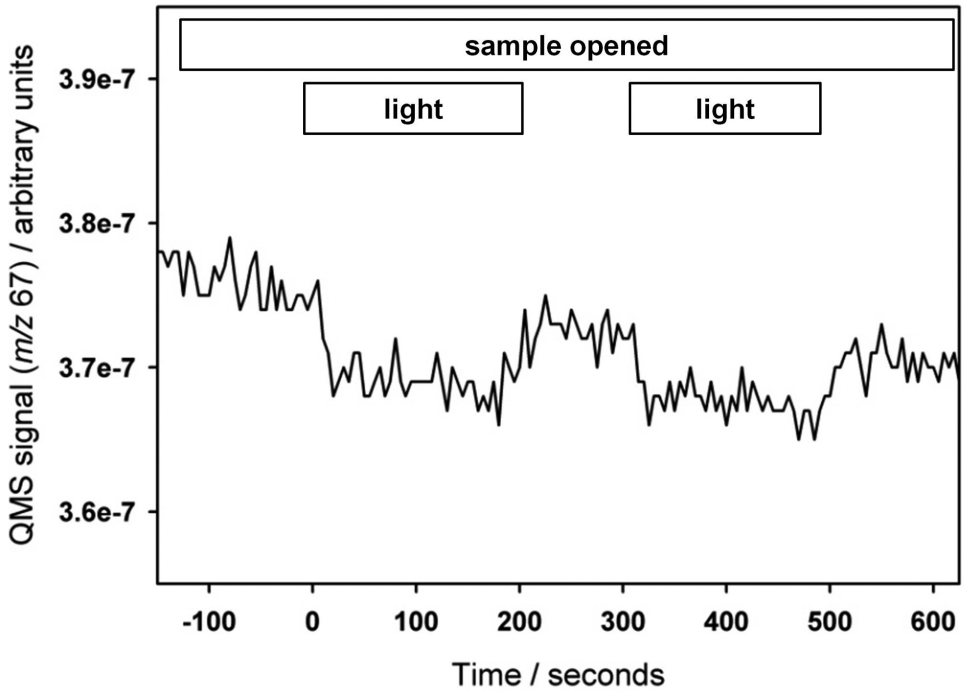

Figure 3-8 Representative QMS trace showing variation in gas-phase cyclohexene QMS signal (*m/z* 67) upon exposure to KNO_3-doped TiO_2 films (film mass 20 mg) under dark and illuminated conditions. Time = 0 indicates when the sample was first illuminated.

3.4 Discussion

The experiments described above show that isopropanol and *n*-propanol are efficiently transformed into acetone and propionaldehyde, respectively, on illuminated

TiO_2 dust. This photooxidation is substantially enhanced in the presence of nitrate anion. These observations are atmospherically significant because they demonstrate that actinically transparent compounds, such as alcohols, may be oxidized to tropospherically photoactive compounds via uptake to mineral dust surfaces, thereby changing the production rate and distribution of organic radical species in the atmosphere.[50]

In order to draw a connection between our experimental conditions (i.e., low pressure, oxygen-free) and conditions in the real atmosphere, we first consider the expected mechanism for acetone production from isopropanol adsorbed on TiO_2 surfaces under ambient conditions:[51, 52]

$TiO_2 + h\nu$ (E > 3.2 eV) → $h^+_{vb} + e_{cb}$ *(2)*

$>TiOH + h^+_{vb}$ → $\{>TiOH\cdot\}^+$ *(3)*

$h^+_{vb} + e_{cb}$ → heat *(4)*

$\{>TiOH\cdot\}^+ + e_{cb}$ → $>TiOH$ *(5)*

$O_2 + e_{cb}$ → $O_2^{-}\cdot$ *(6)*

$h^+_{vb} + (CH_3)_2CHOH$ →→ $(CH_3)_2CO$ *(7)*

$\{>TiOH\cdot\}^+ + (CH_3)_2CHOH$ →→ $(CH_3)_2CO$ *(8)*

$O_2^{-}\cdot + (CH_3)_2CHOH$ →→ $(CH_3)_2CO$ *(9)*

As shown in eq 2, TiO_2 produces electron hole pairs upon illumination. The photoproduced holes, which are strong one- electron oxidizing agents, have the potential to react directly with adsorbed isopropanol and/or to react with the hydrated TiO_2 surface (>TiOH) to yield surface-sorbed hydroxyl radical, which can

subsequently react with adsorbed isopropanol via hydrogen abstraction (see ref 52 for a comprehensive discussion of the mechanisms of heterogeneous photocatalysis on TiO_2). As shown in eqs 4 and 5, the availability of holes for oxidative surface processes is limited by charge-carrier recombination. Under real atmospheric conditions, this recombination is reduced by trapping of photoproduced electrons by adsorbed oxygen molecules (eq 6). However, in the absence of oxygen, as in the present experiments, this electron-trapping pathway is not available. As we will outline in the following paragraphs, both silver ion and nitrate anion can serve this purpose in the Knudsen cell.

As illustrated in Figure 4, a substantial enhancement in isopropanol uptake and acetone production was observed in the presence of both KNO_3 and $AgNO_3$. We attribute this result in part to the electron-trapping effect of nitrate anion, which would act to limit charge-carrier recombination at the TiO_2 surface and thus increase the availability of holes for oxidative processing of adsorbed isopropanol:[53]

$$NO_3^+ + 4H^+ + 3e_{cb} \rightarrow NO + 2H_2O \qquad (E^0 = 0.957\ V) \qquad (10)$$

Our observation of substantial gas-phase NO production from KNO_3-doped TiO_2 in the presence of isopropanol provides support for this mechanism. In addition, the TiO_2-catalyzed photoreduction of nitrate in aqueous solution has previously been observed in the presence of oxalic acid[54] or 2-propanol[55] as hole scavengers; under these conditions, however, the primary product was ammonia.

As shown in Figure 4, films prepared with $AgNO_3$ produced more acetone than films prepared with KNO_3. We attribute this enhancement in acetone production to competitive electron trapping by silver ion:[53, 56]

$$Ag^+ + e_{cb} \rightarrow Ag \qquad (E^0 = 0.80\ V) \qquad (11)$$

The lack of gas-phase NO observed under these conditions provides support for this reaction competing favorably with that shown in eq 10 under our experimental conditions. This enhancement of TiO_2 photochemistry echoes previous observations of enhanced TiO_2 catalytic efficiency in the presence of cosorbed silver species.[57, 58]

In summary, these results imply that the alcohol photooxidation results obtained within our cell are likely lower estimates for the efficiency of these processes in the real atmosphere, where ample oxygen is available to reduce charge-carrier recombination at the TiO_2 surface. Indeed, a number of studies have found that the TiO_2-catalyzed photooxidation of isopropanol is reduced in the absence of gas-phase oxygen.[42, 43]

The results of previous investigations of the photochemistry of nitrate on TiO_2 surfaces[21, 59] suggest a further possibility: that the enhanced production of acetone observed upon illumination of the nitrate-doped TiO_2 film may have arisen in part by the direct reaction of adsorbed isopropanol with oxidatively produced nitrate radical:[51, 60]

$$TiO_2 + h\nu \ (E > 3.2 \text{ eV}) \rightarrow h^+_{vb} + e_{cb} \qquad (2)$$

$$NO_3^+ + h^+_{vb} \rightarrow NO_3\cdot \qquad (E^0 = 2.30 \text{ V}) \qquad (12)$$

$$NO_3\cdot + (CH_3)_2CHOH \rightarrow (CH_3)_2COH\cdot + HNO_3 \qquad (13)$$

$$NO_3\cdot + (CH_3)_2COH\cdot \rightarrow (CH_3)_2CO + HNO_3 \qquad (14)$$

In the gas phase, the reaction of isopropanol with nitrate radical proceeds via hydrogen abstraction with a rate coefficient of 1.4×10^{-15} cm^3 $molecule^{-1}$ s^{-1}.[61] The reaction of nitrate radical with the alkyl radical thus produced has been estimated to proceed with a rate coefficient of 5×10^{-13} cm^3 $molecule^{-1}$ s^{-1}.[62] Given that reactions on surfaces often proceed more quickly than their gas-phase counterparts,[31] these rate

constants likely represent lower limits to those appropriate for the dust surface.

Under our experimental conditions (*i.e.*, in the absence of surface-sorbed oxygen), it is difficult to distinguish between these two potential nitrate enhancement pathways. However, our observations using cyclohexene as the gas-phase reagent provide some experimental evidence for the existence of reactive nitrate radical. In these experiments, whose results are illustrated in Figure 6, we observed a small uptake of cyclohexene to the illuminated surface of TiO_2 prepared from slurries containing KNO_3 but no uptake, either in the dark or under illumination, to unmodified TiO_2 films. Experiments performed using KNO_3-doped SiO_2 films provided evidence that this nitrate-induced enhancement did not arise via reaction of cyclohexene with surface-sorbed hydroxyl radical produced by direct nitrate photolysis. Further, if the nitrate-mediated uptake of cyclohexene had arisen via electron capture by nitrate and subsequent enhanced availability of holes for oxidative processing, as was the case for isopropanol, we would have expected to see a relationship between cyclohexene consumption and NO production. However, we did not observe any gas-phase NO during these experiments.

Given these considerations, we propose that the uptake of cyclohexene by the illuminated KNO_3-doped TiO_2 film was mediated by photoproduced nitrate radical, with which cyclohexene is known to react rapidly: in the gas phase, the reaction rate coefficient is $(6.3 \pm 1.3) \times 10^{-13}$ cm^3 molecule^{-1} s^{-1}, which is 450 times greater than that for the reaction of nitrate radical with isopropanol.[63] Further support for this reactive pathway is afforded by a set of experiments investigating the photochemistry of TiO_2 films prepared from KNO_3 or $AgNO_3$-containing aqueous slurries in the absence of gas-phase isopropanol. These results are presented in the Appendix.

In summary, the results presented above suggest that mineral dust aerosol has the potential to catalyze the oxidative conversion of non-absorbing organic species to those that are photochemically active in the actinic region and thus act as a source of

radicals for further gas-phase and/or heterogeneous chemistry. The enhancement in alcohol photooxidation effected by cosorbed silver ion and nitrate anion implies that the present results represent a lower estimate for the atmospheric efficiency of TiO_2-induced photooxidation. In addition, our observation of enhanced photochemistry on TiO_2 films containing cosorbed nitrate anion suggests that such chemistry may be amplified on atmospherically processed dust particles, which often contain nitrate as a major constituent.[17, 64] Finally, our results provide a first indication that surface nitrate radical produced via mineral dust-catalyzed photooxidation of nitrate anion may be important not only as a photolytic source of gas-phase reactive nitrogen[21] but also as a reagent for surficial processing of adsorbed organics.

3.5 Supporting information

We suggest in the main text that in the absence of a suitable hole scavenger (*i.e.* isopropanol), nitrate anion may undergo photooxidative chemistry at the TiO_2 surface. Here, we provide additional evidence for this photooxidative pathway.

As illustrated in Figure S-1, the illumination of $AgNO_3$-doped TiO_2 films in the absence of gas-phase isopropanol led to the formation of gas-phase NO and smaller quantities of NO_2 and HONO. The illumination of KNO_3-doped films, however, led exclusively to the production of significantly smaller quantities of NO. Insight into this difference is provided by examining the proposed mechanism for photoxidation of nitrate on the TiO_2 surface (adapted from Ndour *et al.*[21]):

$$TiO_2 + h\nu \ (E > 3.2 \text{ eV}) \rightarrow h^+_{vb} + e_{cb} \qquad (S1)$$

$$NO_3^- + h^+_{vb} \rightarrow NO_3\cdot \qquad (S2)$$

$$NO_3\cdot + h\nu \rightarrow NO + O_2 \qquad (S3a)$$

$$\rightarrow NO_2 + O \qquad (S3b)$$

$NO_2 + e_{cb}$ → NO_2^- *(S4)*

$NO_2^- + h\nu$ → $NO + O$ *(S5)*

$NO_2^- + H^+$ → $HONO$ *(S6)*

$HONO + h\nu$ → $NO + OH$ *(S7)*

As shown in this series of reactions, the illumination of nitrate-doped TiO_2 films is believed[21, 59] to lead to the oxidative production of nitrate radical, which can subsequently photolyze to yield NO_2 and NO. The NO_2 thus produced can undergo one-electron reduction by photoproduced electrons to yield NO_2^-, which can subsequently photolyze to yield further NO or interact with adsorbed protons to yield gas-phase HONO. In the absence of oxygen, as was the case in the present experiments, the NO_2 produced via eq S3b would be expected to be rapidly reduced by photoproduced electrons, and thus would not be expected to be emitted to the gas phase. Indeed, as described above, we observed production of NO alone from TiO_2 films prepared using KNO_3.

In the case of $AgNO_3$, however, we observed production not only of NO but also of smaller quantities of NO_2 and HONO. In addition, the production of NO was significantly higher than that observed for KNO_3-doped films. We suggest that both of these observations can be explained by competitive electron trapping by silver ion,[56] which allowed for some escape of NO_2 to the gas phase prior to its reduction via eq S4 and simultaneously enhanced the availability of holes for nitrate oxidation:

$Ag^+ + e_{cb}$ → Ag *(S8)*

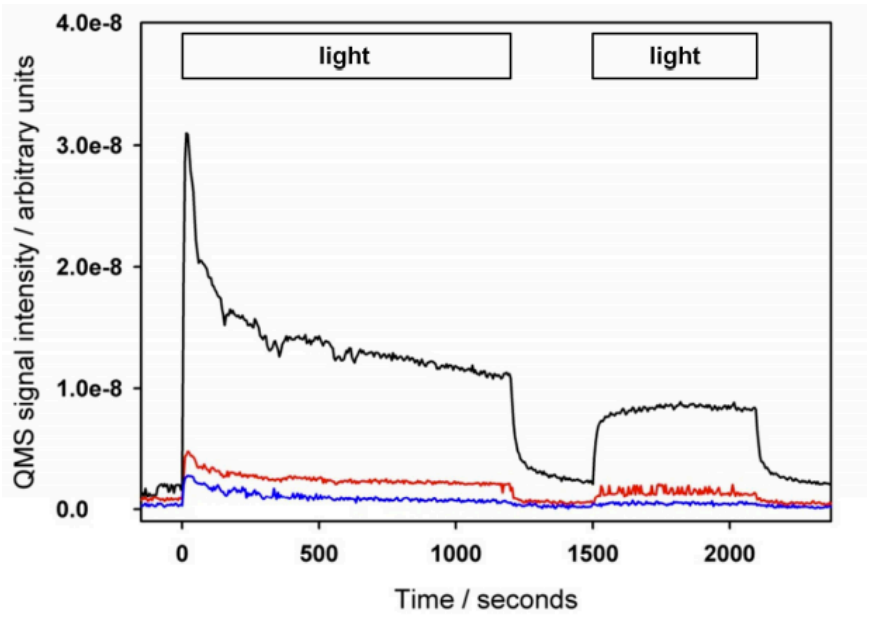

Figure S-1 Representative QMS traces for production of gas-phase NO_2 (*m/z* 46; red trace), NO (*m/z* 30; black trace), and HONO (*m/z* 47; blue trace) upon illumination of $AgNO_3$-doped TiO_2 films (film mass 20 mg).

In summary, these experiments provide support for the existence of an oxidative pathway for phototransformation of nitrate on the TiO_2 surface in the absence of strongly-sorbed hole scavengers such as isopropanol.

In the main text, we describe a set of experiments performed using cyclohexene as the gas-phase probe molecule. In these experiments, we observed no uptake of cyclohexene by an unmodified TiO_2 film, even if the film was illuminated. This observation implies that cyclohexene did not interact with the TiO_2 film and, unlike isopropanol, was not available for the scavenging of photoproduced holes. In the presence of co-sorbed KNO_3, however, a small uptake of cyclohexene was observed. We suggest that this uptake arose as a result of the reaction of cyclohexene with nitrate radical produced via the photooxidation process outlined in the above mechanism.

3.6 References

1. Andreae, M. O.; Rosenfeld, D., Aerosol cloud precipitation interactions. Part 1. The nature and sources of cloud-active aerosols. *Earth-Sci. Rev.* **2008,** *89*, (1 2), 13 41.

2. Solomon, S.; Qin, D.; Manning, M.; Chen, Z.; Marquis, M.; Averyt, K. B.; Tignor, M.; Miller, H. L. *Contribution of Working Group I to the Fourth Assessment Report of the IPCC*; Cambridge, UK and New York, NY, USA.

3. Usher, C. R.; Michel, A. E.; Grassian, V. H., Reactions on mineral dust. *Chem. Rev.* **2003,** *103*, (12), 4883 4939.

4. Perry, K. D.; Cahill, T. A.; Eldred, R. A.; Dutcher, D. D.; Gill, T. E., Long-range transport of North African dust to the eastern United States. *J. Geophys. Res.–Atmos.* **1997,** *102*, (D10), 11225 11238.

5. Kanatani, K. T.; Ito, I.; Al-Delaimy, W. K.; Adachi, Y.; Mathews, W. C.; Ramsdell, J. W.; Toyama Asian Desert Dust and Asthma Study Team, Desert dust exposure is associated with increased risk of asthma hospitalization in children. *Am. J. Respir. Crit. Care Med.* **2010,** *182*, (12), 1475 1481.

6. McNaughton, C. S.; Clarke, A. D.; Kapustin, V.; Shinozuka, Y.; Howell, S. G.; Anderson, B. E.; Winstead, E.; Dibb, J.; Scheuer, E.; Cohen, R. C.; Wooldridge, P.; Perring, A.; Huey, L. G.; Kim, S.; Jimenez, J. L.; Dunlea, E. J.; DeCarlo, P. F.; Wennberg, P. O.; Crounse, J. D.; Weinheimer, A. J.; Flocke, F., Observations of heterogeneous reactions between Asian pollution and mineral dust over the Eastern North Pacific during INTEX-B. *Atmos. Chem. Phys.* **2009,** *9*, (21), 8283 8308.

7. Fairlie, T. D.; Jacob, D. J.; Dibb, J. E.; Alexander, B.; Avery, M. A.; van Donkelaar, A.; Zhang, L., Impact of mineral dust on nitrate, sulfate, and ozone in transpacific Asian pollution plumes. *Atmos. Chem. Phys.* **2010,** *10*, (8), 3999 4012.

8. Li, J. W.; Han, Z. W., A modeling study of the impact of heterogeneous reactions on mineral aerosol surfaces on tropospheric chemistry over East Asia. *Particuology* **2010,** *8*, (5), 433-441.

9. Zhu, S.; Butler, T.; Sander, R.; Ma, J.; Lawrence, M. G., Impact of dust on tropospheric chemistry over polluted regions: a case study of the Beijing megacity. *Atmos. Chem. Phys.* **2010,** *10*, (8), 3855 3873.

10. Mogili, P. K.; Kleiber, P. D.; Young, M. A.; Grassian, V. H., Heterogeneous uptake of ozone on reactive components of mineral dust aerosol: An environmental aerosol reaction chamber study. *J. Phys. Chem. A* **2006,** *110*, (51), 13799 13807.

11. Grassian, V. H., Heterogeneous uptake and reaction of nitrogen oxides and volatile organic compounds on the surface of atmospheric particles including oxides, carbonates, soot and mineral dust: implications for the chemical balance of the troposphere. *Int. Rev. Phys. Chem.* **2001,** *20*, (3), 467 548.

12. Borensen, C.; Kirchner, U.; Scheer, V.; Vogt, R.; Zellner, R., Mechanism and kinetics of the reactions of NO_2 or HNO_3 with alumina as a mineral dust model compound. *J. Phys. Chem. A* **2000,** *104*, (21), 5036 5045.

13. Cwiertny, D. M.; Young, M. A.; Grassian, V. H., Chemistry and photochemistry of mineral dust aerosol. *Annu. Rev. Phys. Chem.* 2008, *59*, 27 51.

14. Fu, H.; Wang, X.; Wu, H.; Yin, Y.; Chen, J., Heterogeneous uptake and oxidation of SO_2 on iron oxides. *J. Phys. Chem. C* **2007,** *111*, (16), 6077 6085.

15. Hanisch, F.; Crowley, J. N., Heterogeneous reactivity of gaseous nitric acid on Al_2O_3, $CaCO_3$, and atmospheric dust samples: a Knudsen cell study. *J. Phys. Chem. A* **2001,** *105*, (13), 3096 3106.

16. Underwood, G. M.; Li, P.; Al-Abadleh, H.; Grassian, V. H., A Knudsen cell study of the heterogeneous reactivity of nitric acid on oxide and mineral dust particles. *J. Phys. Chem. A* **2001,** *105*, (27), 6609 6620.

17. Li, W. J.; Shao, L. Y., Observation of nitrate coatings on atmospheric mineral dust particles. *Atmos. Chem. Phys.* **2009,** *9*, (6), 1863 1871.

18. Hanisch, F.; Crowley, J. N., Ozone decomposition on Saharan dust: an experimental investigation. *Atmos. Chem. Phys.* **2003,** *3*, 119 130.

19. Linke, C.; Moehler, O.; Veres, A.; Mohacsi, A.; Bozoki, Z.; Szabo, G.; Schnaiter, M., Optical properties and mineralogical composition of different Saharan mineral dust samples: a laboratory study. *Atmos. Chem. Phys.* **2006,** *6*, 3315 3323.

20. Parmon, V. N.; Zakharenko, V. S., Photocatalysis and photosorption in the Earth's atmosphere. *Cattech* **2001,** *5*, (2), 96-115.

21. Ndour, M.; Conchon, P.; D'Anna, B.; Ka, O.; George, C., Photochemistry of mineral dust surface as a potential atmospheric renoxification process. *Geophys. Res. Lett.* **2009,** *36*.

22. Ndour, M.; D'Anna, B.; George, C.; Ka, O.; Balkanski, Y.; Kleffmann, J.; Stemmler, K.; Ammann, M., Photoenhanced uptake of NO_2 on mineral dust: Laboratory experiments and model simulations. *Geophys. Res. Lett.* **2008,** *35*, (5).

23. Nicolas, M.; Ndour, M.; Ka, O.; D'Anna, B.; George, C., Photochemistry of atmospheric dust: Ozone decomposition on illuminated titanium dioxide. *Environ. Sci. Technol.* **2009,** *43*, (19), 7437 7442.

24. Carp, O.; Huisman, C. L.; Reller, A., Photoinduced reactivity of titanium dioxide. *Prog. Solid State Chem.* **2004,** *32*, (1 2), 33 177.

25. Gaya, U. I.; Abdullah, A. H., Heterogeneous photocatalytic degradation of organic contaminants over titanium dioxide: A review of fundamentals, progress and problems. *J. Photochem. Photobiol., C* **2008,** *9*, (1), 1 12.

26. Mo, J.; Zhang, Y.; Xu, Q.; Lamson, J. J.; Zhao, R., Photocatalytic purification of volatile organic compounds in indoor air: a literature review. *Atmos. Environ.* **2009,** *43*, (14), 2229 2246.

27. Lagesson-Andrasko, L.; Lagesson, V.; Andrasko, J., The use of gas-phase UV spectra in the 168 330 nm wavelength region for analytical purposes. 1. Qualitative measurements. *Anal. Chem.* **1998,** *70*, (5), 819 826.

28. Martinez, R. D.; Buitrago, A. A.; Howell, N. W.; Hearn, C. H.; Joens, J. A., The near-UV absorption spectra of several aliphatic aldehydes and ketones at 300 K. *Atmos. Environ. A* **1992,** *26*, (5), 785 792.

29. Li, P.; Perreau, K. A.; Covington, E.; Song, C. H.; Carmichael, G. R.; Grassian, V. H., Heterogeneous reactions of volatile organic compounds on oxide particles of the most abundant crustal elements: surface reactions of acetaldehyde, acetone, and propionaldehyde on SiO_2, Al_2O_3, Fe_2O_3, TiO_2, and CaO. *J. Geophys. Res. Atmos.* **2001,** *106*, (D6), 5517 5529.

30. Carlos-Cuellar, S.; Li, P.; Christensen, A. P.; Krueger, B. J.; Burrichter, C.; Grassian, V. H., Heterogeneous uptake kinetics of volatile organic compounds on oxide surfaces using a Knudsen cell reactor: adsorption of acetic acid, formaldehyde, and methanol on alpha-Fe_2O_3, alpha-Al_2O_3, and SiO_2. *J. Phys. Chem. A* **2003,** *107*, (21), 4250 4261.

31. Donaldson, D. J.; Mmereki, B. T.; Chaudhuri, S. R.; Handley, S.; Oh, M., Uptake and reaction of atmospheric organic vapours on organic films. *Faraday Discuss.* **2005,** *130*, 227 239.

32. Stern, K. H., High-temperature properties and decomposition of inorganic salts. Part 3: nitrates and nitrites. *J. Phys. Chem. Ref. Data* **1972,** *1*, (3), 747 772.

33. Kahan, T. F. Experimental investigations of physical and chemical processes at air ice interfaces. PhD Thesis, University of Toronto, 2010.

34. Finlayson-Pitts, B. J.; Pitts, J. N., *Chemistry of the upper and lower atmosphere*. Academic Press: San Diego, CA, 2000.

35. Chaudhuri, S. R. Heterogeneous uptake of atmospheric organic gas phase species by condensed organic film substrates: a low-pressure effusive cell study. MSc Thesis, University of Toronto, 2006.

36. Li, P.; Al-Abadleh, H. A.; Grassian, V. H., Measuring heterogeneous uptake coefficients of gases on solid particle surfaces with a Knudsen cell reactor: complications due to surface saturation and gas diffusion into underlying layers. *J. Phys. Chem. A* **2002,** *106*, (7), 1210 1219.

37. Underwood, G. M.; Li, P.; Usher, C. R.; Grassian, V. H., Determining accurate kinetic parameters of potentially important heterogeneous atmospheric reactions on solid particle surfaces with a Knudsen cell reactor. *J. Phys. Chem. A* **2000,** *104*, (4), 819 829.

38. Sassine, M.; Burel, L.; D'Anna, B.; George, C., Kinetics of the tropospheric formaldehyde loss onto mineral dust and urban surfaces. *Atmos. Environ.* **2010,** *44*, (40), 5468 5475.

39. Zhao, Y.; Chen, Z.; Shen, X.; Zhang, X., Kinetics and mechanisms of heterogeneous reaction of gaseous hydrogen peroxide on mineral oxide particles. *Environ. Sci. Technol.* **2011,** *45*, (8), 3317 3324.

40. Linstrom, P. J.; Mallard, W. G., *NIST Chemistry WebBook, NIST Standard Reference Database 69*. National Institute of Standards and Technology: Gaithersburg, MD, 20899.

41. Vildozo, D.; Ferronato, C.; Sleiman, M.; Chovelon, J., Photocatalytic treatment of indoor air: optimization of 2-propanol removal using a response surface methodology (RSM). *Appl. Catal., B* **2010,** *94*, (3 4), 303 310.

42. Chang, C. P.; Chen, J. N.; Lu, M. C., Characteristics of photocatalytic oxidation of gaseous 2-propanol using thin-film TiO_2 photocatalyst. *J. Chem. Technol. Biotechnol.* **2004,** *79*, (11), 1293 1300.

43. Larson, S. A.; Widegren, J. A.; Falconer, J. L., Transient studies of 2-propanol photocatalytic oxidation on titania. *J. Catal.* **1995,** *157*, (2), 611 625.

44. Xu, W. Z.; Raftery, D., Photocatalytic oxidation of 2-propanol on TiO_2 powder and TiO_2 monolayer catalysts studied by solid-state NMR. *J. Phys. Chem. B* **2001,** *105*, (19), 4343 4349.

45. Vincent, G.; Marquaire, P. M.; Zahraa, O., Photocatalytic degradation of gaseous 1-propanol using an annular reactor: kinetic modelling and pathways. *J. Hazard. Mater.* **2009,** *161*, (2 3), 1173 1181.

46. Mack, J.; Bolton, J. R., Photochemistry of nitrite and nitrate in aqueous solution: a review. *J. Photochem. Photobiol., A* **1999,** *128*, (1 3), 1 13.

47. Ndour, M.; Nicolas, M.; D'Anna, B.; Ka, O.; George, C., Photoreactivity of NO_2 on mineral dusts originating from different locations of the Sahara desert. *Phys. Chem. Chem. Phys.* **2009,** *11*, (9), 1312 1319.

48. Adedokun, J. A.; Emofurieta, W. O.; Adedeji, O. A., Physical, mineralogical and chemical properties of Harmattan dust at Ile-Ife, Nigeria. *Theor. Appl. Climatol.* **1989,** *40*, (3), 161 169.

49. Ghosh, A. K.; Maruska, H. P., Photoelectrolysis of water in sunlight with sensitized semiconductor electrodes. *J. Electrochem. Soc.* **1977,** *124*, (10), 1516 1522.

50. Mu, Y. J.; Mellouki, A., The near-UV absorption cross sections for several ketones. *J. Photochem. Photobiol., A* **2000,** *134*, (1 2), 31 36.

51. Rajeshwar, K., Photoelectrochemistry and the environment. *J. Appl. Electrochem.* **1995,** *25*, (12), 1067 1082.

52. Hoffmann, M. R.; Martin, S. T.; Choi, W. Y.; Bahnemann, D. W., Environmental applications of semiconductor photocatalysis. *Chem. Rev.* **1995,** *95*, (1), 69 96.

53. Haynes, W. M., *CRC Handbook of Chemistry and Physics, 91st Edition (Internet Version 2011)*. CRC Press / Taylor and Francis: Boca Raton, Florida.

54. Li, Y. X.; Wasgestian, F., Photocatalytic reduction of nitrate ions on TiO_2 by oxalic acid. *J. Photochem. Photobiol., A* **1998,** *112*, (2-3), 255 259.

55. Ohtani, B.; Kakimoto, M.; Miyadzu, H.; Nishimoto, S.; Kagiya, T., Effect of surface-adsorbed 2-propanol on the photocatalytic reduction of silver and/or nitrate ions in acidic TiO_2 suspension. *J. Phys. Chem.* **1988,** *92*, (20), 5773 5777.

56. Litter, M. I., Heterogeneous photocatalysis: transition metal ions in photocatalytic systems. *Appl. Catal., B* **1999,** *23*, (2 3), 89 114.

57. Colmenares, J. C.; Aramendia, M. A.; Marinas, A.; Marinas, J. M.; Urbano, F. J., Synthesis, characterization and photocatalytic activity of different metal-doped titania systems. *Appl. Catal., A* **2006,** *306*, 120 127.

58. Crittenden, J. C.; Liu, J. B.; Hand, D. W.; Perram, D. L., Photocatalytic oxidation of chlorinated hydrocarbons in water. *Water Res.* **1997,** *31*, (3), 429 438.

59. Monge, M. E.; D'Anna, B.; George, C., Nitrogen dioxide removal and nitrous acid formation on titanium oxide surfaces an air quality remediation process? *Phys. Chem. Chem. Phys.* **2010,** *12*, (31), 8992 8999.

60. Wardman, P., Reduction potentials of one-electron couples involving free radicals in aqueous solution. *J. Phys. Chem. Ref. Data* **1989,** *18*, (4), 1637 1755.

61. Chew, A. A.; Atkinson, R.; Aschmann, S. M., Kinetics of the gas-phase reactions of NO_3 radicals with a series of alcohols, glycol ethers, ethers and chloroalkenes. *J. Chem. Soc., Faraday Trans.* **1998,** *94*, (8), 1083 1089.

62. Langer, S.; Ljungstrom, E., Rates of reaction between the nitrate radical and some aliphatic alcohols. *J. Chem. Soc., Faraday Trans.* **1995,** *91*, (3), 405 410.

63. Ljungstrom, E.; Wangberg, I.; Langer, S., Absolute rate coefficients for the reaction between nitrate radicals and some cyclic alkenes. *J. Chem. Soc., Faraday Trans.* **1993,** *89*, (16), 2977 2982.

64. Sullivan, R. C.; Guazzotti, S. A.; Sodeman, D. A.; Prather, K. A., Direct observations of the atmospheric processing of Asian mineral dust. *Atmos. Chem. Phys.* **2007,** *7*, 1213 1236.

Chapter 4

Heterogeneous photochemistry of oxalic acid on Mauritanian sand and Icelandic volcanic ash

Contributions:

All experiments were designed and conducted by Sarah A. Styler. Milos Markovic provided assistance with ion chromatography. The manuscript was written by Sarah A. Styler, with critical comments from D. James Donaldson.

4.1 Introduction

Terrestrial volcanism and Aeolian processes emit teragram quantities of solid oxide aerosol into the atmosphere on an annual basis.[1, 2] Although these particles are emitted locally, their smallest size fractions undergo efficient long-range transport, and thus can be distributed widely: Saharan dust, for example, has been detected in the southeastern United States[3] and volcanic ash from the 2010 eruption of Eyjafjallajökull in Iceland was detected over 25 European countries.[4]

During transport, mineral dust mixes with industrial, urban, and biogenic pollutant plumes; in some cases, dust can serve as a vector for the long-range transport of anthropogenic emissions.[5-10] Dust–pollutant interactions can have a profound effect on dust composition, even close to source regions: in one recent study, for example, mineral dust particles in M'Bour, Senegal, were shown to possess an amorphous carbonaceous coating.[11] In addition, chemical analysis of advected Saharan dust has shown it to contain a wide variety of semi-volatile organic compounds, including pesticides, polycyclic aromatic hydrocarbons (PAH), and organic acids.[12] The interaction of gas-phase organic species with mineral dust and its individual components, including Al_2O_3, Fe_2O_3, SiO_2, and TiO_2, has also been explored in the laboratory.[13-20] Together, the results obtained in these field and laboratory studies suggest that the mineral dust surface has the potential to play a significant role in the heterogeneous processing of gas-phase organic species.

Despite the fact that mineral and volcanic aerosols contain a variety of photoactive metal oxides,[21, 22] little attention has been paid to the photochemistry that may occur on these chemically complex surfaces. To date, studies of dust photochemistry have largely focused on the photochemical reactions of adsorbed inorganic species, including ozone,[23, 24] nitrogen dioxide,[22, 25, 26] and nitrate.[27-33] By contrast, few studies have investigated the mineral dust-catalyzed photochemistry of adsorbed organic species.[15, 34-36]

In both urban and remote environments, oxalic acid is typically the most atmospherically abundant aerosol-phase dicarboxylic acid.[37-39] Its atmospheric sources include direct emission from biomass burning[40] and transportation[41] and indirect formation via the gas- and aqueous-phase oxidation of a variety of precursor species, including glyoxal[42-44] and isoprene.[45, 46] Oxalic acid photolyzes only slowly in the gas phase, and its gas-phase reactivity with OH is low.[37] It is, therefore, expected to be removed from the troposphere primarily by wet deposition,[45] with lesser contributions from its atmospheric aqueous-phase photolysis, both direct[47] and iron-catalyzed,[48, 49] and its reaction with dissolved ozone[50] and hydroxyl radical.[45] In arid regions, therefore, its atmospheric residence time might be expected to be lengthy and perhaps modified by the existence of additional, aerosol-phase, loss processes.

A recent spectroscopic investigation of aerosol composition in Tsukuba, Japan showed that 20–80% of aerosol-phase oxalate was present as Ca and Zn oxalate complexes.[51] Given that oxalic acid will also form complexes with iron and other metal ions present in atmospheric aerosols, these observations suggest that metal-catalyzed photochemistry may be an unrecognized loss pathway for aerosol-phase oxalic acid. Indeed, in a study performed as part of the ACE-Asia campaign, Sullivan and Prather[52] found that Gobi and Taklimakan desert dust-associated oxalic acid concentrations exhibited a strong nighttime maximum. Those authors speculated that this maximum did not imply the existence of a significant daytime photochemical loss pathway for this species but rather reflected the nighttime arrival of photochemically processed dust that was rich in oxalic acid. To our knowledge, the diurnal variability in concentrations of dicarboxylic acids associated with Saharan or Australian dust, both of which are richer in iron than Gobi desert dust[53] and thus would be expected to be more photochemically active, has not received study.

In an attempt to assess the importance of metal-catalyzed photochemical processing of aerosol-phase dicarboxylic acids, the heterogeneous photochemistry of oxalic acid was

investigated at the surface of authentic Mauritanian sand and volcanic ash from the eruption of the Icelandic volcano Eyjafjallajökull using our previously developed photochemical Knudsen cell.[15]

4.2 Materials and methods

4.2.1 Experimental apparatus

Experiments were performed in a custom-built photochemical Knudsen cell, which we have previously used to investigate the photooxidation of isopropanol on TiO_2 and TiO_2–KNO_3 films.[15] In brief, the reactor consists of a 730 cm^3 stainless-steel T-shaped chamber, the bottom flange of which is modified to act as a sample compartment (3.1 cm diameter). A quartz inset in the bottom of this compartment allows for the illumination of samples. Pressures within the reactor are maintained at a baseline range of $3–5 \times 10^{-2}$ Pa using a turbopump. Gas-phase reaction products effuse out of the reactor through a 3 mm diameter exit orifice and are detected using a quadrupole mass spectrometer (QMS) with 70 eV electron-impact ionization. Illumination of samples was accomplished using the output beam of a 150 W xenon arc lamp, which was directed through the quartz window of the sample compartment to illuminate samples from below. A 10 cm water filter was used to reduce the infrared component of the illumination beam. The resultant spectral profile is presented in Figure 4-1.

4.2.2 Experimental procedure

Experimental samples were prepared as internal mixtures by suspending 10–50 mg of Fe_2O_3, Mauritanian sand, or Icelandic volcanic ash in 2 mL of 5–10 mM aqueous oxalic acid. The resultant slurry was transferred via pipet to a shallow 3 cm diameter Pyrex sample holder, which was subsequently heated for 1.5 h in a 373 K oven to yield a film of relatively uniform thickness. No further efforts were made to remove

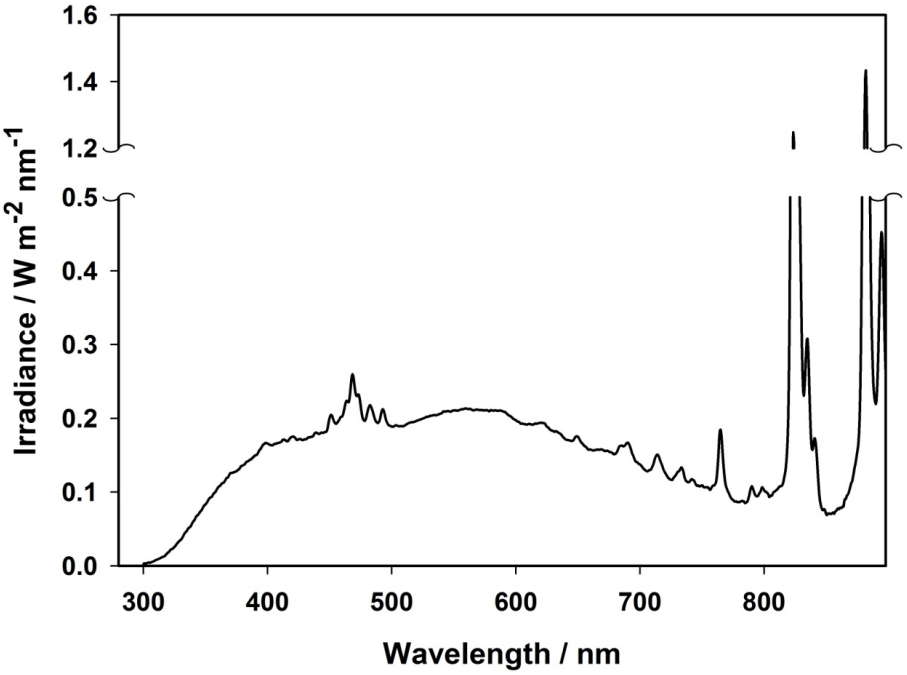

Figure 4-1 Spectral profile of the 120 W Xe arc lamp used for irradiation after its passage through a water filter to remove the bulk of infrared radiation.

---

adsorbed water from the samples. Before each experiment commenced, the sample holder containing the substrate of interest was placed into the reaction chamber, and the apparatus was evacuated for ~1h until a constant background pressure of $\sim 3 \times 10^{-2}$ Pa was reached. At this point, background levels of *m/z* 44 (CO_2) were measured using the QMS. At that time, the sample film was illuminated for time periods ranging from 20–60 min. In some cases, optical long-pass filters were used to restrict the wavelengths of illumination (the transmission spectra of these filters are presented in Figure 4-2). In order to fully capture the desorption of volatile photoproducts, QMS data were recorded not only during the illumination period but also for 15 min after its cessation. A set of experiments was also performed to measure the quantity of

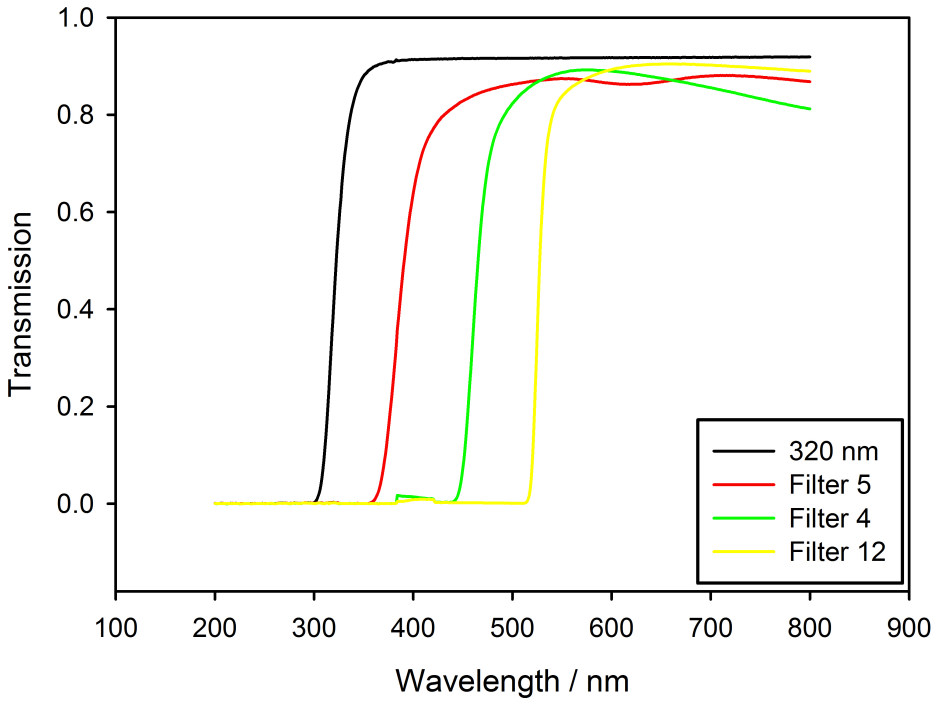

Figure 4-2 Transmission spectra of the long-pass optical filters used to obtain the results in Figure 4-5. The 10% transmission wavelength of each filter is the wavelength used on the x-axis of the action spectrum in Figure 4-5.

---

oxalic acid remaining at the surface of Mauritanian sand films as a function of illumination time. In these experiments, the sample holders were removed from the Knudsen reactor after illumination and immersed in 20 mL of deionized water. A Pasteur pipet was used to mechanically agitate the sand film and disperse it within the extraction volume. The resultant suspensions were centrifuged, diluted by a factor of 250, filtered through a 0.2 μm PTFE membrane (Acrodisc, VWR International), and analyzed using ion chromatography.

4.2.3 Ion chromatography

Ion chromatographic analysis was accomplished using a Dionex ICS-2000 system, which was operated with reagent-free KOH eluent and suppressed conductivity detection. Oxalate was separated using the gradient elution method of VandenBoer et al.[54] on an AS19 hydroxide-selective anion exchange column fitted with a trace anion concentrator column (TAC-ULP1), guard column, and ASRS 300 conductivity suppressor. Samples were quantified using external calibration curves created from a stock solution of oxalic acid (1 mg/mL, Sigma Aldrich).

4.2.4 Chemicals

Oxalic acid (ACS grade, Fisher Scientific), Fe_2O_3 (≥99%, Sigma Aldrich), SiO_2 (99.9%, Alfa Aesar), and TiO_2 (anatase, ≥99%, Sigma Aldrich) were used as received. The Mauritanian sand used in the present experiments, which has previously been shown to catalyze the photochemical reduction of gas-phase NO_2,[22, 25] was generously donated by Dr. Christian George. The Icelandic volcanic ash sample was obtained from a Reykjavik tourist shop following the 2010 Eyjafjallajökull eruption. Both authentic samples were finely ground in a mortar and pestle prior to use.

4.3 Results

4.3.1 Sample characterization

The bulk compositions of the Mauritanian sand and Icelandic volcanic ash samples were determined using wavelength-dispersive X-ray fluorescence spectrometry in the analytical laboratories of the Department of Geology, University of Toronto.

As shown in Table 4-1, the Mauritanian sand is primarily composed of quartz (94 wt % SiO_2), with smaller quantities of aluminum (1.4 wt %), iron (0.2 wt %), and titanium (0.1 wt%). Its orange-red coloration is likely due to a thin surficial layer of iron oxide,

	Icelandic Volcanic Ash		Mauritanian Sand	
	Mass %	Element %	Mass %	Element %
SiO_2	58.66	27.42	94.116	43.99
Al_2O_3	14.25	7.54	2.571	1.36
FeO / Fe_2O_3	8.75	6.80	0.335	0.23
CaO	4.73	3.38	0.041	0.03
Na_2O	4.69	3.48	0.055	0.04
MgO	2.68	1.61	0.135	0.08
K_2O	1.97	1.64	0.181	0.15
TiO_2	1.66	0.99	0.219	0.13
P_2O_5	0.42	0.18	0.022	0.01
SO_3	0.22	0.09	--	--
MnO	0.19	0.15	--	--
Cl	0.16	0.16	--	--
	Trace elements (ppm)			
Ba	450		--	
Br	10		--	
Cu	40		--	
Ga	20		--	
Ni	80		80	
Nb	60		--	
Rb	50		10	
Sr	300		10	
Y	70		--	
Zn	170		--	
Zr	550		340	

Table 4-1 Elemental composition of the Icelandic volcanic ash and Mauritanian sand samples, as determined using wavelength-dispersive X-ray fluorescence spectrometry.

perhaps present in association with clay minerals.[55] These analytical results agree reasonably well with those of Ndour et al.,[22] who previously estimated the iron (1 wt %) and titanium (1 wt %) content of this sand using inductively coupled plasma optical emission spectrometry (ICP-OES).

The elemental composition of Eyjafjallajökull volcanic ash is significantly more complex: this substrate contains substantial quantities of iron (6.8 wt %) and titanium (1 wt %), both of which would be expected to promote photochemistry at the ash surface, and a variety of trace metal species. These results agree well with those of ref 21, which previously reported the bulk composition of this substrate measured using ICP-OES.

4.3.2 Photochemical production of CO_2 from oxalic acid at the surface of Mauritanian sand and Icelandic volcanic ash

As shown in Figures 4-3 and 4-4, the illumination of films prepared from suspensions of Mauritanian sand or Icelandic volcanic ash in deionized water without added oxalic acid resulted in an immediate increase in the QMS signal associated with gas-phase CO_2 (*m/z* 44). When illumination ceased, the CO_2 signal rapidly returned to its initial value. These observations clearly imply that the CO_2 production by these films was photochemical in nature.

In the presence of surface-sorbed oxalic acid, the production of gas-phase CO_2 by these films was enhanced by more than an order of magnitude. The direct photolysis of oxalic acid did not play a substantial role in this enhancement: as illustrated in Figure 4-3, the production of gas-phase CO_2 from oxalic acid at the surface of a SiO_2 film was relatively insignificant and was comparable to that produced by the Mauritanian sand film in the absence of oxalic acid. Together, these results show that while both Mauritanian sand and Icelandic volcanic ash catalyzed the heterogeneous photooxidation of oxalic acid and the resultant production of gas-phase CO_2, SiO_2 did not.

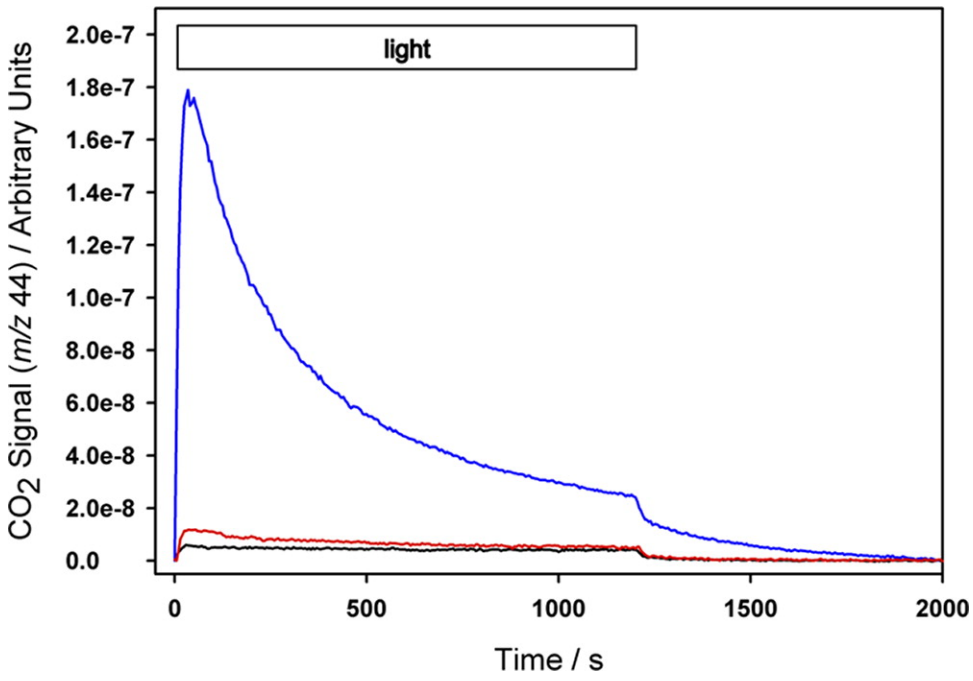

Figure 4-3 Representative QMS traces for production of gas-phase CO_2 (*m/z* 44) from oxalic acid at the surface of Mauritanian sand (5 mM oxalic acid; 50 mg sand; blue trace) and SiO_2 (10 mM oxalic acid; 20 mg SiO_2; red trace). For comparison, the black trace represents production of CO_2 by the Mauritanian sand film (50 mg) in the absence of oxalic acid. Time = 0 indicates when the samples were first illuminated.

In order to gain insight into the mechanism(s) of the observed catalysis, action spectra were obtained for gas-phase CO_2 production integrated over a 20-min illumination period and subsequent 15-min falloff period as a function of illumination wavelength. For purposes of comparison, these experiments were also performed for oxalic acid at the surface of Fe_2O_3 films. As shown in Figure 4-5, the wavelength dependence of CO_2 production at the surface of all three sample types displays a qualitative resemblance to the aqueous-phase absorption spectrum of iron(III) oxalate,[49] which suggests that iron-mediated photochemistry may have contributed to the observed results.

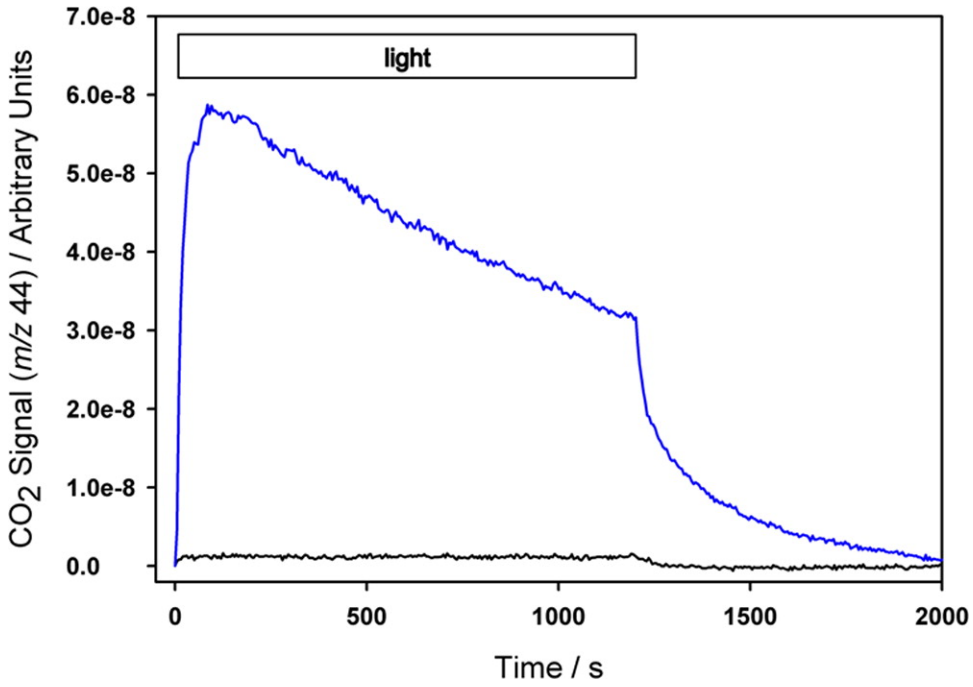

Figure 4-4 Representative QMS trace for production of gas-phase CO_2 (*m/z* 44) from oxalic acid at the surface of Icelandic volcanic ash (5 mM oxalic acid; 50 mg ash; blue trace). For comparison, the black trace represents production of CO_2 by the Icelandic ash film (50 mg) in the absence of oxalic acid. Time = 0 indicates when the samples were first illuminated.

The experiments described thus far were all performed under low-pressure, oxygen-free conditions. In order to assess the relevance of our results under conditions more reflective of the ambient environment, the photochemistry of oxalic acid at the surface of Mauritanian sand, Icelandic volcanic ash, and Fe_2O_3 was also investigated in the presence of ~0.7 Pa oxygen. As illustrated in Figure 4-6a, the presence of oxygen suppressed CO_2 production at the Fe_2O_3 surface. At the surface of Icelandic ash, by contrast, Figure 4-6b shows that the presence of oxygen had no apparent effect on the quantity of CO_2 produced. At the surface of Mauritanian sand, CO_2 production was

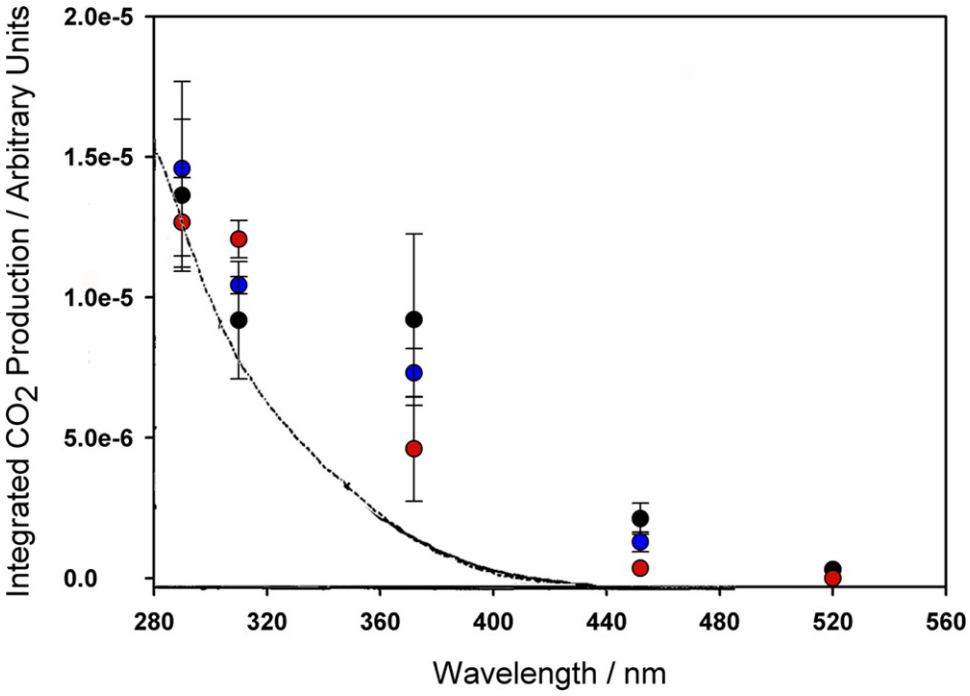

Figure 4-5 Action spectra for gas-phase CO_2 production from oxalic acid at the surface of Mauritanian sand (5 mM oxalic acid; 50 mg sand; blue circles), Icelandic volcanic ash (5 mM oxalic acid; 50 mg ash; red circles), and Fe_2O_3 (10 mM oxalic acid; 10 mg Fe_2O_3; black circles). Each point is the mean of three or more trials. The black trace represents the aqueous-phase absorption spectrum of iron(III) oxalate and is taken from ref 48. Wavelengths are reported as the 10% transmission wavelength of the long-pass optical filter used. The filter transmission spectra are displayed in Figure 4-2.

---

substantially enhanced in the presence of oxygen (Figure 4-6c). In control experiments performed using Mauritanian sand samples prepared from slurries in deionized water without added oxalic acid, however, this oxygen-induced enhancement in CO_2 production was not observed.

As shown in Table 4-1, the Mauritanian sand and Icelandic ash samples contain 0.2 wt % and 1.7 wt % TiO_2, respectively. In order to assess the contribution of Ti-mediated photochemistry to the observed results, the production of gas-phase CO_2 from oxalic acid was investigated at the surface of TiO_2 films in the presence and the

absence of gas-phase oxygen. As illustrated in Figure 4-6d, the production of CO_2 from these films was substantially enhanced in the presence of oxygen.

4.3.3 Photochemical loss of oxalic acid at the surface of Mauritanian sand

In an attempt to explore the photochemical oxidation of oxalic acid from the surface perspective, oxalic acid was extracted from illuminated Mauritanian sand films and quantified as oxalate anion using ion chromatography. The results of these experiments are displayed in Figure 4-7, where the quantity of oxalic acid remaining in the film (normalized to the quantity of oxalic acid remaining in a set of nonilluminated films prepared in an identical manner and subjected to vacuum conditions in the Knudsen cell) is plotted with a representative CO_2 production trace as a function of illumination time.

After ~60 min of illumination, gas-phase CO_2 production by the sand film was negligible; in addition, no further loss of oxalic acid was observed. At this point, the quantity of oxalic acid remaining within the film was ~85% of its preillumination value. This observation implies that the photoreactive pathways explored in the present experiment were available to only ~15% of surface-sorbed oxalic acid molecules and/or that the inherent photoactivity of the film in the absence of gas-phase oxygen was diminished at long time scales.

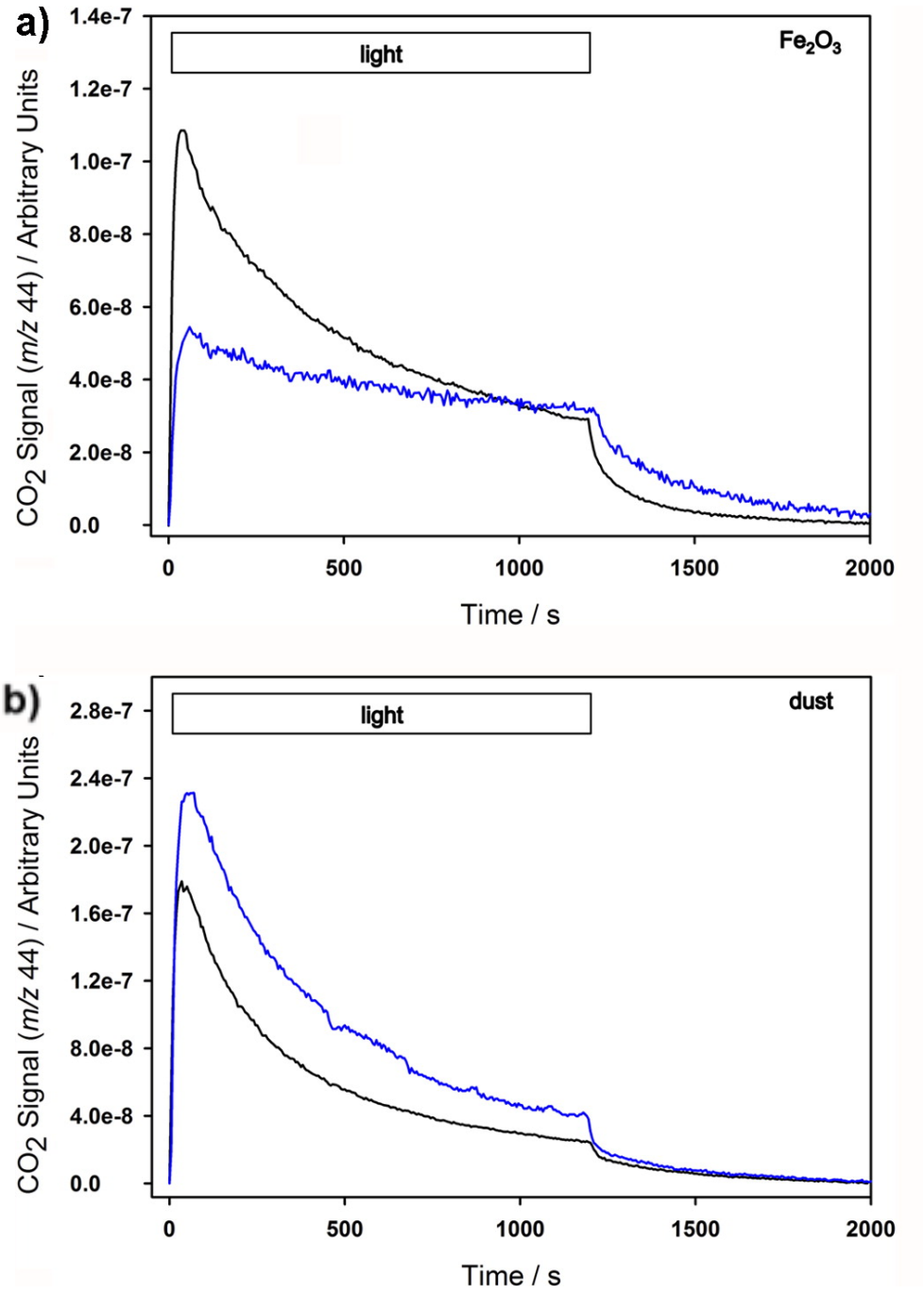

Figure 4-6 Production of gas-phase CO_2 from oxalic acid in the presence (blue trace) and absence (black trace) of 0.7 Pa oxygen, at the surface of a) Fe_2O_3 (10 mM oxalic acid; 10 mg Fe_2O_3) and b) Mauritanian sand (5 mM oxalic acid; 50 mg sand). Time = 0 indicates when the samples were first illuminated.

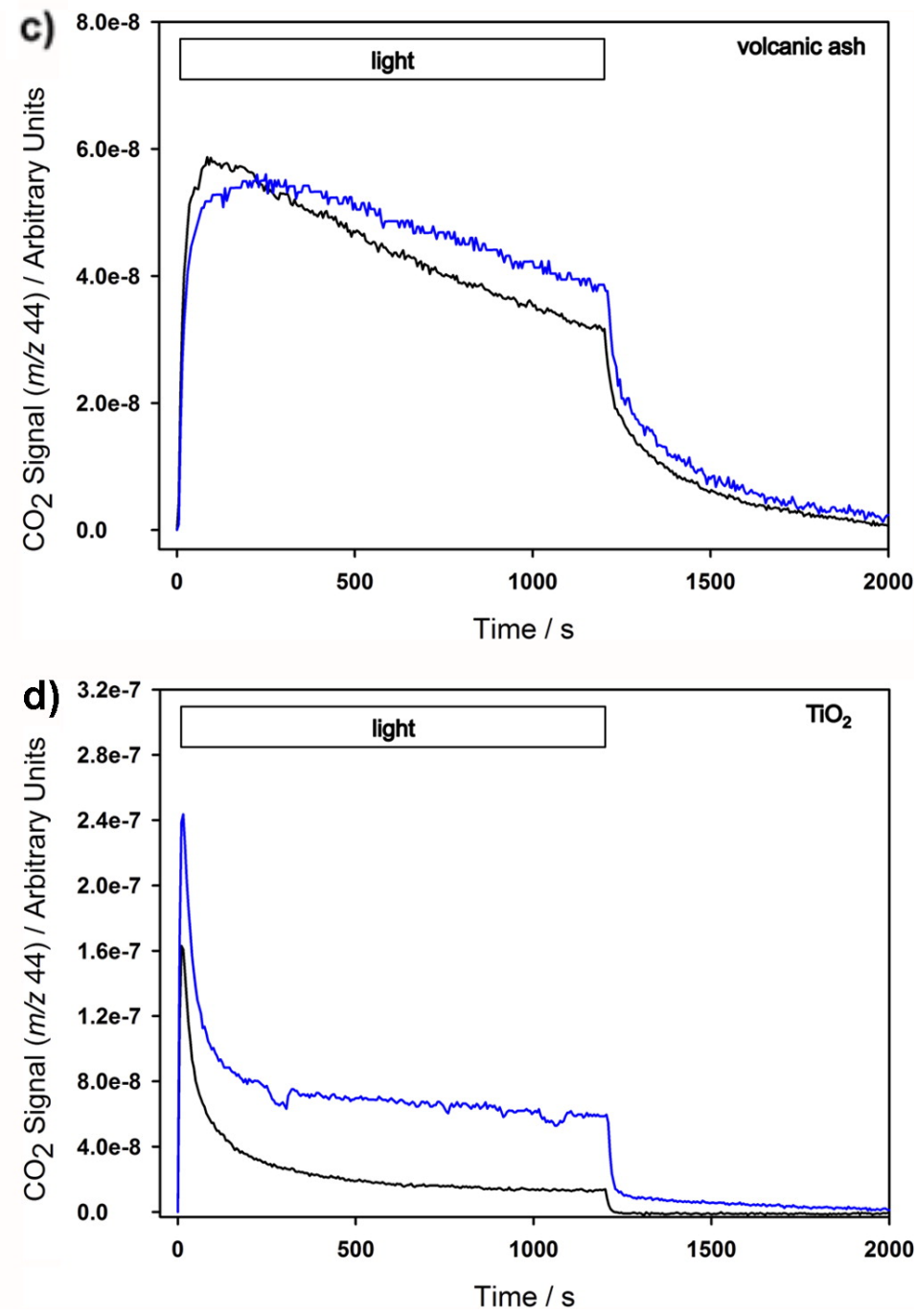

Figure 4-6 Production of gas-phase CO_2 from oxalic acid in the presence (blue trace) and absence (black trace) of 0.7 Pa oxygen, at the surface of c) Icelandic volcanic ash (5 mM oxalic acid; 50 mg ash) and d) TiO_2 (10 mM oxalic acid; 10 mg TiO_2). Time = 0 indicates when the samples were first illuminated.

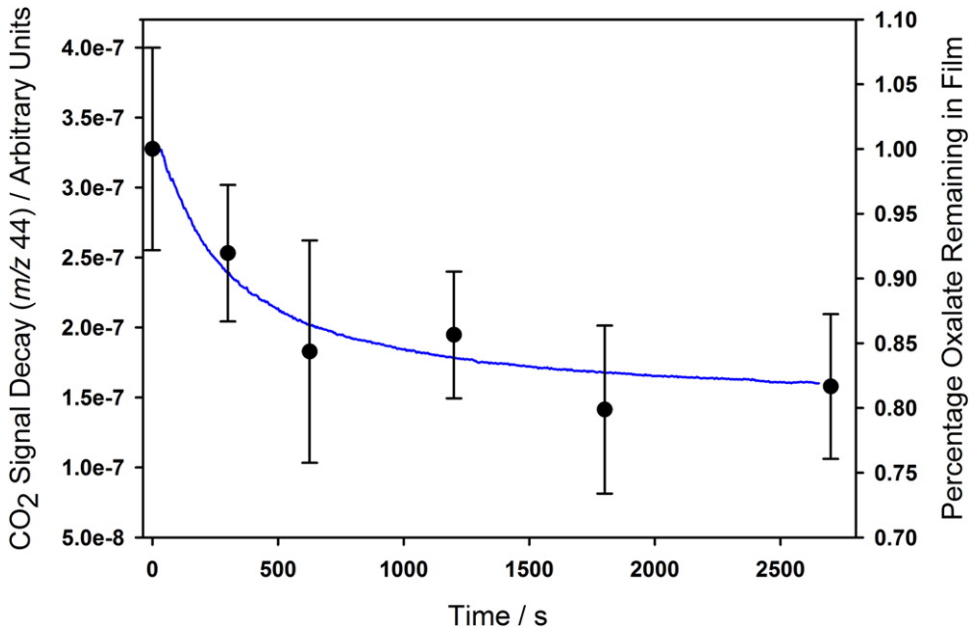

Figure 4-7 Composite figure showing the decay in gas-phase CO_2 signal during illumination of oxalic acid at the surface of Mauritanian dust (5 mM, 50 mg, blue trace, left axis) and the quantity of oxalic acid remaining in the film as a function of illumination time (black circles, right axis), normalized to the quantity of oxalic acid remaining in a set of nonilluminated films prepared in an identical manner and subjected to vacuum conditions in the Knudsen cell. Each data point represents the mean of three trials, each of which was performed using a fresh sample.

4.4 Discussion

4.4.1 CO_2 production from illuminated sand and ash films in the absence of oxalic acid

Figures 4-3 and 4-4 illustrate that the illumination of Mauritanian sand and Icelandic volcanic ash films leads to the production of gas- phase CO_2, even in the absence of added oxalic acid. Although the release of CO_2 upon illumination has previously been observed for TiO_2[56, 57] and a variety of other semiconductors,[58] the present work provides, to our knowledge, the first demonstration of this phenomenon on real

environmental substrates.

It has been proposed that the capture of conduction-band electrons by oxygen molecules physisorbed to surface carbon impurities on semiconductor surfaces leads to the production of chemisorbed carboxyl groups (CO_2–).[59] In the case of TiO_2 nanoparticles, these moieties have also been shown to arise via the interaction of gas-phase CO_2 with the semiconductor surface.[60] Given that our samples were stored under ambient conditions and were not subjected to a high-temperature treatment prior to use, it thus seems reasonable for CO_2– to have been present.

The mechanism of light-induced CO_2 production by semiconductor surfaces is believed to involve the oxidation of chemisorbed CO_2– by photogenerated holes to yield physisorbed CO_2, which can subsequently undergo thermal desorption.[59] These observations have implications for the laboratory study of photochemical reactions occurring at environmental surfaces, since they imply that gas-phase CO_2 produced upon illumination of an organic-coated surface may originate not only from chemistry involving the organic adsorbate but also from photoactive carboxyl functionalities present within the surface itself.

4.4.2 Heterogeneous photooxidation of oxalic acid: mechanistic insights

As shown in Figures 4-3 and 4-4, the illumination of oxalic acid at the surface of Mauritanian sand and Icelandic volcanic ash resulted in the production of gas- phase CO_2; in addition, at least in the case of Mauritanian sand, as shown in Figure 4-7, the production of CO_2 scaled with the loss of surface oxalic acid. The results from experiments at the SiO_2 surface presented in Figure 4-3 provide evidence that the direct photolysis of oxalic acid at the surface of these films did not contribute substantially to the observed CO_2 production and further imply that the photochemical oxidation of oxalic acid was mediated by photoactive species within the films themselves.

Interestingly, comparison of Figures 4-3 and 4-4 also shows that the time dependence of gas-phase CO_2 production at the surface of Mauritanian sand differed significantly from that at the surface of Icelandic ash. This observation, which most likely reflects a convolution of the differing chemical composition, specific surface area, and optical transmittance of these two substrates, highlights the substrate-dependent nature of this photochemistry and provides direct evidence for the value of laboratory experiments performed using authentic environmental samples.

As shown in Figure 4-5, the action spectra for gas-phase CO_2 production at the surface of Mauritanian sand and Icelandic volcanic ash resemble the absorption spectrum of iron(III) oxalate.[49] This observation, coupled with the fact that both substrates contain measurable quantities of iron, suggests that the observed heterogeneous photochemistry of oxalic acid was, at least in part, iron-mediated. In fact, the iron-catalyzed photochemistry of oxalic acid has long been known to be a significant aqueous-phase loss process for this species.[48, 49, 61] Although the precise mechanism of iron oxalate photochemistry in aqueous solution is still the topic of much discussion,[62-64] it is generally agreed that gas-phase CO_2 is the sole oxidative product. The reactions involved in the CO_2 production are proposed to be[62, 65, 66]

$$Fe^{III}\ \ C_2O_4^{2} + h\nu \rightarrow Fe^{II} + C_2O_4\bullet \qquad (1a)$$

$$\rightarrow Fe^{III} + 2\ CO_2\bullet \qquad (1b)$$

$$C_2O_4\bullet \rightarrow CO_2\uparrow + CO_2\bullet \qquad (2)$$

$$CO_2\bullet + Fe^{III}\ C_2O_4^{2} \rightarrow CO_2\uparrow + Fe^{II} + C_2O_4^{2} \qquad (3)$$

In the presence of dissolved oxygen, the carboxyl radical anion may react to produce superoxide anion and, by extension, hydroxyl radical[61]

$$CO_2\bullet + O_2 \rightarrow CO_2\uparrow + O_2\bullet \qquad (4)$$

$O_2 \bullet + H_2O \rightarrow HO_2\bullet + OH$ *(5)*

$HO_2\bullet + HO_2\bullet \rightarrow H_2O_2 + O_2$ *(6)*

$H_2O_2 + h\nu \rightarrow 2\ \bullet OH$ *(7)*

Although literature on the iron-catalyzed photochemistry of oxalic acid in the solid phase is sparse, several older studies have investigated the solid-state photochemistry of potassium trisoxalatoferrate(III) trihydrate.[67-69] These studies have, variously, suggested that the photochemical mechanism is similar to that occurring in aqueous solution,[68] that it involves the formation of bridged intermediates,[67] and that it occurs via the formation of electron–hole pairs in the solid and the subsequent hole-mediated oxidation of oxalate anion.[69]

In the present experiments, we observed that the production of CO_2 from oxalic acid at the Fe_2O_3 surface was reduced in the presence of oxygen. This observation agrees with that of Spencer and Schmidt,[69] who found that the quantum yield for Fe^{II} production from potassium trisoxalatoferrate(III) trihydrate increased at low pressures. Given that oxygen is an efficient electron-capturing agent and would thus be expected to reduce electron–hole recombination and therefore increase the availability of holes at the illuminated Fe_2O_3 surface, these results suggest that the iron-catalyzed photooxidation of oxalic acid at the Fe_2O_3 surface likely did not proceed via a direct, hole-mediated pathway. The resemblance of the action spectrum for CO_2 production at this surface, shown in Figure 4-5, to the absorption spectrum of iron (III) oxalate provides additional evidence for this assertion. These results imply that the importance of iron-catalyzed photochemistry is reduced under ambient conditions. We speculate that this reduction may be attributable to the nonreactive quenching of a long-lived charge-transfer complex by adsorbed oxygen.

Interestingly, this reduction in CO_2 production upon introduction of gas-phase oxygen was observed neither at the surface of Mauritanian sand nor at the surface of

volcanic ash: at the volcanic ash surface, the presence of oxygen did not influence CO_2 production; at the Mauritanian sand surface, the presence of gas-phase oxygen enhanced CO_2 production. The different behavior observed at the sand and ash surfaces is likely attributable to the different chemical composition of these two substrates. Together, these observations imply that iron-mediated chemistry was not the only photochemical pathway available at the surface of these substrates. The most obvious candidate for this new pathway is photochemistry involving TiO_2, which is present in both authentic samples. Evidence for this assertion is provided in Figure 4-6d, which shows that the production of CO_2 by oxalic acid at the surface of an illuminated TiO_2 film was substantially enhanced in the presence of oxygen. The following photo-Kolbe mechanistic pathway is consistent with this observation:[70]

$TiO_2 + h\nu\,(E > 3.2\ eV) \rightarrow h^+_{vb} + e_{cb}$ *(8)*

$h_{vb}^+ + e_{cb} \rightarrow$ *heat* *(9)*

$O_2 + e \rightarrow O_2\bullet$ *(10)*

$C_2O_4^{2-} + h^+_{vb} \rightarrow C_2O_4\bullet$ *(11)*

$C_2O_4\bullet \rightarrow CO_2\uparrow + CO_2\bullet$ *(2)*

$CO_2\bullet + O_2 \rightarrow CO_2\uparrow + O_2\bullet$ *(4)*

4.4.3 Atmospheric significance

In the present set of experiments, we have shown that the illumination of oxalic acid deposited on Mauritanian sand and Icelandic volcanic ash films leads to the production of gas-phase CO_2. Further, we have provided evidence that this phototransformation is mediated by Fe and Ti contained within the films. This is, to our knowledge, the first investigation of oxalic acid photochemistry on authentic solid-phase environmental samples, and one of the first studies to demonstrate

conclusively the role that metal- containing aerosols may play in influencing the lifetime of atmospherically relevant organic compounds.

Adsorbed water is known to play a complex role in photochemistry occurring on mineral surfaces.[71] Although the low-pressure environment of the Knudsen cell precludes the performance of experiments in the presence of water vapor at levels typical of the troposphere, we note that our samples were not subject to intense heating regimes and thus would have been expected to contain some strongly adsorbed water. The formation of oxalic acid in cloud droplets[42-46] and deliquesced aerosol[72] and the aqueous-phase iron-catalyzed photochemistry of oxalic acid[48, 49] have received much research attention. Our results, however, suggest that heterogeneous loss processes exist for this species even under arid conditions.

In a study of oxalic acid in Shanghai aerosol, Yang et al.[72] observed a distinct diurnal trend in the concentration of dust- associated oxalic acid, with significantly higher concentrations occurring at nighttime. The same trend was also observed by He and Kawamura[73] for aerosol-phase oxalic acid in a suburban site north of Beijing. In both cases, these authors attributed these observations to enhanced nighttime production of oxalic acid via the aqueous-phase processing of precursor organic species. However, the results obtained in the present experiments suggest that this phenomenon may also have arisen as a result of the existence of aerosol-catalyzed photochemical loss processes for this species during daylight hours.

The reactive pathways explored in the present study may also be available to other adsorbed carboxylic acids: citric, glyoxalic, malonic, and pyruvic acids are known to undergo iron-catalyzed photochemistry in the aqueous phase,[48, 61] and TiO_2 has been shown to catalyze the aqueous-phase photooxidation of malonic and succinic acids.[74] Unlike oxalic acid, however, whose photochemistry in the presence of oxygen would be expected to produce HO_x via eqs 4–7, the decarboxylation of carboxylate radicals derived from longer-chain acids would ultimately result in the production of peroxy

radicals,[61] which would have the potential to undergo further chemistry at the aerosol surface.

4.5 References

1. Andreae, M. O.; Rosenfeld, D., Aerosol cloud precipitation interactions. Part 1. The nature and sources of cloud-active aerosols. *Earth-Sci. Rev.* **2008,** *89*, (1 2), 13 41.

2. Durant, A. J.; Bonadonna, C.; Horwell, C. J., Atmospheric and environmental impact of volcanic particulates. *Elements* **2010,** *6*, (4), 235 240.

3. Prospero, J. M., Long-term measurements of the transport of African mineral dust to the southeastern United States: implications for regional air quality. *J. Geophys. Res.–Atmos.* **1999,** *104*, (D13), 15,917 15,927, doi:10.1029/1999JD900072.

4. Langmann, B.; Folch, A.; Hensch, M.; Matthias, V., Volcanic ash over Europe during the eruption of Eyjafjallajökull on Iceland, April May 2010. *Atmos. Environ.* **2012,** *48*, 1 8.

5. Huang, K.; Zhuang, G. S.; Li, J. A.; Wang, Q. Z.; Sun, Y. L.; Lin, Y. F.; Fu, J. S., Mixing of Asian dust with pollution aerosol and the transformation of aerosol components during the dust storm over China in Spring 2007. *J. Geophys. Res.–Atmos.* **2010,** *115*, D00K13, doi:10.1029/2009JD013145.

6. Rodriguez, S.; Alastuey, A.; Alonso-Perez, S.; Querol, X.; Cuevas, E.; Abreu-Afonso, J.; Viana, M.; Perez, N.; Pandolfi, M.; de la Rosa, J., Transport of desert dust mixed with North African industrial pollutants in the subtropical Saharan Air Layer. *Atmos. Chem. Phys.* **2011,** *11*, (13), 6663 6685.

7. Petzold, A.; Veira, A.; Mund, S.; Esselborn, M.; Kiemle, C.; Weinzierl, B.; Hamburger, T.; Ehret, G.; Lieke, K.; Kandler, K., Mixing of mineral dust with urban pollution aerosol over Dakar (Senegal): impact on dust physico-chemical and radiative properties. *Tellus B* **2011,** *63*, (4), 619 634.

8. Li, C.; Tsay, S. C.; Fu, J. S.; Dickerson, R. R.; Ji, Q. A.; Bell, S. W.; Gao, Y.; Zhang, W.; Huang, J. P.; Li, Z. Q.; Chen, H. B., Anthropogenic air pollution observed near dust source regions in northwestern China during springtime 2008. *J. Geophys. Res.–Atmos.* **2010,** *115*, D00K22, doi:10.1029/2009JD013659.

9. Erel, Y.; Dayan, U.; Rabi, R.; Rudich, Y.; Stein, M., Trans-boundary transport of pollutants by atmospheric mineral dust. *Environ. Sci. Technol.* **2006,** *40*, (9), 2996 3005.

10. Jaffe, D.; McKendry, I.; Anderson, T.; Price, H., Six 'new' episodes of trans-Pacific transport of air pollutants. *Atmos. Environ.* **2003,** *37*, (3), 391 404.

11. Deboudt, K.; Flament, P.; Choel, M.; Gloter, A.; Sobanska, S.; Colliex, C., Mixing state of aerosols and direct observation of carbonaceous and marine coatings

on African dust by individual particle analysis. *J. Geophys. Res.–Atmos.* **2010,** *115*, D24207, doi:10.1029/2010JD013921.

12. Falkovich, A. H.; Schkolnik, G.; Ganor, E.; Rudich, Y., Adsorption of organic compounds pertinent to urban environments onto mineral dust particles. *J. Geophys. Res.–Atmos.* **2004,** *109*, D02208, doi:10.1029/2003JD003919.

13. Carlos-Cuellar, S.; Li, P.; Christensen, A. P.; Krueger, B. J.; Burrichter, C.; Grassian, V. H., Heterogeneous uptake kinetics of volatile organic compounds on oxide surfaces using a Knudsen cell reactor: adsorption of acetic acid, formaldehyde, and methanol on alpha-Fe_2O_3, alpha-Al_2O_3, and SiO_2. *J. Phys. Chem. A* **2003,** *107*, (21), 4250 4261.

14. Crowley, J. N.; Ammann, M.; Cox, R. A.; Hynes, R. G.; Jenkin, M. E.; Mellouki, A.; Rossi, M. J.; Troe, J.; Wallington, T. J., Evaluated kinetic and photochemical data for atmospheric chemistry: Volume V heterogeneous reactions on solid substrates. *Atmos. Chem. Phys.* **2010,** *10*, (18), 9059 9223.

15. Styler, S. A.; Donaldson, D. J., Photooxidation of atmospheric alcohols on laboratory proxies for mineral dust. *Environ. Sci. Technol.* **2011,** *45*, (23), 10004 10012.

16. Xu, B.; Shang, J.; Zhu, T.; Tang, X., Heterogeneous reaction of formaldehyde on the surface of gamma-Al_2O_3 particles. *Atmos. Environ.* **2011,** *45*, (21), 3569 3575.

17. Zhao, Y.; Chen, Z. M.; Zhao, J. N., Heterogeneous reactions of methacrolein and methyl vinyl ketone on alpha-Al_2O_3 particles. *Environ. Sci. Technol.* **2010,** *44*, (6), 2035 2041.

18. Tong, S. R.; Wu, L. Y.; Ge, M. F.; Wang, W. G.; Pu, Z. F., Heterogeneous chemistry of monocarboxylic acids on alpha-Al_2O_3 at different relative humidities. *Atmos. Chem. Phys.* **2010,** *10*, (16), 7561 7574.

19. Jie, C. Y.; Chen, Z. M.; Wang, H. L.; Hua, W.; Wang, C. X.; Li, S., Atmospheric heterogeneous reaction of acetone: adsorption and desorption kinetics and mechanisms on SiO_2 particles. *Chinese Sci. Bull.* **2008,** *53*, (7), 1004 1010.

20. Hatch, C. D.; Gough, R. V.; Tolbert, M. A., Heterogeneous uptake of the C-1 to C-4 organic acids on a swelling clay mineral. *Atmos. Chem. Phys.* **2007,** *7*, (16), 4445-4458.

21. Gislason, S. R.; Hassenkam, T.; Nedel, S.; Bovet, N.; Eiriksdottir, E. S.; Alfredsson, H. A.; Hem, C. P.; Balogh, Z. I.; Dideriksen, K.; Oskarsson, N.; Sigfusson, B.; Larsen, G.; Stipp, S. L. S., Characterization of Eyjafjallajökull volcanic ash particles and a protocol for rapid risk assessment. *PNAS* **2011,** *108*, (18), 7307 7312.

22. Ndour, M.; Nicolas, M.; D'Anna, B.; Ka, O.; George, C., Photoreactivity of NO_2 on mineral dusts originating from different locations of the Sahara desert. *Phys. Chem. Chem. Phys.* **2009,** *11*, (9), 1312 1319.

23. Nicolas, M.; Ndour, M.; Ka, O.; D'Anna, B.; George, C., Photochemistry of atmospheric dust: ozone decomposition on illuminated titanium dioxide. *Environ. Sci. Technol.* **2009,** *43*, (19), 7437 7442.

24. Chen, H. H.; Stanier, C. O.; Young, M. A.; Grassian, V. H., A kinetic study of ozone decomposition on illuminated oxide surfaces. *J. Phys. Chem. A* **2011,** *115*, (43), 11979 11987.

25. Ndour, M.; D'Anna, B.; George, C.; Ka, O.; Balkanski, Y.; Kleffmann, J.; Stemmler, K.; Ammann, M., Photoenhanced uptake of NO_2 on mineral dust: laboratory experiments and model simulations. *Geophys. Res. Lett.* **2008,** *35*, L05812, doi:10.1029/2007GL032006.

26. Monge, M. E.; D'Anna, B.; George, C., Nitrogen dioxide removal and nitrous acid formation on titanium oxide surfaces an air quality remediation process? *Phys. Chem. Chem. Phys.* **2010,** *12*, (31), 8992 8999.

27. Schuttlefield, J.; Rubasinghege, G.; El-Maazawi, M.; Bone, J.; Grassian, V. H., Photochemistry of adsorbed nitrate. *J. Am. Chem. Soc.* **2008,** *130*, (37), 12210 12211.

28. Navea, J. G.; Chen, H. H.; Huang, M.; Carmichel, G. R.; Grassian, V. H., A comparative evaluation of water uptake on several mineral dust sources. *Environ. Chem.* **2010,** *7*, (2), 162 170.

29. Ndour, M.; Conchon, P.; D'Anna, B.; Ka, O.; George, C., Photochemistry of mineral dust surface as a potential atmospheric renoxification process. *Geophys. Res. Lett.* **2009,** *36*, L05816, doi:10.1029/2008GL036662.

30. Rubasinghege, G.; Grassian, V. H., Photochemistry of adsorbed nitrate on aluminum oxide particle surfaces. *J. Phys. Chem. A* **2009,** *113*, (27), 7818 7825.

31. Rubasinghege, G.; Elzey, S.; Baltrusaitis, J.; Jayaweera, P. M.; Grassian, V. H., Reactions on atmospheric dust particles: surface photochemistry and size-dependent nanoscale redox chemistry. *J. Phys. Chem. Lett.* **2010,** *1*, (11), 1729 1737.

32. Chen, H. H.; Navea, J. G.; Young, M. A.; Grassian, V. H., Heterogeneous photochemistry of trace atmospheric gases with components of mineral dust aerosol. *J. Phys. Chem. A* **2011,** *115*, (4), 490 499.

33. Monge, M. E.; George, C.; D'Anna, B.; Doussin, J. F.; Jammoul, A.; Wang, J.; Eyglunent, G.; Solignac, G.; Daele, V.; Mellouki, A., Ozone formation from illuminated titanium dioxide surfaces. *J. Am. Chem. Soc.* **2010,** *132*, (24), 8234 8235.

34. Isidorov, V.; Klokova, E.; Povarov, V.; Kolkova, S., Photocatalysis on atmospheric aerosols: experimental studies and modeling. *Catal. Today* **1997,** *39*, 233 242.

35. Sassine, M.; Burel, L.; D'Anna, B.; George, C., Kinetics of the tropospheric formaldehyde loss onto mineral dust and urban surfaces. *Atmos. Environ.* **2010,** *44*, (40), 5468 5475.

36. Lackhoff, M.; Niessner, R., Photocatalytic atrazine degradation by synthetic minerals, atmospheric aerosols, and soil particles. *Environ. Sci. Technol.* **2002,** *36*, (24), 5342 5347.

37. Chebbi, A.; Carlier, P., Carboxylic acids in the troposphere, occurrence, sources, and sinks: a review. *Atmos. Environ.* **1996,** *30*, (24), 4233 4249.

38. Ho, K. F.; Ho, S. S. H.; Lee, S. C.; Kawamura, K.; Zou, S. C.; Cao, J. J.; Xu, H. M., Summer and winter variations of dicarboxylic acids, fatty acids and benzoic acid in PM(2.5) in Pearl Delta River Region, China. *Atmos. Chem. Phys.* **2011,** *11*, (5), 2197 2208.

39. Kawamura, K.; Narukawa, M.; Li, S. M.; Barrie, L. A., Size distributions of dicarboxylic acids and inorganic ions in atmospheric aerosols collected during polar sunrise in the Canadian high Arctic. *J. Geophys. Res.–Atmos.* **2007,** *112*, D10307, doi:10.1029/2006JD008244.

40. Falkovich, A. H.; Graber, E. R.; Schkolnik, G.; Rudich, Y.; Maenhaut, W.; Artaxo, P., Low molecular weight organic acids in aerosol particles from Rondônia, Brazil, during the biomass-burning, transition and wet periods. *Atmos. Environ.* **2005,** *5*, 781 797.

41. Kawamura, K.; Kaplan, I. R., Motor exhaust emissions as a primary source for dicarboxylic acids in Los Angeles ambient air. *Environ. Sci. Technol.* **1987,** *21*, (1), 105 110.

42. Rinaldi, M.; Decesari, S.; Carbone, C.; Finessi, E.; Fuzzi, S.; Ceburnis, D.; O'Dowd, C. D.; Sciare, J.; Burrows, J. P.; Vrekoussis, M.; Ervens, B.; Tsigaridis, K.; Facchini, M. C., Evidence of a natural marine source of oxalic acid and a possible link to glyoxal. *J. Geophys. Res.–Atmos.* **2011,** *116*, D16204, doi:10.1029/2011JD015659.

43. Carlton, A. G.; Turpin, B. J.; Altieri, K. E.; Seitzinger, S.; Reff, A.; Lim, H. J.; Ervens, B., Atmospheric oxalic acid and SOA production from glyoxal: results of aqueous photooxidation experiments. *Atmos. Environ.* **2007,** *41*, (35), 7588 7602.

44. Lee, A. K. Y.; Zhao, R.; Gao, S. S.; Abbatt, J. P. D., Aqueous-phase OH oxidation of glyoxal: application of a novel analytical approach employing aerosol mass spectrometry and complementary off-line techniques. *J. Phys. Chem. A* **2011,** *115*, (38), 10517 10526.

45. Myriokefalitakis, S.; Tsigaridis, K.; Mihalopoulos, N.; Sciare, J.; Nenes, A.; Kawamura, K.; Segers, A.; Kanakidou, M., In-cloud oxalate formation in the global troposphere: a 3-D modeling study. *Atmos. Chem. Phys.* **2011,** *11*, (12), 5761 5782.

46. Huang, D.; Zhang, X.; Chen, Z. M.; Zhao, Y.; Shen, X. L., The kinetics and mechanism of an aqueous phase isoprene reaction with hydroxyl radical. *Atmos. Chem. Phys.* **2011,** *11*, (15), 7399 7415.

47. Yang, L. M.; Ray, M. B.; Yu, L. E., Photooxidation of dicarboxylic acids Part II: Kinetics, intermediates and field observations. *Atmos. Environ.* **2008,** *42*, (5), 868 880.

48. Zuo, Y. G.; Hoigne, J., Photochemical decomposition of oxalic, glyoxalic and pyruvic acid catalyzed by iron in atmospheric waters. *Atmos. Environ.* **1994,** *28*, (7), 1231 1239.

49. Zuo, Y. G.; Hoigne, J., Formation of hydrogen peroxide and depletion of oxalic acid in atmospheric water by photolysis of iron(III)-oxalato complexes. *Environ. Sci. Technol.* **1992,** *26*, (5), 1014 1022.

50. Grgic, I.; Nieto-Gligorovski, L. I.; Net, S.; Temime-Roussel, B.; Gligorovski, S.; Wortham, H., Light induced multiphase chemistry of gas-phase ozone on aqueous pyruvic and oxalic acids. *Phys. Chem. Chem. Phys.* **2010,** *12*, (3), 698 707.

51. Furukawa, T.; Takahashi, Y., Oxalate metal complexes in aerosol particles: implications for the hygroscopicity of oxalate-containing particles. *Atmos. Chem. Phys.* **2011,** *11*, (9), 4289 4301.

52. Sullivan, R. C.; Prather, K. A., Investigations of the diurnal cycle and mixing state of oxalic acid in individual particles in Asian aerosol outflow. *Environ. Sci. Technol.* **2007,** *41*, (23), 8062 8069.

53. Usher, C. R.; Michel, A. E.; Grassian, V. H., Reactions on mineral dust. *Chem. Rev.* **2003,** *103*, (12), 4883 4939.

54. VandenBoer, T. C.; Petroff, A.; Markovic, M. Z.; Murphy, J. G., Size distribution of alkyl amines in continental particulate matter and their online detection in the gas and particle phase. *Atmos. Chem. Phys.* **2011,** *11*, (9), 4319 4332.

55. Gardner, R.; Pye, K., Nature, origin, and palaeoenvironmental significance of red coastal and desert dune sands. *Prog. Phys. Geog.* **1981,** *5*, (4), 514 534.

56. Zakharenko, V.; Khromova, S., Photochemical properties of precipitated solid aerosol produced by burning of titanium microparticles under ambient air. *Mater. Sci. Appl.* **2010,** *1*, (2), 97 102.

57. Vanhieu, N.; Lichtman, D., Bandgap radiation induced photodesorption from titanium oxide surfaces. *Surf. Sci.* **1981,** *103*, (2 3), 535 541.

58. Lichtman, D.; Shapira, Y., Photodesorption: a critical review. *CRC Cr. Rev. Sol. State* **1978,** *8*, (1), 93 118.

59. Lichtman, D., Mechanisms of desorption due to electrons or photons. *Surf. Sci.* **1979,** *90*, (2), 579 587.

60. Baltrusaitis, J.; Schuttlefield, J.; Zeitler, E.; Grassian, V. H., Carbon dioxide adsorption on oxide nanoparticle surfaces. *Chem. Eng. J.* **2011,** *170*, (2 3), 471 481.

61. Faust, B. C.; Zepp, R. G., Photochemistry of aqueous iron(III)-polycarboxylate complexes: roles in the chemistry of atmospheric and surface waters. *Environ. Sci. Technol.* **1993,** *27*, (12), 2517 2522.

62. Pozdnyakov, I. P.; Kel, O. V.; Plyusnin, V. F.; Grivin, V. P.; Bazhin, N. M., New insight into photochemistry of ferrioxalate. *J. Phys. Chem. A* **2008,** *112*, (36), 8316 8322.

63. Pozdnyakov, I. P.; Kel, O. V.; Plyusnin, V. F.; Grivin, V. P.; Bazhin, N. M., Reply to "Comment on 'New insight into photochemistry of ferrioxalate'". *J. Phys. Chem. A* **2009,** *113*, (30), 8820 8822.

64. Chen, J.; Dvornikov, A. S.; Rentzepis, P. M., Comment on "New insight into photochemistry of ferrioxalate". *J. Phys. Chem. A* **2009,** *113*, (30), 8818 8819.

65. Chen, J.; Zhang, H.; Tomov, I. V.; Wolfsherg, M.; Ding, X. L.; Rentzepis, P. M., Transient structures and kinetics of the ferrioxalate redox reaction studied by time-resolved EXAFS, optical spectroscopy, and DFT. *J. Phys. Chem. A* **2007,** *111*, (38), 9326 9335.

66. Mulazzani, Q. G.; Dangelantonio, M.; Venturi, M.; Hoffman, M. Z.; Rodgers, M. A. J., Interaction of formate and oxalate ions with radiation-generated radicals in aqueous solution: methylviologen as a mechanistic probe. *J. Phys. Chem.* **1986,** *90*, (21), 5347 5352.

67. Savelyev, G. G.; Medvinskii, A. A.; Shtsherinskii, V. L.; Gevlitch, L. P.; Gavryushov, N. I.; Pavlyukhin, Y. T.; Stepanova, L. I., The photochemistry of potassium trisoxalatoferrate(III) trihydrate in the solid state. *J. Solid State Chem.* **1975,** *12*, (1 2), 92 101.

68. Simmons, E. L.; Wendlandt, W. W., Solid-state photochemical reactions of transition-metal coordination compounds. *Coordin. Chem. Rev.* **1971,** *7*, (1), 11 27.

69. Spencer, H. E.; Schmidt, M. W., Photochemical studies of solid potassium trisoxalatoferrate(III) trihydrate. *J. Phys. Chem.* **1971,** *75*, (19), 2986 2990.

70. Mao, Y.; Schoneich, C.; Asmus, K. D., Identification of organic acids and other intermediates in oxidative degradation of chlorinated ethanes on titania surfaces en route to mineralization: a combined photocatalytic and radiation chemical study. *J. Phys. Chem.* **1991,** *95*, (24), 10080 10089.

71. Henderson, M. A., A surface science perspective on TiO_2 photocatalysis. *Surface Science Reports* **2011,** *66*, (6-7), 185-297.

72. Yang, F.; Chen, H.; Wang, X. N.; Yang, X.; Du, J. F.; Chen, J. M., Single particle mass spectrometry of oxalic acid in ambient aerosols in Shanghai: mixing state and formation mechanism. *Atmos. Environ.* **2009,** *43*, (25), 3876 3882.

73. He, N.; Kawamura, K., Distributions and diurnal changes of low molecular weight organic acids and alpha-dicarbonyls in suburban aerosols collected at Mangshan, North China. *Geochem. J.* **2010,** *44*, (6), E17 E22.

74. Dolamic, I.; Burgi, T., Photocatalysis of dicarboxylic acids over TiO_2: an in situ ATR-IR study. *J. Catal.* **2007,** *248*, (2), 268 276.

Chapter 5

Heterogeneous photooxidation of fluorotelomer alcohols: a new source of aerosol-phase perfluorinated carboxylic acids

Reprinted (adapted) with permission from Styler, S.A.; Myers, A.L.; Donaldson, D.J. "Heterogeneous photooxidation of fluorotelomer alcohols: a new source of aerosol-phase perfluorinated carboxylic acids" in *Environmental Science & Technology* 2013, 47 (12), 6358 6367.

Contributions:

Anne L. Myers designed the extraction and analysis procedure for surface-sorbed perfluorinated species, and carried out this procedure with assistance from Sarah A. Styler. All other experiments were designed and conducted by Sarah A. Styler. The manuscript was written by Sarah A. Styler (with the exception of experimental and supporting material related to the extraction and analysis of surface-sorbed perfluorinated species, which was written by Anne L. Myers), with critical comments from Anne L. Myers and D. James Donaldson.

5.1 Introduction

Fluorotelomer alcohols (FTOHs, $C_nF_{2n+1}CH_2CH_2OH$), a class of volatile high-production-volume chemicals used in the synthesis of a broad range of industrial and consumer products, including oil- and water-repelling coatings and waxes,[1, 2] have been shown to be present in residual quantities (up to 3.8% dry weight) in a number of fluorinated commercial products.[3-5] Trace quantities of FTOHs (ppb) have also been detected in a wide range of environmental matrices, including both urban and remote atmospheres,[6-9] house dust,[10] indoor air,[11] sludge-amended agricultural soils,[12] and precipitation and surface water.[13]

FTOHs have been shown to be biological[14, 15] and photochemical[16] precursors of perfluorinated carboxylic acids (PFCAs, $C_nF_{2n+1}COOH$), which are a toxic[17] and persistent[18] class of chemicals. Despite this, very little is currently known about their atmospheric fate, and the results of the few partitioning and kinetic studies performed under laboratory conditions do not provide a satisfactory explanation for a number of field observations. For example, laboratory measurements have shown unequivocally that FTOHs partition efficiently to organic[19, 20] and mineral[21] surfaces. By contrast, field studies have typically found that the concentration of FTOHs in atmospheric particulate matter is significantly lower than in corresponding gas-phase samples.[22-25] In addition, the only atmospheric reactive loss mechanism proposed to date for FTOHs is gas-phase OH oxidation, which proceeds with a lifetime of ~ 20 days.[26] This process, however, is insufficient to explain recent observations of a significant diurnal concentration gradient for FTOHs in an urban environment.[22]

Although TiO_2 has been shown to catalyze the mineralization of gas-phase 4:2 FTOH under optimized conditions,[27] the photochemical behaviour of FTOHs at the surface of real atmospheric substrates has not yet received study. We have previously shown that Mauritanian sand and Icelandic volcanic ash efficiently catalyze the

photooxidation of surface-sorbed oxalic acid.[28] In the present study, we use a combination of gas- and particle-phase analytical techniques to explore the possibility that heterogeneous photooxidation on sand and ash surfaces may serve not only as an additional loss mechanism for FTOHs but also as a previously unidentified source of particle-sorbed PFCAs.

5.2 Materials and methods

Two distinct types of experiments were performed here. In the first, a Knudsen cell photoreactor was used to investigate a) the uptake of FTOHs by Mauritanian sand, Icelandic volcanic ash, and TiO_2 and b) the gas-phase products of 6:2 FTOH photooxidation at the TiO_2 surface. In the second, the photochemistry of 6:2 FTOH at the surface of Mauritanian sand, Icelandic volcanic ash, TiO_2, Fe_2O_3, and SiO_2 was explored over longer timescales using gas-phase Fourier transform infrared spectroscopy (FTIR). In these experiments, surface-sorbed photoproducts were identified using liquid chromatography-tandem mass spectrometry (LC-MS-MS).

5.2.1 Knudsen cell uptake and photochemistry experiments

5.2.1.1 Experimental apparatus

Experiments were performed in a custom-built multi-sample photochemical Knudsen cell, which is a modification of the cell we have previously used to investigate the photooxidation of isopropanol on TiO_2 and TiO_2 KNO_3 films[29] and of oxalic acid on Mauritanian sand and Icelandic volcanic ash.[28] A schematic of the apparatus is presented in the Appendix (Figure 5-A1).

In brief, the reactor consists of a 2890 cm^3 stainless-steel rectangular box with three quartz-bottomed circular sample compartments (3.1 cm diameter) contained within its removable bottom face. Pressures within the reactor are maintained at a baseline range of 3 5 $\times$ 10^{-2} Pa using a turbopump. Gas-phase reagents are drawn from the

vapour above a liquid reservoir, passed through a variable leak valve, and introduced into the chamber through a length of copper tubing connected to a ¼" stainless-steel injector tube. The liquid samples were subjected to three freeze pump thaw cycles prior to use. Three isolation flanges equipped with Viton o-rings are used to shield samples from gas-phase reagents present in the reactor. The flanges are raised and lowered by stainless-steel rods, which pass through compression fittings on the top face of the reactor. Gas-phase species exit the reactor via a 3 mm diameter orifice and are detected using a quadrupole mass spectrometer (QMS) with 70 eV electron-impact ionization.

Illumination of samples is accomplished using a 150W Xe arc lamp, the output of which is directed through the quartz window of each sample compartment and the bottom face of each Pyrex sample holder using a 3D-printed modular mirror assembly. Each Pyrex sample holder itself serves as a long-pass optical filter, eliminating $\lambda < 310$ nm.

5.2.1.2 Experimental procedure

Samples were prepared by suspending 10 50 mg of TiO_2, Mauritanian sand, or Icelandic volcanic ash in 2 mL of deionized water. In order to investigate the influence of co-sorbed nitrate upon photochemistry at the TiO_2 surface,[29] some samples were prepared using 2 mL of 10 mM aqueous KNO_3. The resultant slurries were transferred via pipet to shallow 3 cm diameter Pyrex sample holders, which were then heated for 1.5 h in a 373 K oven to evaporate water and yield films of relatively uniform thickness. No further efforts were made to remove adsorbed water from the samples.

Before each experiment commenced, the sample holders containing the substrates of interest were placed into the reaction chamber and the apparatus was evacuated until a constant background pressure of $\sim 3 \times 10^{-2}$ Pa was achieved. At this point, background signal intensities of *m/z* 31 (CH_2OH^+; alcohol functional group) and *m/z* 29

(CHO^+; aldehyde functional group) were measured using the QMS. Then, the isolation flanges were lowered and the gas-phase reagent was introduced into the sample chamber. Once the mass spectrometric signal reached a constant level, the first sample cover was opened. The resultant decrease in signal was used to obtain an apparent initial uptake coefficient via the following equation:[30]

$$\gamma_0 = \frac{A_h}{A_s} \frac{I_0 - I}{I}$$

Here, A_h and A_s are the geometric areas of the escape orifice and sample holder, respectively; I_0 is the signal recorded by the QMS with the sample cover closed; and I is the signal recorded by the QMS immediately upon raising the isolation flange. The main advantage of the multi-compartment Knudsen cell is that it allows three uptake coefficients to be determined in quick succession. The results of a typical experiment performed using this apparatus are shown in Figure 5-1.

Several experiments investigating 3,3,3-trifluoropropanol and 6:2 FTOH photochemistry at the TiO_2 surface were performed using the Knudsen cell. In these experiments, the TiO_2 surface was first exposed to the gas-phase reagent of interest under dark conditions. Once the mass spectrometric signal at *m/z* 31 returned to its pre-exposure level, which indicated that the rates of reagent adsorption and desorption at the surface were equal (*i.e.* that equilibrium was reached), the sample was illuminated and the resultant changes in *m/z* 31 and *m/z* 29 were used to deduce the efficiency of oxidative photochemistry taking place at the sample surface.

5.2.2 Product identification experiments

5.2.2.1 Experimental apparatus

Experiments were performed in a 50 cm Pyrex reaction cell equipped with Ge windows and interfaced to a FTIR spectrometer. Gas-phase FTIR spectra of the cell contents were obtained with the sample beam exiting the instrument via a side port,

passing through the reaction cell, and impinging on a liquid-nitrogen-cooled mercury cadmium telluride (MCT) detector. Spectra were analysed using BOMEM-GRAMS/32 software.

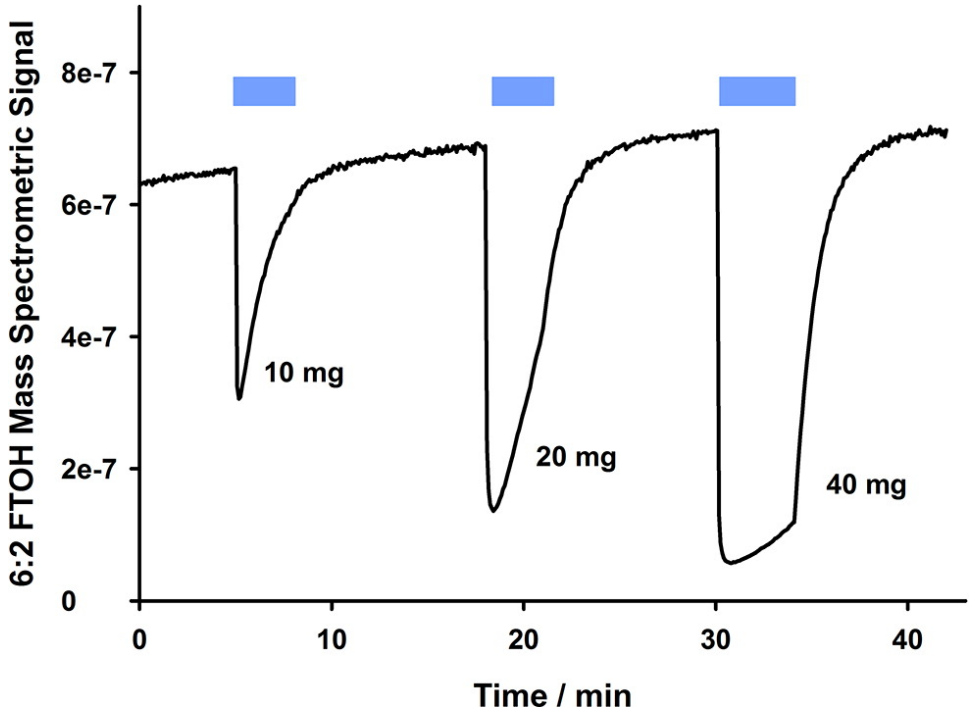

Figure 5-1 Representative QMS trace for uptake of 6:2 FTOH (*m/z* 31) at the surface of Mauritanian sand samples (10 mg; 20 mg; 40 mg). Blue rectangles indicate the times during which the sample compartments were opened.

5.2.2.2 Sample preparation and illumination

Photoactive solid sample films were prepared in quartz reaction boats by heating aqueous suspensions of 100 mg of the sample of interest for ~ 30 minutes in a 423K oven. At the beginning of each experiment, a reaction boat containing the sample film of interest was placed into the FTIR cell, which was then flushed with synthetic air.

After a background reference spectrum was taken, 6:2 FTOH from the vapour above a heated liquid reservoir was introduced to the flow of synthetic air. After ~ 5 min, the inlet and outlet ports of the FTIR cell were closed and the system was allowed to reach gas surface equilibrium, here defined as the point at which the concentration of gas-phase 6:2 FTOH no longer decreased with time (~ 90 min). At this point, the sample film was illuminated for time periods ranging from 30 min to 5 h using the output of the same 150W Xe arc lamp. Gas-phase FTIR spectra were obtained at 5 min intervals for the duration of the experiment.

5.2.2.3 Sample extraction and LC-MS-MS analysis

After illumination, fluorinated surface products were extracted into methanol using a method based on that of De Silva and coworkers.[31] In brief, the quartz boat was placed in a 50 mL polypropylene tube containing 10 mL of methanol, which was then sonicated (15 min), placed on a mechanical shaker (15 min, 360 rpm), and centrifuged (10 min, 6000 rpm). The methanol extract was filtered (0.2 μm nylon syringe filter), evaporated to dryness under a nitrogen flow, and reconstituted in 1 mL HPLC-grade methanol. Sample extracts were refrigerated in polypropylene cryogenic vials until sample analysis.

LC-MS-MS analysis of the methanol extracts was performed using an ultra-performance liquid chromatograph (UPLC) coupled to a triple quadrupole mass spectrometer, which was run in multiple reaction monitoring mode (MRM) using negative electrospray ionization. Separation of analytes was accomplished using a modification of the gradient elution method of Rand and Mabury[32] on a Phenomenex Kinetex C18 analytical UPLC column (50 mm × 4.6 mm, 2.6 μm, 100 Å). Analytes were quantified via internal calibration using ^{13}C-labelled internal standards.

Further information regarding the chromatographic, mass spectrometric, and quantification methods employed is available in the Appendix.

5.2.2.4 Quality assurance / quality control (QA/QC)

Blank samples representing experimental, extraction and analytical procedures were analyzed to ensure that contamination was not contributing to observed perfluoroalkyl substance (PFAS) concentrations. Spike and recovery studies were performed to assess the extraction efficiency of PFASs. In these experiments, ash and sand samples (100mg) were spiked with 6 ng native PFASs and subjected to the extraction procedure outlined above. Recoveries ranged from 60 90%, and experimental values were not recovery-corrected. As indicated by error bars in Figures 5-6 and 5-7, precision in the experimental procedure was assessed through replicate experiments. Instrumental precision was determined by duplicate LC-MS-MS analysis of each sample. Further details of QA/QC procedures are available in the Appendix.

5.2.3 Chemicals

3,3,3-trifluoropropanol (98%), 4:2 FTOH (99%), and 6:2 FTOH (97%) were obtained from SynQuest Laboratories and used as received. TiO_2 (anatase, ≥99%), SiO_2 (99.5%, 99.8 ppm TiO_2 as quoted in the certificate of analysis), Fe_2O_3 (≥99%), and KNO_3 (ACS grade) were obtained from Sigma Aldrich and used as received. The Mauritanian sand used in the present experiments, which we have previously shown to catalyze the photochemical oxidation of oxalic acid,[28] was generously donated by Dr. Christian George. The Icelandic volcanic ash sample was obtained from a Reykjavik tourist shop following the 2010 Eyjafjallajökull eruption. Sand and ash samples were finely ground in a mortar and pestle prior to use. The elemental concentrations of Fe (0.2% sand, 6.8% ash) and Ti (0.1% sand, 1.0% ash) in these natural samples were previously determined using wavelength-dispersive X-ray fluorescence spectrometry.[28]

HPLC-grade methanol (>99.8%) was purchased from EMD Chemicals, Inc. Native and mass-labelled perfluoroalkyl substance (PFAS) standards (>99%) were donated by Wellington Laboratories, Inc. Native PFAS solutions included perfluoropentanoic

acid (PFPeA), perfluorohexanoic acid (PFHxA), perfluoroheptanoic acid (PFHpA), and 6:2 fluorotelomer unsaturated carboxylic acid (6:2 FTUCA). Mass-labelled PFAS solutions were used as internal standards and included [$^{13}C_2$] PFHxA, [$^{13}C_4$] PFOA, and [$^{13}C_2$] 6:2 FTUCA.

5.3 Results

5.3.1 Dark uptake experiments

In order to gain insight into the mechanism of uptake at the mineral surface (*vide infra*), we first determined the apparent initial uptake coefficient, γ_0, of 3,3-trifluoropropanol, 4:2 FTOH, and 6:2 FTOH as a function of solid-phase sample mass. The results of these experiments are displayed in Figures 5-2 and 5-3a b. At the surface of Mauritanian sand, each of these fluorinated alcohols exhibited a plateau in γ_0 at the highest masses under study. At lower sample masses, however, their behaviour differed substantially: while the apparent initial uptake coefficient for 3,3,3-trifluoropropanol increased linearly with increasing sample mass, those for 4:2 FTOH and 6:2 FTOH increased in a non-linear fashion as a function of sample mass.

In an attempt to determine whether this non-linear mass dependence was specific to the Mauritanian sand surface, we also measured the uptake of 6:2 FTOH at the TiO_2 surface and at the surface of Icelandic volcanic ash as a function of substrate mass. Figure 5-4a shows that at the volcanic ash surface, γ_0 also increased non-linearly with increasing sample mass. However, as illustrated in Figure 5-4b, a linear dependence of γ_0 on sample mass was observed at the TiO_2 surface. In both cases, γ_0 reached a plateau at the highest masses under study.

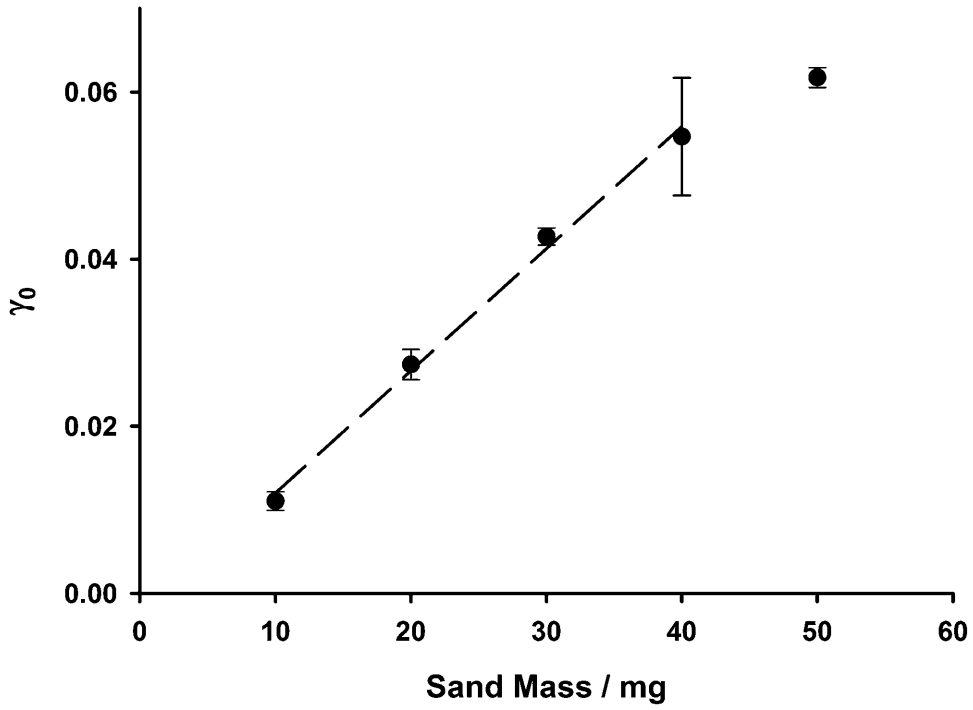

Figure 5-2 Apparent initial uptake coefficient γ_0 for 3,3,3-trifluoropropanol at the surface of Mauritanian sand as a function of sand mass. Error bars represent the standard error associated with three individual trials.

5.3.2 Gas-phase products from the TiO_2-catalyzed photooxidation of 6:2 FTOH

We have previously shown that the illumination of an *n*-propanol-saturated TiO_2 film leads to the production of gas-phase propionaldehyde.[29] In the present work, we investigated the photooxidation of this alcohol's fluorinated analogue, 3,3,3-trifluoropropanol. The illumination of a TiO_2 film saturated with this species led to an increase in the mass spectrometric signal associated with the CHO^+ fragment (*m/z* 29) and a concomitant decrease in the signal associated with the CH_2OH^+ fragment (*m/z* 31), which suggests that 3,3,3-trifluoropropanol is oxidatively converted to 3,3,3-trifluoropropionaldehyde at the illuminated TiO_2 surface.

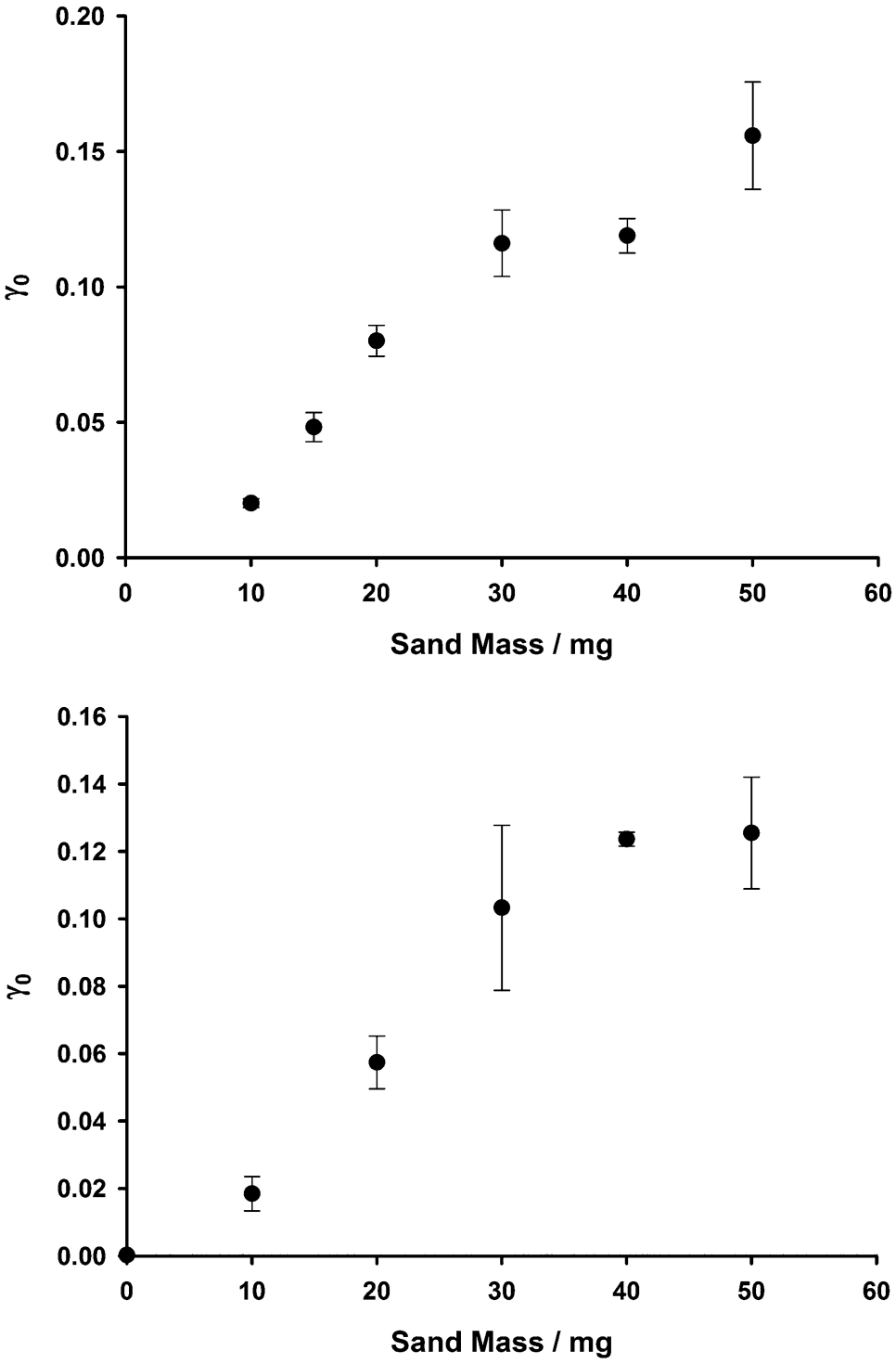

Figure 5-3 Apparent initial uptake coefficient γ_0 for a) 4:2 FTOH and b) 6:2 FTOH at the surface of Mauritanian sand as a function of sand mass. Error bars represent the standard error associated with three individual trials.

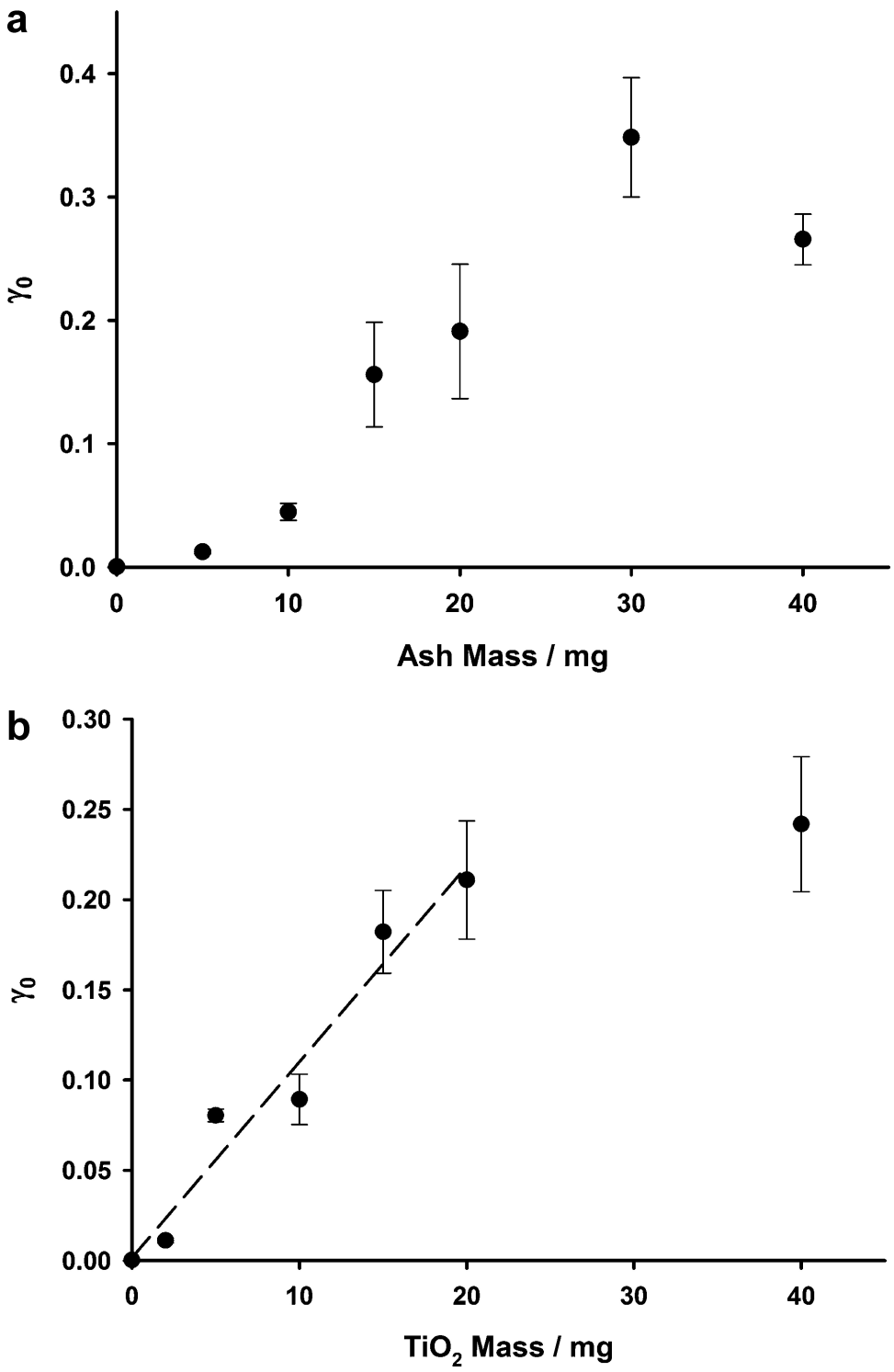

Figure 5-4 Apparent initial uptake coefficients γ_0 for 6:2 FTOH at the surface of a) Icelandic volcanic ash and b) TiO_2 as a function of substrate mass. Error bars represent the standard error associated with three individual trials.

As shown in Figure 5-5a, illumination of a 6:2 FTOH-saturated TiO_2 film in the photochemical Knudsen cell led to the same increase in the CHO^+ fragment and decrease in the CH_2OH^+ fragment as was observed for 3,3,3-trifluoropropanol. In agreement with the work of Kutsuna and co-workers,[27] who investigated the photochemistry of 4:2 FTOH at the TiO_2 surface, we attribute this observation to the photochemical loss of 6:2 FTOH and the concurrent formation and emission to the gas phase of its aldehydic oxidation products, 6:2 fluorotelomer aldehyde (6:2 FTAL) and/or 6:2 fluorotelomer unsaturated aldehyde (6:2 FTUAL).

This assignment is corroborated by the results obtained by gas-phase FTIR measurements at ambient pressure and over longer time-scales: as shown in Figure 5-5b, illumination of 6:2 FTOH-saturated TiO_2 films led to the production of aldehydic oxidation products with absorbances at 1686, 1713, and 1751 cm^{-1}. We attribute these absorbances to 6:2 FTAL (CH=O, 1751 cm^{-1}) and 6:2 FTUAL (CH=O, 1713 cm^{-1}; C=C, 1686 cm^{-1}).[27, 33]

The Knudsen cell experiments described thus far were performed under oxygen-free conditions. Previously, we have shown that the presence of oxygen has a complex influence on the photooxidation of oxalic acid at the surface of Mauritanian sand and Icelandic ash.[28]

In addition, in our previous investigation of the photochemical conversion of isopropanol to acetone at the TiO_2 surface,[29] we found that the presence of nitrate – a characteristic component of processed mineral dust aerosol – led to a substantial enhancement in both isopropanol loss and acetone formation. Here, we used the photochemical Knudsen cell to investigate the influence of gas-phase oxygen (~ 0.7 Pa) and surface-sorbed nitrate upon the TiO_2-catalyzed photooxidation of 6:2 FTOH. Interestingly, neither oxygen nor surface-sorbed nitrate enhanced the photochemical production of gas-phase aldehydic oxidation products (CHO^+, *m/z* 29). Since these gas-phase measurements are influenced not only by surface oxidation rates but also by the

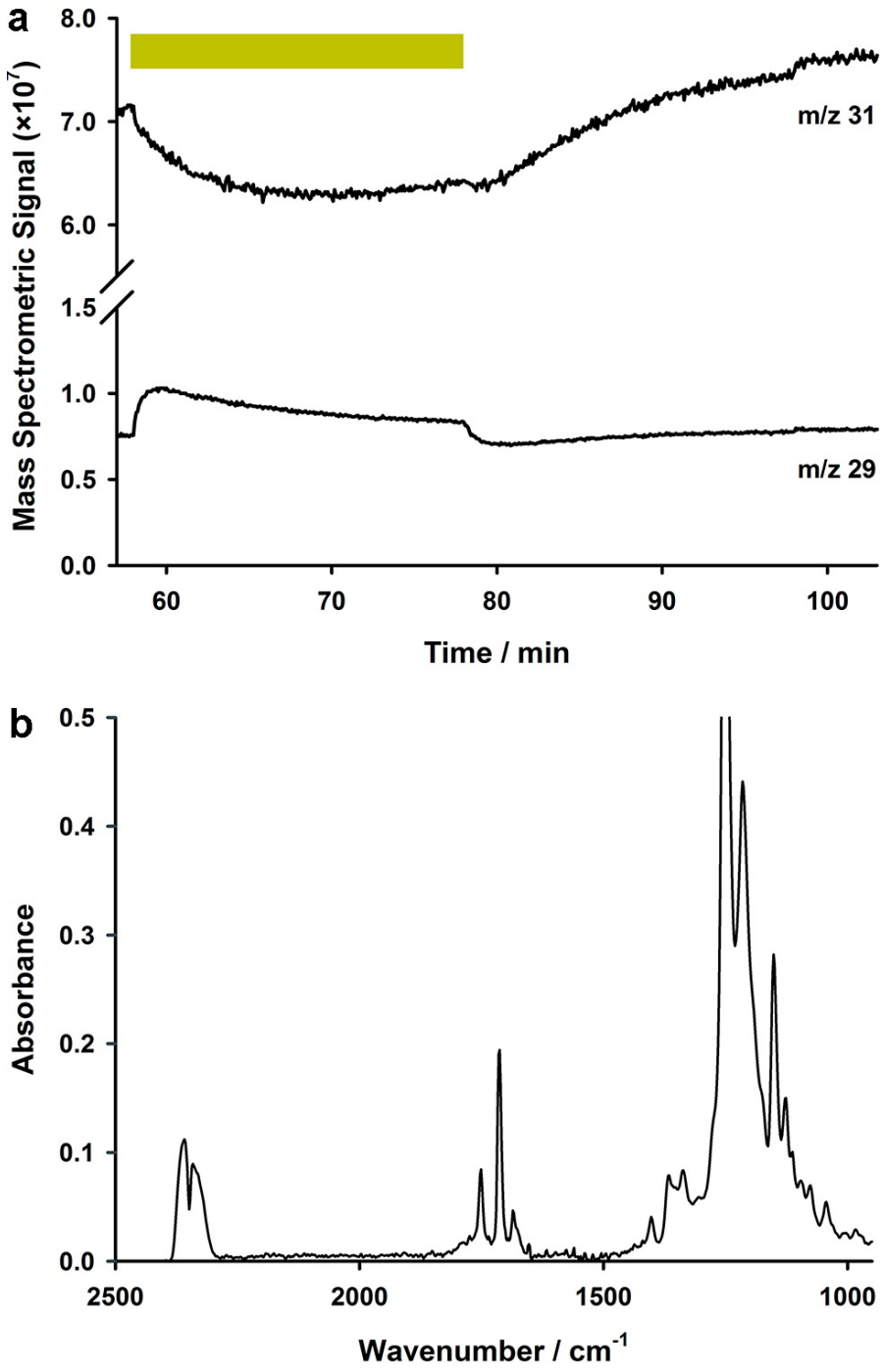

Figure 5-5 a) Representative QMS trace for conversion of 6:2 FTOH (*m*/*z* 31) to 6:2 FTAL/6:2 FTUAL (*m*/*z* 29) at the illuminated TiO_2 surface. A yellow rectangle indicates the time period during which the samples were illuminated. b) Gas-phase FTIR spectrum obtained for the photooxidation of 6:2 FTOH at the TiO_2 surface after 2.5 h of illumination.

surface-to-gas transfer of oxidation products, we suggest that this observation reflects the fact that the initial aldehydic products of FTOH photooxidation may have remained at the TiO_2 surface and undergone further oxidation to yield involatile fluorinated species. This possibility is explored further in the subsequent section.

5.3.3 Surface-sorbed products from the heterogeneous photooxidation of 6:2 FTOH

As illustrated in Figure 5-6, the photooxidation of 6:2 FTOH at the TiO_2 surface led to the production of a variety of surface-sorbed species, including 6:2 FTUCA, PFHpA, PFHxA, and PFPeA. Although 6:2 fluorotelomer carboxylic acid (6:2 FTCA) was also observed, it was not quantified in these experiments. At the Fe_2O_3 surface, the oxidation of 6:2 FTOH also resulted in the production of substantial quantities of 6:2FTCA (not quantified), 6:2 FTUCA, and PFHxA, but only minor quantities of PFHpA and PFPeA. In a control experiment performed at the SiO_2 surface, in which the sample was not illuminated but no attempts were made to exclude ambient laboratory lighting, small but measurable quantities of each of the analytes described above were observed. Photochemistry at the SiO_2 surface was significantly less efficient than at the surface of Fe_2O_3 and TiO_2, but nevertheless resulted in enhanced levels of PFPeA, PFHxA, and PFHpA over those observed in the absence of illumination.

With these observations as a framework, we investigated the photooxidation of 6:2 FTOH at the surface of real environmental samples. In these experiments, the results of which are illustrated in Figure 5-7, we measured 6:2 FTUCA and the C5 – C7 PFCAs at the surface of Mauritanian sand and Icelandic volcanic ash as a function of illumination time. At both surfaces, the dominant species observed was PFHxA: at the ash surface, its concentration reached a maximum after 2.5h of illumination; at the sand surface, however, its concentration increased monotonically over the time period studied (up to 5h). At the ash surface, PFPeA, PFHpA, and 6:2 FTUCA were detected

at all illumination time points, but were present in significantly lower concentrations than PFHxA. At the sand surface, however, these photoproducts were observed only after 5h of illumination.

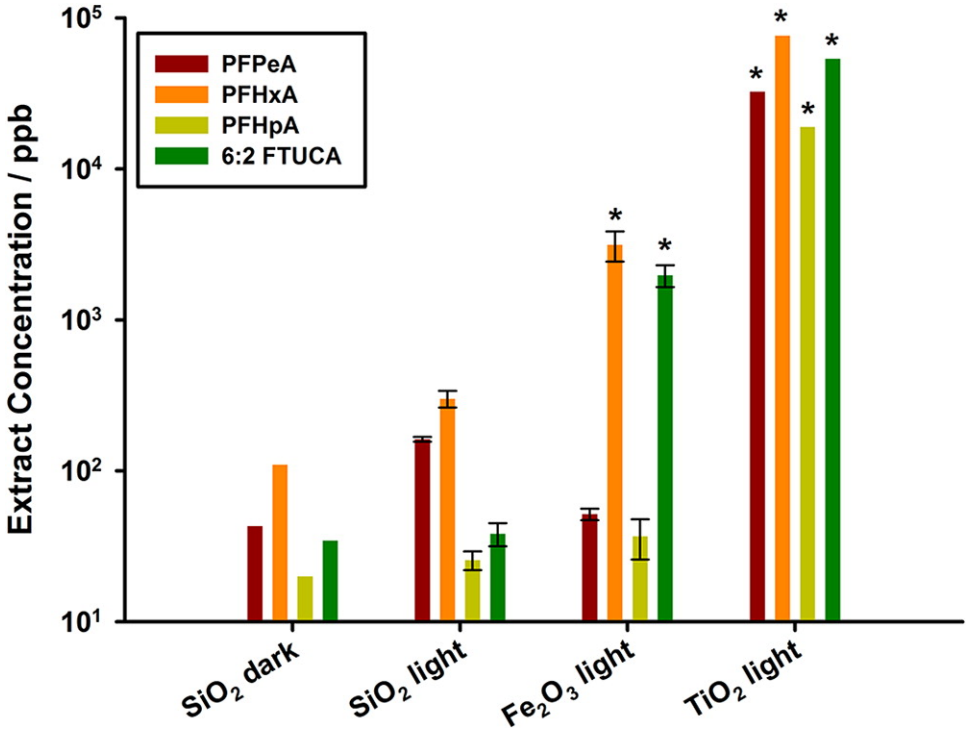

Figure 5-6 Fluorinated photoproduct concentrations in extracts from films exposed to 6:2 FTOH for 1.5 h under dark conditions and subsequently illuminated for 2.5 h. The SiO_2 dark control was exposed to 6:2 FTOH under dark conditions for 2.5 h. Results are displayed on a logarithmic scale. Where present, error bars represent the standard error associated with two individual trials. Asterisks indicate that extract concentrations were higher than those associated with the highest standard used for quantification. Analyte concentrations in blank samples are too small to fit on the scale.

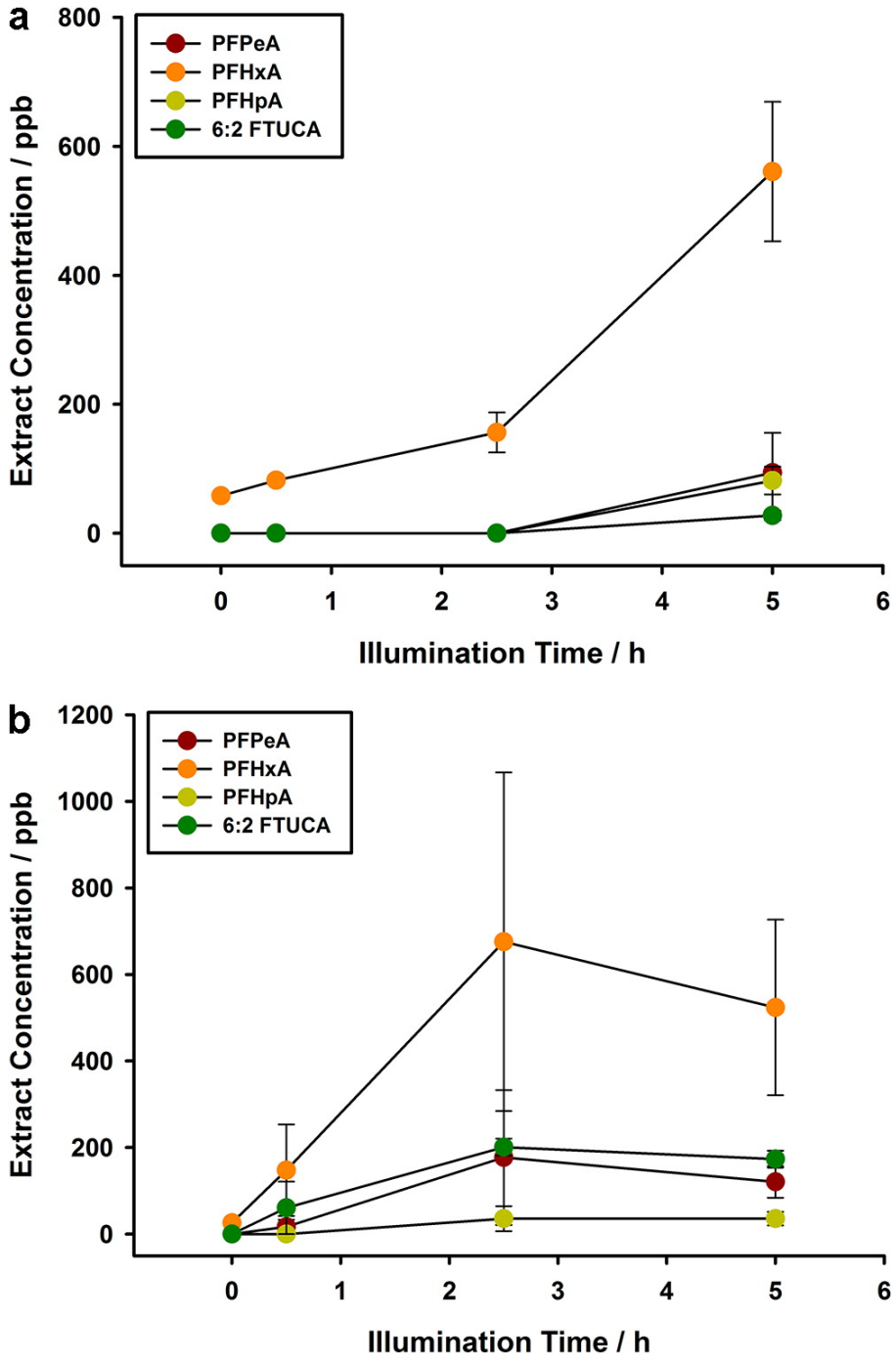

Figure 5-7 Fluorinated photoproduct concentrations in extracts from a) sand and b) ash films exposed to 6:2 FTOH for 1.5 h under dark conditions and subsequently illuminated for periods of time ranging from 0 to 5h. Error bars represent the standard error associated with two individual trials.

5.4 Discussion

5.4.1 Fluorinated alcohols partition efficiently to environmental surfaces

As shown in Figures 5-2, 5-3, and 5-4, the apparent initial uptake coefficients, γ_0, for fluorotelomer alcohols were substantial at all of the mineral surfaces under study. At the surface of TiO_2, γ_0 for 6:2 FTOH was greater than that which we previously observed for isopropanol under similar experimental conditions.[29] This result, when coupled with previous laboratory observations of substantial uptake to the octanol surface[19] and efficient equilibrium partitioning to quartz, Al_2O_3, and $CaCO_3$,[21] stresses the need for a comprehensive investigation of the heterogeneous fate of this class of compounds.

As a result of efficient diffusion into underlying sample layers, γ_0 of gas-phase species on solid samples measured in a Knudsen cell generally first increases linearly with sample mass this is referred to as the linear mass-dependent (LMD) regime.[34] At elevated sample masses, however, where the adsorbate molecules cannot access the entire sample via diffusion over the time-scale of the uptake experiment, a plateau in this relationship is observed.[34] We have previously observed this uptake behaviour for isopropanol at the TiO_2 surface;[29] and, as shown in Figure 5-2, we observed the same behaviour for 3,3,3-trifluoropropanol at the Mauritanian sand surface.

In the LMD regime, by definition, the number of surface sites available for adsorption increases linearly as a function of sample mass. Therefore, if uptake is governed exclusively by adsorbate surface interactions, there should also be a linear relationship between γ_0 and sample mass. As illustrated in Figures 5-3a and 5-3b, however, the apparent initial uptake coefficient of the 4:2 and 6:2 FTOHs at the surface of Mauritanian sand exhibited a non-linear increase with increasing sample mass followed by a plateau at the highest sample masses. As shown in Figure 5-4a, the same behaviour was observed for 6:2 FTOH at the Icelandic ash surface. This

observation suggests that intermolecular forces involving only the FTOHs species hydrogen bonding or van der Waals interactions, for example may have contributed to the observed uptake. This type of favourable adsorbate adsorbate interaction has been previously invoked to explain the self-association of polycyclic aromatic hydrocarbons at the surface of ice[35] and snow[36] and the formation of oleic acid 'islands' at the surface of both polar and non-polar aerosol mimics.[37]

Since the gas-phase organic uptake studies performed to date on atmospheric particulate matter have been performed nearly exclusively with small molecules,[38, 39] it is not currently known whether our results are specific to the fluorinated alcohols or are a general observation for larger adsorbates. Two characteristics of the fluorotelomer alcohols, however, suggest that the contribution of adsorbate adsorbate interactions to observed uptake may be more pronounced for these species than for their hydrogenated analogues: first, the ability of the hydroxyl head group to participate in hydrogen-bonding interactions with the mineral surface is diminished in the FTOHs by the presence of a substantial intramolecular hydrogen bond;[21, 40] second, access to adsorptive sites may be impeded by the stiff, helical fluorinated tail of these molecules.[40] In any event, this non-linear increase in uptake coefficient as a function of sample mass is not universally observed for this class of compounds: as shown in Figure 5-4b, a typical linear mass dependence was observed at the TiO_2 surface. This observation, which may have arisen from strong bonding to hydroxyl groups present at the TiO_2 surface,[41] suggests that the surface partitioning behaviour of fluorotelomer alcohols may depend sensitively on the specific nature of the substrate surface, which could itself depend on ambient temperature and relative humidity.

5.4.2 Heterogeneous photochemistry of 6:2 FTOH: mechanistic insights

In an attempt to gain insight into the mechanism of heterogeneous 6:2 FTOH oxidation on real atmospheric surfaces, we first examine the relative production of

surface-sorbed PFCAs at the surface of TiO_2 and Fe_2O_3. At the Fe_2O_3 surface, the only PFCA observed in significant quantities was PFHxA. At the TiO_2 surface, by contrast, we saw significant production not only of PFHxA but also of PFHpA and PFPeA. We suggest that these observations can be explained by the different photooxidation pathways available at the surface of these two semiconductors. These pathways are displayed schematically in Scheme 5-1.[16, 42]

At the Fe_2O_3 surface, we propose that the oxidation of 6:2 FTOH is mediated by hydroxyl radical produced by photochemical oxidation of surface-sorbed water[43-45] and yields both 6:2 FTCA and 6:2 FTUCA as intermediates. The slower rate of OH-mediated hydrogen abstraction from the saturated 6:2 FTCA, which would ultimately yield PFHpA, as compared to OH addition to 6:2 FTUCA, which would ultimately yield PFHxA, explains the dominance of the latter PFCA in these experiments. In addition, since PFCAs are known to be recalcitrant with respect to reaction with OH,[46] additional evidence for this OH-mediated reactive mechanism is provided by the fact that no oxidation of PFHxA to yield PFPeA was observed at the Fe_2O_3 surface.

At the TiO_2 surface, oxidation can be effected not only by photochemically produced hydroxyl radical but also directly by photoproduced valence-band holes (h^+_{vb}).[47] Our observation of PFHpA at the TiO_2 surface provides support for the latter mechanism, since the hole-mediated oxidation of 6:2 FTUCA and 6:2 FTCA would be expected to proceed at similar rates. Unlike Fe_2O_3, TiO_2 has been previously shown to mediate the photochemical oxidation of PFCAs.[48] The same is true in the present work, where we observed significant production of PFPeA, which can arise only from reaction of its C7 and C6 PFCA precursors, upon illumination.

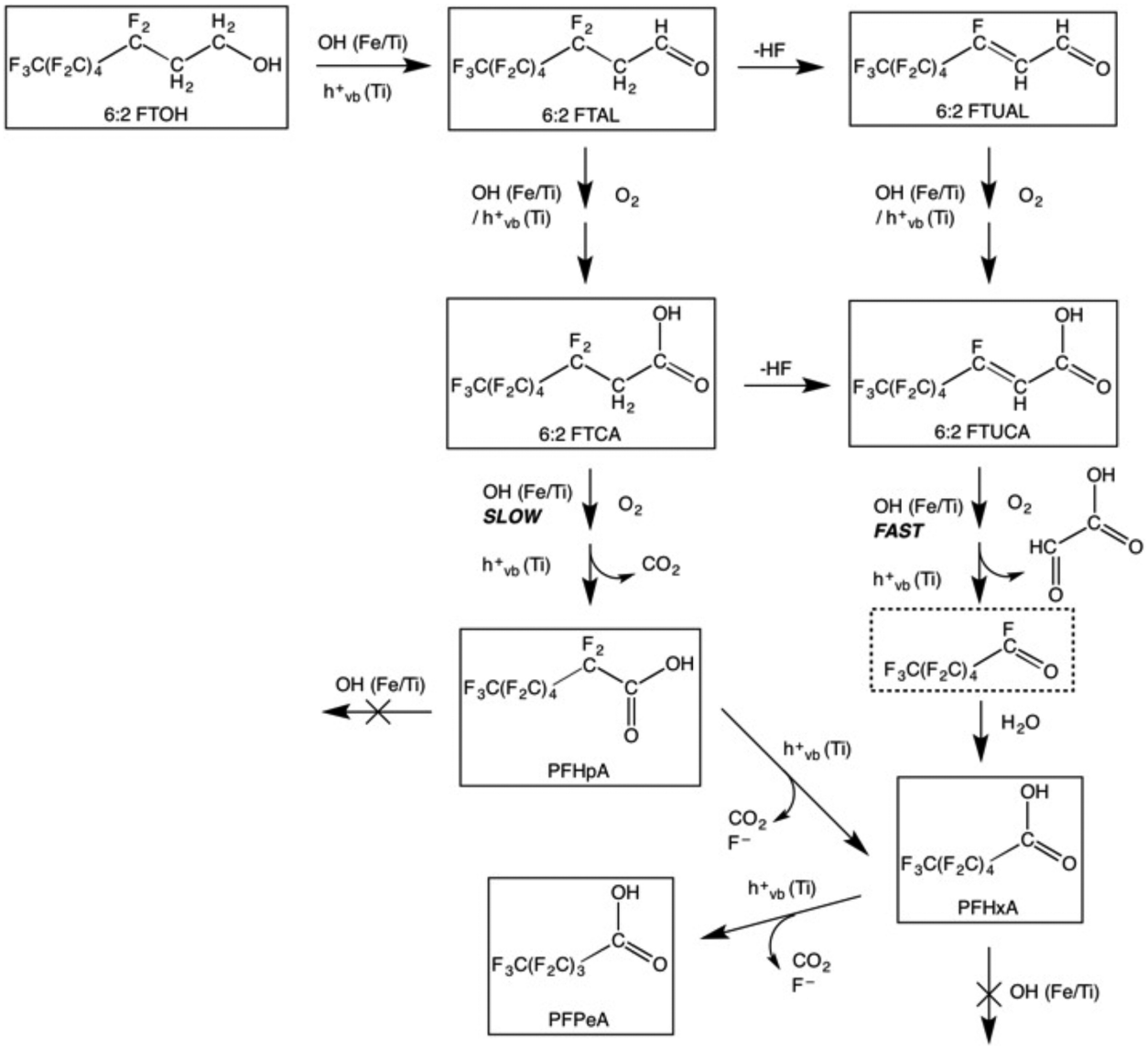

Scheme 5-1 Suggested mechanisms for photoproduction of PFAS from surface-sorbed FTOHs. Species in solid rectangles were observed in the present experiments.

Unexpectedly, we also saw photoproduction of PFPeA, PFHxA, and PFHpA at the surface of SiO_2, a wide band-gap insulator, albeit at significantly lower quantities. We suggest that the following considerations may have contributed to these observations: first, the SiO_2 used had a small particle size (~ 2.8 μm), and would therefore have been expected to have a large surface area for adsorption of 6:2 FTOH; second, the SiO_2

contained trace (~ 100 ppm) quantities of TiO_2, which we have already shown to efficiently promote the oxidation of 6:2 FTOH. In addition, it may also be possible that direct photolysis of 6:2 FTOH proceeds more rapidly on surfaces than in bulk media, in this case perhaps owing to efficient light scattering and/or reflection at the SiO_2 surface, which may have exposed adsorbed species to significantly enhanced light levels.

As shown in Figures 5-7a and 5-7b, the oxidation of 6:2 FTOH at the surface of Mauritanian sand and Icelandic ash samples also led to the production of PFHxA and lesser quantities of 6:2 FTUCA, PFPeA, and PFHpA. Strong evidence for the substrate-mediated nature of the oxidation is provided by the fact that both the magnitude and temporal evolution of surface-sorbed photoproducts were different at the sand than at the ash surface: while PFHxA levels at the sand surface increased slowly but monotonically as a function of illumination time, those at the ash surface increased more rapidly but decreased at the longest illumination time (5h); in addition, the production of PFPeA at the ash surface occurred earlier and at a higher level than at the sand surface. These observations can be rationalized by considering the elemental concentrations of Fe (0.2% sand, 6.8% ash) and Ti (0.1% sand, 1.0% ash) in these natural samples[28] in the context of the proposed photochemical mechanism described above. Since levels of Fe and Ti, both of which can catalyze the photooxidation of 6:2 FTOH, are significantly higher in the ash sample than in the sand sample, it is unsurprising that the production of PFHxA was higher in the former than in the latter. In addition, the recalcitrance of PFHxA at the sand surface as compared to at the ash surface can be explained by the lower levels of Ti present in the sand.

5.4.3 Atmospheric significance

We have shown here that fluorotelomer alcohols are efficiently taken up on TiO_2 and on Mauritanian sand and Icelandic volcanic ash samples. Further, we have provided

evidence that the photochemical oxidation of 6:2 FTOH on TiO_2, Fe_2O_3, sand, and ash results in the production of surface-sorbed perfluorinated carboxylic acids. This work, which to our knowledge represents the first investigation of heterogeneous photoprocessing of fluorotelomer alcohols on real environmental surfaces, provides evidence that this process may contribute to aerosol-phase PFCA loadings, even close to source regions.

In a number of field studies, gas-phase FTOH concentrations have been reported to be significantly higher than those in the particle phase; in some cases, particle-phase concentrations have been reported to be negligible.[22-25] Although these observations have been largely attributed to the volatility of fluorotelomer alcohols[25] as compared to their hydrogenated analogues and to sampling challenges associated with this class of compounds,[49] our results suggest that particle-phase FTOHs may undergo efficient photochemical transformation, and therefore that the gas particle partitioning of these compounds cannot be readily inferred from field measurements in the absence of kinetic data concerning their photochemical reactivity in the aerosol phase. In the sole study performed to date that investigated diurnal trends in FTOH concentrations, Mueller and coworkers[22] observed a diel pattern in gas-phase FTOH concentrations, with lower concentrations observed in the daytime than at night. Although these authors attributed this observation to nocturnal enrichment of these species in the stable boundary layer, it is also possible that these observations may have arisen as a result of efficient uptake and photooxidation of gas-phase FTOHs by atmospheric particulate matter. This interpretation is supported by concurrent measurements of particle-sorbed PFCAs, which showed that the C4 C6 congeners exhibited the opposite diel pattern, with higher concentrations observed in the daytime than at night.

Our observations of efficient conversion of 6:2 FTOH to PFHxA on the Fe_2O_3 surface have a number of interesting atmospheric implications. First, these results imply that

mineral dust[50] and coal fly ash[51] may rapidly become enriched in surface-sorbed PFCAs, since these species are not expected to be fully mineralized on the Fe-rich surface of these aerosols. The long-range transport of these aerosols, therefore, may represent a potential additional source of PFCAs to remote regions, including the Arctic environment.[25, 52-55] Second, since iron-catalyzed photochemistry would also be expected to occur at the surface of agricultural soils,[56] our results indicate that the production of PFCAs in sewage sludge-amended soils may occur not only via biochemical pathways[14] but also via photochemical processes at or near the soil surface.

Although our results are compelling, they represent only a first attempt to investigate the heterogeneous photoprocesses by which FTOHs may react in the environment. We recommend that future studies investigate a variety of other plausible aerosol-phase mechanisms via which fluorotelomer alcohols and PFCAs may be transformed, including their interaction with aerosol-phase oxalic acid in the presence of TiO_2,[57] photo-Fenton processes in mixed organic aqueous aerosol,[58] or via photo-complexation of PFCAs with dissolved iron (III).[59]

5.5 References

1. Howard, P. H.; Muir, D. C. G., Identifying new persistent and bioaccumulative organics among chemicals in commerce. *Environ. Sci. Technol.* **2010,** *44*, (7), 2277 2285.

2. Buck, R. C.; Franklin, J.; Berger, U.; Conder, J. M.; Cousins, I. T.; de Voogt, P.; Jensen, A. A.; Kannan, K.; Mabury, S. A.; van Leeuwen, S. P. J., Perfluoroalkyl and polyfluoroalkyl substances in the environment: terminology, classification, and origins. *Integr. Environ. Assess. Manage.* **2011,** *7*, (4), 513 541.

3. Dinglasan-Panlilio, M. J. A.; Mabury, S. A., Significant residual fluorinated alcohols present in various fluorinated materials. *Environ. Sci. Technol.* **2006,** *40*, (5), 1447 1453.

4. Sinclair, E.; Kim, S. K.; Akinleye, H. B.; Kannan, K., Quantitation of gas-phase perfluoroalkyl surfactants and fluorotelomer alcohols released from nonstick cookware and microwave popcorn bags. *Environ. Sci. Technol.* **2007,** *41*, (4), 1180 1185.

5. Herzke, D.; Olsson, E.; Posner, S., Perfluoroalkyl and polyfluoroalkyl substances (PFASs) in consumer products in Norway a pilot study. *Chemosphere* **2012,** *88*, (8), 980 987.

6. Shoeib, M.; Harner, T.; Vlahos, P., Perfluorinated chemicals in the Arctic atmosphere. *Environ. Sci. Technol.* **2006,** *40*, (24), 7577 7583.

7. Del Vento, S.; Halsall, C.; Gioia, R.; Jones, K.; Dachs, J., Volatile per- and polyfluoroalkyl compounds in the remote atmosphere of the western Antarctic Peninsula: an indirect source of perfluoroalkyl acids to Antarctic waters? *Atmos. Poll. Res.* **2012,** *3*, (4), 450 455.

8. Jahnke, A.; Ahrens, L.; Ebinghaus, R.; Temme, C., Urban versus remote air concentrations of fluorotelomer alcohols and other polyfluorinated alkyl substances in Germany. *Environ. Sci. Technol.* **2007,** *41*, (3), 745 752.

9. Li, J.; Del Vento, S.; Schuster, J.; Zhang, G.; Chakraborty, P.; Kobara, Y.; Jones, K. C., Perfluorinated compounds in the Asian atmosphere. *Environ. Sci. Technol.* **2011,** *45*, (17), 7241 7248.

10. Xu, Z.; Fiedler, S.; Pfister, G.; Henkelmann, B.; Mosch, C.; Volkel, W.; Fromme, H.; Schramm, K.-W., Human exposure to fluorotelomer alcohols, perfluorooctane sulfonate and perfluorooctanoate via house dust in Bavaria, Germany. *Sci. Total Environ.* **2013,** *443*, 485 90.

11. Liu, W.; Takahashi, S.; Sakuramachi, Y.; Harada, K. H.; Koizumi, A., Polyfluorinated telomers in indoor air of Japanese houses. *Chemosphere* **2013,** *90*, (5), 1672 1677.

12. Yoo, H.; Washington, J. W.; Ellington, J. J.; Jenkins, T. M.; Neill, M. P., Concentrations, distribution, and persistence of fluorotelomer alcohols in sludge-applied soils near Decatur, Alabama, USA. *Environ. Sci. Technol.* **2010,** *44*, (22), 8397 8402.

13. Mahmoud, M. A. M.; Karrman, A.; Oono, S.; Harada, K. H.; Koizumi, A., Polyfluorinated telomers in precipitation and surface water in an urban area of Japan. *Chemosphere* **2009,** *74*, (3), 467 472.

14. Dinglasan, M. J. A.; Ye, Y.; Edwards, E. A.; Mabury, S. A., Fluorotelomer alcohol biodegradation yields poly- and perfluorinated acids. *Environ. Sci. Technol.* **2004,** *38*, (10), 2857 2864.

15. Martin, J. W.; Mabury, S. A.; O'Brien, P. J., Metabolic products and pathways of fluorotelomer alcohols in isolated rat hepatocytes. *Chem. Biol. Interact.* **2005,** *155*, (3), 165 180.

16. Ellis, D. A.; Martin, J. W.; De Silva, A. O.; Mabury, S. A.; Hurley, M. D.; Andersen, M. P. S.; Wallington, T. J., Degradation of fluorotelomer alcohols: a likely atmospheric source of perfluorinated carboxylic acids. *Environ. Sci. Technol.* **2004,** *38*, (12), 3316 3321.

17. Lau, C.; Anitole, K.; Hodes, C.; Lai, D.; Pfahles-Hutchens, A.; Seed, J., Perfluoroalkyl acids: a review of monitoring and toxicological findings. *Toxicol. Sci.* **2007,** *99*, (2), 366 394.

18. Prevedouros, K.; Cousins, I. T.; Buck, R. C.; Korzeniowski, S. H., Sources, fate and transport of perfluorocarboxylates. *Environ. Sci. Technol.* **2006,** *40*, (1), 32 44.

19. Li, Y. Q.; Demerjian, K. L.; Williams, L. R.; Worsnop, D. R.; Kolb, C. E.; Davidovits, P., Heterogeneous uptake of 8:2 fluorotelomer alcohol on liquid water and 1-octanol droplets. *J. Phys. Chem. A* **2006,** *110*, (21), 6814 6820.

20. Thuens, S.; Dreyer, A.; Sturm, R.; Temme, C.; Ebinghaus, R., Determination of the octanol air partition coefficients (K_{OA}) of fluorotelomer alcohols. *J. Chem. Eng. Data* **2008,** *53*, (1), 223 227.

21. Arp, H. P. H.; Niederer, C.; Goss, K.-U., Predicting the partitioning behavior of various highly fluorinated compounds. *Environ. Sci. Technol.* **2006,** *40*, (23), 7298 7304.

22. Mueller, C. E.; Gerecke, A. C.; Bogdal, C.; Wang, Z.; Scheringer, M.; Hungerbuehler, K., Atmospheric fate of poly- and perfluorinated alkyl substances (PFASs): I. Day-night patterns of air concentrations in summer in Zurich, Switzerland. *Environ. Pollut.* **2012,** *169*, 196 203.

23. Cai, M.; Xie, Z.; Moeller, A.; Yin, Z.; Huang, P.; Cai, M.; Yang, H.; Sturm, R.; He, J.; Ebinghaus, R., Polyfluorinated compounds in the atmosphere along a cruise pathway from the Japan Sea to the Arctic Ocean. *Chemosphere* **2012,** *87*, (9), 989 997.

24. Ahrens, L.; Shoeib, M.; Del Vento, S.; Codling, G.; Halsall, C., Polyfluoroalkyl compounds in the Canadian Arctic atmosphere. *Environ. Chem.* **2011,** *8*, (4), 399 406.

25. Dreyer, A.; Weinberg, I.; Temme, C.; Ebinghaus, R., Polyfluorinated compounds in the atmosphere of the Atlantic and Southern Oceans: evidence for a global distribution. *Environ. Sci. Technol.* **2009,** *43*, (17), 6507 6514.

26. Ellis, D. A.; Martin, J. W.; Mabury, S. A.; Hurley, M. D.; Andersen, M. P. S.; Wallington, T. J., Atmospheric lifetime of fluorotelomer alcohols. *Environ. Sci. Technol.* **2003,** *37*, (17), 3816 3820.

27. Kutsuna, S.; Nagaoka, Y.; Takeuchi, K.; Hori, H., TiO_2-induced heterogeneous photodegradation of a fluorotelomer alcohol in air. *Environ. Sci. Technol.* **2006,** *40*, (21), 6824 6829.

28. Styler, S. A.; Donaldson, D. J., Heterogeneous photochemistry of oxalic acid on Mauritanian sand and Icelandic volcanic ash. *Environ. Sci. Technol.* **2012,** *46*, (16), 8756 8763.

29. Styler, S. A.; Donaldson, D. J., Photooxidation of atmospheric alcohols on laboratory proxies for mineral dust. *Environ. Sci. Technol.* **2011,** *45*, (23), 10004 10012.

30. Finlayson-Pitts, B. J.; Pitts, J. N., *Chemistry of the upper and lower atmosphere*. Academic Press: San Diego, CA, 2000.

31. De Silva, A. O.; Allard, C. N.; Spencer, C.; Webster, G. M.; Shoeib, M., Phosphorus-containing fluorinated organics: polyfluoroalkyl phosphoric acid diesters (diPAPs), perfluorophosphonates (PFPAs), and perfluorophosphinates (PFPIAs) in residential indoor dust. *Environ. Sci. Technol.* **2012,** *46*, (22), 12575 12582.

32. Rand, A. A.; Mabury, S. A., Covalent binding of fluorotelomer unsaturated aldehydes (FTUALs) and carboxylic acids (FTUCAs) to proteins. *Environ. Sci. Technol.* **2013,** *47*, (3), 1655 1663.

33. Leveque, L.; Le Blanc, M.; Pastor, R., Synthesis of per(poly)fluoroalkyl aldehydes R-F$(CH_2)_{(n)}$CHO. *Tetrahedron Lett.* **1998,** *39*, (48), 8857 8860.

34. Underwood, G. M.; Li, P.; Usher, C. R.; Grassian, V. H., Determining accurate kinetic parameters of potentially important heterogeneous atmospheric reactions on solid particle surfaces with a Knudsen cell reactor. *J. Phys. Chem. A* **2000,** *104*, (4), 819 829.

35. Kahan, T. F.; Donaldson, D. J., Heterogeneous ozonation kinetics of phenanthrene at the air ice interface. *Environ. Res. Lett.* **2008,** *3*, (4), 045006.

36. Heger, D.; Nachtigallova, D.; Surman, F.; Krausko, J.; Magyarova, B.; Brumovsky, M.; Rubes, M.; Gladich, I.; Klan, P., Self-organization of 1-methylnaphthalene on the surface of artificial snow grains: a combined experimental computational approach. *J. Phys. Chem. A* **2011,** *115*, (41), 11412 11422.

37. Garland, E. R.; Rosen, E. P.; Clarke, L. I.; Baer, T., Structure of submonolayer oleic acid coverages on inorganic aerosol particles: evidence of island formation. *Phys. Chem. Chem. Phys.* **2008,** *10*, (21), 3156 3161.

38. Levitt, N. P.; Zhang, R. Y.; Xue, H. X.; Chen, J. M., Heterogeneous chemistry of organic acids on soot surfaces. *J. Phys. Chem. A* **2007,** *111*, (22), 4804 4814.

39. Shen, X.; Zhao, Y.; Chen, Z.; Huang, D., Heterogeneous reactions of volatile organic compounds in the atmosphere. *Atmos. Environ.* **2013,** *68*, 297 314.

40. Stock, N. L.; Ellis, D. A.; Deleebeeck, L.; Muir, D. C. G.; Mabury, S. A., Vapor pressures of the fluorinated telomer alcohols limitations of estimation methods. *Environ. Sci. Technol.* **2004,** *38*, (6), 1693 1699.

41. Chen, H.; Nanayakkara, C. E.; Grassian, V. H., Titanium dioxide photocatalysis in atmospheric chemistry. *Chem. Rev.* **2012,** *112*, (11), 5919 5948.

42. Gauthier, S. A.; Mabury, S. A., Aqueous photolysis of 8:2 fluorotelomer alcohol. *Environ. Toxicol. Chem.* **2005,** *24*, (8), 1837 1846.

43. Ahmmad, B.; Leonard, K.; Islam, M. S.; Kurawaki, J.; Muruganandham, M.; Ohkubo, T.; Kuroda, Y., Green synthesis of mesoporous hematite (alpha-Fe_2O_3) nanoparticles and their photocatalytic activity. *Adv. Powder Technol.* **2013,** *24*, (1), 160 167.

44. Chatterjee, S.; Sarkar, S.; Bhattacharyya, S. N., Photodegradation of phenol by visible light in the presence of colloidal Fe_2O_3. *J. Photochem. Photobiol., A* **1994,** *81*, (3), 199 203.

45. Ohko, Y.; Nakamura, Y.; Fukuda, A.; Matsuzawa, S.; Takeuchi, K., Photocatalytic oxidation of nitrogen dioxide with TiO_2 thin films under continuous UV-light illumination. *J. Phys. Chem. C* **2008,** *112*, (28), 10502 10508.

46. Hori, H.; Hayakawa, E.; Einaga, H.; Kutsuna, S.; Koike, K.; Ibusuki, T.; Kiatagawa, H.; Arakawa, R., Decomposition of environmentally persistent perfluorooctanoic acid in water by photochemical approaches. *Environ. Sci. Technol.* **2004,** *38*, (22), 6118 6124.

47. Hoffmann, M. R.; Martin, S. T.; Choi, W. Y.; Bahnemann, D. W., Environmental applications of semiconductor catalysis. *Chem. Rev.* **1995,** *95*, (1), 69 96.

48. Ochiai, T.; Iizuka, Y.; Nakata, K.; Murakami, T.; Tryk, D. A.; Koide, Y.; Morito, Y.; Fujishima, A., Efficient decomposition of perfluorocarboxylic acids in aqueous suspensions of a TiO_2 photocatalyst with medium-pressure ultraviolet lamp irradiation under atmospheric pressure. *Ind. Eng. Chem. Res.* **2011,** *50*, (19), 10943 10947.

49. Ahrens, L.; Harner, T.; Shoeib, M.; Lane, D. A.; Murphy, J. G., Improved characterization of gas particle partitioning for per- and polyfluoroalkyl substances in the atmosphere using annular diffusion denuder samplers. *Environ. Sci. Technol.* **2012,** *46*, (13), 7199 7206.

50. Formenti, P.; Schuetz, L.; Balkanski, Y.; Desboeufs, K.; Ebert, M.; Kandler, K.; Petzold, A.; Scheuvens, D.; Weinbruch, S.; Zhang, D., Recent progress in understanding physical and chemical properties of African and Asian mineral dust. *Atmos. Chem. Phys.* **2011,** *11*, (16), 8231 8256.

51. Chen, H.; Laskin, A.; Baltrusaitis, J.; Gorski, C. A.; Scherer, M. M.; Grassian, V. H., Coal fly ash as a source of iron in atmospheric dust. *Environ. Sci. Technol.* **2012,** *46*, (4), 2112 2120.

52. Benskin, J. P.; Muir, D. C. G.; Scott, B. F.; Spencer, C.; De Silva, A. O.; Kylin, H.; Martin, J. W.; Morris, A.; Lohmann, R.; Tomy, G.; Rosenberg, B.; Taniyasu, S.; Yamashita, N., Perfluoroalkyl acids in the Atlantic and Canadian Arctic Oceans. *Environ. Sci. Technol.* **2012,** *46*, (11), 5815 5823.

53. Webster, E.; Ellis, D. A., Potential role of sea spray generation in the atmospheric transport of perfluorocarboxylic acids. *Environ. Toxicol. Chem.* **2010,** *29*, (8), 1703 1708.

54. Young, C. J.; Furdui, V. I.; Franklin, J.; Koerner, R. M.; Muir, D. C. G.; Mabury, S. A., Perfluorinated acids in arctic snow: new evidence for atmospheric formation. *Environ. Sci. Technol.* **2007,** *41*, (10), 3455 3461.

55. Armitage, J. M.; MacLeod, M.; Cousins, I. T., Modeling the global fate and transport of perfluorooctanoic acid (PFOA) and perfluorooctanoate (PFO) emitted

from direct sources using a multispecies mass balance model. *Environ. Sci. Technol.* **2009,** *43*, (4), 1134 1140.

56. Frank, R.; Ishida, K.; Suda, P., Metals in agricultural soils of Ontario. *Can. J. Soil Sci.* **1976,** *56*, (3), 181 196.

57. Wang, Y.; Zhang, P. Y., Photocatalytic decomposition of perfluorooctanoic acid (PFOA) by TiO_2 in the presence of oxalic acid. *J. Hazard. Mater. 192*, (3), 1869 1875.

58. Tang, H.; Xiang, Q.; Lei, M.; Yan, J.; Zhu, L.; Zou, J., Efficient degradation of perfluorooctanoic acid by UV Fenton process. *Chem. Eng. J.* **2012,** *184*, 156 162.

59. Hori, H.; Yamamoto, A.; Koike, K.; Kutsuna, S.; Osaka, I.; Arakawa, R., Photochemical decomposition of environmentally persistent short-chain perfluorocarboxylic acids in water mediated by iron(II)/(III) redox reactions. *Chemosphere* **2007,** *68*, (3), 572 578.

5.6 Appendix

5.6.1 The multi-compartment Knudsen cell

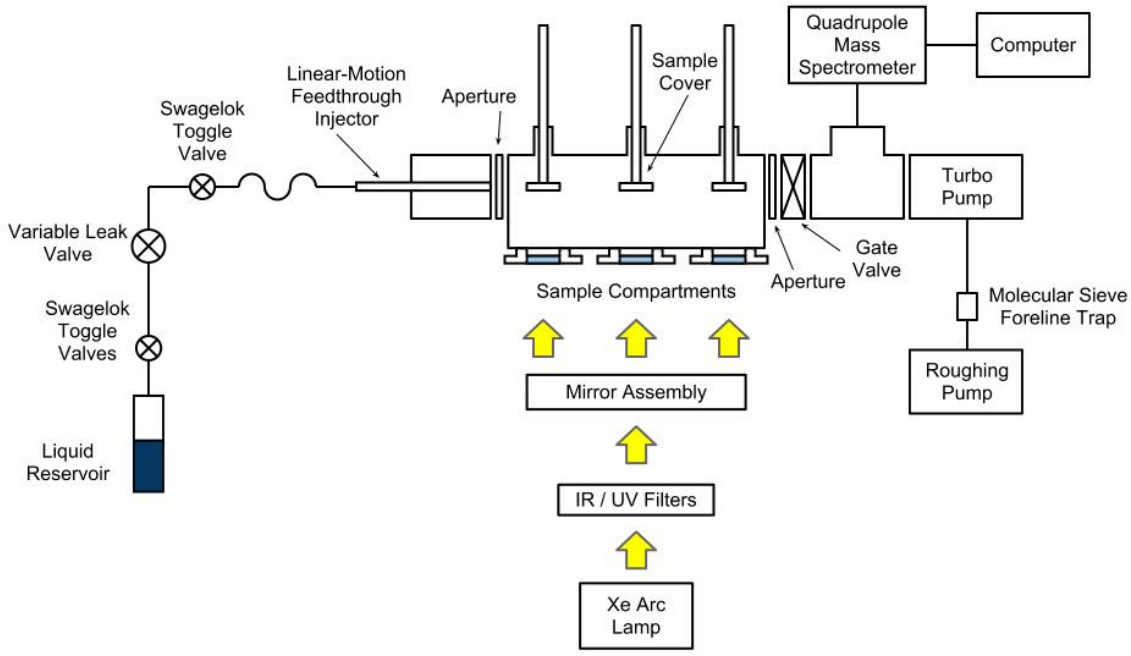

Figure 5A-1 Schematic drawing of the multicompartment photochemical Knudsen cell

5.6.2 LC-MS-MS analysis

Analysis was performed using a Waters Aquity ultra-performance liquid chromatograph (UPLC) (Waters, Mississauga, ON, CAN) coupled to an AB Sciex API4000 triple quadrupole mass spectrometer (AB Sciex, Concord, ON, CAN). The column used was a Phenomenex Kinetex C18 analytical UPLC column (50 mm x 4.60 mm, 2.6 µm, 100 Å, Torrence, CA, USA). The injection volume was 10 µL, the column temperature was 40°C, and the sample temperature was 10°C.

The following gradient method was used (0.6 mL min^{-1} flow rate):

Time (minutes)	10mM Ammonium Acetate Water (%)	10mM Ammonium Acetate Methanol (%)
0	65	35
3	5	95
5	5	95
5.5	65	35
8	65	35

The analysis was run in multiple reaction monitoring (MRM) mode using negative electrospray ionization. The following mass spectrometry parameters were used:

Analyte	Parent Ion Mass (Da)	Progeny Ion Mass (Da)	Declustering Potential (V)	Collision Energy (eV)
PFPeA	263.0	219.0	-25	-13
PFHxA	313.0	269.0	-30	-14
PFHpA	363.0	319.0	-30	-14
6:2 FTUCA	357.0	293.0	-35	-18
6:2 FTCA	377.0	293.0	-35	-18
[$^{13}C_2$]PFHxA	315.0	270.0	-30	-14
[$^{13}C_4$]PFOA	417.0	372.0	-35	-15
[$^{13}C_2$]6:2 FTCA	379.0	294.0	-35	-18
[$^{13}C_2$]6:2 FTUCA	359.0	294.0	-35	-18

Analytes were quantified using internal standard calibration (calibration standards: 1, 5 20, 50, 100, 135 ng/mL). Native and ^{13}C-labelled PFC standards were obtained from Wellington Laboratories (Guelph, ON, CAN). Native analytes were quantified using ^{13}C-labelled internal standards as follows: $^{13}C_2$-PFHxA for PFPeA and PFHxA, $^{13}C_4$-PFOA for PFHpA, and $^{13}C_2$-6:2 FTUCA for 6:2 FTUCA. 6:2 FTCA could not be quantified due to lack of native 6:2 FTCA standard (*i.e.* no 6:2 FTCA calibration curve for quantification).

Samples were prepared in 50:50 methanol:water. Extracts were diluted as necessary prior to LC analysis. 15µL of a 50 ng/mL ^{13}C-labelled PFC standard in methanol was added to each sample and standard to give an internal standard concentration of 2.5ng/mL.

5.6.3 QA/QC results

Blank concentrations of fluorinated photoproducts in the various matrices under study (n = 1) were quantified by subjecting 100 mg samples to the same extraction procedure as was described in the Materials and Methods section. In all cases, blank concentrations were < 1 ppb, which was significantly lower than samples exposed to 6:2 FTOH, and therefore no blank corrections were made to experimental values.

The extraction efficiency for PFASs in ash and sand was evaluated using a spike and recovery method. 100 mg samples of sand (n=5) and ash (n=5) were placed in glass scintillation vials containing ~ 2 mL deionized water and dried in a 423K oven. Each dried sample was spiked with 20µL of a 300 ng/mL native PFAS methanol standard solution and the solvent was allowed to evaporate overnight in a fume hood. The samples were then subjected to the extraction procedure described in the Materials and Methods section, alongside 100 mg blank sand and ash samples used to account for contamination during extraction. In these experiments, low ppb contamination of PFHxA was observed in the blank ash and sand samples; therefore, reported

recoveries for PFHxA have been blank-corrected. The results of these experiments are presented in Figure 5A-2.

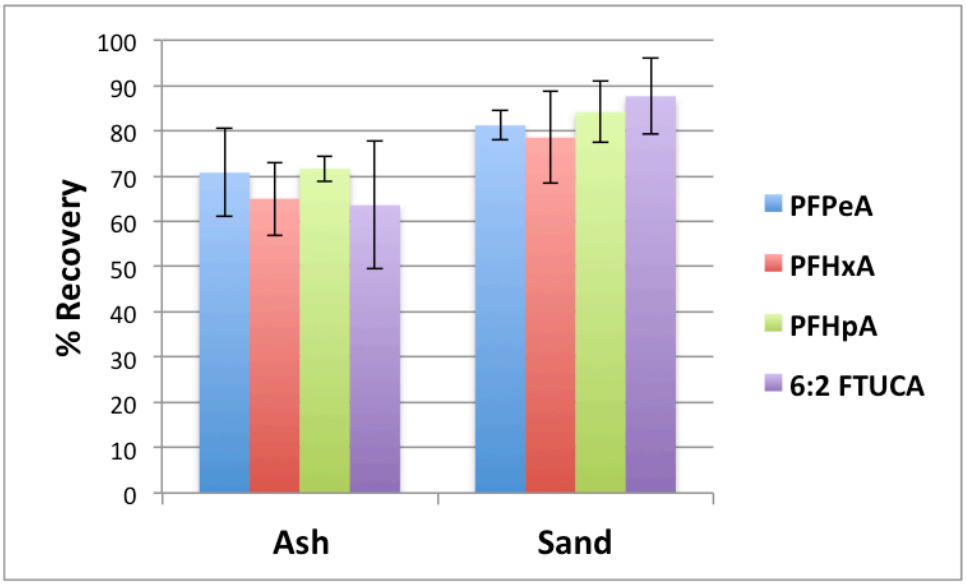

Figure 5A-2 Results of spike and recovery experiments designed to quantify extraction efficiency of fluorinated photoproducts. Error bars represent the standard deviation associated with five individual trials. Recoveries for PFHxA were blank-corrected.

Chapter 6

Light-induced interactions of SO_2 with authentically generated mineral dust

Contributions:

Sarah A. Styler designed the overall experimental strategy with assistance from D. James Donaldson, Jean-Francois. Doussin, and Paola Formenti. All experiments performed at the University of Toronto were designed and conducted by Sarah A. Styler. Experiments in the CESAM atmospheric chamber were performed by Sarah A. Styler with assistance from Jean-François Doussin, Paola Formenti, Claudia di Biagio, and Edouard Pangui. The manuscript was written by Sarah A. Styler, with critical comments from D. James Donaldson.

6.1 Introduction

Teragram quantities of mineral dust are emitted annually from source regions in Africa and Central Asia.[1, 2] Emitted dust undergoes efficient transport to distant receptor regions, where it can contribute to local reductions in air quality: for example, the springtime atmosphere in Beijing, China is characterized by episodes of high particulate matter concentrations, which arise from the windblown transport of dust from desert regions west of the city.[3] The interaction between advected dust and local pollutant plumes is especially important in East Asia, where emissions from highly populated urban and industrial centres result in elevated concentrations of SO_2 and other pollutants.[4, 5]

In a modeling study performed as part of the Asian Pacific Regional Aerosol Characterization Experiment (ACE-Asia), which aimed in part to provide insight into aerosol trace gas interactions in this region, dust was found to contribute to a 55% loss in gas-phase SO_2 concentrations.[6] The uptake of SO_2 by dust is important for two main reasons. First, it ultimately leads to the formation of surface-sorbed sulfate, which enhances dust hygroscopicity and thus influences its cloud-forming and light-scattering properties.[7, 8] Second, strong evidence exists to suggest that SO_2-mediated enhancements in aerosol acidity can increase the solubility and bioavailability of iron in dust deposited to the ocean, and thereby influence oceanic primary productivity.[9, 10]

For the reasons described above, the uptake of SO_2 by mineral dust has been explored in a number of laboratory studies.[11-16] Surface characterization studies have shown that the uptake of SO_2 by individual metal oxides and authentic mineral dust samples results in the formation of surface-bound sulfites, which can subsequently be converted to sulfates by oxidants such as co-sorbed O_3 and NO_2.[17-22]

In recent years, researchers have begun to investigate the light-induced oxidation of SO_2 at the surface of photoactive metal oxides, including TiO_2 and Fe_2O_3. At the TiO_2

surface, the presence of light effects the transformation of adsorbed sulfite to adsorbed sulfate[23, 24] and enhances the total sulfur adsorption capacity.[25] At the illuminated Fe_2O_3 surface, the uptake of gas-phase SO_2 is thought to be enhanced by the presence of reactive Fe^{2+} sites.[26]

To date, only two studies have investigated the photochemistry of SO_2 in the presence of real mineral dust. In the first study, Saharan dust was exposed to gas-phase SO_2 and the accumulation of surface sulfate was measured using scanning electron microscopy with energy-dispersive X-ray detection (SEM-EDX) in the presence and absence of humidity, ozone, and light.[27] Although no statistically significant sulfate formation was observed in the presence of light alone, the authors of this study note that the SEM-EDX technique, which probes the outer ~ 1 μm of the dust grains, is not particularly sensitive to the accumulation of sulfate at the dust surface, since the surface signal is 'diluted' by signal from the underlying bulk sample.[27] In the second study, the exposure of Arizona test dust to gas-phase SO_2 in the presence of light and humidity was shown to lead to new particle formation.[28] This observation was attributed to the oxidation of SO_2 by gas-phase OH produced by the illuminated dust surface.[28]

The present collaborative study represents an attempt to further our understanding of the light-induced interactions of SO_2 with mineral dust. The first phase of the study, which was performed at the University of Toronto, investigated the uptake of SO_2 and light-mediated production of sulfate at the surface of individual mineral dust components and authentic African and Asian source sands. The second phase of the study, which was performed in the CESAM atmospheric chamber at the Université Paris Est Créteil, investigated mineral dust-mediated particle formation in the presence of light and SO_2.

6.2 Materials and methods

6.2.1 Knudsen cell uptake and photochemistry experiments

In these experiments, a photochemical Knudsen cell reactor was used to measure the uptake of SO_2 at the surface of mineral dust components and sand obtained from dust source regions in Niger and China under light and dark conditions. Then, light-induced changes in the relative quantities of sulfite and sulfate formed at the surface of these samples were determined using ion chromatography.

6.2.1.1 Experimental apparatus

Experiments were performed in a custom-built multi-sample photochemical Knudsen cell, which was first used for the study of fluorotelomer alcohol (FTOH) photochemistry on sand and ash surfaces.[29] A schematic and description of the apparatus is presented in Chapter 5.

Gas-phase SO_2 is introduced into the Knudsen cell reaction chamber through a length of copper tubing connected to a ¼" stainless-steel injector tube. The introduction of SO_2 into the chamber is controlled using a variable leak valve. Three isolation flanges equipped with o-rings are used to shield samples from gas-phase SO_2. Viton o-rings are especially susceptible to SO_2-mediated degradation; the resultant leakage of SO_2 into sample compartments manifests as an apparent reduction in uptake by the surface under study. For this reason, the Knudsen cell flanges were equipped with SO_2-resistant EPDM o-rings, and new o-rings were used for each experiment.

6.2.1.2 Experimental procedure

Samples were prepared by suspending 5 150 mg of TiO_2, illite, Arizona test dust, or sand obtained from Niger or China in ~ 1.5 mL of deionized water. The resultant slurries were transferred via pipet to shallow 3 cm diameter Pyrex sample holders,

which were then heated for 45 minutes in a 373 423 K oven to evaporate water and yield films of relatively uniform thickness. No further efforts were made to remove adsorbed water from the samples.

Prior to each experiment, the sample holders containing the substrates of interest were placed into the Knudsen cell reaction chamber and the apparatus was evacuated until a constant background pressure of $\sim 3 \times 10^{-2}$ Pa was achieved ($\sim$ 1 hour). At this point, SO_2 background signal intensity (*m/z* 64) was measured using the quadrupole mass spectrometer (QMS) interfaced to the chamber. Then, the isolation flanges were lowered and gas-phase SO_2 was introduced into the sample chamber.

Once the mass spectrometric signal reached a relatively constant level, the first sample cover was opened. Uptake of SO_2 by the sample gave rise to an immediate decrease in the QMS signal at *m/z* 64 followed by a slow increase toward its initial value, the latter of which reflects the saturation of available surface sites. Typically, surface saturation was achieved in < 5 min. Representative QMS traces illustrating this uptake behaviour are displayed in Figure 6-4. The apparent initial uptake coefficient for reaction was calculated using the following equation:[30]

$$\gamma_0 = \frac{A_h}{A_s} \frac{I_0 - I}{I}$$

Here, A_h and A_s are the geometric areas of the escape orifice and sample holder, respectively; I_0 is the signal recorded by the QMS with the sample cover closed; and I is the lowest signal recorded by the QMS after raising the isolation flange.

In experiments designed to investigate heterogeneous SO_2 photochemistry, samples were illuminated from below during SO_2 exposure using a 100 W Xe arc lamp, the output of which resembles the actinic radiation spectrum (see Figure 4-1). The Pyrex sample holders served as long-pass optical filters, eliminating $\lambda < 310$ nm. All

photochemical experiments were conducted in the presence of gas-phase oxygen (~ 0.7 Pa), which was introduced into the chamber through a variable leak valve.

6.2.1.3 Determination of sulfite and sulfate in SO_2-exposed samples

Sulfite (S^{IV}) is efficiently oxidized to sulfate (S^{VI}) in aqueous solution, especially in the presence of iron.[31] One common S^{IV} stabilizer is aqueous formaldehyde (formalin), which reacts with sulfite to form the stable hydroxymethanesulfonate adduct.[32] Although treatment of sample extracts with formalin allows for the determination of S^{VI} without interference from sulfite oxidation, the hydroxymethanesulfonate adduct is poorly retained on the ion chromatographic column and therefore cannot be quantified under the conditions employed in the present experiment. For this reason, the quantity of S^{IV} in each sample was determined indirectly.

After exposure to gas-phase SO_2, samples were divided in half and placed in two 15 mL polypropylene tubes (T1 and T2). 2 5 mL of deionized water and 10 mg of Fe_2O_3 (as sulfite oxidant) was added to T1, while 2 5 mL of 1% or 5% v/v aqueous formalin solution prepared using deionized water was added to T2. Both tubes were manually shaken (1 min) and centrifuged (10 min; 4180 rpm). The centrifuged samples were passed through a 0.2 μm syringe filter (Fisher Scientific) and the sulfate content in each was determined using ion chromatography. The sulfate (S^{VI}) content and total sulfur content (S^{IV} + S^{VI}) of the sample itself were then obtained by doubling the sulfate peak areas measured for T2 and T1, respectively.

6.2.1.4 Ion chromatography

The sulfate content of sample extracts was analyzed via ion chromatography using a HPLC system equipped with a Perkin-Elmer Series 200 pump, an Alltech 550 conductivity detector with self-regenerating suppressor, and a 25 μL sample loop. The analytical column used was a Dionex STAR-ION A300 (4.6 x 100 mm). The

mobile phase was 1.8 mM/1.7 mM carbonate/bicarbonate and the flow rate was 1.5 mL min^{-1}. Under these conditions, sulfate eluted at ~ 6.3 min.

6.2.2 Atmospheric chamber experiments

The interaction of authentically generated dust with gas-phase SO_2 was explored in the CESAM atmospheric chamber at the Université Paris Est Creteil. Information regarding CESAM is provided in Section 1.3.2.3 and in a detailed paper by Wang *et al.*[33]

6.2.2.1 Dust generation technique

Dust was generated from Nigerien and Chinese source sands using a technique designed to mimic the sandblasting process that is responsible for dust emission in the real environment.[34] As shown in Figure 6-1, the dust generation apparatus consists of an Erlenmeyer flask affixed to a vibrating plate. The upper opening of the flask is connected to a wide-bore vertical metal cylinder, which in turn is connected to the CESAM chamber. All connections are made using rubber tubing, which minimizes particle loss via electrostatic deposition.

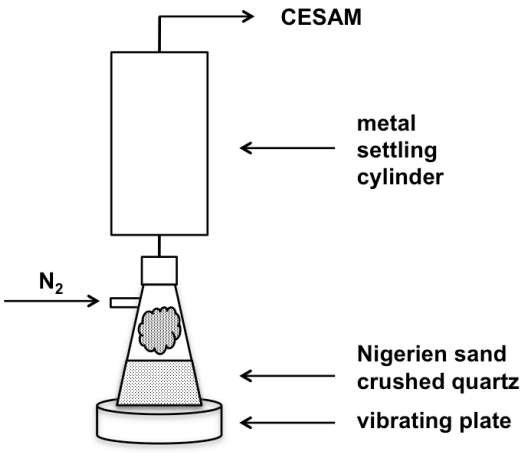

Figure 6-1 System used at CESAM for generation of dust from source sands.

Before each experiment, equal quantities of sand and crushed pure quartz (typically ~ 60 g) were placed into the Erlenmeyer flask and the entire apparatus was flushed with N_2. At this point, the vibrating plate was turned to its maximum level (100 Hz) and the sample was agitated for 30 minutes. After the agitation period, the generated dust was entrained in a flow of N_2; passed through the metal settling cylinder, where the largest size fraction was removed via sedimentation; and injected into the chamber.

Some control experiments were performed using dry NaCl particles instead of mineral dust. In these experiments, particles were produced by nebulizing an aqueous solution of NaCl (30 mM) and passing the resultant particle stream through a diffusion dryer. This generation technique resulted in particles with a broad size distribution centred around ~ 300 nm.

6.2.2.2 Experimental procedure

Experiments began by introducing gas-phase water into the CESAM chamber. After the relative humidity within the chamber reached ~ 50%, gas-phase SO_2 (~ 4 mL at standard temperature and pressure) was introduced into the chamber in a nitrogen flow. Typical SO_2 concentrations within the chamber at the beginning of an experiment were ~ 800 ppb. In order to determine background wall loss within the chamber, SO_2 concentrations were first monitored for ~ 1h in the absence of other species. Then, dust was introduced into the chamber using the technique described in Section 6.2.2.1. After 30 minutes, the chamber was illuminated. At this time, the relative humidity in the chamber was ~ 40%. All experiments were performed at room temperature and atmospheric pressure.

6.2.2.3 Instrumentation

Gas-phase SO_2 concentrations within the chamber were measured using an ambient sulfur dioxide monitor (APSA-370, Horiba). Particle number counts were measured using a condensation particle counter (CPC model 3775; TSI®). Particle size distributions were measured using an aerodynamic particle sizer (APS model 3321; TSI®) and a

scanning mobility particle sizer (SMPS; DMA model 3080, CPC model 3010; TSI®).

6.2.3 Chemicals

TiO_2 (anatase, ≥ 99%) and Fe_2O_3 (≥ 99%) were obtained from Sigma Aldrich. Arizona test dust (0 5 μm) was obtained from Powder Technology Inc. Illite (IMt-1) was obtained from the Source Clays Repository of the Clay Minerals Society. Sand samples were obtained from Banizoumbou, Niger and the Ulan Buh area in the Gobi desert, China.[34] TiO_2, Fe_2O_3, and the Chinese sand sample were rinsed repeatedly in deionized water to remove surface-sorbed sulfate prior to use.

6.3 Results

6.3.1 Knudsen cell uptake and photochemistry experiments

6.3.1.1 Dark uptake experiments

In order to gain insight into the dependence of SO_2 uptake on particle mineralogy, mass-dependent uptake coefficients were determined for SO_2 at the surface of TiO_2, illite, Arizona test dust, and Chinese sand using the photochemical Knudsen cell. The results of these experiments are displayed in Figures 6-2 and 6-3.

Experiments were not performed to characterize SO_2 uptake at the surface of Niger sand as a function of sample mass. However, individual uptake experiments were performed using both coarse (< 1000 μm) and fine (20 63 μm) fractions of the Niger sand sample. As shown in Figure 6-4, a significantly larger loss of gas-phase SO_2 was observed in the presence of the fine sample than in the presence of an identical mass of the coarse sample.

All of the uptake experiments described in this section were performed under dark conditions. In a set of preliminary experiments conducted under illumination, no change in uptake behaviour was observed.

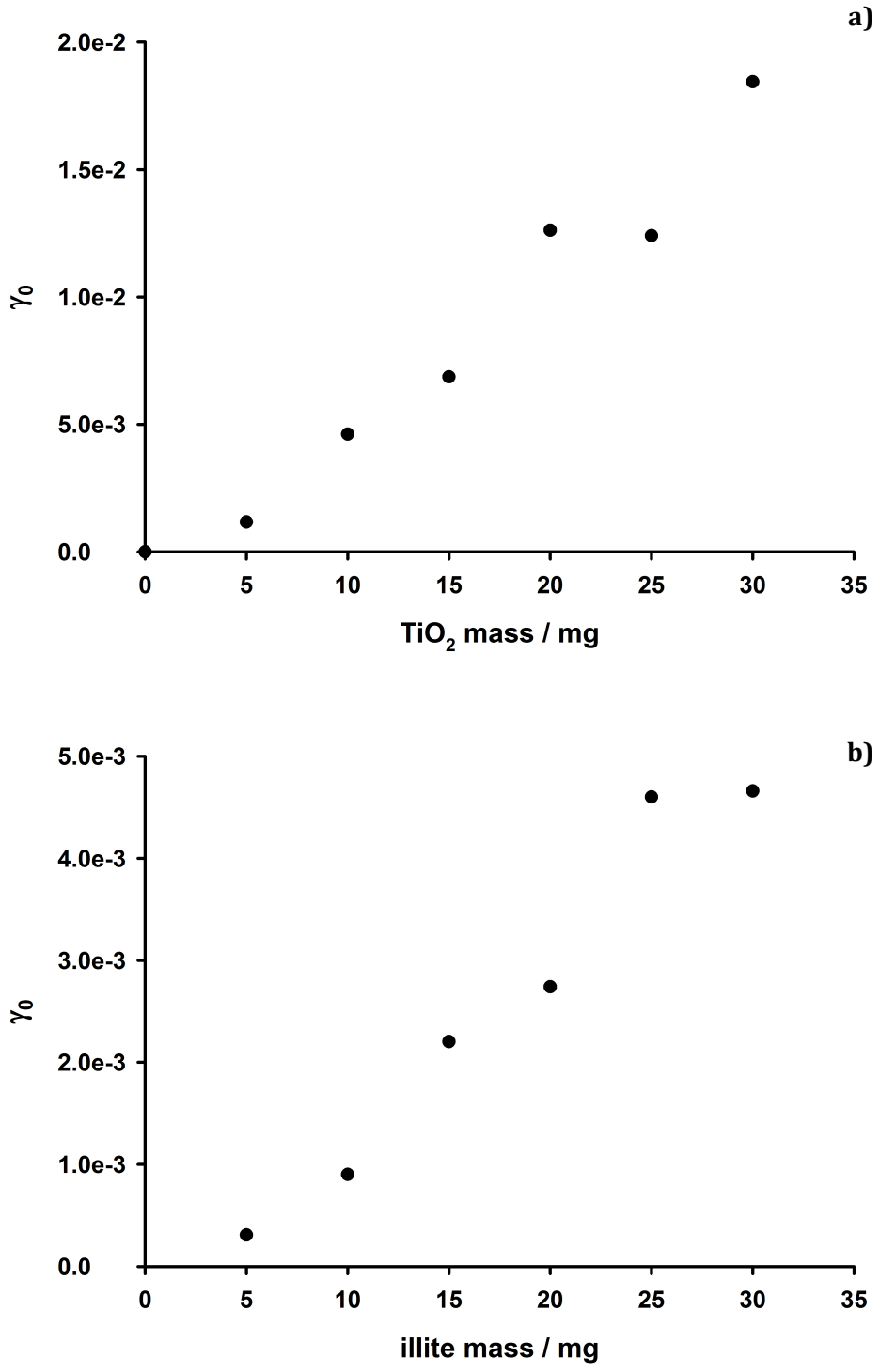

Figure 6-2 Apparent initial uptake coefficients γ_0 for SO_2 at the surface of a) TiO_2 and b) illite as a function of sample mass.

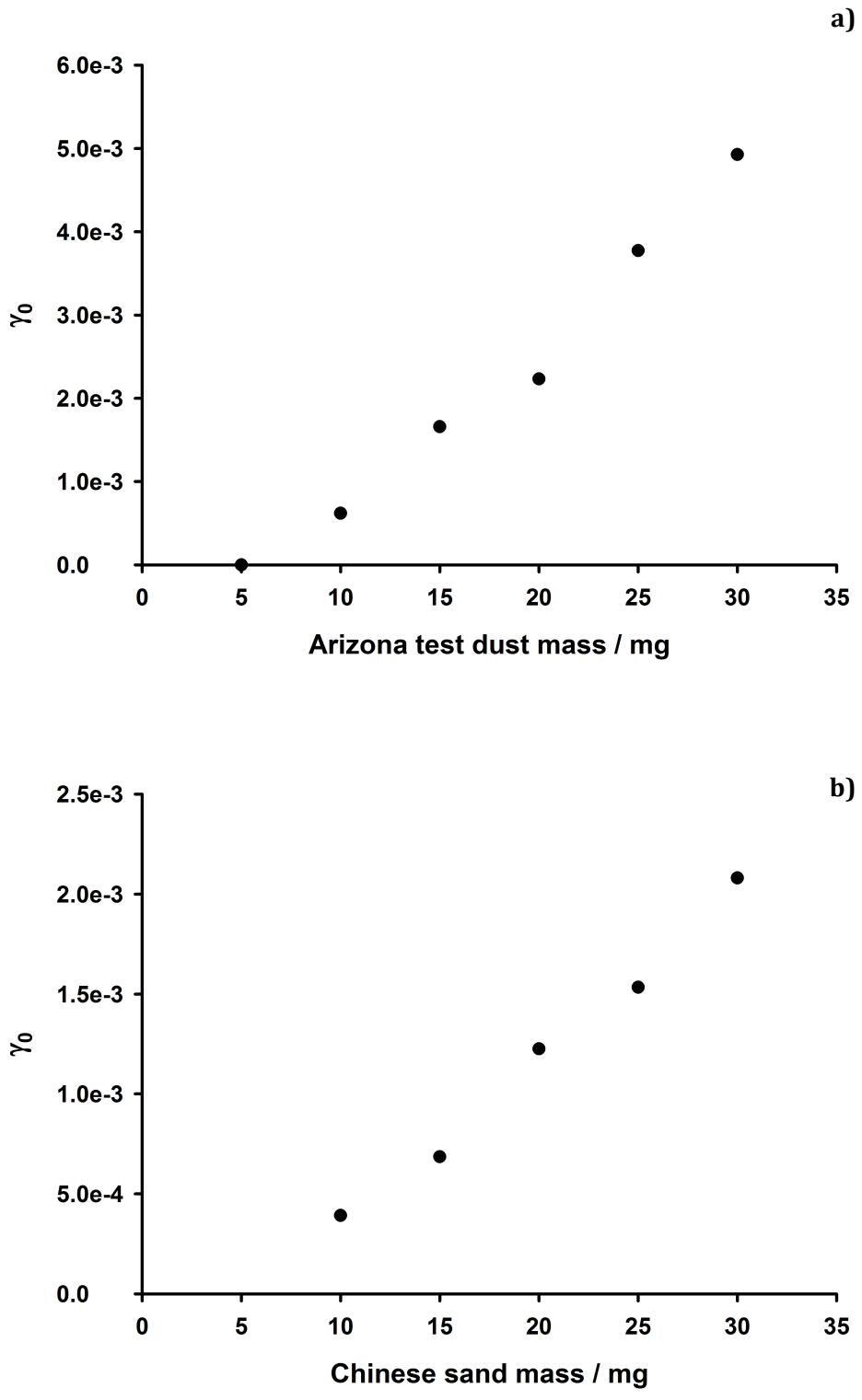

Figure 6-3 Apparent initial uptake coefficients γ_0 for SO_2 at the surface of a) Arizona test dust and b) Chinese sand as a function of sample mass.

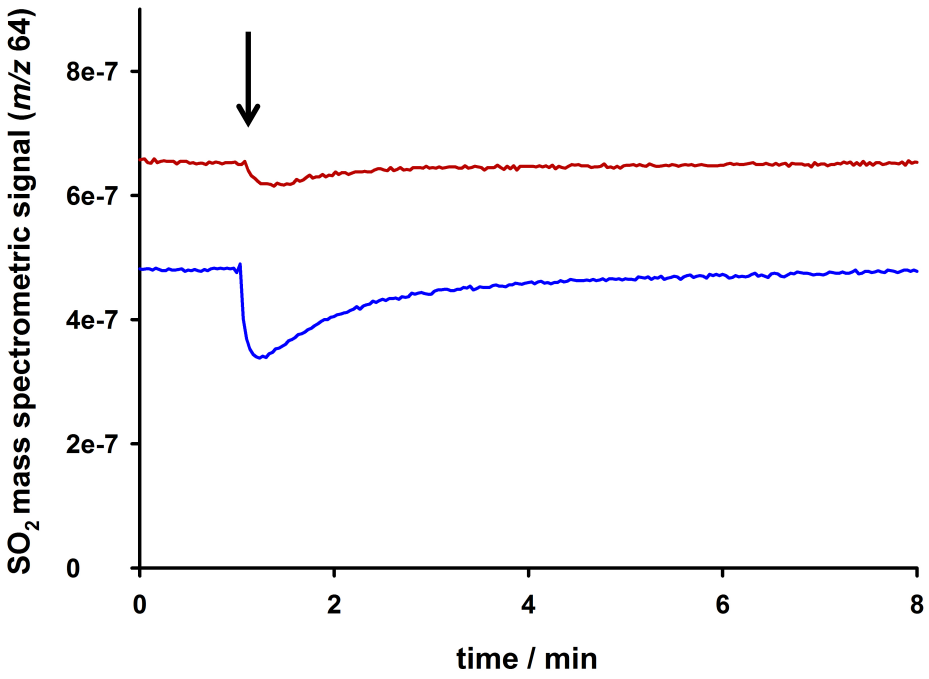

Figure 6-4 Uptake of SO_2 at the surface of 100 mg of coarse (< 1000 μm; red trace) and fine (20–63 μm; blue trace) Niger sand. The plot shows the results of two separate experiments. The black arrow indicates the time at which the samples were exposed to gas-phase SO_2. Experiments were conducted in the presence of gas-phase oxygen (~ 0.7 Pa), and both samples were ground in a mortar and pestle prior to the experiments.

6.3.1.2 Photochemical production of sulfate at the surface of illuminated sand

The production of sulfate at the surface of illuminated coarse and fine size fractions of Nigerien sand and Fe_2O_3 upon exposure to SO_2 was determined using ion chromatography. The results of these experiments are plotted in Figures 6-5 to 6-7. For Nigerien sand (Figures 6-5 and 6-6), the sulfur content of SO_2-exposed samples is reported in terms of absolute sulfur (VI) and total sulfur (S^{VI} + S^{IV}) peak areas within sample extracts. For Fe_2O_3 (Figure 6-7), the sulfur content of SO_2-exposed samples is

reported both in terms of absolute sulfate peak areas S_{ABS} and fractional sulfate content S_{FRA} (*i.e.* S^{VI}/S^{TOTAL}, where $S^{TOTAL} = S^{IV} + S^{VI}$) within sample extracts.

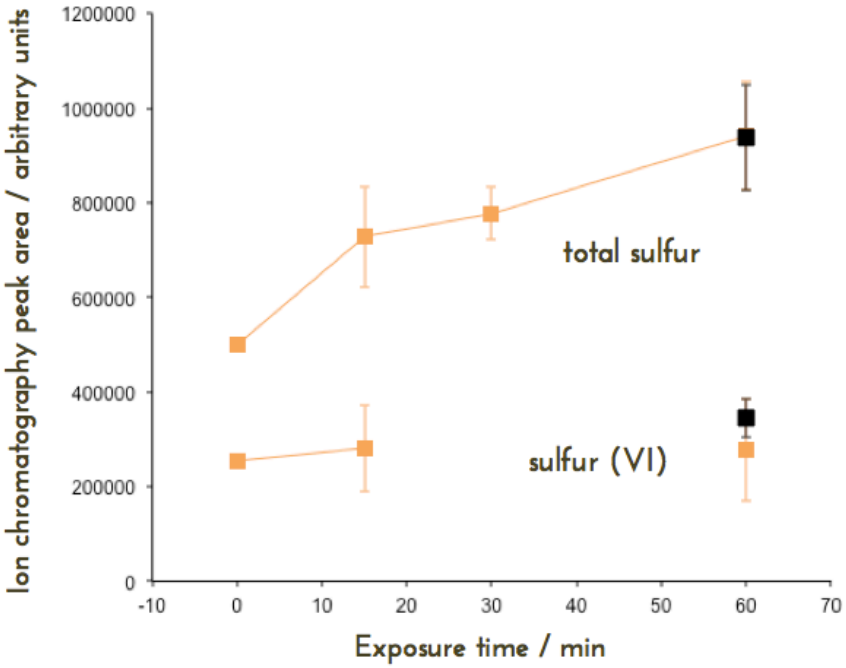

Figure 6-5 Sulfur (VI) and total sulfur ($S^{IV} + S^{VI}$) at the surface of the coarse fraction of Nigerien sand (< 1000 μm; 150 mg) as a function of exposure to gas-phase SO_2. The orange and black squares represent the absolute peak areas for SO_2-exposed sand samples under light and dark conditions, respectively. Each data point represents the mean of three trials, each of which was performed with a fresh sample.

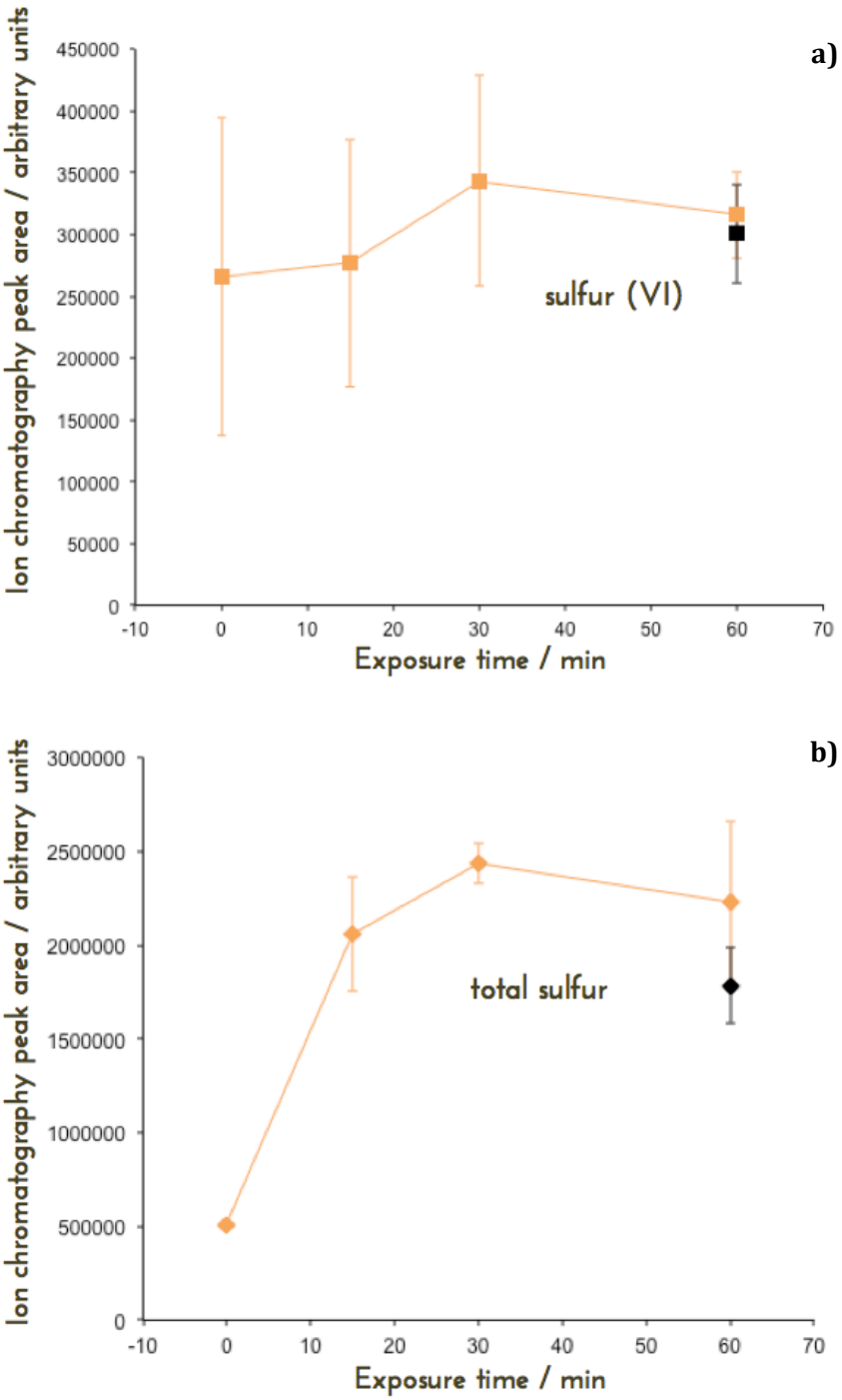

Figure 6-6 a) Sulfur (VI) and b) total sulfur (S^{IV} + S^{VI}) at the surface of the fine fraction of Nigerien sand (20–63 μm; 150 mg) as a function of exposure to gas-phase SO_2. The orange and black symbols represent the absolute sulfur peak areas for SO_2-exposed sand samples under light and dark conditions, respectively. Each data point represents the mean of three trials, each of which was performed with a fresh sample.

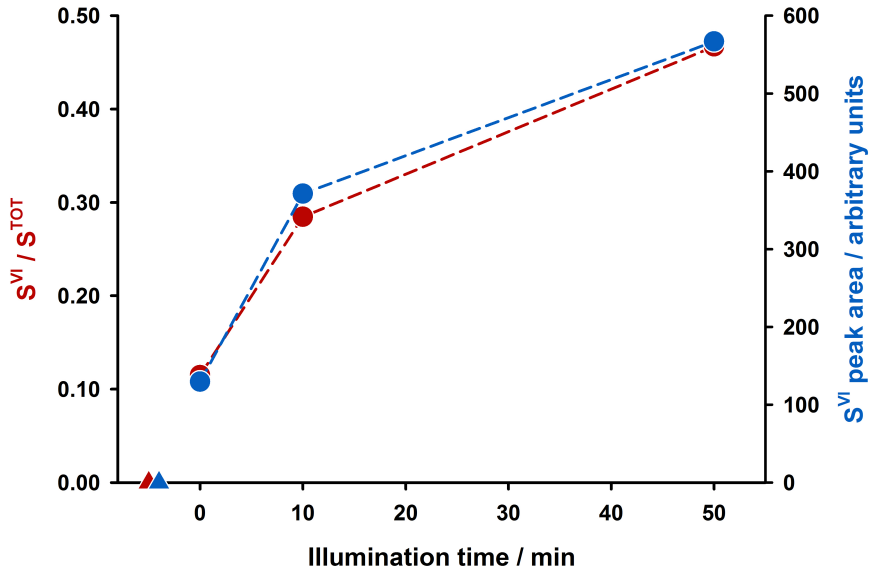

Figure 6-7 Light-induced sulfate production at the surface of 20 mg of Fe_2O_3. Here, the red circles and red triangles represent the fractional sulfate contents of SO_2-exposed and control sand samples, respectively (left axes). The blue circles and blue triangles represent the absolute sulfate peak areas for SO_2-exposed and control sand samples, respectively (right axes).

6.3.2 Atmospheric chamber experiments

6.3.2.1 Dust size distribution within the CESAM chamber

In the present experiments, dust was generated using a method designed to replicate the natural processes responsible for the release of dust from source soils.[34] The APS number size distribution of the generated dust within the CESAM chamber is shown in Figure 6-8 as a function of residence time within the chamber. As illustrated by this figure, the peak of the size distribution moved toward smaller particle diameters with increasing residence time, which implies that the largest particles were preferentially removed via sedimentation.

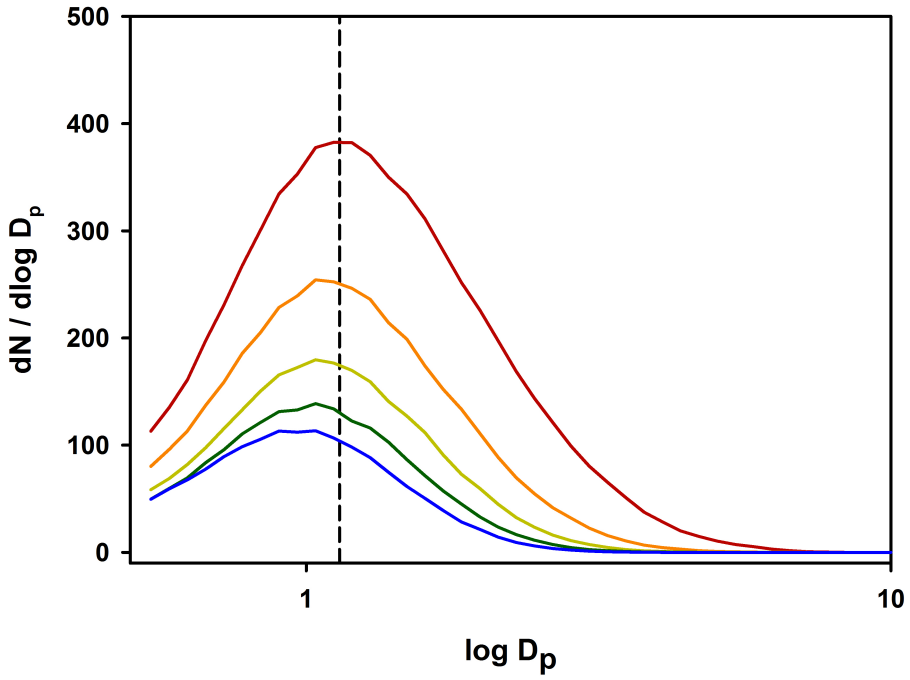

Figure 6-8 APS dust particle number size distribution within the CESAM chamber as a function of residence time (red = 0 min; orange = 30 min; yellow = 60 min; green = 90 min; blue = 120 min). The black dashed line represents the peak of the size distribution immediately after injection (~ 1.14 μm). The APS measurements presented here are not corrected for dilution effects within the chamber.

6.3.2.2 Background chamber reactivity: light-induced nucleation in the presence of gas-phase SO_2

In a set of control experiments designed to characterize background SO_2 nucleation within the CESAM chamber, SO_2 was illuminated in the presence of gas-phase water (RH ~ 40%) but in the absence of introduced particulate matter. As shown in Figure 6-9, this resulted in significant new particle formation.

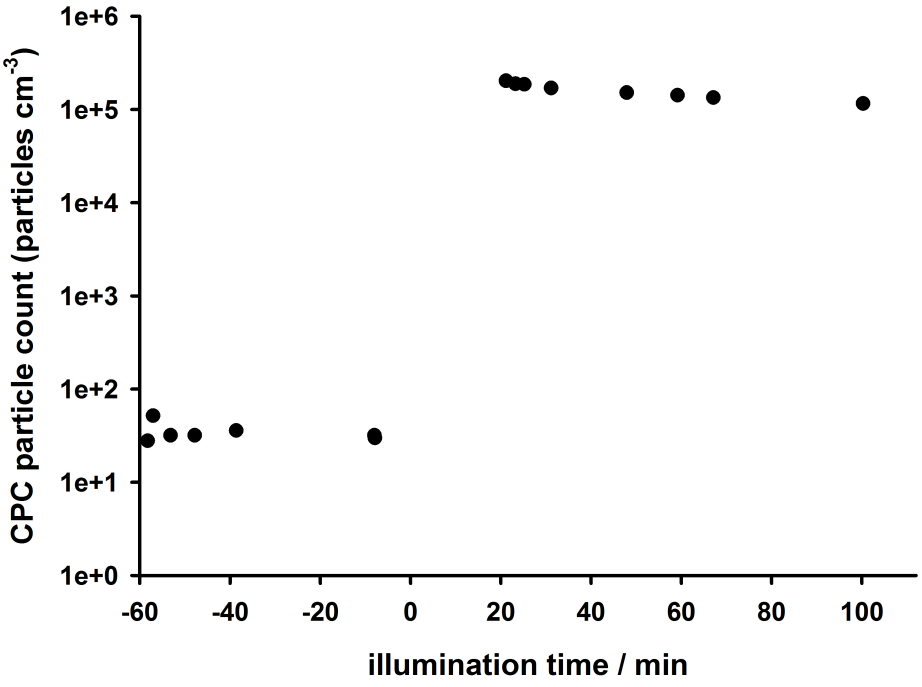

Figure 6-9 CPC particle count (particles cm^{-3}) within the CESAM chamber as a function of illumination time reveals significant new particle formation, even in the absence of mineral dust. The experiment was conducted with ~ 800 ppb SO_2 and at ~ 40% RH.

6.3.2.3 New particle formation in the presence of SO_2, mineral dust, and light

As shown in Figure 6-10, illumination of SO_2 in the presence of gas-phase water (RH ~ 40%) and NaCl particles (~ 100 nm diameter) results in a suppression of the background nucleation observed in the absence of introduced particles. By contrast, as illustrated in Figure 6-11, illumination of SO_2 in the presence of gas-phase water (RH ~ 40%) and mineral dust produced from either Nigerien or Chinese source samples leads to significant new particle formation. These experiments were performed under similar particle surface area loadings (< 50% difference as determined using SMPS and APS data).

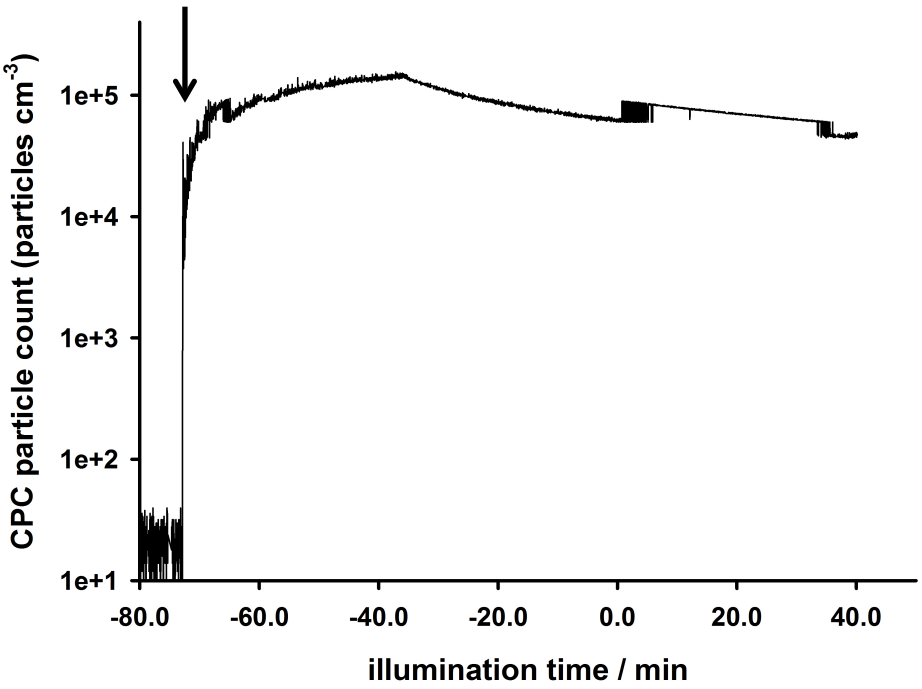

Figure 6-10 CPC particle count (particles cm^{-3}) within the CESAM chamber as a function of illumination time in the presence of NaCl particles (~ 100 nm diameter; surface area loading comparable within ~ 50% to that of dust experiments shown in Figure 6-11). These experiments were conducted with ~ 800 ppb SO_2 and at ~ 40% RH. The black arrow indicates the time at which NaCl particles were injected into the chamber. Illumination was halted at ~ 35 min. The apparent stepwise increase and decrease in particle number upon initiation and cessation of illumination arose from an electronic interference from the lamps and/or chamber cooling system.

6.4 Discussion

6.4.1 Uptake of SO_2 under dark conditions

As shown in Figures 6-2 and 6-3, SO_2 uptake is observed at all of the surfaces under study. The highest uptake was observed at the surface of TiO_2; the uptakes at the surface of illite, Arizona test dust, and Chinese sand were comparable. The uptake of SO_2 at the surface of each of these samples displays a quasi-linear dependence upon sample mass. As outlined by Underwood and coworkers,[35] a linear correlation between uptake and sample mass implies that the entire sample mass is accessible to the gas-phase

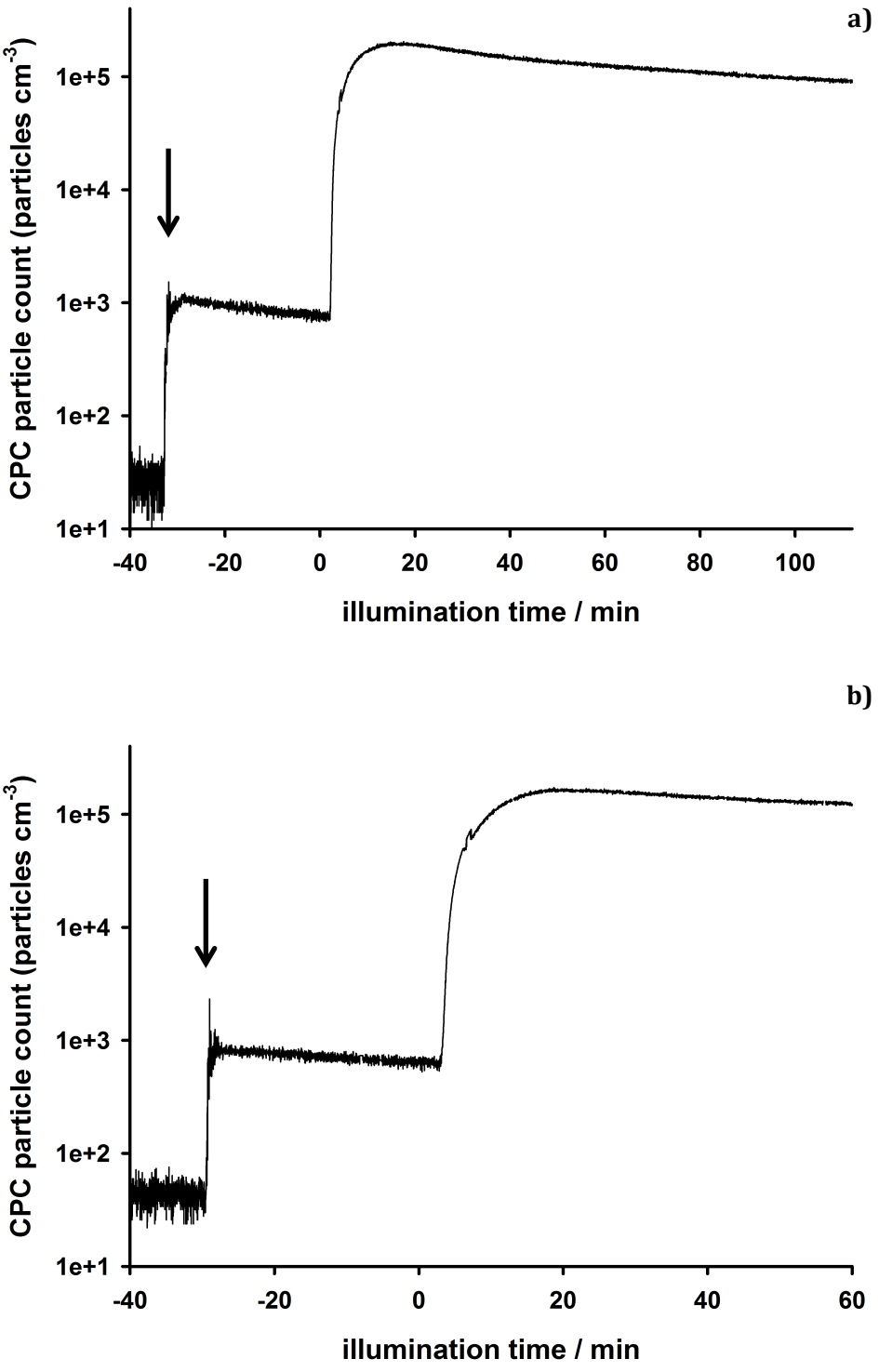

Figure 6-11 CPC particle count (particles cm^{-3}) within the CESAM chamber as a function of illumination time in the presence of dust produced from a) Chinese and b) Nigerien source samples. These experiments were conducted with ~ 800 ppb SO_2 and at ~ 40% RH. The black arrows indicate the times at which dust particles were injected into the chamber.

reagent over the time scale of the uptake reaction. It should be noted, however, that the uptake coefficients calculated at the lowest sample masses under study are typically lower than would be expected for a truly linear relationship this is especially apparent for the illite, Arizona test dust, and China sand samples. This observation is not without precedent for SO_2, although it has generally been presented without comment in the atmospheric literature.[19, 36]

As illustrated in Figure 6-4, the uptake of SO_2 at the surface of fine Niger sand is significantly greater than at the surface of coarse sand. This observation may be explained by the fact that larger sand particles contain higher relative quantities of quartz (SiO_2),[37] which is largely unreactive to SO_2.[20]

6.4.2 Photochemical production of sulfate at the surface of illuminated sand

The first set of photochemical experiments was conducted using coarse sand samples (< 1000 μm) from Niger. As illustrated in Figure 6-5, these natural samples contained detectable quantities of both S^{IV} and S^{VI} prior to SO_2 exposure. This observation is unsurprising given the results of a recent field study, which found that dust-associated sulfate in the Taklimakan desert of China originated primarily from the surface soil itself rather than from post-mobilization atmospheric processing.[38] Exposure of these samples to gas-phase SO_2 under illuminated conditions resulted in a substantial increase in total sulfur but only a minor, insignificant increase in S^{VI}. This result implies that SO_2 is primarily taken up as sulfite or bisulfite at the source of coarse Niger sand, even in the presence of light. Additional evidence for the insignificant role played by photochemistry at the coarse sand surface is provided by the fact that both the total sulfur and the S^{VI} contents of the films were, within experimental error, the same under dark and light conditions.

Recall from Section 6.4.1 that the uptake of SO_2 at the surface of Nigerien sand displayed a distinct size dependence: significantly higher uptake was observed at the

surface of fine (20 63 μm) sand than at the surface of coarse sand. Similarly, the fine fraction of Niger sand exhibited enhanced photochemical activity as illustrated in Figure 6-6, illumination of fine sand samples during SO_2 exposure led to a small enhancement in their total sulfur and S^{VI} contents over those observed under dark conditions. These results provide some (limited) evidence for light-catalyzed production of sulfate at the surface of mineral dusts in the atmosphere.

The smallest size fractions of mineral dust are often enriched in photoactive minerals, including Fe and Ti.[40, 41] As shown in Figure 6-7, highly efficient sulfate production was observed at the surface of Fe_2O_3 samples exposed to SO_2 and light. This result provides evidence, although indirect, that Fe-mediated chemistry may have contributed to the enhanced photochemical activity observed for the fine fraction of Niger sand.

6.4.3 Illumination of mineral dust in the presence of SO_2 leads to new particle formation

As shown in Figure 6-9, SO_2 undergoes light-induced nucleation in the CESAM chamber even in the absence of mineral dust. This apparent homogeneous nucleation is well-known in the atmospheric community, although its mechanism is still not fully understood.[42, 43]

In order to control for this chamber artefact, SO_2 was illuminated under identical experimental conditions but in the presence of NaCl particles, which would be expected to provide sufficient depositional/reactive surface area to suppress homogeneous nucleation. Indeed, the presence of NaCl particles did suppress nucleation: as shown in Figure 6-11, no particle formation was observed under these conditions (the small apparent stepwise increase in particle number upon illumination is attributable to a currently unresolved electronic interference from the lamps and/or chamber cooling system rather than to photochemistry within the chamber).

By contrast, as illustrated in Figure 6-10, illumination of SO_2 in the presence of Niger or China dust samples led to significant new particle formation. Since these experiments were performed using a similar total particle surface area to that employed in the NaCl experiment, the mineral dust would also have been expected to serve as a significant depositional sink for newly formed particles. The fact that net production of particles (as opposed to suppression of background nucleation, which was the case for the NaCl experiment) was observed in these experiments, therefore, is consistent with the dust surface itself acting as a significant source of new particles.

These results echo those obtained by Dupart and coworkers,[28] who observed under different experimental conditions that illumination of SO_2 in the presence of Arizona test dust led to significant new particle formation.

6.4.4 Atmospheric implications

The results obtained in the present study suggest that SO_2 mineral dust interactions under illumination may promote not only the production of sulfate at the mineral dust surface but also new particle formation from gas-phase SO_2. These results have important climatic implications, since the first pathway has the potential to influence the cloud-forming propensity of mineral dust aerosol and the second has the potential to change the net scattering properties of mineral dust-containing air masses.

One of the most important observations made in this study is that the uptake and photochemistry of SO_2 is enhanced at the surface of the fine fraction of Niger sand as compared to the coarse fraction. The size distribution of advected dust is known to shift toward smaller diameters during long-range transport;[44, 45] the results obtained in this study provide the first direct experimental evidence that the inherent heterogeneous (photo)reactivity of advected dust may be enhanced as a result of this transport-induced size fractionation. Since any increase in inherent dust reactivity would be necessarily offset during transport by dust particle dilution, transport-

induced reactivity enhancements would be expected to be most pronounced in polluted areas relatively close to source regions, where dust contributes significantly to particulate mass loadings Beijing and its industrial surroundings, for example.[3]

This observation of size-dependent reactivity underscores that it is critical to perform laboratory experiments using realistically generated dust samples. The dust generation method used for the CESAM chamber nucleation studies produced particles with a modal diameter of ~ 1.1 μm. These particles are similar in size to the smallest of three particle populations (~ 1.5 μm) produced in a laboratory study designed to investigate the size distribution of mineral aerosol produced by wind erosion,[46] and comparable to the smallest of the two dust coarse modes typically observed in field campaigns.[47]

The nucleation results obtained in the CESAM chamber, therefore, can be applied directly to the ambient environment, at least with respect to the inherent reactivity of the mineral dust under study. Further experiments should probe the photoinduced formation of sulfate at the surface of these authentically generated dust samples, however, since the reactivity of even the 'fine' Niger sample (20 63 μm) studied in the present work would be expected to be less than that of ambient mineral dust.

Although these results are not discussed in this chapter, the experimental campaign in CESAM also involved the measurement of dust size distributions using a broad range of analytical instrumentation, including two GRIMM optical particle counters, a WELAS light-scattering spectrometer, a scanning mobility particle sizer (SMPS), an aethalometer, and a nephelometer. In future, the data obtained from these instruments will be analyzed to see whether the uptake and photooxidation of SO_2 leads to a change in the dust size distribution, perhaps as a result of enhanced dust hygroscopicity and subsequent water uptake in the presence of surface-sorbed sulfate. In addition, dust optical properties were measured using Fourier transform infrared spectroscopy (FTIR). In future, these data will be analyzed to determine whether

production of surface sulfate results in a change in the dust spectral signature in the infrared region.

6.5 References

1. Tanaka, T. Y.; Chiba, M., A numerical study of the contributions of dust source regions to the global dust budget. *Global Planet. Change* **2006,** *52*, (1 4), 88 104.

2. Shao, Y.; Wyrwoll, K.-H.; Chappell, A.; Huang, J.; Lin, Z.; McTainsh, G. H.; Mikami, M.; Tanaka, T. Y.; Wang, X.; Yoon, S., Dust cycle: an emerging core theme in Earth system science. *Aeolian Res.* **2011,** *2*, (4), 181 204.

3. Dillner, A. M.; Schauer, J. J.; Zhang, Y. H.; Zeng, L. M.; Cass, G. R., Size-resolved particulate matter composition in Beijing during pollution and dust events. *J. Geophys. Res.–Atmos.* **2006,** *111*, (D5).

4. Lu, Z.; Streets, D. G.; Zhang, Q.; Wang, S.; Carmichael, G. R.; Cheng, Y. F.; Wei, C.; Chin, M.; Diehl, T.; Tan, Q., Sulfur dioxide emissions in China and sulfur trends in East Asia since 2000. *Atmos. Chem. Phys.* **2010,** *10*, (13), 6311 6331.

5. Wang, T.; Wei, X. L.; Ding, A. J.; Poon, C. N.; Lam, K. S.; Li, Y. S.; Chan, L. Y.; Anson, M., Increasing surface ozone concentrations in the background atmosphere of Southern China, 1994 2007. *Atmos. Chem. Phys.* **2009,** *9*, (16), 6217 6227.

6. Tang, Y. H.; Carmichael, G. R.; Kurata, G.; Uno, I.; Weber, R. J.; Song, C. H.; Guttikunda, S. K.; Woo, J. H.; Streets, D. G.; Wei, C.; Clarke, A. D.; Huebert, B.; Anderson, T. L., Impacts of dust on regional tropospheric chemistry during the ACE-Asia experiment: a model study with observations. *J. Geophys. Res.–Atmos.* **2004,** *109*, (D19).

7. Kojima, T.; Buseck, P. R.; Iwasaka, Y.; Matsuki, A.; Trochkine, D., Sulfate-coated dust particles in the free troposphere over Japan. *Atmos. Res.* **2006,** *82*, (3 4), 698 708.

8. Fan, S. M.; Horowitz, L. W.; Levy, H.; Moxim, W. J., Impact of air pollution on wet deposition of mineral dust aerosols. *Geophys. Res. Lett.* **2004,** *31*, (2).

9. Meskhidze, N.; Chameides, W. L.; Nenes, A.; Chen, G., Iron mobilization in mineral dust: can anthropogenic SO_2 emissions affect ocean productivity? *Geophys. Res. Lett.* **2003,** *30*, (21).

10. Solmon, F.; Chuang, P. Y.; Meskhidze, N.; Chen, Y., Acidic processing of mineral dust iron by anthropogenic compounds over the north Pacific Ocean. *J. Geophys. Res.–Atmos.* **2009,** *114*.

11. Adams, J. W.; Rodriguez, D.; Cox, R. A., The uptake of SO_2 on Saharan dust: a flow tube study. *Atmos. Chem. Phys.* **2005,** *5*, 2679 2689.

12. Horita, Y.; Sorimachi, A.; Takada, H.; Sekiguchi, K.; Wang, Q. Y.; Ishihara, H.; Nishikawa, M.; Sakamoto, K., *Influence of nitrogen oxides on heterogeneous uptake and oxidation of sulfur dioxide on yellow sand particles*. 2007.

13. Tonegawa, Y.; Kawashima, Y.; Horita, Y.; Ishihara, H.; Sakamoto, K., *Determination of SO2 deposition velocity and uptake coefficient onto yellow sand particles collected in Lanzhou, china*. 2007; p 196-199.

14. Seisel, S.; Keil, T.; Lian, Y.; Zellner, R., Kinetics of the uptake of SO_2 on mineral oxides: improved initial uptake coefficients at 298 K from pulsed Knudsen cell experiments. *Int. J. Chem. Kinet.* **2006,** *38*, (4), 242 249.

15. Fu, H.; Wang, X.; Wu, H.; Yin, Y.; Chen, J., Heterogeneous uptake and oxidation of SO_2 on iron oxides. *J. Phys. Chem. C* **2007,** *111*, (16), 6077 6085.

16. Seisel, S.; Keil, T.; Zellner, R., The uptake of SO_2 on alpha-Fe_2O_3 and mineral dust surfaces in the temperature range 250 K to 600 K. *Z. Phys. Chem.* **2009,** *223*, (12), 1477 1495.

17. Ullerstam, M.; Vogt, R.; Langer, S.; Ljungstrom, E., The kinetics and mechanism of SO_2 oxidation by O_3 on mineral dust. *Phys. Chem. Chem. Phys.* **2002,** *4*, (19), 4694 4699.

18. Usher, C. R.; Al-Hosney, H.; Carlos-Cuellar, S.; Grassian, V. H., A laboratory study of the heterogeneous uptake and oxidation of sulfur dioxide on mineral dust particles. *J. Geophys. Res.–Atmos.* **2002,** *107*, (D23).

19. Ullerstam, M.; Johnson, M. S.; Vogt, R.; Ljungstrom, E., DRIFTS and Knudsen cell study of the heterogeneous reactivity of SO_2 and NO_2 on mineral dust. *Atmos. Chem. Phys.* **2003,** *3*, 2043 2051.

20. Zhang, X. Y.; Zhuang, G. S.; Chen, J. M.; Wang, Y.; Wang, X.; An, Z. S.; Zhang, P., Heterogeneous reactions of sulfur dioxide on typical mineral particles. *J. Phys. Chem. B* **2006,** *110*, (25), 12588 12596.

21. Li, L.; Chen, Z. M.; Zhang, Y. H.; Zhu, T.; Li, J. L.; Ding, J., Kinetics and mechanism of heterogeneous oxidation of sulfur dioxide by ozone on surface of calcium carbonate. *Atmos. Chem. Phys.* **2006,** *6*, 2453 2464.

22. Liu, C.; Ma, Q. X.; Liu, Y. C.; Ma, J. Z.; He, H., Synergistic reaction between SO_2 and NO_2 on mineral oxides: a potential formation pathway of sulfate aerosol. *Phys. Chem. Chem. Phys.* **2012,** *14*, (5), 1668 1676.

23. Nanayakkara, C. E.; Pettibone, J.; Grassian, V. H., Sulfur dioxide adsorption and photooxidation on isotopically labeled titanium dioxide nanoparticle surfaces: roles of surface hydroxyl groups and adsorbed water in the formation and stability of adsorbed sulfite and sulfate. *Phys. Chem. Chem. Phys.* **2012,** *14*, (19), 6957 6966.

24. Shang, J.; Li, J.; Zhu, T., Heterogeneous reaction of SO_2 on TiO_2 particles. *Sci. China–Chem.* **2010,** *53*, (12), 2637 2643.

25. Baltrusaitis, J.; Jayaweera, P. M.; Grassian, V. H., Sulfur dioxide adsorption on TiO_2 nanoparticles: influence of particle size, coadsorbates, sample pretreatment, and light on surface speciation and surface coverage. *J. Phys. Chem. C* **2011,** *115*, (2), 492 500.

26. Fu, H. B.; Xu, T. G.; Yang, S. G.; Zhang, S. C.; Chen, J. M., Photoinduced formation of Fe(III) sulfato complexes on the surface of alpha-Fe_2O_3 and their photochemical performance. *J. Phys. Chem. C* **2009,** *113*, (26), 11316 11322.

27. Harris, E.; Sinha, B.; Foley, S.; Crowley, J. N.; Borrmann, S.; Hoppe, P., Sulfur isotope fractionation during heterogeneous oxidation of SO_2 on mineral dust. *Atmos. Chem. Phys.* **2012,** *12*, (11), 4867 4884.

28. Dupart, Y.; King, S. M.; Nekat, B.; Nowak, A.; Wiedensohler, A.; Herrmann, H.; David, G.; Thomas, B.; Miffre, A.; Rairoux, P.; D'Anna, B.; George, C., Mineral dust photochemistry induces nucleation events in the presence of SO_2. *PNAS* **2012,** *109*, (51), 20842 20847.

29. Styler, S. A.; Myers, A. L.; Donaldson, D. J., Heterogeneous photooxidation of fluorotelomer alcohols: a new source of aerosol-phase perfluorinated carboxylic acids. *Environ. Sci. Technol.* **2013,** *47*, (12), 6358 6367.

30. Finlayson-Pitts, B. J.; Pitts, J. N., *Chemistry of the upper and lower atmosphere*. Academic Press: San Diego, CA, 2000.

31. Michigami, Y.; Ueda, K., Sulfite stabilizer in ion chromatography. *J. Chromatogr. A* **1994,** *663*, (2), 255 258.

32. Hansen, L. D.; Richter, B. E.; Rollins, D. K.; Lamb, J. D.; Eatough, D. J., Determination of arsenic and sulfur species in environmental samples by ion chromatography. *Anal. Chem.* **1979,** *51*, (6), 633 637.

33. Wang, J.; Doussin, J. F.; Perrier, S.; Perraudin, E.; Katrib, Y.; Pangui, E.; Picquet-Varrault, B., Design of a new multi-phase experimental simulation chamber for atmospheric photosmog, aerosol, and cloud chemistry research. *Atmos. Meas. Tech.* **2011,** *4*, (11), 2465 2494.

34. Alfaro, S. C.; Lafon, S.; Rajot, J. L.; Formenti, P.; Gaudichet, A.; Maille, M., Iron oxides and light absorption by pure desert dust: an experimental study. *J. Geophys. Res.–Atmos.* **2004,** *109*, (D8).

35. Underwood, G. M.; Li, P.; Usher, C. R.; Grassian, V. H., Determining accurate kinetic parameters of potentially important heterogeneous atmospheric reactions on solid particle surfaces with a Knudsen cell reactor. *J. Phys. Chem. A* **2000,** *104*, (4), 819 829.

36. Ma, Q. X.; Liu, Y. C.; Liu, C.; Ma, J. Z.; He, H., A case study of Asian dust storm particles: chemical composition, reactivity to SO_2, and hygroscopic properties. *J. Environ. Sci.–China* **2012,** *24*, (1), 62 71.

37. Glaccum, R. A.; Prospero, J. M., Saharan aerosols over the tropical North Atlantic: mineralogy. *Mar. Geol.* **1980,** *37*, (3 4), 295 321.

38. Wu, F.; Zhang, D.; Cao, J.; Xu, H.; An, Z., Soil-derived sulfate in atmospheric dust particles at Taklimakan desert. *Geophys. Res. Lett.* **2012,** *39*.

39. Clements, A. L.; Buzcu-Guven, B.; Fraser, M. P.; Kulkarni, P.; Chellam, S., Role of particulate metals in heterogenous secondary sulfate formation. *Atmos. Environ.* **2013,** *75*, 233 240.

40. Castillo, S.; Moreno, T.; Querol, X.; Alastuey, A.; Cuevas, E.; Herrmann, L.; Mounkaila, M.; Gibbons, W., Trace element variation in size-fractionated African desert dusts. *J. Arid Environ.* **2008,** *72*, (6), 1034 1045.

41. Jeong, G. Y., Bulk and single-particle mineralogy of Asian dust and a comparison with its source soils. *J. Geophys. Res.–Atmos.* **2008,** *113*, (D2).

42. Shen, C. H.; Springer, G. S., Photochemical particulate formation in sulfur dioxide air mixtures. *Atmos. Environ.* **1976,** *10*, (3), 235 239.

43. Friend, J. P.; Barnes, R. A.; Vasta, R. M., Nucleation by free radicals from the photooxidation of sulfur dioxide in air. *J. Phys. Chem.* **1980,** *84*, (19), 2423 2436.

44. Maring, H.; Savoie, D. L.; Izaguirre, M. A.; Custals, L.; Reid, J. S., Mineral dust aerosol size distribution change during atmospheric transport. *J. Geophys. Res.–Atmos.* **2003,** *108*, (D19).

45. Mori, I.; Nishikawa, M.; Tanimura, T.; Quan, H., Change in size distribution and chemical composition of kosa (Asian dust) aerosol during long-range transport. *Atmos. Environ.* **2003,** *37*, (30), 4253 4263.

46. Alfaro, S. C.; Gaudichet, A.; Gomes, L.; Maille, M., Mineral aerosol production by wind erosion: aerosol particle sizes and binding energies. *Geophys. Res. L.* **1998,** *25*, (7), 991 994.

47. Formenti, P.; Schuetz, L.; Balkanski, Y.; Desboeufs, K.; Ebert, M.; Kandler, K.; Petzold, A.; Scheuvens, D.; Weinbruch, S.; Zhang, D., Recent progress in understanding physical and chemical properties of African and Asian mineral dust. *Atmos. Chem. Phys.* **2011,** *11*, (16), 8231 8256.

Chapter 7

Conclusions and future directions

Contributions:

The manuscript was written by Sarah A. Styler, with critical comments from D. James Donaldson.

7.1 Summary of thesis results

"The photochemistry of gases adsorbed onto mineral dust particles is largely unknown…"

- Kolb *et al.*, 2010[1]

Over a billion tons of dust are emitted into the atmosphere each year from source regions in Africa and Central Asia.[2] Once emitted, dust undergoes efficient long-range transport, during which it can interact with industrial and urban pollutant plumes.[3-5]

Although a number of laboratory studies have measured the uptake of gas-phase pollutants at the dust surface,[6] fewer have investigated the role that photochemical reactions occurring on dust and other photoactive surfaces may play in influencing the concentration and lifetime of gas-phase species typical of urban environments. Fewer still have directly studied photochemistry on real mineral dust samples: the majority of the experiments conducted to date have been performed using Ti oxides as proxies for the photoactive components of mineral aerosol.[7]

My doctoral work focused on designing methods to explore the photochemical reactivity of dust and other photoactive substrates in controlled laboratory settings. To this end, I performed five separate studies, each of which explored a different aspect of atmospheric heterogeneous photochemistry.

In the first study, I investigated the photoenhanced ozonation of pyrene, a carcinogenic product of incomplete combustion, at three surfaces designed to mimic different chemical attributes of "urban grime", the complex chemical film that develops on buildings and roadways in urban environments. I found that the photochemical behaviour of pyrene depends strongly on the type of surface used to mimic the urban grime environment: while the heterogeneous ozonation of pyrene solid films displayed a light enhancement, the ozonation of pyrene at the air-octanol film interface did not; moreover, the ozone-induced loss of pyrene at the illuminated

air-aqueous interface not only occurred more quickly than in the dark but also occurred via a different mechanistic pathway. These experiments highlighted a major disadvantage of the typical reductive laboratory approach: there is no guarantee that a molecule's reactivity on simplified surfaces is representative of its reactivity in the real environment.

In the second study, I explored the photochemical behaviour of atmospheric alcohols on TiO_2 and TiO_2/KNO_3 films, which I used as proxies for the photochemically active fraction of newly emitted and atmospherically processed mineral dust, respectively.[8] I found that isopropanol was efficiently converted to acetone on the illuminated TiO_2 surface, and that this conversion was enhanced in the presence of co-sorbed nitrate. These results are important because they indicate that mineral dust has the potential to catalyze the oxidation of non-absorbing species to those that are photochemically active in the actinic region, and therefore serve as a source of reactive organic radicals for further gas- or surface-phase chemistry. In addition, these studies serve as the first demonstration that the photochemical activity of mineral dust may be influenced by atmospheric processing.

In the third study, I investigated the photochemistry of oxalic acid, the most atmospherically abundant particulate-phase dicarboxylic acid, at the surface of Mauritanian sand and Icelandic volcanic ash.[9] These experiments showed that oxalic acid is efficiently oxidized to gas-phase CO_2 on sand and ash surfaces, and that this oxidation is catalyzed by Fe and Ti contained within these substrates. These results provided the first evidence that aqueous-phase iron-catalyzed photochemistry may not be the only substantial chemical loss mechanism for oxalic acid, especially in arid regions.

In the fourth study, I explored the atmospheric fate of fluorotelomer alcohols (FTOHs), a class of chemicals used in the production of water- and oil-repelling surface coatings.[10] Using both surface- and gas-phase analytical techniques, I showed that these compounds sorb strongly to sand and ash surfaces, where they can undergo

photooxidation to yield toxic and persistent perfluorinated carboxylic acids (PFCAs). These results suggest that the metal-catalyzed heterogeneous oxidation of FTOHs may act as a source of aerosol-phase PFCAs close to source regions. Furthermore, long-range transport of these aerosol-sorbed PFCAs has the potential to join oceanic transport and local gas-phase FTOH oxidation as a source of PFCA contamination in remote Arctic regions.

In the fifth study, I moved away from dust-catalyzed organic chemistry to focus on the light-mediated interactions of SO_2 with mineral dust. I found that illumination of Niger and China sand in the presence of gas-phase SO_2 led to the production of surface-sorbed sulfate; in the case of Niger sand, the uptake and photochemistry of SO_2 were both enhanced at the surface of the fine fraction as compared to the coarse fraction. These results are important because they provide the first direct experimental evidence that the heterogeneous (photo)reactivity of advected dust may be enhanced as a result of transport-induced size fractionation. In a set of chamber studies, I found that illumination of SO_2 in the presence of authentically generated mineral dust led to substantial new particle formation.

The implications of the work performed in this thesis extend beyond the role that mineral dust photochemistry may play in determining the atmospheric lifetime and ultimate fate of the set of organic species studied to include issues as broad as human health and climate. For example, the production of recalcitrant PFCAs from the heterogeneous photooxidation of FTOHs represents a pathway for the enhancement of urban particle toxicity. Mineral dust can also influence air quality indirectly: the photooxidative production of light-absorbing species, for example, has the potential to influence the local atmospheric oxidative capacity, and by extension the atmospheric persistence of urban pollutants of health concern. The formation of new particles by illuminated SO_2 dust mixtures is important in a climate context, since it provides a mechanism by which the scattering activity of polluted air parcels may be enhanced.

Finally, since the dust-catalyzed oxidation of oxalic acid is accompanied by the production of soluble Fe(II) from insoluble Fe(III), this reactive pathway has the potential not only to act as a sink for oxalic acid but also to enhance the extent to which oceanic dust deposition promotes primary productivity, and thus atmospheric CO_2 uptake.

7.2 Future research directions

The experiments performed in this thesis provide significant new insights into heterogeneous atmospheric photochemistry at the surface of dust and other photoactive substrates. However, our understanding of these processes is still far from complete the studies performed in this thesis represent virtually the only comprehensive investigations of organic photochemistry at the surface of mineral dust. It is obvious, therefore, that the scope of organic species and dust substrates studied should be widened. What is less obvious, however, is how a project of this magnitude should be approached. In the following sections, I highlight three overarching strategies that I believe will improve our understanding of heterogeneous photochemistry in an efficient and thorough manner.

7.2.1 Moving beyond model substrates

To date, the vast majority of experiments investigating heterogeneous photochemical processes have been performed using model systems. An ideal model system must be simple enough to allow researchers to extract a mechanistic understanding of chemical transformations yet complex enough to capture the attributes of environmental surfaces that fully define their reactivity.

While the model systems used to date have largely met the first criterion, it is not always clear whether they have fulfilled the second: the assumption that the reaction

environment provided by simple proxy systems is sufficiently representative of that provided by real environmental surfaces has rarely been interrogated.

Explicit evidence for the pitfalls of the typical reductive laboratory approach is provided in Chapter 2, which reports the results of investigations of the photochemical ozonation of pyrene solid films and pyrene at the air aqueous and air octanol interfaces. Although each of these simple environments could be considered a 'reasonable' proxy for environmental surfaces, the behaviour of pyrene was different at each. Which substrate is *more* 'reasonable', then? Which substrate best reflects the characteristics of the real environments in which pyrene is found? How would one go about inferring pyrene's behaviour in the real environment from its behaviour at these model surfaces? These are not easy questions to answer for this reason, most likely, they are questions that are rarely asked.

One approach to addressing this challenge is to perform experiments using real atmospheric samples. Some studies have already taken this approach: the uptake of ozone has been investigated on depositional Saharan dust samples collected in the Cape Verde islands, for example.[11]

The use of depositional dust samples is not without disadvantages, however. Experiments performed using these samples necessarily interrogate chemical processes on an ensemble of particles that have been subject to a range of (largely unknown) transport paths and gas-phase pollutant exposure scenarios. A first step toward measuring the inherent reactivity of dust is provided in Chapter 6, where a method for the generation of dust from authentic source samples is reported.

In my opinion, the following course of action will provide the greatest insight into chemistry occurring at the dust surface:

1. Build upon the method reported in Chapter 6 for the generation of dust from source samples: develop laboratory techniques to mimic the various dust generation processes occurring in the real environment.

2. Measure the uptake, chemistry, and photochemistry of gas-phase species on these authentically generated samples.

3. Characterize the size-dependent composition of these authentically generated samples. Building upon the preliminary results reported in Chapter 6 for the uptake and photochemistry of SO_2 at the surface of Niger sand, perform experiments using size-selected dust samples, and look for correlations between composition and (photo)reactivity.

4. Systematically expose dust samples to a variety of pollutants, both alone and in combination. Then, perform experiments using dust samples that have been subjected to this simulated atmospheric processing.

While I believe this approach will be useful for mineral dust, it will be less so for 'urban grime' and other complex photoactive surfaces, which are not emitted from point sources but rather are formed *in situ*. For 'urban grime', I suggest the following strategy:

1. Examine the uptake and reaction of trace atmospheric gases at the surface of collected urban grime samples (see Baergen *et al.*[12] for the first demonstration of this strategy).

2. Explore the photochemical loss of semivolatile organic species at the surface of urban grime. In order to circumvent issues of sample complexity, spike samples with isotopically labeled versions of the compounds of interest.

Finally, as outlined in Section 1.4.2.2, humic acid has been shown to promote the photoreductive uptake of both NO_2 and O_3.[13, 14] Although this substrate has typically

been used as a proxy for organic aerosol, it is also a major constituent of humic substances, which in turn comprise the majority of organic matter in soils.[15] It is reasonable to expect, therefore, that soils in agricultural regions downwind of urban regions the San Joaquin Valley in California, for example may serve as photochemical reactive sinks for some urban pollutants. To date, however, no studies have investigated this possibility. As a first attempt to address this gap in knowledge, I suggest that researchers investigate the photochemical uptake of O_3 and NO_2 at the surface of agricultural soils.

7.2.2 Moving beyond 'TiO_2-type' oxidative photochemistry

Studies of mineral dust photochemistry have largely been predicated upon the fact that it contains TiO_2, a known photosensitizer.[16] For this reason, the majority of studies investigating photochemistry at this surface have focused on semiconductor-type oxidative processes.[7]

This implicit experimental bias, however, does not preclude the existence of other mineral dust-mediated photoreactive pathways: in Chapter 4, for example, I showed that the lifetime of oxalic acid at the mineral dust surface may be limited by iron-mediated photochemistry.[9]

I recommend that future work in this area expand the working definition of photochemistry beyond TiO_2-mediated oxidative processes to include the following, as yet largely unstudied, reactive pathways:

1. Studies have shown that illumination of insulating metal oxides and soil surfaces leads to the production of singlet oxygen.[17, 18] Reaction with surface-sorbed singlet oxygen has the potential to be a significant loss pathway for gas-phase alkenes, aromatics, and other electron-rich organic species.[19]

2. The illumination of TiO_2 leads to the production of not only oxidizing holes but also reducing electrons.[16] Although these electrons have been implicated in the

photoreduction of NO_2 on the mineral dust surface,[20] their potential role in the reduction of organic species has yet to be investigated. I recommend that the photochemistry of halogen-containing organics, including polybrominated diphenyl ethers (PBDEs) and biogenic organobromides, be investigated at the mineral dust surface.

3. Mineral dust and ambient urban particulate matter both contain a wide variety of trace metals,[21] the photochemical reactivity of which has largely been unexplored. I recommend that the atmospheric chemistry community make a concerted effort to engage with the catalytic and inorganic literature in order to discover atmospherically relevant reactive pathways that may be the subject of much study in different contexts.

7.2.3 Including heterogeneous organic photochemistry in atmospheric models

The results obtained in this thesis suggest that substrate-promoted heterogeneous photochemistry may play a role in determining the atmospheric lifetime and ultimate fate of a variety of organic species. Although a full assessment of the conditions under which heterogeneous photochemistry represents a significant sink for organic pollutants and/or a significant production pathway for oxidized particle-bound species is beyond the scope of this work, I here apply results obtained in Chapter 4 to obtain a simple estimate of the potential contribution of particle-phase photochemistry to the removal of oxalic acid from the atmosphere under arid conditions.

As noted by Chebbi and Carlier, the primary loss process for carboxylic acids in the atmosphere recognized to date is dry deposition.[22] Assuming a boundary layer height of 400 m and a deposition velocity of 1 cm s^{-1},[22] the first-order depositional loss rate for gas-phase oxalic acid is thus 0.09 h^{-1}, which corresponds to an atmospheric lifetime of ~ 11h. Assuming an identical boundary layer height and a particle deposition velocity ranging from 0.01 1 cm s^{-1} for small (< 1 μm) and large (> 1 μm) particles,

respectively,[23] the first-order depositional loss rate for particle-phase oxalic acid ranges from 9×10^{-4} 0.09 h^{-1}, which corresponds to an atmospheric lifetime of 11 1100 h.

Field studies have shown that approximately 90% of oxalic acid is found in the particle phase.[24] The overall non-reactive loss rate for oxalic acid in the atmosphere, therefore, can be calculated by summing the weighted loss rates for gas-phase (*i.e.* 0.1×0.09 h^{-1}) and particle-phase (*i.e.* $0.9 \times [9 \times 10^{-4}$ 0.09 $h^{-1}]$) oxalic acid. The loss rate determined in this manner ranges from 9.81×10^{-3} h^{-1} (*i.e.* in cases where oxalic acid is present at the surface of small particles, which undergo relatively slow deposition) to 0.09 h^{-1} (*i.e.* in cases where oxalic acid is present at the surface of larger particles, which undergo relatively rapid deposition). These loss rates correspond to an atmospheric lifetime of 11 102 h.

The results obtained in Chapter 4, however, suggest that particle-catalyzed photochemistry may also contribute to oxalic acid loss in arid environments. At the surface of Mauritanian sand, the rate of photochemical oxalate loss is ~ 7.56 h^{-1} (this value is obtained from a first-order fit to the ion chromatographic data presented in Figure 4-7). If we assume, as an upper limit, that this pathway is available to 20% of particle-associated oxalic acid, then the loss rate of oxalic acid present in larger particles can be determined by summing the weighted loss rates for particle-phase oxalic acid present in non-reactive (*i.e.* 0.8×0.09 h^{-1}) and reactive (*i.e.* $0.2 \times [7.56$ h^{-1} + 0.09 $h^{-1}]$) environments. The loss rate determined in this manner is ~ 1.6 h^{-1} for both larger and smaller particles (*i.e.* the particle size dependence in dry depositional loss rates is insignificant when compared to photoreactive loss at the particle surface).

The overall loss rate for oxalic acid in the atmosphere again calculated by summing the weighted loss rates for gas-phase (*i.e.* 0.1×0.09 h^{-1}) and particle-phase (*i.e.* $0.9 \times$ 1.6 $h^{-1}]$) oxalic acid also increases substantially, to ~ 1.45 h^{-1}, which corresponds to an atmospheric lifetime of ~ 0.7h. Clearly, this simple calculation suggests that the particle-phase photooxidation of oxalic acid may contribute significantly to its loss in

arid environments, where its atmospheric lifetime is otherwise determined by dry deposition.

To my knowledge, only a few studies have attempted to model the contribution of heterogeneous chemistry to the loss of organic pollutants,[25, 26] and none have considered heterogeneous photochemistry. I suggest, therefore, that researchers in this field collaborate with experts in chemical modelling to develop strategies to incorporate heterogeneous photochemistry into chemical fate and transport models.

7.3 References

1. Kolb, C. E.; Cox, R. A.; Abbatt, J. P. D.; Ammann, M.; Davis, E. J.; Donaldson, D. J.; Garrett, B. C.; George, C.; Griffiths, P. T.; Hanson, D. R.; Kulmala, M.; McFiggans, G.; Poeschl, U.; Riipinen, I.; Rossi, M. J.; Rudich, Y.; Wagner, P. E.; Winkler, P. M.; Worsnop, D. R.; O' Dowd, C. D., An overview of current issues in the uptake of atmospheric trace gases by aerosols and clouds. *Atmos. Chem. Phys.* **2010,** *10*, (21), 10561 10605.

2. Tanaka, T. Y.; Chiba, M., A numerical study of the contributions of dust source regions to the global dust budget. *Global Planet. Change* **2006,** *52*, (1 4), 88 104.

3. Tang, Y. H.; Carmichael, G. R.; Kurata, G.; Uno, I.; Weber, R. J.; Song, C. H.; Guttikunda, S. K.; Woo, J. H.; Streets, D. G.; Wei, C.; Clarke, A. D.; Huebert, B.; Anderson, T. L., Impacts of dust on regional tropospheric chemistry during the ACE-Asia experiment: a model study with observations. *J. Geophys. Res.–Atmos.* **2004,** *109*, (D19).

4. Erel, Y.; Dayan, U.; Rabi, R.; Rudich, Y.; Stein, M., Trans-boundary transport of pollutants by atmospheric mineral dust. *Environ. Sci. Technol.* **2006,** *40*, (9), 2996 3005.

5. Falkovich, A. H.; Schkolnik, G.; Ganor, E.; Rudich, Y., Adsorption of organic compounds pertinent to urban environments onto mineral dust particles. *J. Geophys. Res.–Atmos.* **2004,** *109*, D02208, doi:10.1029/2003JD003919.

6. Usher, C. R.; Michel, A. E.; Grassian, V. H., Reactions on mineral dust. *Chem. Rev.* **2003,** *103*, (12), 4883 4939.

7. Chen, H. H.; Nanayakkara, C. E.; Grassian, V. H., Titanium dioxide photocatalysis in atmospheric chemistry. *Chem. Rev.* **2012,** *112*, (11), 5919 5948.

8. Styler, S. A.; Donaldson, D. J., Photooxidation of atmospheric alcohols on laboratory proxies for mineral dust. *Environ. Sci. Technol.* **2011,** *45*, (23), 10004 10012.

9. Styler, S. A.; Donaldson, D. J., Heterogeneous photochemistry of oxalic acid on Mauritanian sand and Icelandic volcanic ash. *Environ. Sci. Technol.* **2012,** *46*, (16), 8756 8763.

10. Styler, S. A.; Myers, A. L.; Donaldson, D. J., Heterogeneous photooxidation of fluorotelomer alcohols: a new source of aerosol-phase perfluorinated carboxylic acids. *Environ. Sci. Technol.* **2013,** *47*, (12), 6358 6367.

11. Hanisch, F.; Crowley, J. N., Ozone decomposition on Saharan dust: an experimental investigation. *Atmos. Chem. Phys.* **2003,** *3*, 119 130.

12. Baergen, A. M.; Donaldson, D. J., Photochemical renoxification of nitric acid on real urban grime. *Environ. Sci. Technol.* **2013,** *47*, (2), 815 820.

13. D'Anna, B.; Jammoul, A.; George, C.; Stemmler, K.; Fahrni, S.; Ammann, M.; Wisthaler, A., Light-induced ozone depletion by humic acid films and submicron aerosol particles. *J. Geophys. Res.–Atmos.* **2009,** *114*, (12), D12301, doi:10.1029/2008JD001237.

14. Stemmler, K.; Ammann, M.; Donders, C.; Kleffmann, J.; George, C., Photosensitized reduction of nitrogen dioxide on humic acid as a source of nitrous acid. *Nature* **2006,** *440*, (7081), 195-198.

15. Essington, M. E., *Soil and water chemistry: an integrative approach*. CRC Press: Boca Raton, FL, 2003.

16. Hoffmann, M. R.; Martin, S. T.; Choi, W. Y.; Bahnemann, D. W., Environmental applications of semiconductor photocatalysis. *Chem. Rev.* **1995,** *95*, (1), 69 96.

17. Gohre, K.; Miller, G., Photochemical generation of singlet oxygen on non-transition-metal oxide surfaces. *J. Chem. Soc., Faraday Trans. 1* **1985,** *81*, (3), 793 800.

18. Gohre, K.; Miller, G., Singlet oxygen generation on soil surfaces. *J. Agric. Food. Chem.* **1983,** *31*, (5), 1104 1108.

19. Kearns, D. R., Physical and chemical properties of singlet molecular oxygen. *Chem. Rev.* **1971,** *71*, (4), 395 427.

20. Ndour, M.; Nicolas, M.; D'Anna, B.; Ka, O.; George, C., Photoreactivity of NO_2 on mineral dusts originating from different locations of the Sahara desert. *Phys. Chem. Chem. Phys.* **2009,** *11*, (9), 1312 1319.

21. Clements, A. L.; Buzcu-Guven, B.; Fraser, M. P.; Kulkarni, P.; Chellam, S., Role of particulate metals in heterogenous secondary sulfate formation. *Atmos. Environ.* **2013,** *75*, 233 240.

22. Chebbi, A.; Carlier, P., Carboxylic acids in the troposphere, occurrence, sources, and sinks: a review. *Atmos. Environ.* **1996,** *30*, (24), 4233 4249.

23. Seinfeld, J. H.; Pandis, S. N., *Atmospheric Chemistry and Physics—From Air Pollution to Climate Change, 2nd edition*. 2nd edition ed.; J. Wiley: New York, United States, 2006.

24. Yao, X. H.; Fang, M.; Chan, C. K., Size distributions and formation of dicarboxylic acids in atmospheric particles. *Atmospheric Environment* **2002,** *36*, (13), 2099-2107.

25. Navea, J. G.; Young, M. A.; Xu, S.; Grassian, V. H.; Stanier, C. O., The atmospheric lifetimes and concentrations of cyclic methylsiloxanes octamethylcyclotetrasiloxane (D-4) and decamethylcyclopentasiloxane (D-5) and the influence of heterogeneous uptake. *Atmos. Environ.* **2011,** *45*, (18), 3181 3191.

26. Kwamena, N. O. A.; Clarke, J. P.; Kahan, T. F.; Diamond, M. L.; Donaldson, D. J., Assessing the importance of heterogeneous reactions of polycyclic aromatic hydrocarbons in the urban atmosphere using the Multimedia Urban Model. *Atmos. Environ.* **2007,** *41*, (1), 37 50.

Chapter 8

Appendix—dust and ash absorption spectra

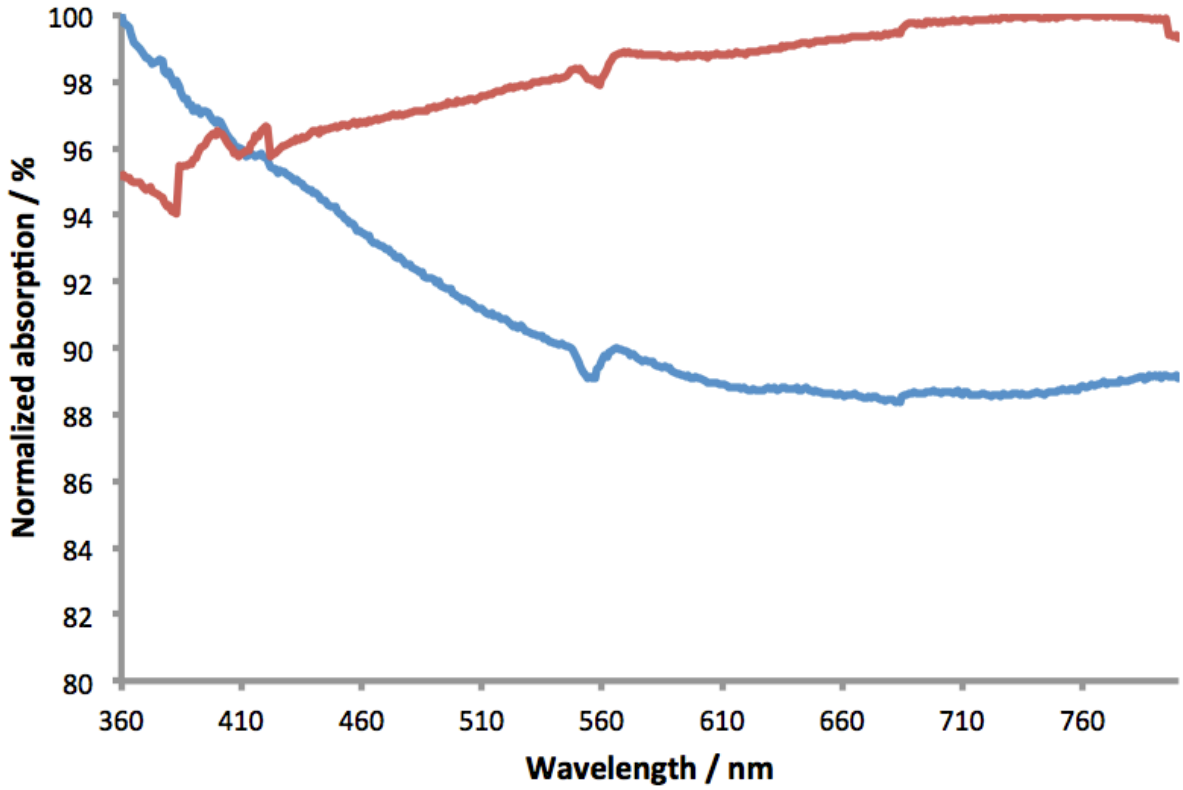

Figure 8-1 Normalized UV-Vis absorption spectra of thin films of Niger sand (20–63 μm particle size; blue trace) and Icelandic volcanic ash (red trace). Samples were ground in a mortar and pestle prior to use. UV-Vis spectra were normalized to the maximum absorption over the wavelength range 360–800 nm.